Spring 1-1-2011

Stream-Sediment Bed Exchange of Colloids and Colloid-Associated Metals in Acid Mine Drainage-Affected Environments

Audrey Salena Norvell Coleman
University of Colorado at Boulder, audrey.norvell@colorado.edu

STREAM-SEDIMENT BED EXCHANGE OF COLLOIDS AND COLLOID-ASSOCIATED METALS IN ACID MINE DRAINAGE-AFFECTED ENVIRONMENTS

By

Audrey Salena Norvell Coleman
B.S., Mercer University, 2006
M.S., University of Colorado, 2009

A thesis submitted to the
Faculty of the Graduate School of the
University of Colorado in partial fulfillment
of the requirement for the degree of
Doctor of Philosophy
Department of Civil, Environmental, and Architectural Engineering
2011

This thesis entitled:

Stream-Sediment Bed Exchange Of Colloids And Colloid-Associated Metals In Acid Mine Drainage-Affected Environments

written by
Audrey Salena Norvell Coleman

has been approved for the Department of Civil, Environmental, and Architectural Engineering

_____
Joseph N. Ryan

_____
Diane M. McKnight

_____
Harihar Rajaram

_____
Robert L. Runkel

_____

Alexis Templeton

Date_____

The final copy of this thesis has been examined by the signatories, and we find that both the content and the form meet acceptable presentation standards of scholarly work in the above mentioned discipline.

Coleman, Audrey Salena Norvell (Ph.D., Civil Engineering; Department of Civil, Architectural and Environmental Engineering)

Stream-Sediment Bed Exchange Of Colloids And Colloid-Associated Metals In Acid Mine Drainage-Affected Environments

Thesis directed by Professor Joseph N. Ryan

Abstract

A key component of human and ecological risk assessments of acid mine drainage is predicting the fate and transport of metals in receiving streams. Some contaminant metals are associated with colloids; therefore, better understanding of the transport and removal of colloids in stream systems is needed. The hyporheic exchange process transports water from the stream channel into the hyporheic zone and may play an important role in the removal of both metals and colloids.

In order to learn more about the processes that control metal removal in the stream, we studied the exchange of water, metals, and colloids with the hyporheic zone of Left Hand Creek, a stream contaminated by acid mine drainage in northwestern Boulder County, Colorado. We installed a set of mini-piezometers in the streambed and sampled the hyporheic pore waters along a 90 m reach of the creek for metals, colloids, and other geochemical parameters in the water and sediments. Though a transient storage model describing solute transport indicated that subsurface exchange was limited, piezometer measurements indicated that the rapid subsurface interactions occur over the upper 5 cm of the streambed and that the hyporheic zone may extend to depths of 40 cm in some locations. Large fractions of lead and copper were associated with colloids composed primarily of iron, manganese, and aluminum, while zinc was not significantly associated with colloids. Comparison of the colloidal concentrations with dissolved concentrations in the subsurface relative to surface concentrations indicated that colloids

facilitated transport of lead, copper, and zinc. Sequential extractions of the sediments showed that trace metals were incorporated in iron and manganese oxide coatings found on the streambed sediments.

We injected synthesized ferric (oxy)hydroxide colloids into a stream contaminated by acid mine drainage and monitored their transport in the stream and subsurface pore waters. A one-dimensional transient storage model (OTIS) was used to quantify parameters describing the transport of the ferric (oxy)hydroxide colloids and bromide, which was injected to serve as a conservative tracer. Based on integration of the area under the tracer dilution plot, 12.3% of the colloids were lost over the 61 m reach. Of the colloids entering the hyporheic zone, greater than 98% attenuation occurred within the upper 40 cm of the streambed at four locations downstream of the injection. Transient storage and first-order removal in the storage zone accounted for the loss of the ferrihydrite colloids from the stream. The rapid decline in the concentrations of colloids in the tail of the breakthrough curves indicates irreversible removal and indicates that modeling using first-order removal is acceptable.

The transport of metals strongly associated with colloids, lead and copper, was compared with the transport of zinc, a metal which tends to remain in the dissolved phase in stream systems. A continuous step injection of dissolved lead, copper, zinc, and a conservative tracer (bromide) was performed on a short reach of a low-order subalpine stream contaminated with acid mine drainage metals. Approximately 17.6% of lead and 4.6% of copper were lost from the main channel of the stream over the reach, while zinc was transported conservatively through the reach (0.061% removal). Zinc was found to be almost entirely dissolved, while colloids played a role in the transport of lead and copper in the reach.

Acknowledgements

My family, friends, and husband have all been supportive of my pursuit of a doctoral degree. I would like to especially thank my husband, Steve Coleman, for endless encouragement, fiscal sustainment, and contribution of labor in the field to accomplish research objectives.

Many thanks also go to Rebecca Cohen, Sanjay Mohanty, Marc Serravezza, Tim Dittrich, Alison Craven, Chase Gerbig, Anna Herring, and Katy Gerretch of the University of Colorado Boulder for helping with the field work. My advisor, Dr. Joseph Ryan, was instrumental in this work by providing assistance in the field, discussion of the experiments and results, and critiques of the thesis. Dr. Robert Runkel and Dr. Diane McKnight also provided helpful discussions of the results.

This research was supported by the National Science Foundation grant EAR-0538265. Howard Taylor, David Roth, Kirk Nordstrom, Blaine McCleskey, Dennis Eberl, Dave Metge and Arvind Mohanram at the United States Geological Survey in Boulder, Colorado, provided instruments and assistance with sample analysis. Fred Luiszer and John Drexler at the Laboratory for Environmental and Geological Studies (LEGS) in the Department of Geological Science at the University of Colorado also provided sample analysis. Colloids were characterized at the Nanomaterials Characterization Facility at the University of Colorado.

TABLE OF CONTENTS

LIST OF TABLES

LIST OF FIGURES

CHAPTER 1 - INTRODUCTION

BACKGROUND

Historical mining sites are responsible for discharging heavy metal-laden waters into streams throughout mining regions of America. The U.S. Environmental Protection Agency and the Department of Energy (2004) lists over 600,000 abandoned mine sites and estimates remediation cost from $32 to $72 billion. Metal contamination impairs aquatic ecosystems. Some metals accumulate in fish and create additional risk for the people who ingest them. Also, the loss of fish habitats adversely affects tourist economies. As America's population increases, the risk of human exposure to contaminated drinking water has become an increasingly critical issue. Therefore, local communities, mining industry leaders, and environmental regulators are under significant pressure to restore abandoned mine sites and affected streams.

A key component of human and ecological risk assessments and the prioritization of abandoned mine cleanups is predicting the impact that heavy metal-laden waters will have on affected streams. Researchers who observed high concentrations of metals when acid mine drainage leaks into pristine streams, have also observed that the metal concentrations decrease rapidly downstream (Theobald et al., 1963; Chapman et al., 1983; Rampe and Runnells, 1989; Kimball et al., 1995; Munk et al., 2002; Ranville et al., 2004). High concentrations of metals are attenuated in streambed sediments affected by acid mine drainage (Axtmann and Luoma, 1991; Nagorski et al., 2002; Galán et al., 2003) and hyporheic exchange has been cited as a means of introducing dissolved metals to sorption sites in the sediments (Benner et al., 1995; Fuller and Harvey, 2000). Some metals, such as lead and copper, are largely associated with colloids; they may sorb or co-precipitate as colloids form (oxy)hydroxides (Johnson, 1986; Kimball et al.,

1995; Ganguli et al., 2000; Tonkin et al., 2002). Understanding metal transport and removal from streams will also require understanding colloid transport and removal.

Hyporheic exchange may play an important role in metal removal from contaminated streams. The hyporheic zone is defined as the region where surface water enters the subsurface beneath and lateral to a stream and returns to the stream surface farther downstream (Harvey and Wagner, 2000). Streambed topography, such as pools and riffles, causes the exchange of water between the stream and streambed (Bencala, 1984; Harvey and Bencala, 1993). Hyporheic exchange plays an important role in stream biogeochemistry, nutrient cycling, and contaminant removal (Triska et al., 1989; Benner et al., 1995). Short hyporheic flowpaths – where water enters the hyporheic zone and returns to the stream within centimeters to meters – have the greatest interaction with the stream. Mixing of surface and ground water in the hyporheic zone leads to the formation of physical (temperature) and geochemical (pH, organic matter, oxidation-reduction) gradients in the hyporheic zone (Triska et al., 1989).

Hyporheic exchange may play an important role in the removal of metals and colloids from the stream (Figure 1.1). Hyporheic exchange brings metals into contact with the sediments, where they may sorb to immobile surfaces. Alternately, colloids may influence metal transport if metals are adsorbed or coprecipitated with colloids. Colloids play a key role in determining the transport of some metals and other contaminants. This is well understood in saturated porous media, where the enhanced groundwater transport of contaminants is referred to as "colloid-facilitated transport" (McCarthy and Zachara, 1989). Three basic criteria have been developed to assess the importance of colloids in contaminant transport in porous media: (1) the colloids are present in abundance, (2) the contaminants associate extensively with the colloids, and (3) the colloids offer enhanced transport. For example, if colloids are mobile relative to dissolved

metals, they will increase the transport of adsorbed metals. For colloid-facilitated transport to be important, desorption of metals from colloids must be slow relative to travel time. Colloids provide enhanced transport when they move the bound contaminants through the porous media, in this case the hyporheic zone, faster than the dissolved contaminants will move on their own.

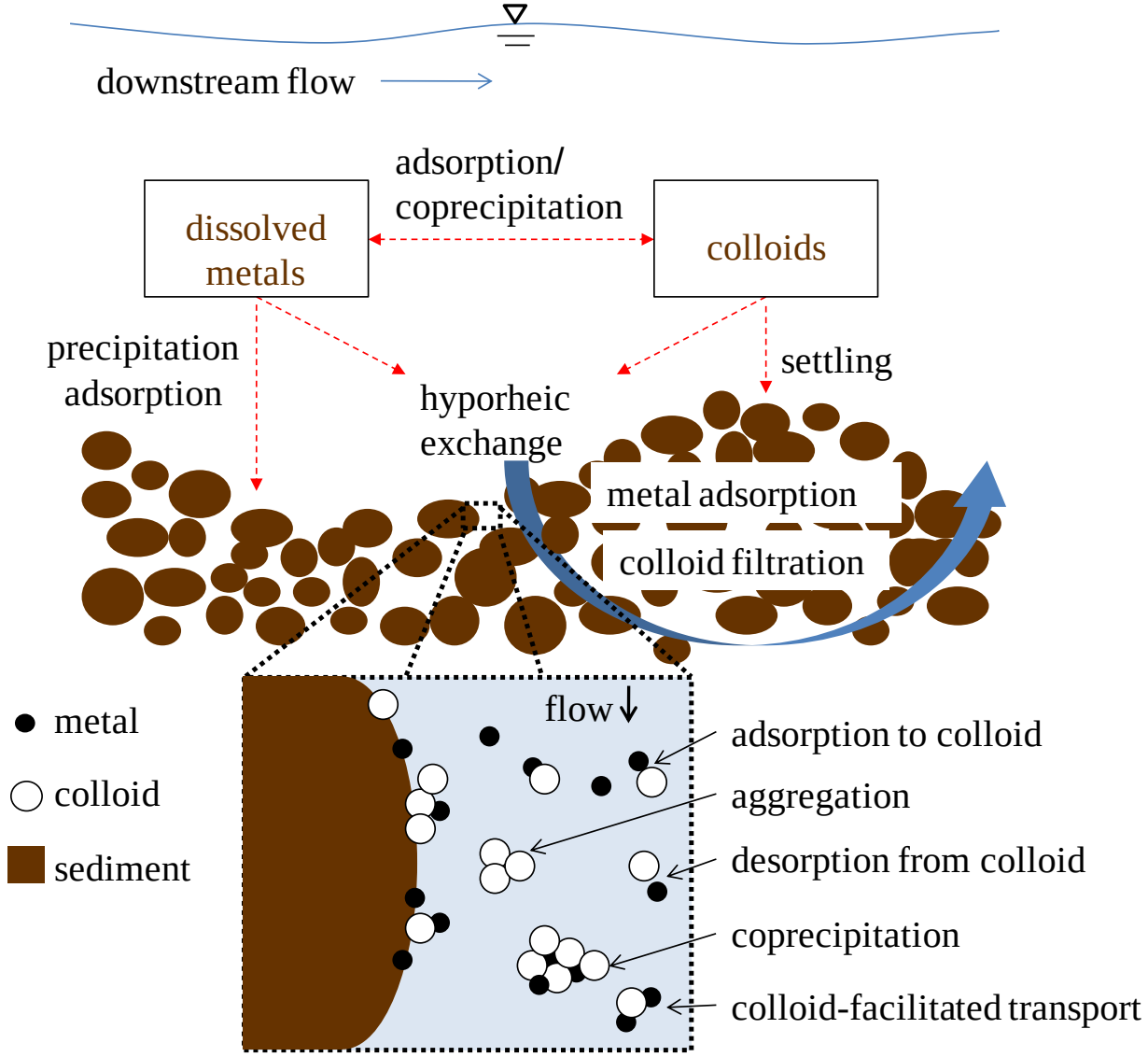

Figure 1.1. Metal and colloid removal processes in a stream-subsurface system, along with grain-scale view of metal, colloid, and sediment interactions, including metal adsorption to colloids and sediments, metal desorption, coprecipitation, colloid aggregation, colloid filtration, and colloid-facilitated metal transport.

TRANSIENT STORAGE MODELING

Bencala and Walters (1983) first developed the transient storage model (TSM), to analyze the results of a stream tracer experiment. This practice has since become a standard approach to quantifying stream hydrodynamics (Runkel et al., 2003). Transient storage refers to areas of water that moves slowly relative to the fast moving flow in the center of a stream, including eddies and subsurface flow. To apply the TSM, Runkel developed the one-dimensional transport with inflow and storage (OTIS) model (1998). The governing equation for the OTIS model is the advection-dispersion equation with additional terms to account for transient storage, lateral inflow, first-order decay and sorption. The conceptual model depicts two zones: the main channel and the storage zone. In the main channel, solutes are transported downstream by advection and dispersion:

$$\frac{\partial C}{\partial t} = -\frac{Q}{A}\frac{\partial C}{\partial x} + \frac{1}{A}\frac{\partial}{\partial x}(AD\frac{\partial C}{\partial x}) + \frac{q_{LIN}}{A}(C_L - C) + \alpha(C_S - C) \quad (1)$$

The solute concentration in the storage zone is driven by the process of transient storage, which is modeled as a first-order mass transfer process.

$$\frac{\partial C_S}{\partial t} = \alpha\frac{A}{A_S}(C - C_S) \quad (2)$$

where A is the main channel cross-sectional area, A_S is the storage zone cross-sectional area, C is the main channel solute concentration, C_L is the lateral inflow solute concentration, C_S is the storage zone solute concentration, D is the dispersion coefficient, Q is the volumetric flow rate, q_{LIN} is the lateral inflow rate, t is the time, x is distance and α is the storage zone exchange coefficient.

The OTIS model uses a Crank-Nicolson finite difference solution to solve for the advection-dispersion equation and associated equations. The application of the model involves a

trial-and –error approach to match simulations with observed tracer concentrations by adjusting parameter estimates. OTIS has been modified by coupling the governing equation with a nonlinear regression package in OTIS-P. OTIS-P automates the parameter estimation process by minimizing the squared differences between the simulated and observed concentrations.

The transient storage model has several limitations described by Runkel et al. (2003). First, the model is empirical and does not model exchange in a mechanistic way. The typical stream tracer approach does not provide for mechanistic model, because of the challenge to make accurate measurements required in a stream system.

Second, the concept of the storage zone combines surface storage and hyporheic zone storage. The two storage areas are difficult to separate except in systems where one is clearly dominant; a series of log jams would suggest surface storage dominates, while a well-defined channel with no eddies would suggest hyporheic exchange dominates.

Third, longer time scales, on the order of days, which may not be identified using stream tracer data. Since short time scales have a greater impact on in-stream tracer concentration, the stream tracer approach is biased toward representing short time scales (Harvey et al., 1996).

The fourth and final limitation deals with the parameters obtained in the model's simulation, which provides average properties. Using generic parameters are not likely to be very meaningful for heterogeneous systems.

Field-scale experiments involving metal and colloid transport have been examined using the OTIS model. Runkel et al. (1999) modeled reactive copper transport with the transient storage model coupled with a surface complexation submodel considering sorption to both immobile sediment surfaces and mobile freshly precipitated hydrous ferric oxide colloids. Runkel and Kimball (2002) simulated the effect of remediation on an acid mine drainage stream

and showed the importance of pH and metal oxide precipitation on lead removal. These experiments emphasize the importance of pH-dependent sorption of metals to colloids and sediments. In one study of colloid transport in streams, Karwan and Saiers (2009) used the transient storage model with irreversible sorption to account for colloid removal. They found that sub-micron sized titanium dioxide colloids can be removed from the stream despite low settling velocities and suggested that colloid removal from the stream channel was due to porous medium filtration in the streambed after introduction to the subsurface through hyporheic exchange.

METAL ADSORPTION TO COLLOIDS AND SEDIMENT

Metals span a wide range of ionic radius, charge, electronegativity and hardness, or covalent index. The hardness of the metal most directly impacts its stability with a given ligand. The A-type or "hard" metals have high spherical symmetry and they bind preferentially with hard ligands to form a highly polarized bond similar to purely ionic interactions (Pearson, 1986a; 1986b). The B-type or "soft" metals tend to have increased strength of covalent bonding. Pb(II), Cu(II), and Zn(II) – three metals that are common in acid mine drainage – span a range of covalent indices with Pb(II) having the highest covalent index ("softest"), followed by Cu(II), and then Zn(II) (Nieboer and Richardson, 1980). The relative extent of adsorption of Pb(II), Cu(II), and Zn(II) often observed in soils, sediments, and colloids in acid mine drainage environments follows the order Pb > Cu > Zn (Johnson, 1986; Evans and Davies, 1994; Rose and Ghazi, 1998; Lee et al., 2002). In addition to adsorption, co-precipitation may result in new surface phases at high adsorbate concentrations (Dzombak and Morel, 1990). Co-precipitation usually results in more tightly bound metals and co-precipitates of heavy metals in iron oxides can provide long-term sinks of these metals (Martinez and McBride, 1998). Metal precipitation

can also occur. However, metals typically adsorb to other surfaces at a lower pH than the pH at which they would precipitate. Therefore, the presence of other sorbents limits the likelihood of precipitation.

Metal sorption is strongly dependent on pH. At low pH, protons compete with metals for sorption sites on surface hydroxyls. As pH increases, less competition from protons allows for increasing metal sorption. Adsorption edges (plots of the amount of metal adsorbed versus pH) clearly show a line at which the pH has increased sufficiently to allow metal sorption to rise from near zero percent to near one hundred percent within a small pH range. Sorption edges of lead, copper and zinc to amorphous iron oxyhydroxides obtained by Benjamin and Leckie (1981) show the sorption edge occurring at the lowest pH for lead, followed by copper, then zinc due to their affinities for sorption as described above. The binding of metals to surface hydroxyls of iron oxides is given by:

$$\equiv SOH + Me^{2+} + H_2O \rightarrow \equiv SOMeOH_2^+ + H^+ \qquad K_{int}$$

The trend observed by Benjamin and Leckie (1981) is supported by the intrinsic surface complexation constants (K_{int}) for these metals: $10^{4.65}$, $10^{2.89}$, $10^{0.99}$ for lead, copper, and zinc, respectively (Dzombak and Morel, 1990).

Adsorption kinetics control metal transport. Metal adsorption reactions on (hydr)oxides are usually characterized by a rapid then slow reaction. Rapid reactions that occur on the order of seconds typically involve a chemical reaction or film diffusion. The slow reactions include inter-particle or intra-particle diffusion in pores and solids sites of low energy or reactivity as well at "surface" precipitation. The rate of sorption reaction depends on the type of sorbent and type of surface complex formed. A surface with more sorption sites will increase the rate of sorption. Metals forming an outer sphere complex are typically rapid and reversible. Those

metals forming an inner-sphere complex typically occur more slowly and may appear irreversible. Desorption rates may be slower for those metals that form bidentate rather than monodentate inner-sphere complexes.

Colloid Filtration in Porous Media

Colloids become immobilized in porous media through physicochemical filtration and straining (Yao et al., 1971; Bradford et al., 2003; Tufenkji and Elimelech, 2004). The kinetics of filtration depend on the rate of collision and the probability that the collision results in attachment. The hydrodynamics of the system control the frequency of collisions and the surface chemistry between colloid and immobile soil grains controls attachment. Collisions between colloids and sediment grains are caused by Brownian diffusion, sedimentation, and interception. The probability of attachment, according to DLVO (Derjaguin and Landau, 1941; Verwey and Overbeek, 1948) theory, depends on the surface-chemical interactions, where electrostatic attraction favors attachment and electrostatic repulsion inhibits attachment. Straining is the trapping of colloids in down-gradient pore throats that are too small to allow passage (McDowell-Boyer et al., 1986). Whether a colloid will be stable, aggregated, filtered, or will settle in porous media depends on density, size, and surface chemistry.

Acid Mine Drainage Colloids and Metal/Colloid Transport in the Hyporheic Zone

Colloids in streams impacted by acid mine drainage are commonly formed by the oxidation of Fe^{2+} and the precipitation of Fe-(oxy)hydroxides (Kimball et al., 1992). High concentrations of aluminum and manganese are also associated with acid mine drainage (Wentz, 1974) and these may also form colloids (Hart et al., 1992). Manganese colloids are less common than ferric iron colloids because of the kinetic limitation on oxidation of Mn^{2+}, but the oxidation rate can be enhanced by the adsorption of Mn^{2+} onto the surfaces of ferric oxyhydroxides and

aluminum oxides (Davies and Morgan, 1989). These ferric iron, aluminum, and manganese oxides have a strong ability to scavenge other metals whether they are in the form of colloids or coatings on streambed sediment (Kimball et al., 1992; Munk et al., 2002; Gandy et al., 2007; Schemel et al., 2007).

Metals may be removed from the stream through sorption directly to streambed sediments or, if they associate with colloids, the colloids may provide a mechanism for metal transport or removal in the stream sediments depending on the chemical composition (Ren and Packman, 2004a, 2004b, 2005). Colloid-associated metals will be removed from streams affected by acid mine drainage if the colloids are effectively immobilized by attachment to hyporheic zone sediments and the metals do not desorb from the colloids. The extent of the association between metals and colloids depends on environmental factors such as pH, ionic strength, size and type of colloid, concentrations of both the metal and colloid as well as other competing ions, reaction time and temperature, organic matter, microbes, and photochemistry.

Coupled metal and colloid transport in the subsurface has been modeled and verified at the laboratory scale. Ren and Packman (2004a) developed a process-based model that predicted stream-subsurface exchange incorporating colloidal contaminant transport. The modeling results explained zinc transport coupled with silica and kaolinite colloids (Ren and Packman, 2004b) and the transport of hematite colloids in the presence of zinc, copper and phosphate (Ren and Packman, 2005). These studies emphasize the importance of considering colloid and contaminant transport simulataneously because colloid-contaminant interactions can alter both colloid and contaminant mobility.

The parameters required for modeling in terms of underlying physical processes are difficult to measure and apply to field investigations. In addition to streamflow parameters such

as stream velocity, slope, and depth, streambed parameters, colloid parameters, and contaminant parameters must be considered. The filtration coefficient for colloid removal and sorption capacities of both colloids and sediment surfaces will vary due to geochemical heterogeniety in the streambed. The colloid filtration coefficient, λ_f, is a function of porosity, the diameter of sediment grains, the attachment efficiency (α), and the single collector contact efficiency (η_0). Due to subsurface heterogeniety, hydraulic conductivity and porosity may vary significantly along a reach. These will cause variations in subsurface flowpaths. The chemical characteristics of the subsurface, such as pH and ionic strength, will influence the collision efficiency and the single collector contact efficiency by controlling the surface charge and extent of the electrical double layer at the surfaces of colloids and sediments. This will in turn control colloid stability and size and the favorability of attachment. Gradients in the subsurface due to mixing of stream and groundwater will cause variability in these important chemical characteristics.

Integration of surface and subsurface transport of metals and colloids at the field scale is lacking. Laboratory studies have examined metal and colloid exchange in controlled flume experiments and applied a process-based modeling approach. Field experiments involving colloid and metal in-stream transport have been performed and modeled using the transient storage model. Further examination of the subsurface as well surface monitoring is necessary to understand the coupled transport of metals and colloids.

HYPOTHESES TESTED IN THIS RESEARCH

The focus of this study was to assess the abundance and behavior of metals and colloids in hyporheic zone waters and sediments and the exchange of the metals and colloids between stream water and the hyporheic zone. To assess these points, we installed a set of mini-piezometers in the streambed of a low-order subalpine stream in the Colorado Front Range

affected by acid mine drainage and sampled surface waters, hyporheic pore waters, and sediments. We also performed a series of tracer additions involving a conservative tracer, colloids, and metals.

Hypothesis 1. The links between hydrology and geochemistry of the hyporheic zone and the resulting impact on metal and colloid transport are not well known. It is hypothesized that geochemical gradients in the hyporheic zone will influence the phase of metals, dissolved or colloidal, and therefore transport in the hyporheic zone. Chapter 2 describes the physicochemical parameters affecting metal transport in the hyporheic zone.

Hypothesis 2. Colloid transport at the field scale is largely unresearched. It is hypothesized that colloids will contact the sediments through hyporheic exchange and be removed through filtration in the sediments. Chapter 3 describes an experiment examining surface and subsurface transport of synthesized iron (oxy)hydroxide colloids.

Hypothesis 3. It is hypothesized that metals more strongly associated with colloids (e.g., lead) will be removed from the stream to a greater extent than metals that bind more weakly (e.g., zinc). If colloids are immobilized in the hyporheic zone, they will provide a means for additional removal of associated metals. The strong link between colloid and metal must be considered in predicting the fate of metals. Chapter 4 describes an injection of dissolved metals and the downstream colloid association and metal removal in the subsurface. Appendix 1 describes the results of colloid and metal filtration in sediments determined from column experiments.

REFERENCES

Axtmann, E.V., Luoma, S.N. (1991) Large-scale distribution of metal contamination in the finegrained sediments of the Clark Fork River, Montana, USA. *Applied Geochemistry* 6 (1) 75-88.

Bencala, K. E., Walters, R. A. (1983) Simulation of solute transport in a mountain pool-and-riffle stream - a transient storage model. *Water Resources Research* 19 (3) 718-724.

Bencala, K.E. (1984) Interactions of solutes and streambed sediment 2. A dynamic analysis of coupled hydrologic and chemical processes that determine solute transport. *Water Resources Research* 20 (12) 1804-1814.

Benjamin, M. M., Leckie, J. O. (1981) Multiple-site adsorption of Cd, Cu, Zn, and Pb on amorphous iron oxyhydroxide. *Journal of Colloid and Interface Science 79* (1) 209-221.

Benner, S.G., Smart, E.W., Moore, J.N. (1995) Metal behavior during surface groundwater interaction, Silver-Bow Creek, Montana. *Environmental Science & Technology* 29 (7) 1789-1795.

Bradford, S. A., Simunek, J., Bettahar, M., Van Genuchten, M. T. and Yates, S. R. (2003) Modeling colloid attachment, straining, and exclusion in saturated porous media. *Environmental Science & Technology*, 37, 2242-2250.

Chapman, B.M., Jones, D.R., Jung, R.F. (1983) Processes controlling metal-ion attenuation in acid-mine drainage streams. *Geochimica et Cosmochimica Acta* 47 (11) 1957-1973.

Davies, S.H.R., Morgan, J.J. (1989) Manganese(II) oxidation-kinetics on metal-oxide surfaces. *Journal of Colloid and Interface Science* 129 (1) 63-77.

Derjaguin, B. V. and Landau, L. (1941) Theory of the stability of strongly charged lyophobic sols and the adhesion of strongly charged particles in solutions of electrolytes. *Acta Physicochimica URSS* 14, 633-662.

Dzombak, D. A. and Morel, F. M. M. (1990) Surface Complexation Modeling: Hydrous Ferric Oxide. John Wiley & Sons: New York, 393 pp.

Evans, D. and Davies, B. E. (1994) The influence of channel morphology on the chemical partitioning of Pb and Zn in contaminated river sediments. *Applied Geochemistry* 9, 45-52.

Feris, K.P., Ramsey, P.W., Gibbons, S.M., Frazar, C., Rillig, M.C., Moore, J.N., Gannon, J.E., Holben, W.E. (2009) Hyporheic microbial community development is a sensitive indicator of metal contamination. *Environmental Science & Technology* 43 (16) 6158-6163.

Fuller, C. C., Harvey, J. W. (2000) Reactive uptake of trace metals in the hyporheic zone of a mining-contaminated stream, Pinal Creek, Arizona. *Environmental Science & Technology* 34 (7) 1150-1155.

Galán, E., Gomez-Ariza, J.L., Gonzalez, I., Fernandez-Caliani, J.C., Morales, E., Giraldez, I. (2003) Heavy metal partitioning in river sediments severely polluted by acid mine drainage in the Iberian Pyrite Belt. *Applied Geochemistry* 18 (3) 409-421.

Gandy, C.J., Smith, J.W.N., Jarvis, A.P. (2007) Attenuation of mining-derived pollutants in the hyporheic zone: A review. *Science of the Total Environment* 373 (2-3) 435-446.

Ganguli, P.M., Mason, R.P., Abu-Saba, K.E., Anderson, R.S., Flegal, A.R. (2000) Mercury speciation in drainage from the New Idria mercury mine, California. *Environmental Science & Technology* 34 (22) 4773-4779.

Hart, B.T., Noller, B.N., Legras, C., Currey, N. (1992) Manganese speciation in Magela Creek, Northern Australia. *Australian Journal of Marine and Freshwater Research* 43 (2) 421-441.

Harvey, J.W., Bencala, K.E. (1993) The effect of streambed topography on surface-subsurface water exchange in mountain catchments. *Water Resources Research* 29 (1) 89-98.

Harvey, J. W., Wagner, B. J., Bencala, K. E. (1996) Evaluating the reliability of the stream tracer approach to characterize stream-subsurface water exchange. *Water Resources Research 32* (8) 2441-2451.

Harvey, J.W., Wagner, B.J. (2000) Quantifying hydrologic interactions between streams and their subsurface hyporheic zones. In *Streams and Ground Waters*, Jones, J.B., Mulholland, P.J. (Eds.), Academic Press, San Diego, p. 3.

Johnson, C.A. (1986) The regulation of trace-element concentrations in river and estuarine waters contaminated with acid-mine drainage – The adsorption of Cu and Zn on amorphous Fe oxyhydroxides. *Geochimica et Cosmochimica Acta* 50 (11) 2433-2438.

Karwan, D. L., Saiers, J. E. (2009). Influences of seasonal flow regime on the fate and transport of fine particles and a dissolved solute in a New England stream. *Water Resources Research 45* (11) doi:10.1029/2009WR008077.

Kimball, B.A. Callender, E., Axtmann, E.V., (1995) Effects of colloids on metal transport in a river receiving acid-mine drainage, Upper Arkansas River, Colorado, USA. *Applied Geochemistry* 10 (3) 285-306.

Kimball, B.A., Mcknight, D.M., Wetherbee, G.A., Harnish, R.A. (1992) Mechanisms of iron photoreduction in a metal-rich, acidic stream (St. Kevin Gulch, Colorado, USA). *Chemical Geology* 96 (1-2) 227-239.

Kuwabara, J. S., Leland, H. V., Bencala, K. E. (1984) Copper transport along a sierra-nevada stream. *Journal of Environmental Engineering-ASCE 110* (3) 646-655.

Lee, G., Bigham, J. M. and Faure, G. (2002) Removal of trace metals by coprecipitation with Fe, Al and Mn from natural waters contaminated with acid mine drainage in the Ducktown Mining District, Tennessee. *Applied Geochemistry* 17, 569-581.

Martinez, C. E. and McBride, M. B. (1998) Solubility of Cd^{2+}, Cu^{2+}, Pb^{2+}, and Zn^{2+} in aged coprecipitates with amorphous iron hydroxides. *Environmental Science & Technology* 32, 743-748.

McCarthy, J. F. and Zachara, J. M. (1989) Subsurface transport of contaminants. *Environmental Science & Technology* 23, 496-502.

McDowell-Boyer, L. M., Hunt, J. R. Sitar, N. (1986) Particle transport through porous media *Water Resources Research* 22 (13) 1901-1921.

Munk, L., Faure, G., Pride, D.E., Bigham, J.M. (2002) Sorption of trace metals to an aluminum precipitate in a stream receiving acid rock-drainage; Snake River, Summit County, Colorado. *Applied Geochemistry* 17 (4) 421-430.

Nagorski, S.A., Moore, J.N., Smith, D.B. (2002) Distribution of metals in water and bed sediment in a mineral-rich watershed, Montana, USA. *Mine Water and the Environment* 21 (3) 121-136.

Nieboer, E., Richardson, D. H. S. (1980) The replacement of the nondescript term `heavy metals' by a biologically and chemically significant classification of metal ions. *Environmental Pollution Series B, Chemical and Physica1*1 (1) 3-26.

Pearson, R. G. (1986a) Hard and soft acids and bases, HSAB part 1: fundamental principles. *Journal of Chemical Education* 45, 581-587.

Pearson, R. G. (1986b) Hard and soft acids and bases, HSAB part 2: underlying theories. *Journal of Chemical Education*, 45, 643-648.

Rampe, J.J., Runnells, D.D. (1989) Contamination of water and sediment in a desert stream by metals from an abandoned gold mine and mill, Eureka District, Arizona, USA. *Applied Geochemistry* 4 (5) 445-454.

Ranville, M., Rough, D., Flegal, A.R. (2004) Metal attenuation at the abandoned Spenceville copper mine. *Applied Geochemistry* 19 (5) 803-815.

Ren, J.H., Packman, A.I. (2004a) Modeling of simultaneous exchange of colloids and sorbing contaminants between streams and streambeds. *Environmental Science & Technology* 38 (10) 2901-2911.

Ren, J.H., Packman, A.I. (2004b) Stream-subsurface exchange of zinc in the presence of silica and kaolinite colloids. *Environmental Science & Technology* 38 (24) 6571-6581.

Ren, J.H., Packman, A.I. (2005) Coupled stream-subsurface exchange of colloidal hematite and dissolved zinc, copper, and phosphate. *Environmental Science & Technology* 39 (17) 6387-6394.

Ren, J.H., Packman, A.I., Welty, C. (2000) Correlation of colloid collision efficiency with hydraulic conductivity of silica sands. *Water Resources Research* 36 (9), 2493-2500.

Rose, S. and Ghazi, A. M. (1998) Experimental study of the stability of metals associated with iron oxyhydroxides precipitated in acid mine drainage. *Environmental Geology* 36, 364-369.

Runkel, R. L. (1998) One-dimensional transport with inflow and storage (OTIS): A solute transport model for streams and rivers. Water-Resources Investigations Report 98-4018, U.S. Geological Survey, Denver, Colorado.

Runkel, R. L., Kimball, B. A., McKnight, D. M., Bencala, K. E. (1999) Reactive solute transport in streams: A surface complexation approach for trace metal sorption. *Water Resources Research 35* (12) 3829-3840.

Runkel, R. L., Kimball, B. A. (2002) Evaluating remedial alternatives for an acid mine drainage stream: Application of a reactive transport model. *Environmental Science & Technology 36* (5) 1093-1101.

Runkel, R. L., McKnight, D.M., Rajaram H. (2003) Modeling hyporheic zone processes. *Advances in Water Resources* 26 (9) 901-905.

Schemel, L.E., Kimball, B.A., Runkel, R.L., Cox, M.H. (2007) Formation of mixed Al-Fe colloidal sorbent and dissolved-colloidal partitioning of Cu and Zn in the Cement Creek - Animas River confluence, Silverton, Colorado. *Applied Geochemistry* 22 (7) 1467-1484.

Theobald, P.K., Lakin, H.W., Hawkins, D.B. (1963) The precipitation of aluminum, iron and manganese at the junction of Deer Creek with the Snake River in Summit County, Colorado. *Geochimica et Cosmochimica Acta* 27 (2) 121-132.

Tonkin, J.W., Balistrieri, L.S., Murray, J.W. (2002) Modeling metal removal onto natural particles formed during mixing of acid rock drainage with ambient surface water. *Environmental Science & Technology* 36 (3) 484-492.

Triska, F.J., Kennedy, V.C., Avanzino, R.J., Zellweger, G.W., Bencala, K.E. (1989) Retention and transport of nutrients in a third-order stream: channel processes. *Ecology* 70 (6) 1877-1892.

Tufenkji, N. and Elimelech, M. (2004) Correlation equation for predicting single-collector efficiency in physicochemical filtration in saturated porous media. *Environmental Science & Technology* 38, 529-536.

USEPA/DOE, 2004. Mine waste technology program: Annual report 2004. United States Environmental Protection Agency and the Department of Energy, 51 p. (accessed March on 17, 2011, at http://www.epa.gov/nrmrl/std/mtb/mwt/annual/annual2004/annual2004.htm).

Verwey, E. J. W. and Overbeek, J. T. G. (1948) Theory of the Stability of Lyophobic Colloids. Elsevier: Amsterdam, 218 pp.

Wentz, D.A. (1974) Effect of mine drainage on the quality of streams in Colorado, 1971-72. *Colorado Water Resources Circular* 21, Colorado Water Conservation Board: Denver. 117 p.

Yao, K.-M., Habibian, M. T. and O'Melia, C. R. (1971) Water and waste water filtration. Concepts and applications. *Environmental Science & Technology,* 5, 1105-1112.

CHAPTER 2 - GEOCHEMICAL CONTROLS ON REMOVAL OF METALS AND COLLOIDS IN THE HYPORHEIC ZONE OF AN ACID MINE DRAINAGE-CONTAMINATED STREAM

ABSTRACT

A key component of human and ecological risk assessments of acid mine drainage is predicting the fate and transport of metals in receiving streams. In order to learn more about the processes that control metal removal in the stream, we studied the role of colloids and the exchange of stream water with the hyporheic zone in Left Hand Creek, a stream contaminated by acid mine drainage in northwestern Boulder County, Colorado. We installed a set of mini-piezometers in the streambed and sampled the hyporheic pore waters along a 77 m reach of the creek for metals, colloids, and other geochemical parameters in the water and sediments during high flow and low flow. We conducted tracer dilution tests to determine the extent and time scale of hyporheic exchange. Piezometer measurements indicate that hyporheic exchange occurred on the order of hours through the upper 40 cm of the streambed and more slowly through the deeper streambed to depths of 100 cm. A transient storage model describing solute transport indicated that transient storage (assumed to be hyporheic exchange) accounts for only 0.1% of the total reach travel time under low flow conditions. Large fractions of lead and copper were associated with colloids composed primarily of iron, manganese, and aluminum, while zinc was not significantly associated with colloids. Comparison of the colloidal concentrations with dissolved concentrations in the subsurface relative to surface concentrations indicated that colloids facilitated transport of lead, copper, and zinc. Sequential extractions of the sediments showed that trace metals were incorporated in iron and manganese oxide coatings found on the streambed sediments. These coatings possess high sorption capacities for metals and may enhance removal of colloids and colloid-associated metals.

INTRODUCTION

Historical mining sites are responsible for decades of discharge of heavy metal-laden waters to streams throughout mining regions of America. The U.S. Environmental Protection Agency and the Department of Energy (2004) lists over 600,000 abandoned mine sites with an estimated cost of remediation of at least US$32 billion. Metal contamination impairs aquatic ecosystems. Some metals accumulate in fish and create additional risk for the people who ingest them. Tourism economies may also be adversely affected by the loss of fish habitats. As the population increases, the demand for drinking water has made the risk of human exposure through drinking water a larger issue. Local communities, mining industry leaders, and environmental regulators are under pressure to restore abandoned mine sites and contaminated streams.

A key component of human and ecological risk assessments and the prioritization of abandoned mine cleanups is predicting the fate and transport of metals in acid mine drainage-affected streams. Near acid mine drainage inputs, metal concentrations are high, but attenuation is often rapid as metals are transported downstream (Theobald et al., 1963; Chapman et al., 1983; Rampe and Runnells, 1989; Kimball et al., 1995; Munk et al., 2002; Ranville et al., 2004). Metal attenuation results in high metal concentrations in streambed sediments (Axtmann and Luoma, 1991; Nagorski et al., 2002; Galán et al., 2003; Ranville et al., 2004). The accumulation of metals in streambed sediments has been attributed to hyporheic exchange and adsorption of metals to minerals in the streambed sediments (Benner et al., 1995; Fuller and Harvey, 2000). Metal deposition has been investigated by measuring metal sorption on cleaned sediment or ceramic beads placed in the streambed, estimating metal uptake within the hypothec zone based

on pore water measurements, as well as by considering sorption in modeling dissolved metal transport (Bencala, 1983; Kennedy, 1984; Benner et al., 1995; Fuller and Harvey, 2000).

Some metals, such as lead and copper, associate to some degree with colloids in acid mine drainage environments (Johnson, 1986; Kimball et al., 1995; Ganguli et al., 2000; Schemel et al., 2000; Tonkin et al., 2002); therefore, understanding of metal transport and removal in streams and the hyporheic zone also requires understanding of colloid transport and removal. Colloids in streams affected by acid mine drainage are often formed by the oxidation of ferrous iron and precipitation of ferric oxyhydroxides (Kimball et al., 1992). Aluminum and manganese may also precipitate as hydroxides and oxide colloids (Hart et al., 1992). These ferric iron, aluminum, and manganese oxyhdyroxides, whether in the form of colloids or coatings on streambed sediment, have a strong affinity for other metals (Kimball et al., 1992; Munk et al., 2002; Gandy et al., 2007; Schemel et al., 2007).

The behavior of colloids and colloid-associated metals in the hyporheic zone is not well known. Runkel et al. (1999) considered the role of "mobile precipitate" and "mobile sorbed" phases of metals in a model of trace metal transport in streams. The phases were considered to be colloidal metal hydroxides and ferric oxyhydroxide-adsorbed metals that were removed from the water column to the streambed sediments by settling. Ren and Packman (2004a, b, 2005) demonstrated the importance of hyporheic exchange in the removal of metals and colloids in a laboratory flume, and they incorporated processes of removal for both metals (adsorption) and colloids (colloid filtration theory – Brownian motion, interception, and settling) into a more mechanistic model of metal removal in the hyporheic zone. Their experiments and modeling demonstrated that colloids can enhance or inhibit metal transport depending on the ability of the streambed sediments to collect colloids and colloid-associated metals.

To assess the role of the hyporheic zone in the removal of colloids, we need to know the nature of the hyporheic zone, which is defined as the region where surface water enters into and returns from the subsurface beneath and lateral to a stream (Harvey and Wagner, 2000). Streambed topography, such as the pools and riffles in high-gradient alpine streams, causes the exchange of water between the stream and streambed (Bencala, 1984; Harvey and Bencala, 1993). Short hyporheic flowpaths – where water enters the hyporheic zone and returns to the stream within centimeters to meters of horizontal distance – have the greatest interaction with the stream. Seasonal changes in stream flow may cause fluctuations in the size of the hyporheic zone (Wroblicky et al., 1998; Harvey and Wagner, 2000; Storey et al., 2003) and the physical (temperature) and geochemical gradients that exist in the hyporheic zone (Triska et al., 1989; Malcolm et al., 2004). The geochemical gradients (e.g., pH, ionic strength, organic matter concentration, oxidation-reduction potential) will affect the transport of both metals and colloids (Gandy et al., 2007).

Colloid and metal transport in the stream and subsurface is largely controlled by the physicochemical properties of the system. Physicochemical properties give an understanding of the processes that may occur in the stream and subsurface. Physical properties, head gradient and hydraulic conductivity, give an indication of the potential for exchange flow into the hyporheic zone. Electrical conductivity, pH, and dissolved oxygen give an indication of the reduction-oxidation potential, the stability of colloids and the likely distribution of metals between dissolved and sorbed phases (Gandy et al., 2007).

Our objective for this study was to better understand the behavior of metals, colloids, and colloid-associated metals in the hyporheic zone of a stream affected by acid mine drainage. We expected that the speciation of metals and the transport of colloids would be affected by

geochemical gradients in the hyporheic zone. To address this objective, we installed a set of piezometers in the streambed of a low-order subalpine stream affected by acid mine drainage and sampled the stream water, the hyporheic pore waters, and the hyporheic zone sediments for metals and colloids. We performed tracer dilution tests during high flow and low flow to assess the effect of seasonal changes in flow on metal and colloid transport.

METHODS

Field Site

Field investigations into the role of hyporheic exchange on the removal of metals and colloids were conducted in Left Hand Creek along the reach where acid mine drainage from the Big Five Tunnel enters the stream (Figure 2.1). Left Hand Creek is a low-order alpine stream that originates in glacial and snow-melt waters at an elevation of approximately 4,200 m near the continental divide in northwestern Boulder County. The creek flows through the Ward Mining District, which produced gold and silver from veins that contained pyrite, galena, and chalcopyrite from 1858 to 1993 (Cobb, 1988; Davis and Streufert, 1990; USEPA, 2003). The legacy of this mining is significant metal contamination, with lead, copper, and zinc being the most abundant metals in the mine water.

The flow rate in Left Hand Creek in the vicinity of the site ranges from about 0.015 $m^3 s^{-1}$ at low flow to 0.15 $m^3 s^{-1}$ at high flow during the spring snow-melt (Wood, 2004). Flow in Left Hand Creek is regulated by releases from the Left Hand Park Reservoir, which is located 5.5 km upstream of the study site. The study reach is characterized by a step-pool configuration with an average slope of 7% (Figure 2.1).

Field Piezometer Installation

Piezometers bundles were installed in October 2007 to sample pore waters and measure hydraulic head in the hyporheic zone. The piezometers were made of polyethylene tubing (0.32 cm inside diameter, 0.64 cm outside diameter) with perforated tips (2.5 cm length, 0.1 cm diameter holes) covered by nylon mesh (0.5 mm) attached with duct tape, a design adapted from Wanty and Winter (2000). Piezometers of nine different lengths were bundled together and installed in the streambed at depths ranging from 5 cm to 100 cm (Figure 2.1). The bundles were installed by driving a steel pipe (5.1 cm diameter) filled with a steel rod into the streambed with a 27 kg electric hammer, removing the rod, inserting the piezometer bundle into the pipe, and withdrawing the pipe with a winch hoist and tripod while the piezometer bundle position was maintained. The target depth was 100 cm, but boulders limited the depth of driving to 60-95 cm in all but one sample location. The piezometer bundles were installed at six locations in the stream: one upstream of the acid mine drainage, one at the inflow of the acid mine drainage, and four downstream of the acid mine drainage (Figure 2.1). The piezometer bundles were placed as near as possible to the thalweg of the stream if not prevented by boulders. Four of the piezometer bundles were located in pools at distances of -21 m, 16 m, 23 m, and 77 m relative to the acid mine drainage inflow at 0 m. The remaining two piezometer bundles at distances of 0 m and 42 m were located in riffles.

Prior to sampling, the piezometers were developed to obtain good flow by using a syringe to withdraw water (60 mL) three times at intervals of approximately 5 d. From most piezometer tubes, water was freely withdrawn from the hyporheic zone. For those from which water was not freely withdrawn, 600 mL of stream water was injected into the piezometers several times until

water was freely withdrawn. After development, the piezometer bundles were left in place for six months before collecting samples for this study.

Surface and Hyporheic Zone Water Collection

Samples for cation and anion analyses were collected once in the spring at high flow (June 4, 2008) and once at fall low flow (October 20, 2008). Dissolved oxygen, pH, electrical conductivity, and head gradient were measured at least once at high flow and once at low flow at all of the piezometer bundle locations. Three piezometer bundle locations (0 m, 23 m, and 77 m) were sampled five times on an almost monthly basis from high flow to low flow. Hydraulic conductivity was measured once in September 2008.

Water samples were collected in bottles (high-density polyethylene, 30 mL) that were washed in acid (10% nitric acid), rinsed three times with ultrapure water, and rinsed three times with stream water. Samples of hyporheic zone water were collected from the piezometers by withdrawing water with a syringe (polypropylene, 30 mL) at a rate of about 15 mL min^{-1} after purging about 1.5 volumes of water standing in the piezometers. The pore volume of each piezometer was calculated based on the length of the tubing below the water line. The depth of the stream was measured to the nearest centimeter prior to drawing water and used to estimate the volume of water standing in the tube. Purging and sample volumes were kept small to avoid cross-sampling between piezometers at nearby depths. A new syringe was used to take a sample from each piezometer with the only cleaning procedure being rinsing the syringe with the purged water. Surface water samples were also collected with syringes rinsed with stream water. Surface and hyporheic zone water samples were transferred to three bottles (high-density polyethylene, 30 mL) for analysis of (1) total cation concentrations, (2) dissolved cation concentrations, and (3) total anion concentrations. Samples collected for the dissolved cation

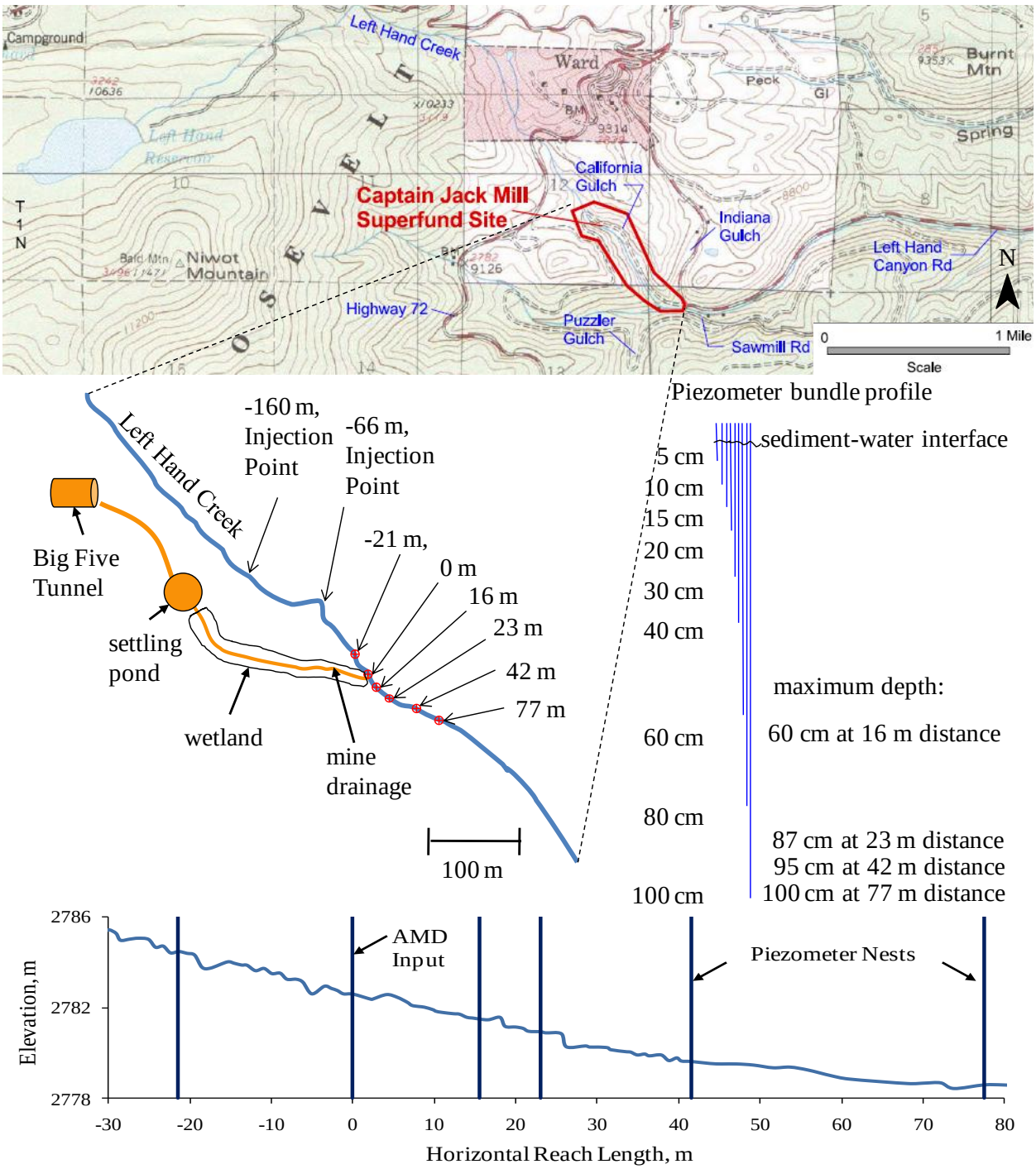

Figure 2.1. Topographic map (USGS 1:24,000; UTM zone 13, NAD 27) of study region along with sketch of field site including major features, sampling locations, piezometer bundle depths, and streambed profile with piezometer locations. The acid mine drainage enters the stream at 0 m. Upstream sites are referred to as negative distances and downstream sites are referred to as positive distances from the acid mine drainage. Due to the presence of large boulders in the streambed, some piezometers could not be installed to the intended 100 cm depth – for these, the maximum piezometer depth achieved is noted.

analysis were filtered through 0.1 µm polycarbonate membranes (Whatman Nuclepore). Samples for total and dissolved cation analysis were acidified to pH less than 2 with trace metal-grade nitric acid. The colloidal fraction was considered to be the difference between the total and dissolved cation concentration.

Dissolved oxygen, pH, and electrical conductivity were measured immediately after collection of samples. Dissolved oxygen was measured with a high-range (0-15.0 mg L^{-1}) dissolved oxygen method and colorimeter (Hach DR/890). Dissolved oxygen saturation was calculated based on the temperature when the sample was collected. To allow for comparison over time, the dissolved oxygen was presented as a percentage of saturation. Measurements were not duplicated because of the small sample volumes. Electrical conductivity was measured with a conductivity meter and electrode (Thermo Orion, model 105 meter; model 011050 electrode, 1.0-cm cell constant) and pH was measured with a pH meter and a combination electrode (Thermo Orion, model 250A+ meter; model 9107BN electrode).

Hydraulic head differences between the surface water and piezometers were measured using a manometer as described by Lee and Cherry (1978). The change in the water levels in the manometer indicated the difference in pressure between the surface and the subsurface water at the depth that the piezometer was installed. The head difference between the stream water and each piezometer was measured and then divided by the depth of the piezometer into the streambed to obtain the average head gradient over that depth. Care was taken to ensure that no air bubbles were introduced during the measurement.

Hydraulic conductivity was estimated using a falling head test (Lee and Cherry, 1978). A graduate burette (1 cm diameter) was attached to a piezometer and filled. The time for the water to fall a set distance was measured. The falling head test was performed three times for each

piezomete. These values were used to calculate an average hydraulic conductivity using the Hvorslev (1951) method.

Sediment Collection

Sediments from the streambed were collected using a modified freeze-core technique (Cahoon et al., 1996; Hill, 1999). The sediment samples were collected by driving a capped steel pipe into the ground with a 27 kg electric hammer to depths of 40-100 cm, filling the pipe with liquid nitrogen to freeze the surrounding sediment, and withdrawing the pipe and frozen sediment with a winch hoist and tripod. The sediment sample was divided into subsamples by thawing the sediment sample over a tray segmented for depth intervals of 2 cm over the first 10 cm, 5 cm over the second 10 cm, 10 cm over the next 40 cm, and 20 cm over the last 40 cm (total depth of 100 cm). As the sediment sample began to thaw, sediment was chipped into tray bins corresponding to the depth the sediment sample. Sediment samples were collected within 2 m of each of the piezometer bundles. Retrieval of sediments beyond a depth of 40 cm occurred in only two of the sampling locations due to the rocky nature of the streambed. The upper 2 cm at the 0 m distance and the upper 10 cm at the 16 m distance were lost upon removal from the stream, perhaps due to uneven or incomplete freezing along the pipe.

Laboratory Analysis

The stream and hyporheic water samples were analyzed for major cations and metals (Na, Mg, K, Ca, Al, Mn, Fe, Cu, Zn, Pb) by inductively coupled plasma-mass spectrometry (ICP-MS; Varian 810MS) and for anions (Cl^-, SO_4^{2-}, and Br^-) by ion chromatography (IC; Dionex DX-500). Detection limits for each element are given in Table 2.1. Iron, which normally does not give consistent results on the ICP-MS, was checked by running 1 in 15 samples by inductively coupled plasma-atomic emission spectrometry (ICP-AES; ARL 3410+). The iron concentration

measurements by ICP-MS and ICP-AES were similar in selected samples. Measurements of samples with iron concentrations less than 0.9 μM appeared to be more reliable on the ICP-MS than on the ICP-AES, which has an iron detection limit of about 0.2 μM.

Table 2.1. Detection limits for elements measured by ICP-MS (cations and metals) and IC (anions).

element	detection limit (μM)	element	detection limit (μM)
Na	0.016	Cu	0.0027
Mg	0.038	Zn	0.012
K	0.13	Pb	0.00039
Ca	0.18	Cl^-	0.56
Al	0.0080	SO_4^{2-}	0.42
Mn	0.0047	Br^-	0.63
Fe	0.039		

The size and elemental composition of suspended sediment collected on the filters was characterized by scanning electron microscopy/energy dispersive x-ray (SEM-EDX) analysis using both low vacuum (LVSEM; JEOL JSM-6480LV, 15 kV accelerating voltage) and field emission (FESEM; JEOL JSM-7401F; 4 kV accelerating voltage) SEMs. The air-dried filters were cut and taped to aluminum mounts with double-sided carbon tape (Nisshin EM Co., NEM Tape) and sputter-coated for 30-40 s to deposit as 2.6-4.8 nm layer of gold and palladium (Denton Vacuum, Inc. Desk II Cold Sputter/Etch Unit; 50 millitorr, 40 milliamp). Colloids were also analyzed for size and zeta potential using dynamic light scattering (DLS) and laser Doppler microelectrophoresis in acid mine drainage and stream water samples at 21°C (Particle Sizing Systems; 380 ZLS). Samples for DLS and zeta potential were analyzed five times and the results averaged. Zeta potential values are based on measurements of electrophoretic mobilities which were converted to zeta potentials using the Smoluchowski equation.

Material in the water was analyzed by x-ray diffraction (XRD; D5000 Siemens) to identify mineral structure. A 5 L water sample was collected at high flow 16 m downstream of

the acid mine drainage. Approximately 2.1 L was filtered through 0.1 μm Supor filters by vacuum filtration. The filters were allowed to leach in deionized water for 24 hours and then the submerged filters were sonicated for 1 minute to release any remaining material on the filters. The colloids were then transferred to a silicon wafer and dried on a hot plate. The sample was analyzed between 5 and 65° 2θ at 0.02° steps with a 5 s count per step using Cu K_α radiation. The diffraction patterns were analyzed with Jade 5 (Materials Data Inc.) software.

Sequential extractions were conducted on the streambed sediment cores to assess the association of metals with the sediments as a function of depth. The sediment samples were dried (20ºC, 24 h) and sieved to exclude the >2.0 mm fraction (No. 10 mesh, stainless steel). A 0.2 g portion of each sediment sample was treated with the following extractions (Ranville et al., 2004): (1) 0.25 M hydroxylamine hydrochloride/0.25 M hydrochloric acid solution for 30 min in a 50˚C water bath (amorphous ferric and manganese oxides), (2) 4 M hydrochloric acid for 30 min in a 94˚C water bath (crystalline ferric and manganese oxides), and (3) 12 M hydrochloric/0.5 M sodium chlorate acid solution for 45 min at room temperature; 4 M nitric acid for 40 min in a 100˚C water bath (sulfides). The extractions were carried out in centrifuge tubes (polypropylene, 15 mL) with 10 mL of each solution. Following each extraction, the sediment samples were centrifuged (Beckman GS-6) at 5,200 *g* for 30 min. The extraction solutions were decanted and stored for metal analysis. In preparation for the following extraction, the residual sediment was rinsed with high-purity water (greater than 18 MΩ cm^{-1} resistivity) and centrifuged at 5,200 *g* for 30 min, after which the water was decanted and the remainder was evaporated before the next extraction. The concentrations of metals (Al, Cu, Fe, Mn, Pb, Zn) in the decanted solutions were determined by ICP-AES.

The sediment samples were examined by SEM-EDX to determine the morphology and composition of the sediment grains and coatings. Approximately 1 g of the sieved sediment from each subsample of the cores taken from 16 m and 77 m were cast in epoxy to produce a polished mount for individual grain and coating examination. These mounts allowed for the examination of a cross section of the grains and associated coatings by LVSEM (15 kV accelerating voltage). The use of EDX line scans allow for identification of elemental composition at many points along a chosen line on a sample surface. Line scans were run on grains starting at the inside of the grain and going past the edge to identify differences in composition between the underlying grain and any surface coatings for each mount.

Tracer Dilution Tests

To determine seasonal differences in stream flow and the connection between the stream and hyporheic zone, injections of a conservative tracer (bromide, added as sodium bromide) were carried out during high flow (June 10, 2008) and low flow (October 18, 2008) conditions. For both injections, a polyethylene tank (378 L) was filled with stream water and sodium bromide was added to create the tracer solution. The tracer dilution test at high flow was conducted as an injection of 1.0 M NaBr introduced 66 m upstream of the acid mine drainage at a rate of 0.60 ± 0.01 L min^{-1} (1.0×10^{-5} m^3 s^{-1}) for 9.0 h (from 0900 to 1800 h). The low flow tracer dilution test was conducted as an injection of 0.9 M NaBr introduced 166 m above the acid mine drainage input at a rate of 0.60 ± 0.04 L min^{-1} (1.0×10^{-5} m^3 s^{-1}) for 9.0 h (from 0900 to 1800 h). During both injections, surface samples were collected at distances of 56 m upstream and 23 m and 77 m downstream of acid mine drainage. Subsurface samples were collected from the 5 cm, 40 cm, and 100 cm (or the deepest) piezometer depths. Samples were collected periodically throughout the injection until one hour after the end of the injection. A single

sample was collected the day after the injection, approximately 25 h after the start of the injections.

Nominal travel times and the relative connectivity of the subsurface with the main channel were calculated for the each location and depth. Nominal travel time was calculated as

$$T_{travel} = T_{sub} - T_{surf} \quad (2.1)$$

where T_{sub} (h) is the time for the tracer concentration to reach half-plateau concentration in the subsurface water collected from a piezometer and T_{surf} (h) is the time for the tracer concentration to reach a plateau in the surface water. The relative connectivity (RC) is the proportion of stream water present in a piezometer at equilibrium when a steady concentration was reached in the piezometer (Wondzell, 2006):

$$\text{RC (\%)} = 100 \times \frac{C_{sub} - C_{bg,sub}}{C_{surf} - C_{bg,surf}} \quad (2.2)$$

where C_{sub} is the steady concentration in the subsurface or the maximum concentration reached by the end of the experiment (approximately 25 h after the start of the injection) if no steady concentration was reached, $C_{bg,sub}$ is the background concentration in the subsurface, C_{surf} is the background-subtracted steady concentration in the surface water, and $C_{bg,surf}$ is the background concentration in the surface water.

Tracer Dilution Test Modeling

The surface concentrations from the tracer injections were modeled using OTIS (One-Dimensional Transport with Inflow and Storage; Runkel (1998)). The model allows for the estimation of four transport parameters using nonlinear regression techniques (OTIS-P): dispersion (D) [$m^2 s^{-1}$], stream cross-sectional area (A) [m^2], storage zone cross-sectional area (A_S) [m^2], and storage zone exchange coefficient (α) [s^{-1}]. The transient storage model includes

any bodies of stationary water, including eddies and side pools, compared with the fast moving waters of the main channel to be part of the transient storage zone. For the purposes of this study, the hyporheic zone is assumed to be equivalent to the model storage zone due to the lack of observed eddies or pools in the reach.

For each dataset, the model considered three reaches in order to constrain the flow. The first reach comprised the distance from the injection site to the acid mine drainage input (the high flow injection was located at -66 m and the low flow injection was located at -160 m). The second reach started at the acid mine drainage input (0 m) and ended at 16 m. The final reach spanned from 16 m to the most downstream sampling point at 77 m. One set of model parameters was used to describe transport in all three reaches based on the observations at 77 m.

The high flow data showed evidence of variation in flow after 13:00. Model complexity increases considerably in the case of unsteady flow because of the need for time-variable flow parameters. A flow-routing model must be used to provide time-varying lateral inflows, channel flow rates, and cross-sectional areas. Detailed flow data was not collected during the experiment, so application of the more complex model was not expected to yield more useful results. Therefore, the model simulation was run under the steady state assumption with the constant flow data collected prior to 13:00. The velocity of the stream during high flow (approximately 1.1 m s^{-1}) resulted in a travel time through all three reaches of about 2 min. The model was able to match the observed data by considering advection and dispersion only; transient storage was estimated to be negligible at high flow.

Several metrics are available for quantifying the importance of transient storage based on the model parameters (Runkel, 2002): (1) the relative size of the hyporheic zone (A_S/A), (2) the average storage zone residence time ($T_{Stor} = A_S/\alpha A$), the hydraulic retention factor (average time

water remains in storage relative to the hydraulic turnover length, $R_h = A_S/Q$), and (3) the fraction of median travel time due to transient storage (F_{med}):

$$F_{med} \cong (1-e^{-L(\alpha/u)}) \frac{A_S}{A+A_S} \tag{2.3}$$

where Q is the average flow in the reach, u is advective velocity (Q/A), and L is the reach length (m) was also determined. F_{med} was evaluated at the standard distance by setting L equal to 200 m (F_{med}^{200}) for comparison with other datasets. A Damkohler number for transient storage (DaI_α) was calculated as:

$$DaI_\alpha = \frac{\alpha\left(1+\frac{A}{A_S}\right)L}{u} \tag{2.4}$$

The Damkohler number gives the ratio of the time scale of transient storage to the time scale of advection through the reach.

Statistical Analysis

In order to determine the controls on metal speciation in the hyporheic zone, we analyzed the solute concentration and water chemistry data using principle component analysis (PCA) and parallel factor analysis (PFA). PCA and PFA are multivariate statistical techniques used to identify important components or factors that explain most of the variances in a system. Both analyses were implemented using R 2.9.2 (R Development Core Team, 2009). These tools were used to quantify the extent to which the measured parameters explain the variability in the subsurface data sets. PCA involves the transformation of a dataset into a set of values of uncorrelated variables called principle components. The principle components can be used to explore the relationships between different variables in the original dataset. PCA was performed on total, dissolved, and colloidal concentrations of Fe, Mn, Al, Pb, Cu, and Zn, dissolved

chloride, and physical and chemical parameters including head gradient, hydraulic conductivity, dissolved oxygen, pH, and electrical conductivity for high flow and low flow. Chloride was included in the analysis because it was transported conservatively as a dissolved ion and could act as a non-reactive tracer of hydrologic interactions between the stream and subsurface. This is the case for other ions such as bromide, but Cl^- was selected because background levels were well above the detection limit in the stream and subsurface. For PCA, the data were centered around zero by subtracting the mean and dividing by the standard deviation of each parameter. PFA was used with all of the colloidal metal concentrations, chloride, and the physical and chemical parameters listed above for high flow and low flow to determine the most important parameters.

RESULTS

Physicochemical Properties of Stream and Streambed

The majority of the hydraulic head gradients measured at both high and low flow conditions were negative, indicating downward flow of water in the streambed (Figure 2.2). The piezometer bundle at the input of the acid mine drainage showed positive head gradients from June to September. The largest variations in head gradient occur in the upper 20 cm of the streambed. Piezometers at distances of 16, 23, and 77 m downstream of the acid mine drainage had large positive gradients between 10 and 15 cm depth in June. The head gradients also change on a seasonal basis, becoming more negative from high flow to low flow. The seasonal variation of the head gradients was most notable at pools (-21 m, 16 m, 23 m, and 77 m), while the riffles (0 m, 42 m) had much more consistent head gradients throughout the sampling season. The hydraulic conductivity generally decreased with depth in the hyporheic zone (Figure 2.3). Some sites show a sharp increase between the 5 and 10 cm depths before the decline. The

hydraulic conductivity measurements (6×10^{-3} to 1.8×10^{-2} cm s^{-1}) were in the range of medium sand with a grain size between 0.25 and 0.50 mm.

The electrical conductivity gives an indication of the concentration of ions and is a surrogate for ionic strength. Ionic strength is an important control on colloidal stability and the extent of interaction between metals, colloids, and sediment surfaces. High ionic strength promotes colloid aggregation and deposition in the subsurface sediment of the hyporheic zone. Increasing ionic strength will also increase competition between the metals of interest and other cations for sorption sites on colloid or sediment surfaces and the thinner electrical double layer at the solid-water interface will limit interaction between metal ion and surface.

The conductivity profiles for locations downstream of the acid mine drainage were fairly stable throughout the season from high flow to low flow, with either a nearly constant value with depth or an increase occurring between 20 and 40 cm (Figure 2.4). At 21 m upstream of the acid mine drainage input, the conductivity was essentially constant with depth from the surface down to the deepest piezometer at 80 cm and the highest values occurred during high flow. At the acid mine drainage input (0 m), the conductivity in the hyporheic water was close to that of the acid mine drainage from 5 to 60 cm depths.

The pH of stream and hyporheic zone waters is an indication of the effects of acid mine drainage. The pH plays an important role in metal solubility and adsorption and colloid mobility. The pH varied over a range of 5.6 to 7.0 at all locations except the acid mine drainage, for which the pH ranged from 3.6 to 4.5 (Figure 2.5). The pH values were almost constant with depth from the surface to the deepest depths measured at the site 21 m upstream of the acid mine drainage. At the acid mine drainage site (0 m), the subsurface waters have pH values similar to the acid mine drainage from 5 cm to 60 cm deep. Profiles at distances 16 and 42 m, which were

only sampled in May and October, showed sharp decreases in pH from the surface to the subsurface in May, while in October, the pH was similar in the surface and shallow subsurface before decreasing beyond 10-20 cm depths. The May profiles also showed a sharp decrease in pH from the surface to the 5 cm depth at all but the upstream location. Of the locations with monthly measurements, the pH was generally lower the subsurface than the surface water and remained fairly constant with depth at 23 m, while the 77 m location showed large seasonal variations in the upper 40 cm and a marked decline in pH from the 40 to 60 cm depths.

Dissolved oxygen is an indicator of the redox conditions of the hyporheic zone. The dissolved oxygen concentration generally decreased from saturation in the surface water to less than 40% of saturation in the subsurface (Figure 2.6). Dissolved oxygen saturation was approximated based on the measured water temperature and an estimate for the barometric pressure based on altitude according to standard methods (American Public Health Association, 2005). The most marked declines occur at distances of 0, 16, and 77 m. The percent of saturation for nearly every location occur in May, whose profiles also tend to show the widest range in dissolved oxygen saturation. Dissolved oxygen solubility increases with decreasing temperature and a lack of biotic uptake shortly after the winter thaw may explain the higher degrees of saturation that occur.

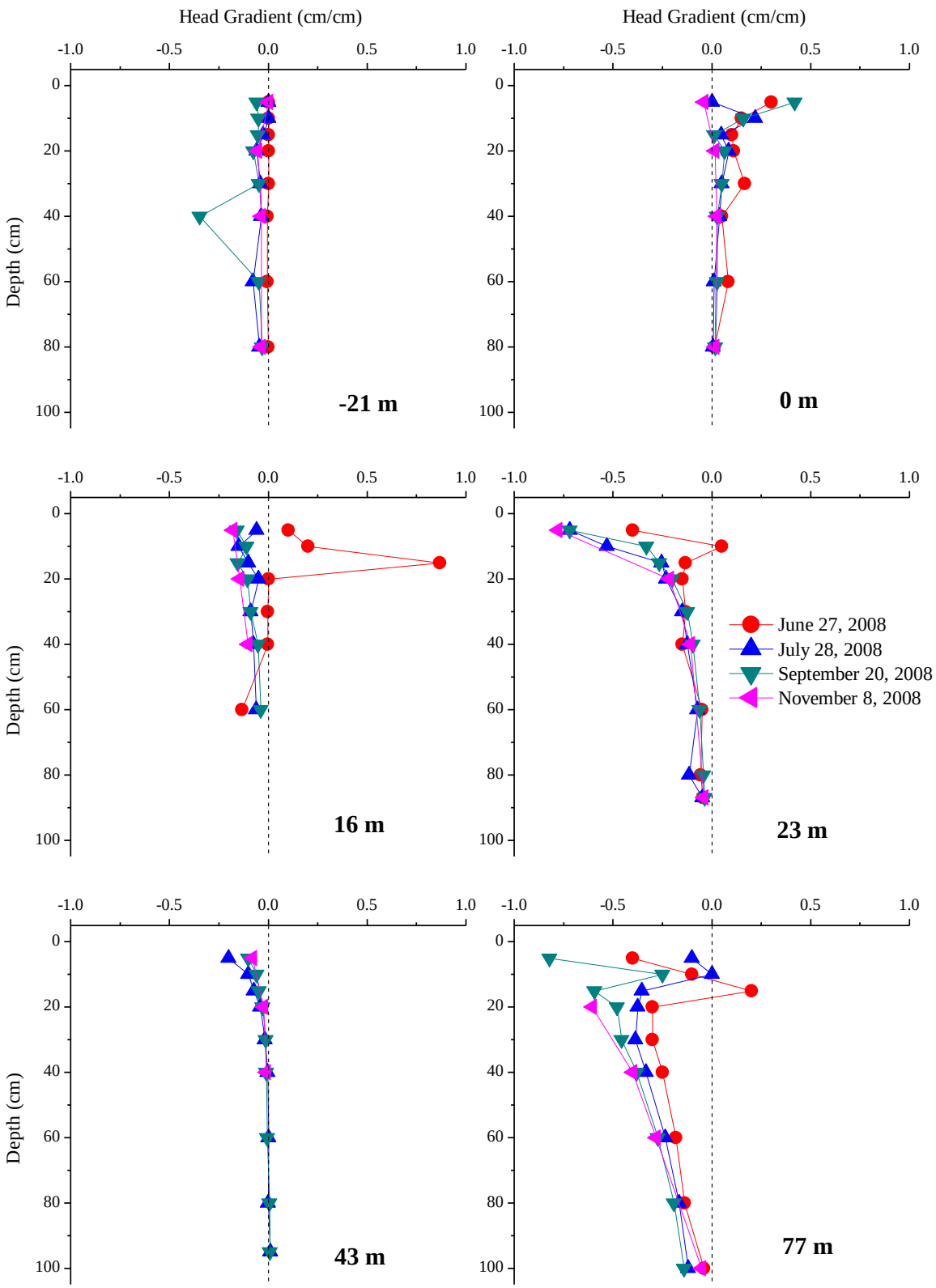

Figure 2.2. Seasonal variations in head gradient profiles measured in piezometers located at -21 m, 0 m, 16 m, 23 m, 42 m, and 77 m. Negative values indicate downward flow.

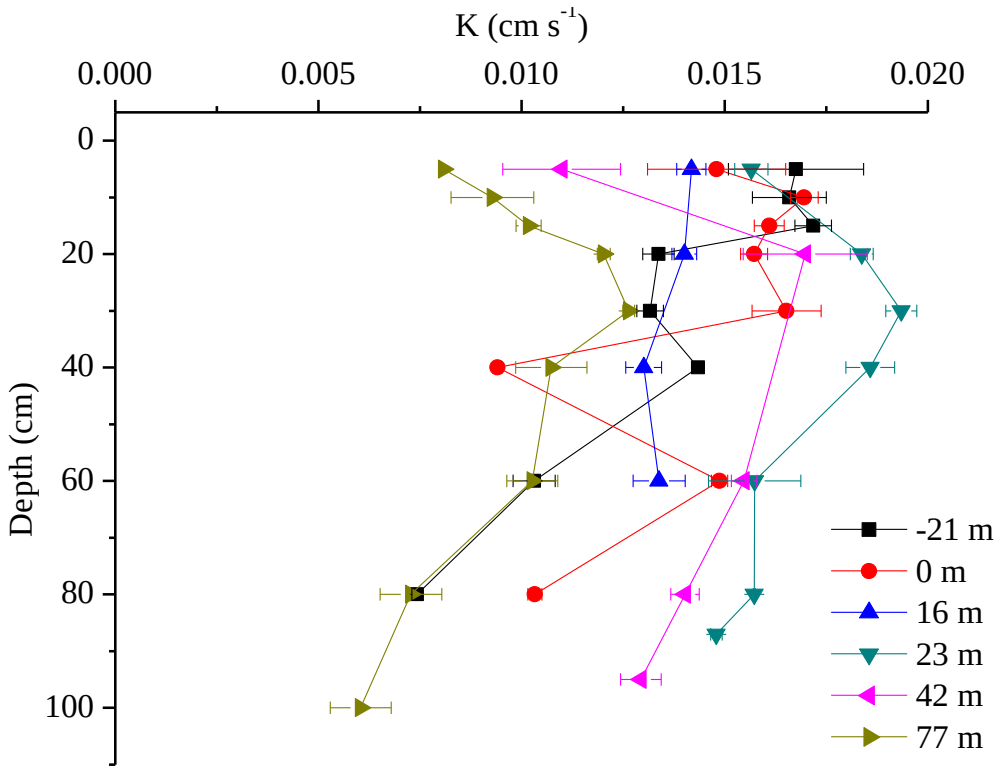

Figure 2.3. Hydraulic conductivity (K) profiles measured at each piezometer site along the study reach. Error bars represent one standard deviation based on three measurements with the exception of the 5 cm depth at the 77 m distance, which was only measured once.

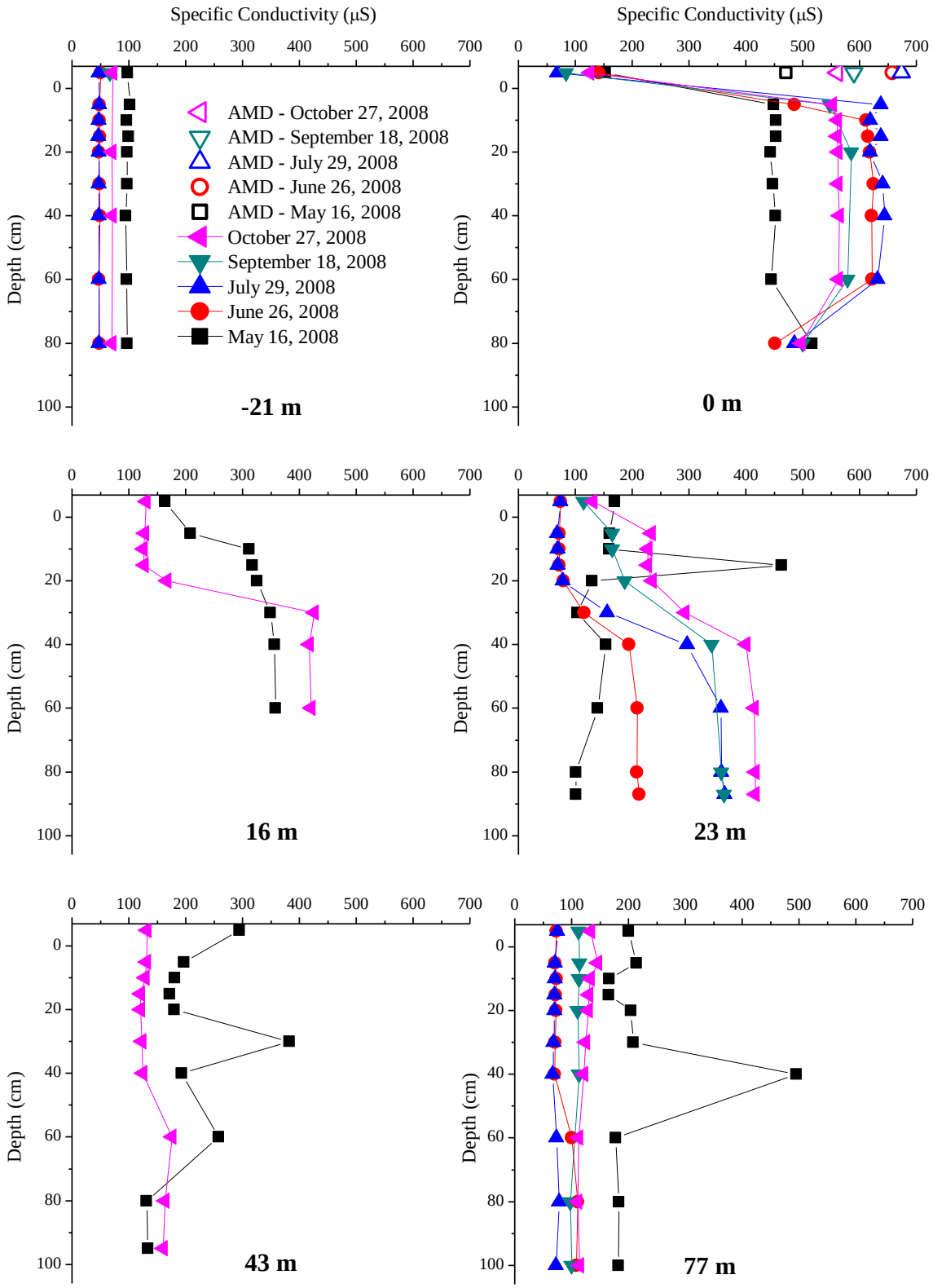

Figure 2.4. Seasonal variations in conductivity profiles measured in piezometers located at -21 m, 0 m, 16 m, 23 m, 43 m, and 77 m. Values displayed 5 cm above the stream-sediment interface represent surface water measurements.

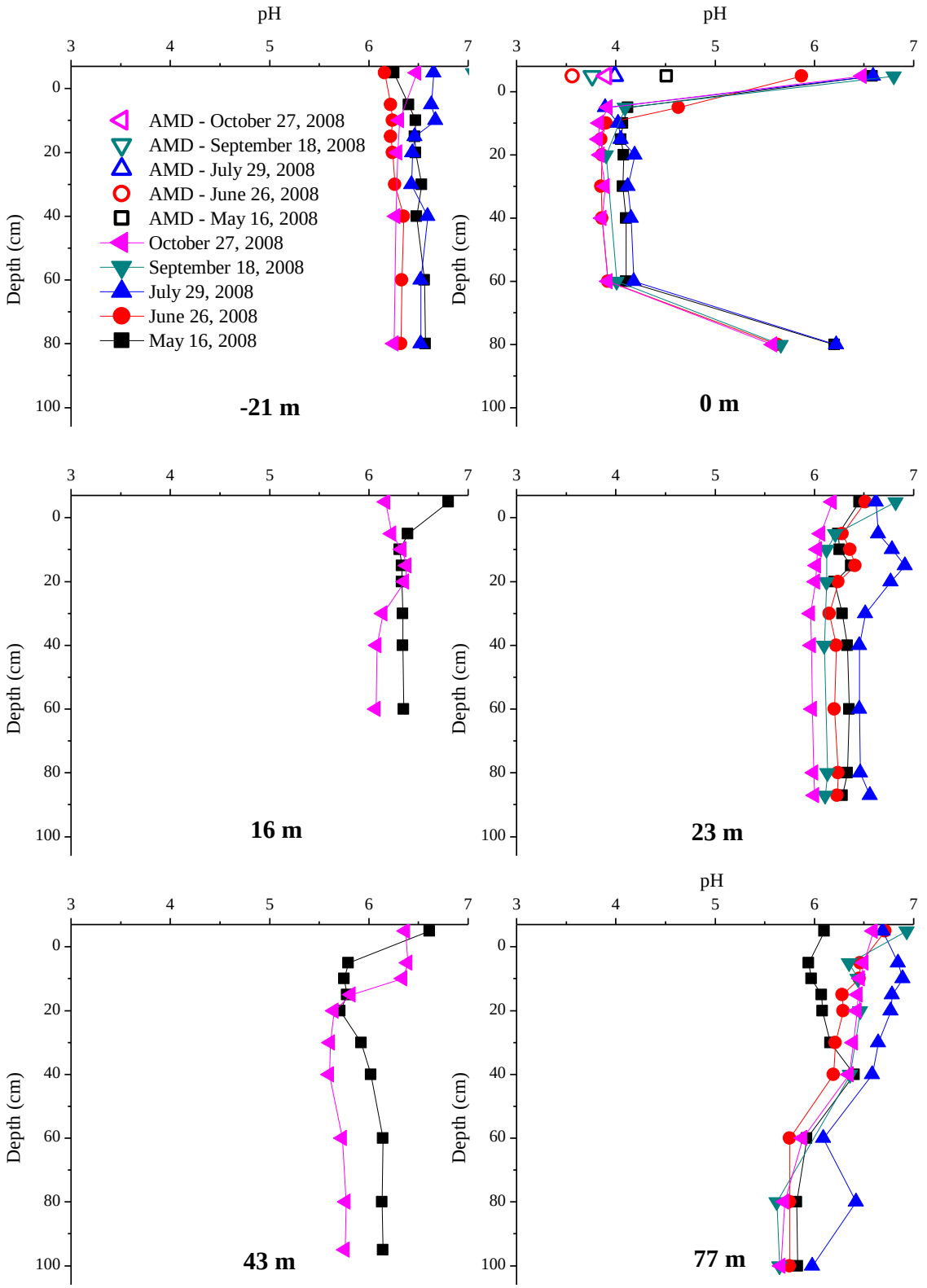

Figure 2.5. Seasonal variations in pH profiles measured in piezometers located at -21 m, 0 m, 16 m, 23 m, 43 m, and 77 m. Values 5 cm above the stream-sediment interface represent surface water measurements.

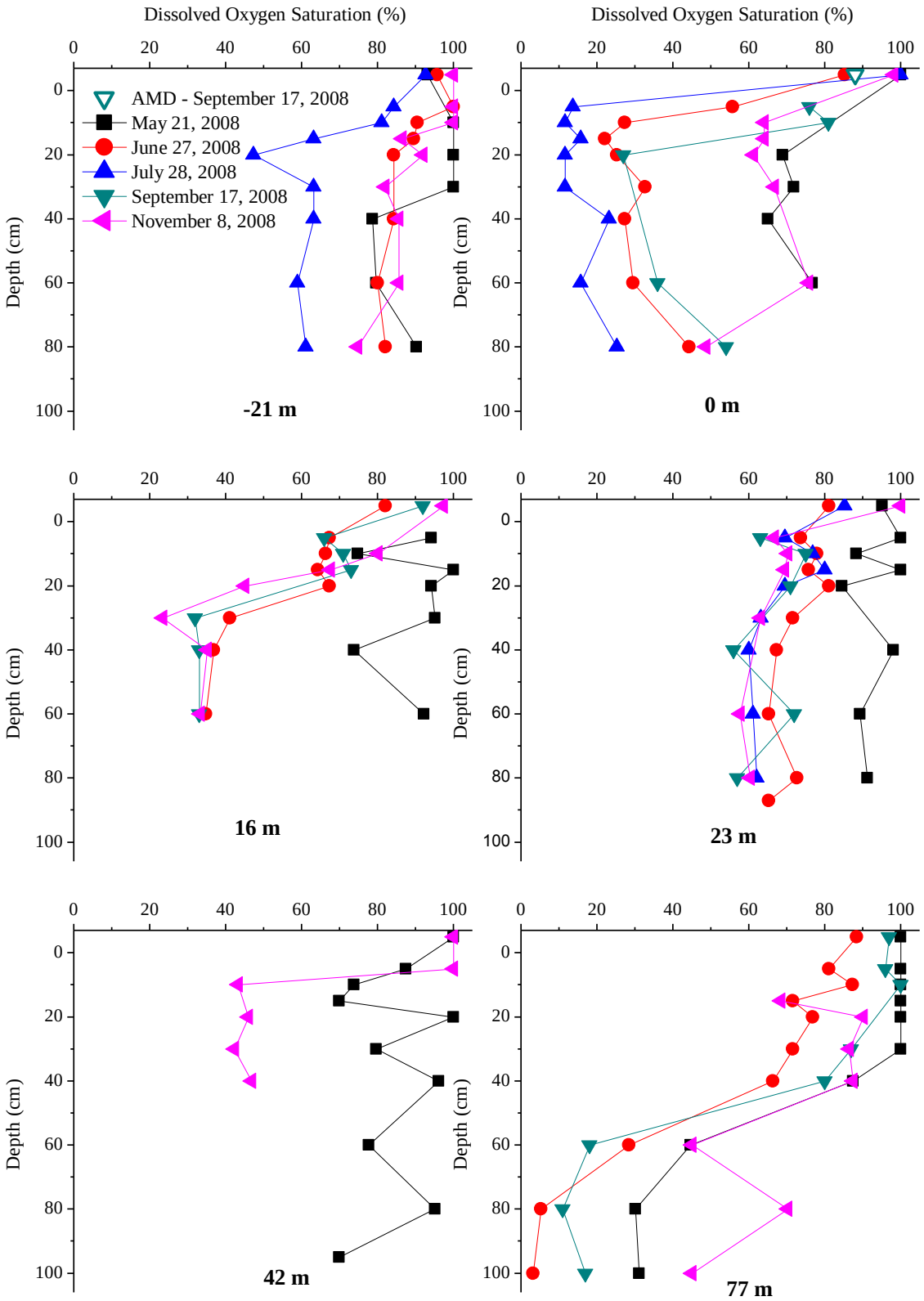

Figure 2.6. Seasonal variations in dissolved oxygen profiles measured in piezometers located at -21 m, 0 m, 16 m, 23 m, 43 m, and 77 m. Values 5 cm above the stream-sediment interface represent surface water measurements.

Tracer Dilution Tests

The tracer injections were conducted at high flow and low flow to evaluate differences in hyporheic exchange resulting from the differences in flow. For the high flow injection, the flow was 0.14 ± 0.01 $m^3 s^{-1}$ at 56 m upstream of the acid mine drainage. At 16 m downstream of the acid mine drainage, the flow was 0.18 ± 0.01 $m^3 s^{-1}$. For the low flow injection, the stream flow was 0.019 $m^3 s^{-1}$ ± 0.001 $m^3 s^{-1}$ at 56 m upstream of the acid mine drainage and 0.020 ± 0.001 $m^3 s^{-1}$ at 16 m downstream of the acid mine drainage. The uncertainties given for flows are based on one standard deviation of the steady state flow as determined based on the tracer injection. The increase in the flow between the -56 m and 16 m distances is attributed to the acid mine drainage input, which added about 23% to the stream flow at high flow and about 9% to the stream flow at low flow.

The results for the breakthrough of the conservative tracer (bromide) in the stream and hyporheic zone were normalized for comparison by dividing the bromide concentrations at 16 m and 77 m by the maximum concentration from the breakthrough at 56 m upstream of the acid mine drainage (Figure 2.7). At high flow, the concentration of bromide dropped off at approximately 15:00 hours due to an apparent increase in flow. The creek is fed by a reservoir, so a release causing this type of flow increase is not unusual. The background concentration of bromide prior to injection was below the detection limit, 0.63 µM, during both the high flow injection (0.84% of the plateau concentration at -56 m) and the low flow injection (0.08% of the plateau concentration at -56 m).

Nominal travel time in the hyporheic zone and connectivity at each piezometer location and depth was determined for those piezometers whose bromide concentration reached a steady concentration over the course of the experiment (Table 2.2). For those piezometers that did not

reach a steady plateau, the maximum connectivity is given. All the hyporheic zone locations show the highest breakthrough for piezometers at the 5 cm depth, with most reaching 90% of the surface concentration (Figure 2.8). A few locations showed evidence of longer flowpaths. At distances of 42 m and 77 m, elevated bromide concentrations were observed at 100 cm depths approximately 25 h after the start of the injection. Similar connectivities at high flow and low flow indicate that hyporheic zone size and exchange rate were relatively constant.

Table 2.2. Nominal travel time and connectivity of the subsurface with the stream in piezometers during high flow and low flow tracer dilution tests.

	travel time in hyporheic zone (h)						connectivity (%)					
piezometer	high flow			low flow			high flow			low flow		
distance/depth	5 cm	40 cm	100 cm	5 cm	40 cm	100 cm	5 cm	40 cm	100 cm	5 cm	40 cm	100 cm
-21 m	0.1	0.6	0.9	0.6	0.9	2	88	78	77	99	95	91
0 m	0.4	NI[a]	--	NI	NI	NI	69	0	--	0	0	0
16 m	0.6	3.5	--	0.9	1.9	--	90	10	--	93	5	--
23 m	0.9	4.2	NI	2.9	4.5	NI	97	1	0	58	1	0
42 m	1.7	8.9	>13	0.9	>13	>13	47	5[b]	1[b]	87	4[b]	2[b]
77 m	0.3	2.1	>13	0.7	3.3	>13	99	97	4[b]	93	86	6[b]

[a] NI: no increase in concentration during the experiment.
[b] piezometers did not reach a steady state in bromide concentration during the experiment; the maximum connectivity measured during the experiment was given.

For the high flow injection, the model fits for the dispersion and stream cross-sectional area were very uncertain as indicated by their coefficients of variance (Table 2.3). The high flow experiment did not show evidence of transient storage and no storage parameters were estimated. At low flow, the coefficient of variance indicates uncertainty in the model estimate of the subsurface exchange rate coefficient. The metrics obtained from the model parameters indicate minimal transient storage in the low flow injection. The relative size of the hyporheic zone

(A_s/A) was 0.03 and the fraction of median travel time due to transient storage evaluated at 200 m (F_{med}^{200}) was 0.1%, which indicates minor stream water exchange with the subsurface. The hydraulic turnover length (L_s), which is the average distance water travels downstream within the main channel prior to entering the storage zone, was 5.1 km. The average storage zone residence time was 0.4 h and the hydraulic retention factor was 0.3 s m^{-1}. The Damkohler number with respect to transient storage, DaI_α, was 0.4, which indicates that the time scale of exchange was slow compared with advection in the reach.

Table 2.3. Stream flow characteristics and solute transport parameters are given from the OTIS model for tracer dilution tests at high flow and low flow tracer. The coefficient of variance is given in parenthesis. For the high flow experiment the model was fit without transient storage – no values are given for A_S and α.

parameter	high flow	low flow
Q ($m^3 s^{-1}$)	0.19	0.021
v ($m s^{-1}$)	1.1	0.12
D ($m^2 s^{-1}$)	12 (81)	0.27 (0.10)
A (m^2)	0.17 (52)	0.18 (0.010)
A_S (m^2)	--	0.0058 (0.48)
α (s^{-1})	--	2.3×10^{-5} (1.1)
RSS	0.089	6.3

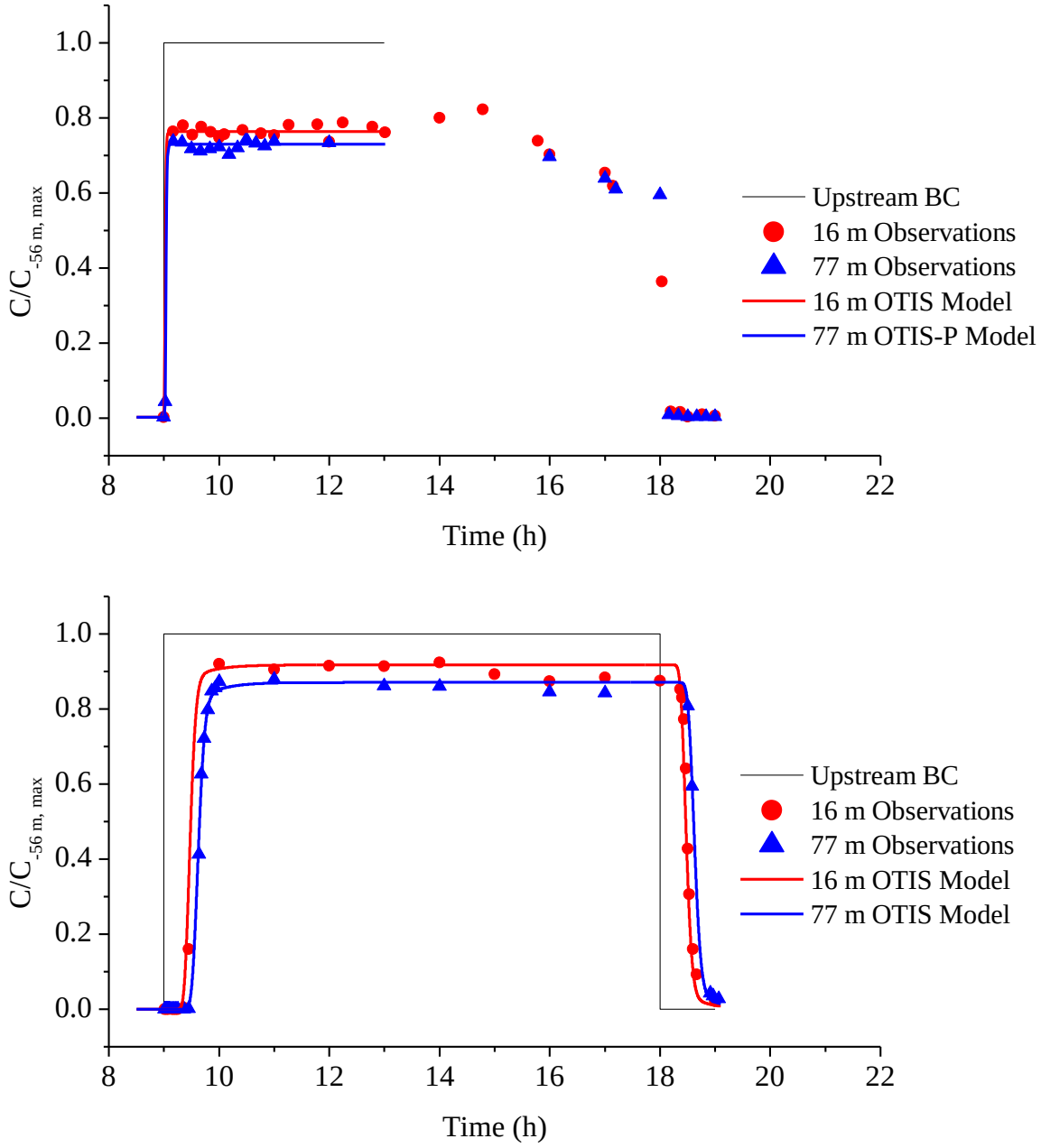

Figure 2.7. Surface bromide tracer measurements and models for high flow (top) and low flow (bottom) at locations 16 and 77 m downstream of the acid mine drainage. In both cases, the injection began at 09:00 and ended at 18:00 and the observations at -56 m were used to define the upstream boundary conditions in the models.

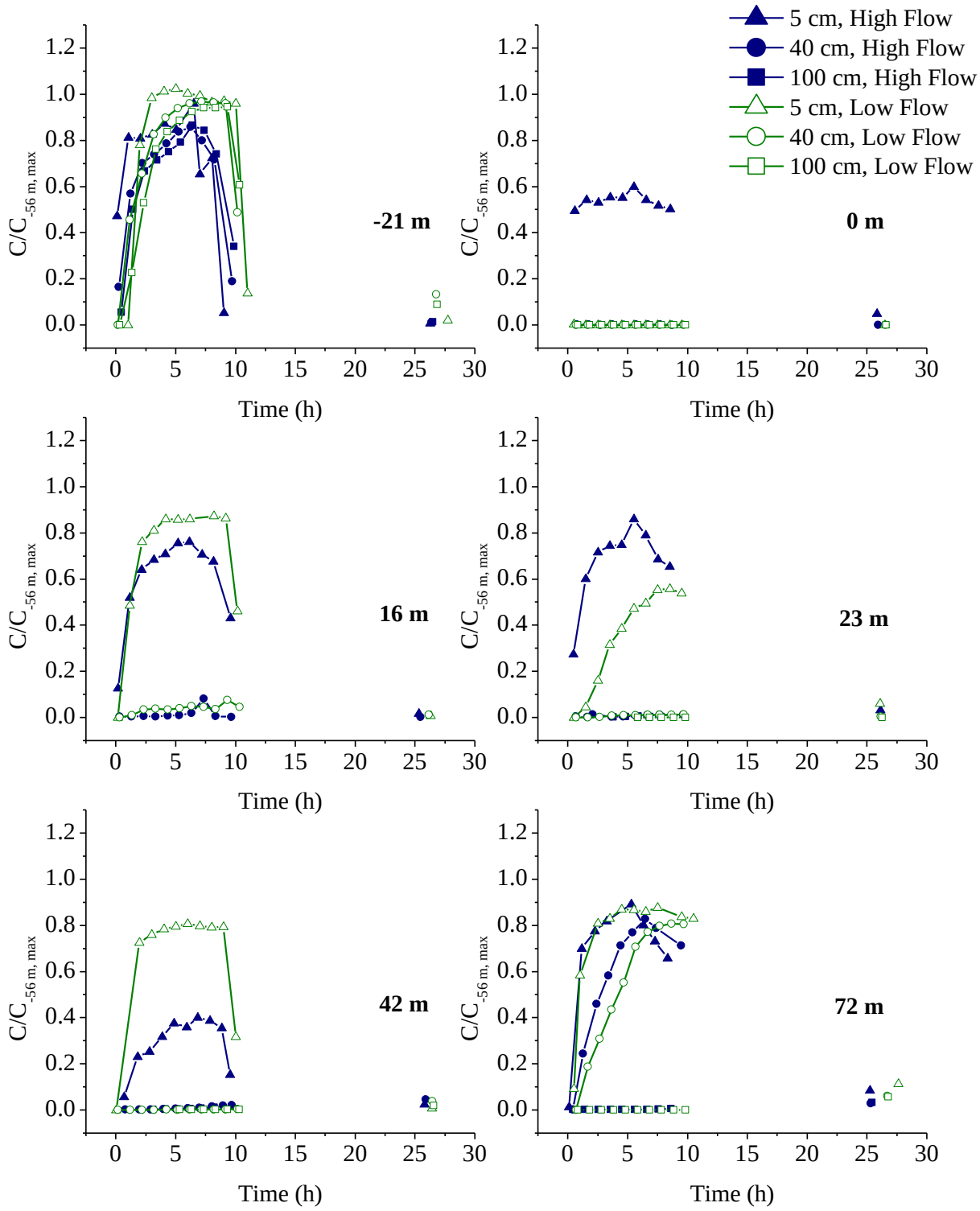

Figure 2.8. Subsurface bromide tracer concentration for hyporheic zone waters normalized to the plateau bromide concentration measured in the stream.

Metals

Metals were measured in samples collected from the surface water and at all piezometers during high flow and low flow. Surface concentrations were normalized to account for possible incomplete mixing at the AMD input by dividing by sodium, which we considered to be a relatively conservative solute, sodium (Figure 2.9). These data were collected as background samples, not during a tracer injection. For example, the normalized iron concentration is

$$[Fe]_{normalized} = [Fe]/[Na^{+}]$$

These normalized concentrations along the stream reach show that metal concentrations decrease rapidly with distance downstream from the acid mine drainage source. Dissolved and colloidal metal concentrations for iron, aluminum, manganese, zinc, copper, and lead are presented for each stream location and time corresponding to high- and low flow conditions. Results for the acid mine drainage are incorporated into the data for the stream at the input of the acid mine drainage.

Subsurface profiles for iron, manganese, and aluminum show similar trends for all locations along the reach (Figures 2.10, 2.11, 2.12). Peaks in concentration tended to occur at the same depths for all three metals. The upstream site showed an increase in metal concentration to a peak at 20 cm depth only for the low flow sampling event, which indicates another source of metal input – probably seepage of acid mine drainage from the wetlands near Left Hand Creek. Iron at the input of the acid mine drainage was largely colloidal, while manganese and aluminum were mostly dissolved. All locations downstream showed mainly colloidal iron, manganese, and aluminum.

Upstream of the acid mine drainage input (Figure 2.13, -21 m), concentrations of zinc, copper, and lead were low relative to downstream of the acid mine input, except for lead during

the low flow sampling. Lead concentrations at the upstream site had a peak concentration of 0.30 µM compared with a maximum of 0.21 µM at the acid mine drainage input site. Lead and copper were predominantly in the colloidal phase. At the acid mine drainage input (0 m transport distance), zinc, copper and lead concentrations were elevated and largely dissolved in the subsurface.

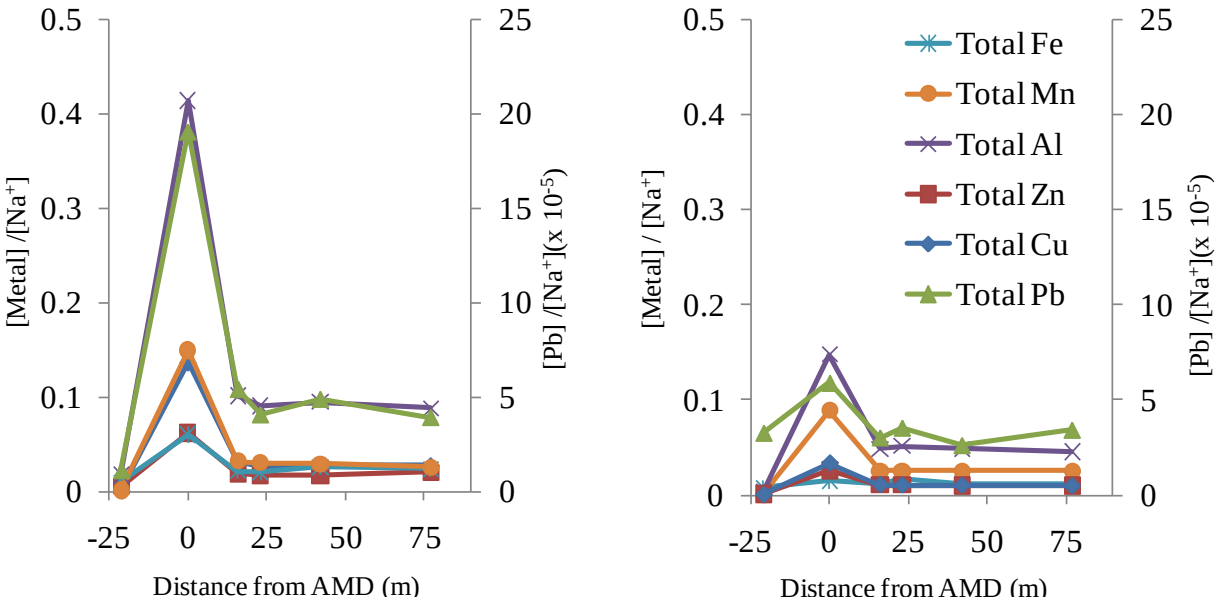

Figure 2.9. Normalized surface metal concentrations with distance downstream from the AMD input for high flow conditions (A) and low flow conditions (B). Metal concentrations are normalized to account for possible incomplete mixing at the AMD input by dividing by a conservative solute, sodium.

Downstream of the acid mine drainage, a range from essentially zero to nearly one hundred percent of lead and copper were associated with colloids (Figures 2.14 and 2.15). The median colloidal percentage of lead are 65% at high flow and 66% at low flow and for copper, 26% at high flow and 46% at low flow. Zinc is mostly in the dissolved phase, with a maximum colloidal fraction of 32%. The highest concentrations of lead, copper, and zinc were typically

located in the upper 30 cm of the subsurface, with the exception of the high concentrations of lead and zinc at the 77 m transport distance at the deepest depths in the hyporheic zone.

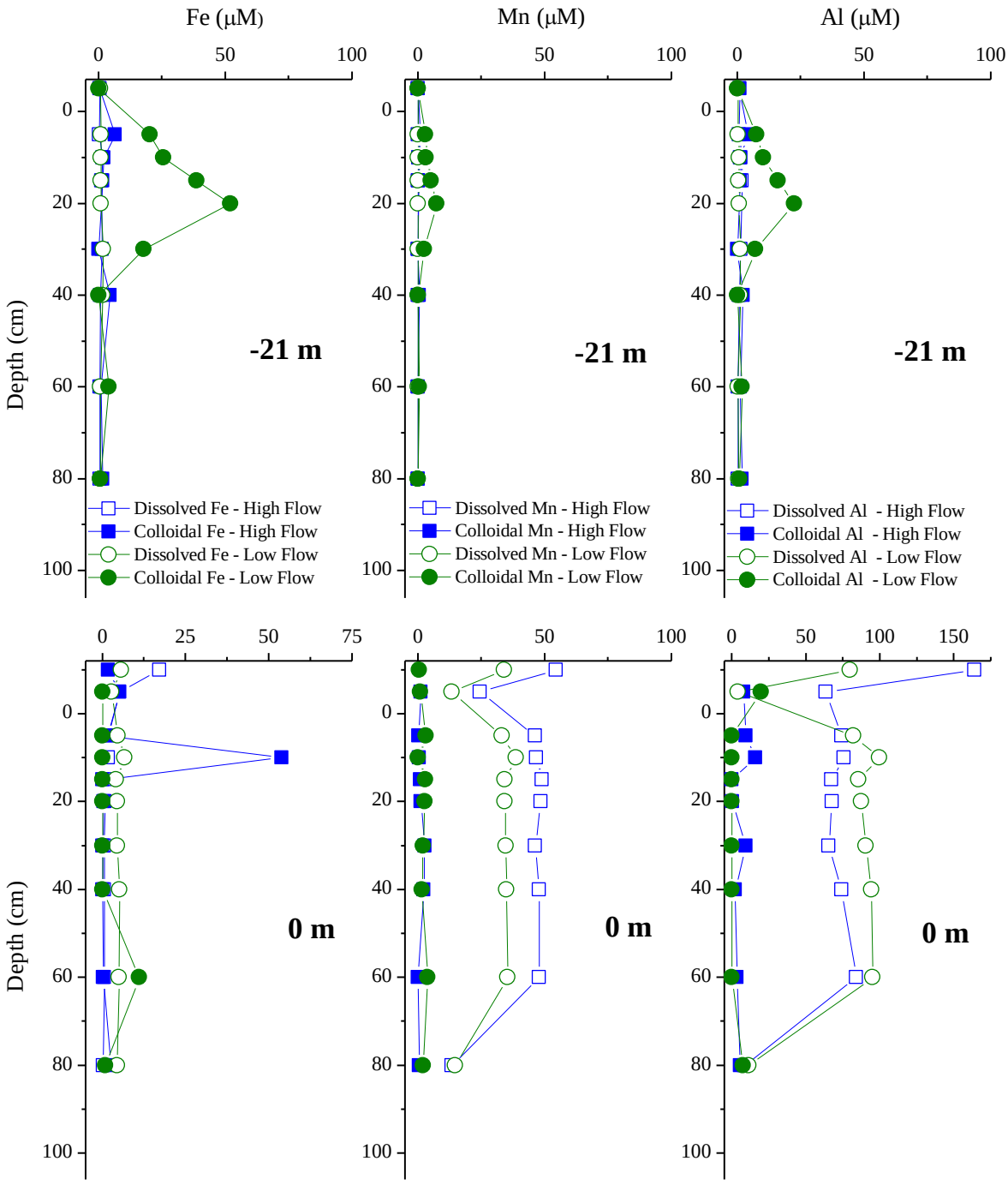

Figure 2.10. Iron, manganese, and aluminum depth profiles for 21 m upstream and 0 m downstream of AMD input. Values 5 cm above the stream-sediment interface represent stream measurements. Values 10 cm above the stream-sediment interface represent acid mine drainage measurements.

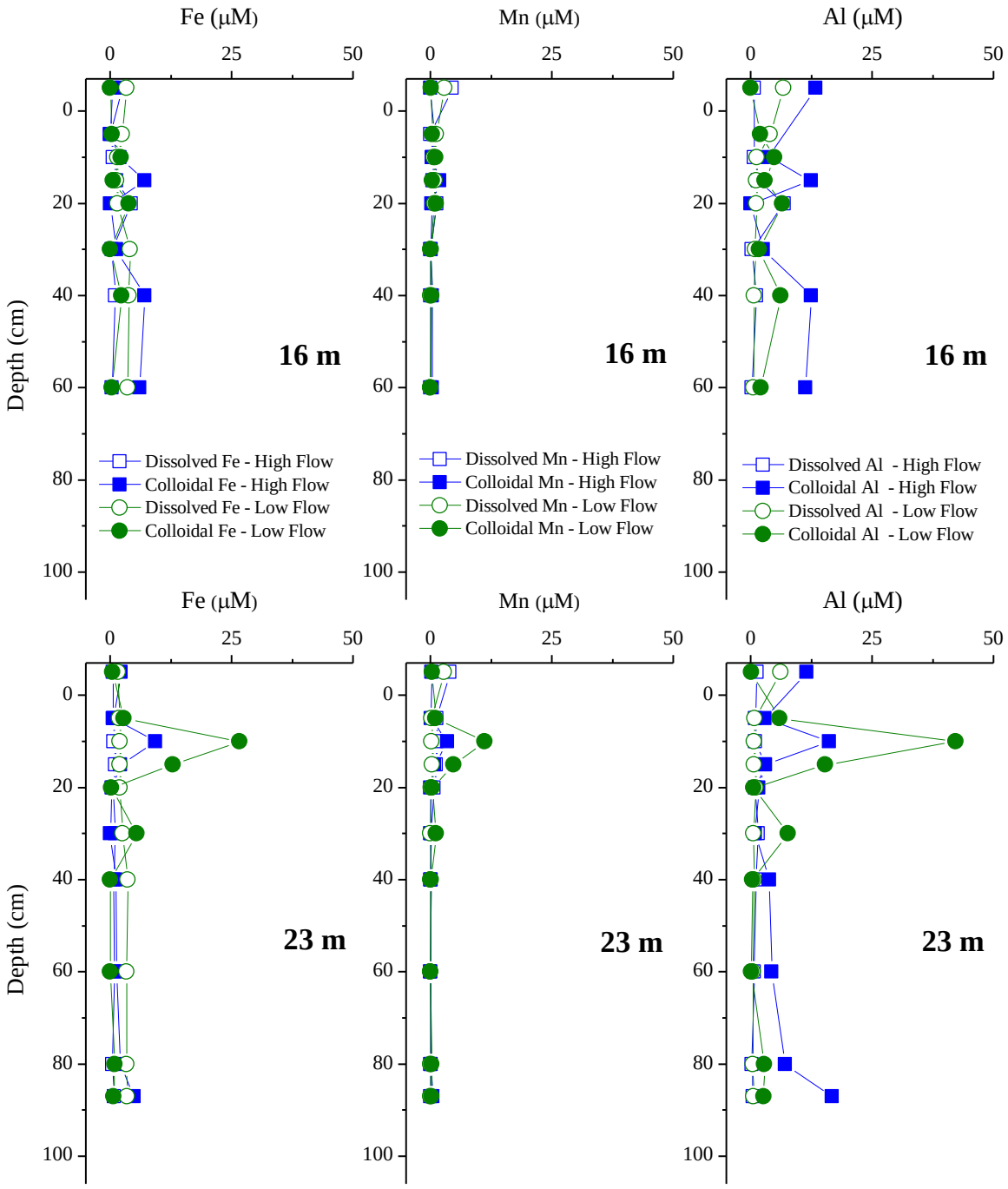

Figure 2.11. Iron, manganese, and aluminum depth profiles for 16 m and 23 m downstream of AMD input. Values 5 cm above the stream-sediment interface represent stream measurements.

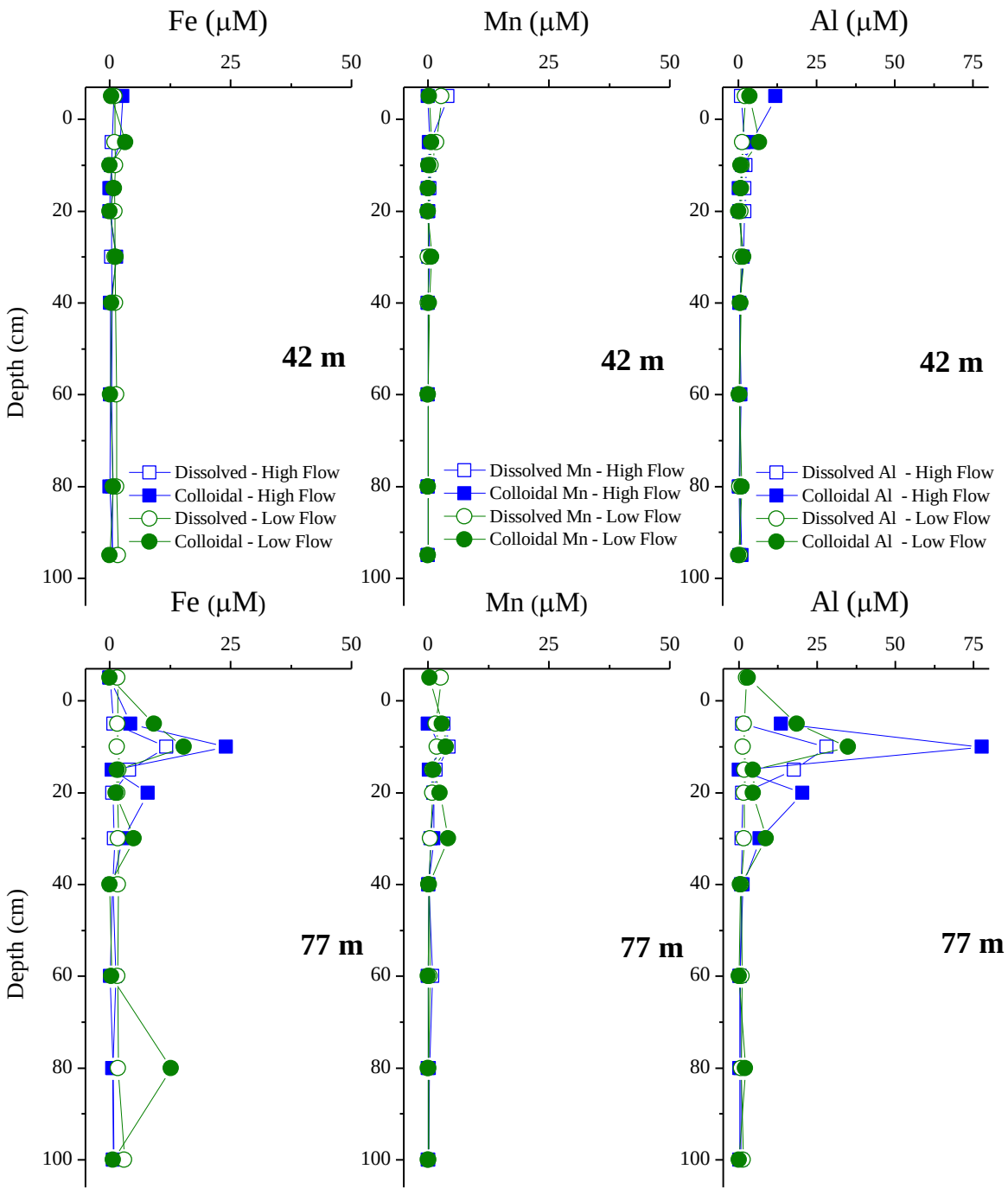

Figure 2.12. Iron, manganese, and aluminum depth profiles for 42 m and 77 m downstream of AMD input. Values 5 cm above the stream-sediment interface represent stream measurements.

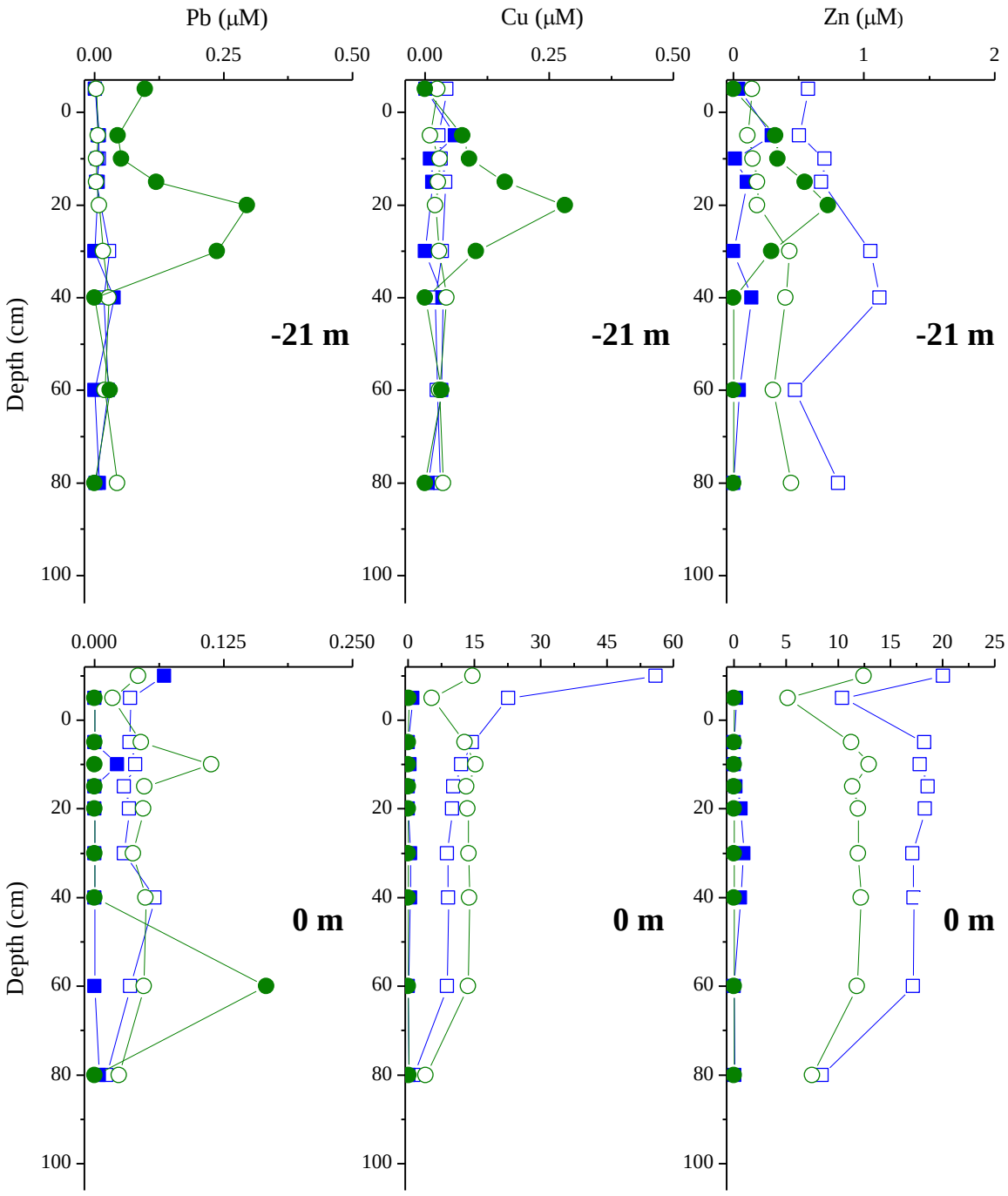

Figure 2.13. Lead, copper, and zinc depth profiles for 21 m upstream and 0 m downstream of the acid mine drainage input. Note that the metal concentration scales vary between graphs. Values 5 cm above the stream-sediment interface represent stream measurements. Values 10 cm above the stream-sediment interface represent acid mine drainage measurements.

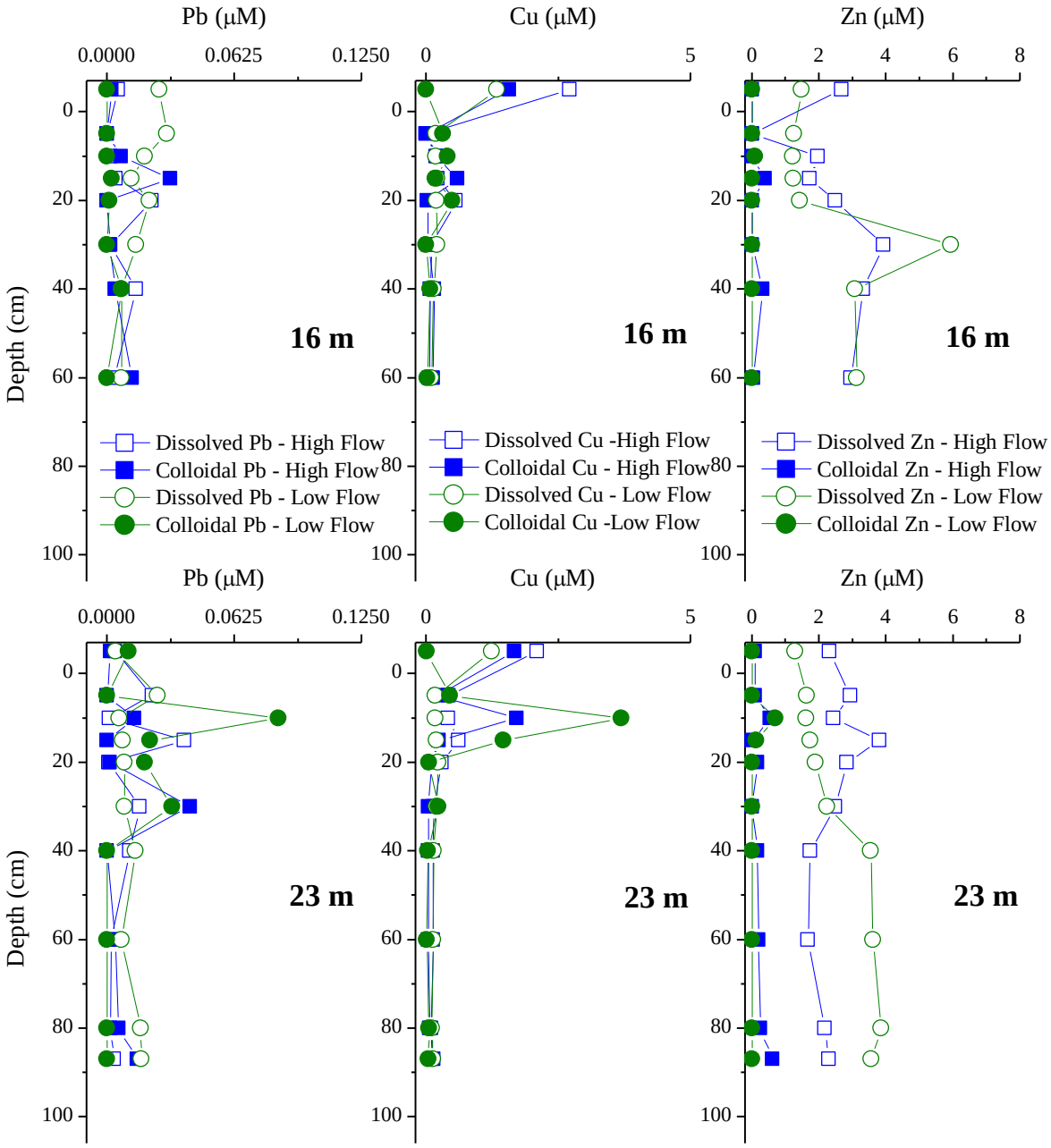

Figure 2.14. Lead, copper, and zinc depth profiles for 16 m and 23 m downstream of AMD input. Values 5 cm above the stream-sediment interface represent stream measurements.

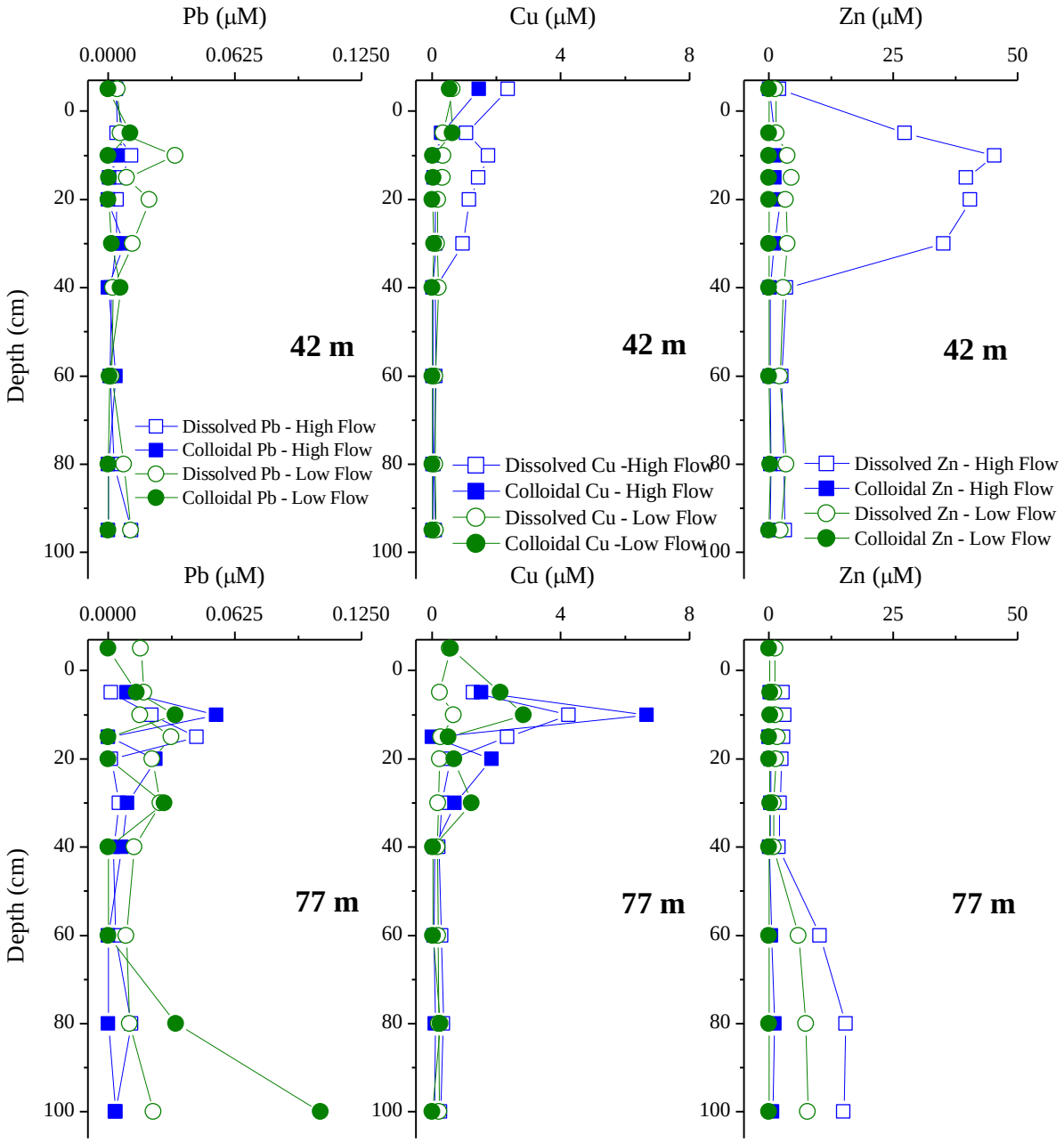

Figure 2.15. Lead, copper, and zinc depth profiles for 42 m and 77 m downstream of AMD input. Values 5 cm above the stream-sediment interface represent stream measurements.

Colloids

Colloids analyzed by a variety of methods showed a wide range of colloidal sizes. SEM micrographs of the material collected on the filters appeared to be large 1-100 µm aggregates

made up of smaller colloids. These smaller colloids were in the size range of 10-100 nm (Figure 2.16). The aggregation of the primary colloids may have occurred during filtration. Dynamic light scattering analysis of the colloids in acid mine drainage and stream water samples resulted in number-weighted size distributions of 150 ± 520 nm and 140 ± 390 nm, respectively. Zeta potential measurements for the acid mine drainage and stream water were 6.66 ± 0.814 mV and -21.9 ± 1.09 mV, respectively. The pH of the acid mine drainage and stream water were 6.19 and 3.17, respectively.

EDX measurements show that the material was consistently composed carbon, oxygen, silicon, aluminum, and iron (Figure 2.17). Carbon was present in the filter and mount material and was an artifact. Sulfur was present in quantities less than about 1%. According to Reed (1996) the theoretical detection limits in SEM–EDS measurements are about 0.08 wt%. EDX is limited to measuring the composition of aggregates greater than 1 μm in diameter. XRD indicated that stream water colloids were composed of clays – kaolinite, illite, and vermiculite or chlorite. A broad peak was observed between 13 and 17 2Θ° that indicated amorphous material.

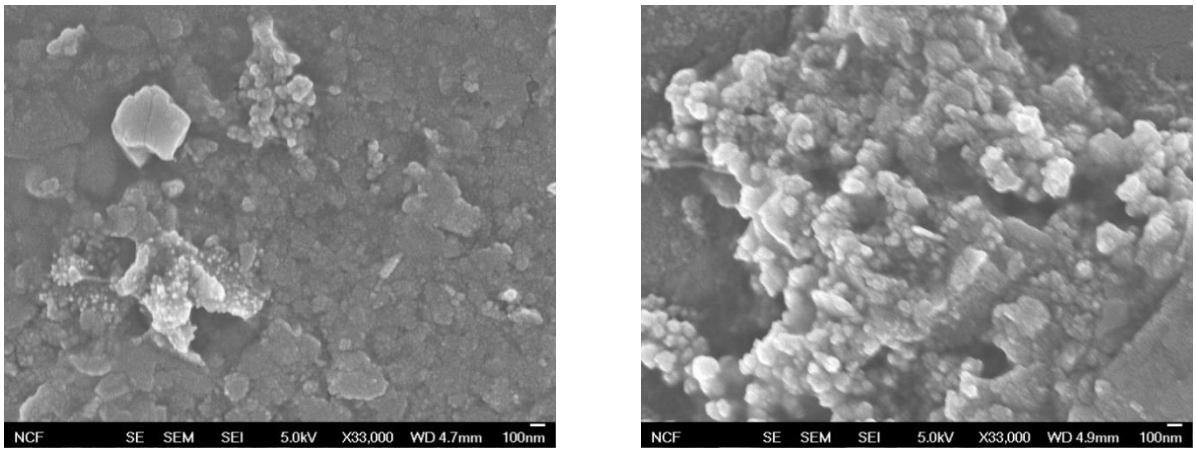

Figure 2.16. Images of colloidal material from the subsurface pore waters collected during sampling at high flow (left) and low flow (right) using a field emission SEM. Scale bars showing the length of 100 nm are located in the lower right corner of each image.

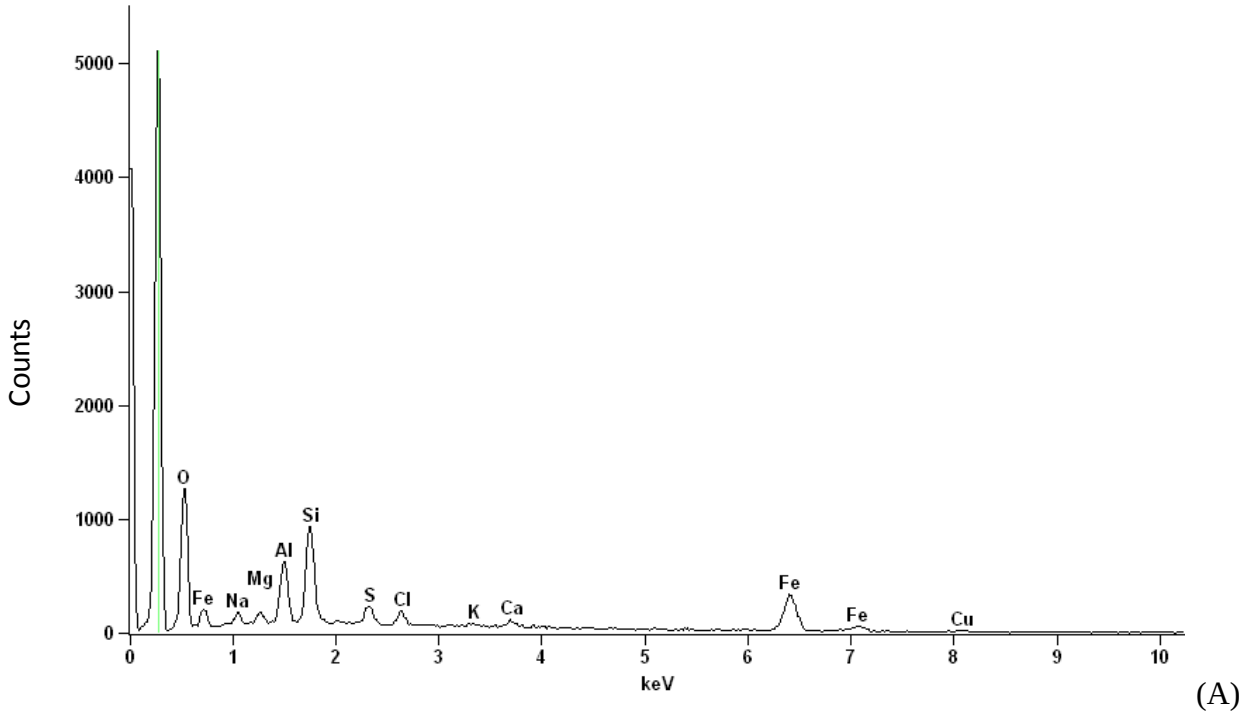

(A)

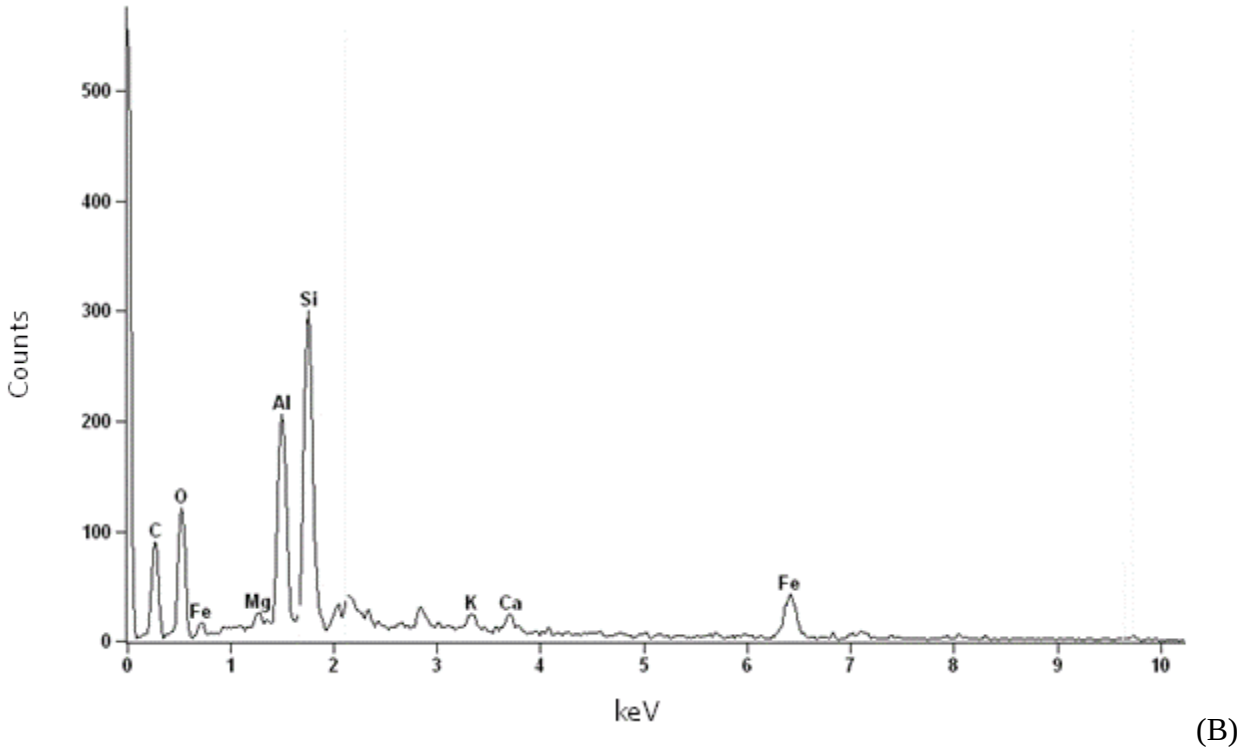

(B)

Figure 2.17. EDX spectra of aggregated material from subsurface pore waters collected during sampling at high flow (upper) and low flow (lower) on a 0.1 µm filter.

Sediment Metal Extraction

Sediment cores downstream of the acid mine drainage were collected and divided into subsamples based on depth (Figure 2.18). Depths of up to 80 cm were sampled, but most cores only yielded sediment to a depth of 40 cm due to the prevalence of large boulders throughout the streambed. Metals were removed from sediment samples by sequential extraction, which enabled the determination of metal concentrations bound in three fractions: (1) 0.25 M hydroxylamine hydrochloride/0.25 M hydrochloric acid solution for 30 min in a 50˚C water bath (amorphous iron-manganese oxides), (2) 4 M hydrochloric acid for 30 min in a 94˚C water bath (crystalline iron-manganese oxides), and (3) 12 M hydrochloric/sodium chlorate acid solution for 45 minutes at room temperature; 4 M nitric acid for 40 minutes in a 100˚C water bath (sulfides).


(A)


(B)


(C)

Figure 2.18. Sediment cores collected at (A) 23 m, (B) 42 m, and (C) 77 m. The core at 42 m is pictured as it was being hoisted from the sediment. We were able to immobilize large rocks as well as fine sediments using the freeze core method. The sediment is missing from about 35 – 55 cm from the core collected at 77 m, possibly due to uneven freezing along the pipe. Partitions on the tray were 2 cm wide for the first 10 cm, then 5 cm wide from 10 cm-20 cm, then 10 cm wide for the 30-60 cm, and 20 cm wide for the remaining 40 cm.

It is expected that deposition of colloids from the acid mine drainage formed coatings on the sediment grains and these coatings are represented by the amorphous iron-manganese oxide fraction. These reducible iron and manganese oxides are considered to be chemically mobile, because these phases could release trace metals to the environment under certain geochemical conditions, i.e. reducing conditions could remobilize metals. The iron and aluminum were mostly in the crystalline oxide fractions while most of the manganese was found in the amorphous oxide fraction. The average concentration of aluminum found in the amorphous Fe/Mn oxide fraction of the sediment extraction was about 60 μmol g^{-1} (Figure 2.19). The average concentration of both iron and manganese in the amorphous Fe/Mn oxide fraction of the sediment extraction was about 30 μmol g^{-1} (Figures 2.20 and 2.21). This represented the majority of the manganese, while the iron and aluminum were largely in the crystalline oxide fractions. Zinc, copper, and lead are found in much smaller concentrations and are predominantly in the amorphous Fe/Mn oxide fraction (Figures 2.22-2.24). Concentrations of metals tend to be highest in the upper 15 cm of the sediment and decrease with depth, most notably at the 77 m location and with regard to Al, Mn, Cu, and Pb. The more difficult to extract fractions (crystalline Fe/Mn oxides and sulfides) represent underlying grain composition and indicate that the streambed is composed of iron and aluminum-rich sulfide and iron minerals.

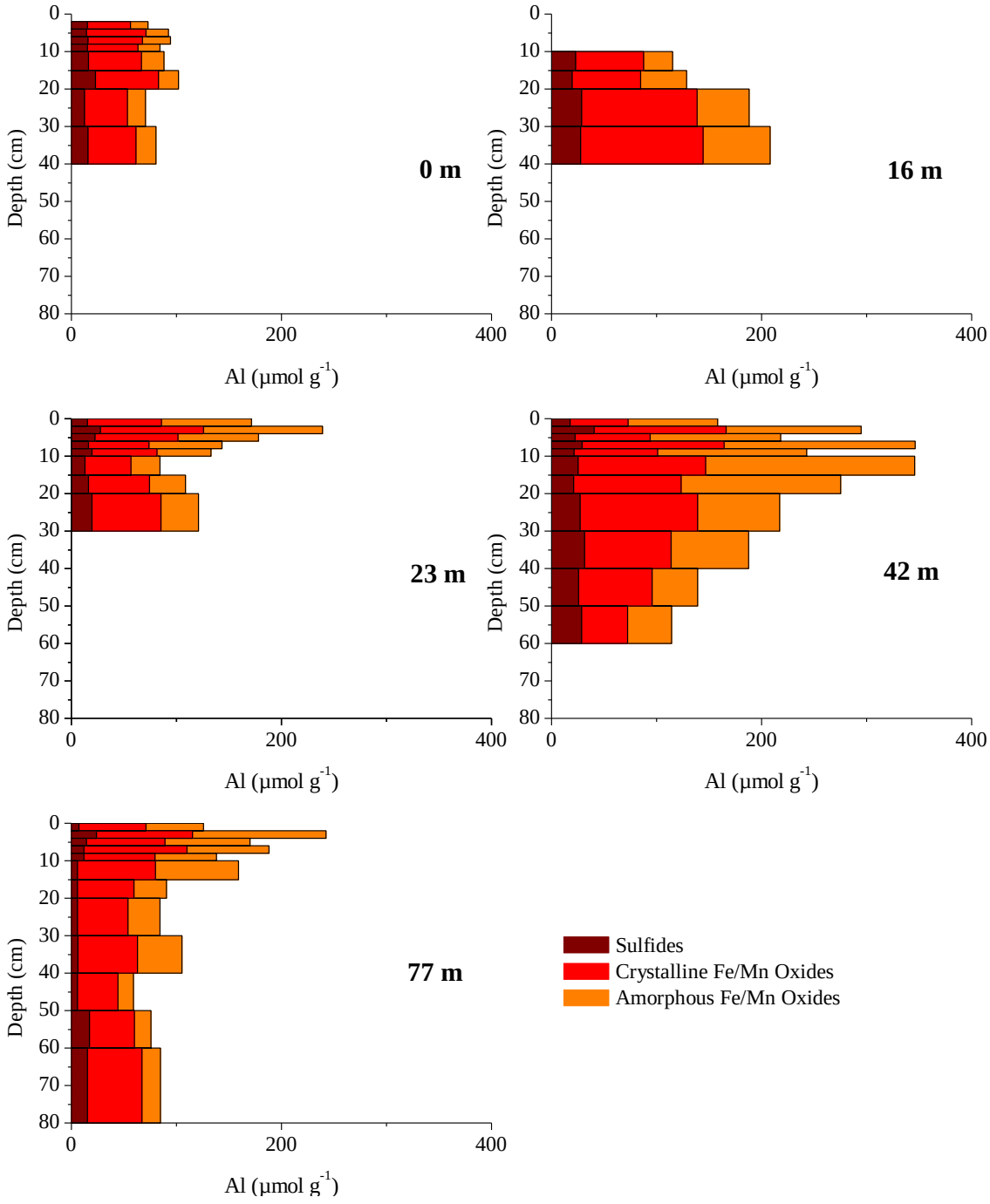

Figure 2.19. Aluminum from extraction of metals from sediment collected downstream of the input of acid mine drainage from the Big Five Tunnel into Left Hand Creek. Distances on each graph represent the downstream location of each core collected with 0 m being the point where the drainage enters the creek.

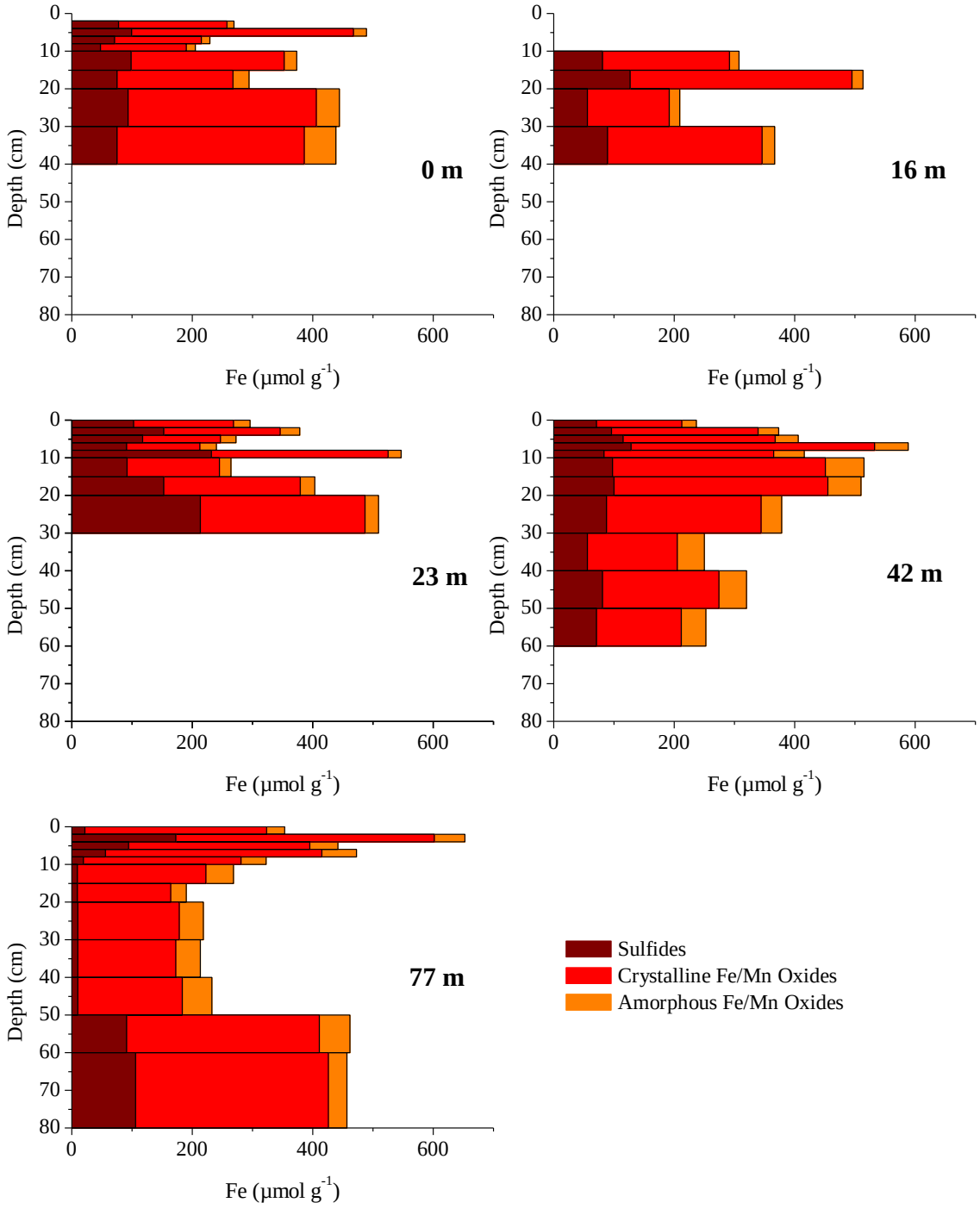

Figure 2.20. Iron from extraction of metals from sediment collected downstream of the input of acid mine drainage from the Big Five Tunnel into Left Hand Creek. Distances on each graph represent the downstream location of each core collected with 0 m being the point where the acid mine drainage enters the creek.

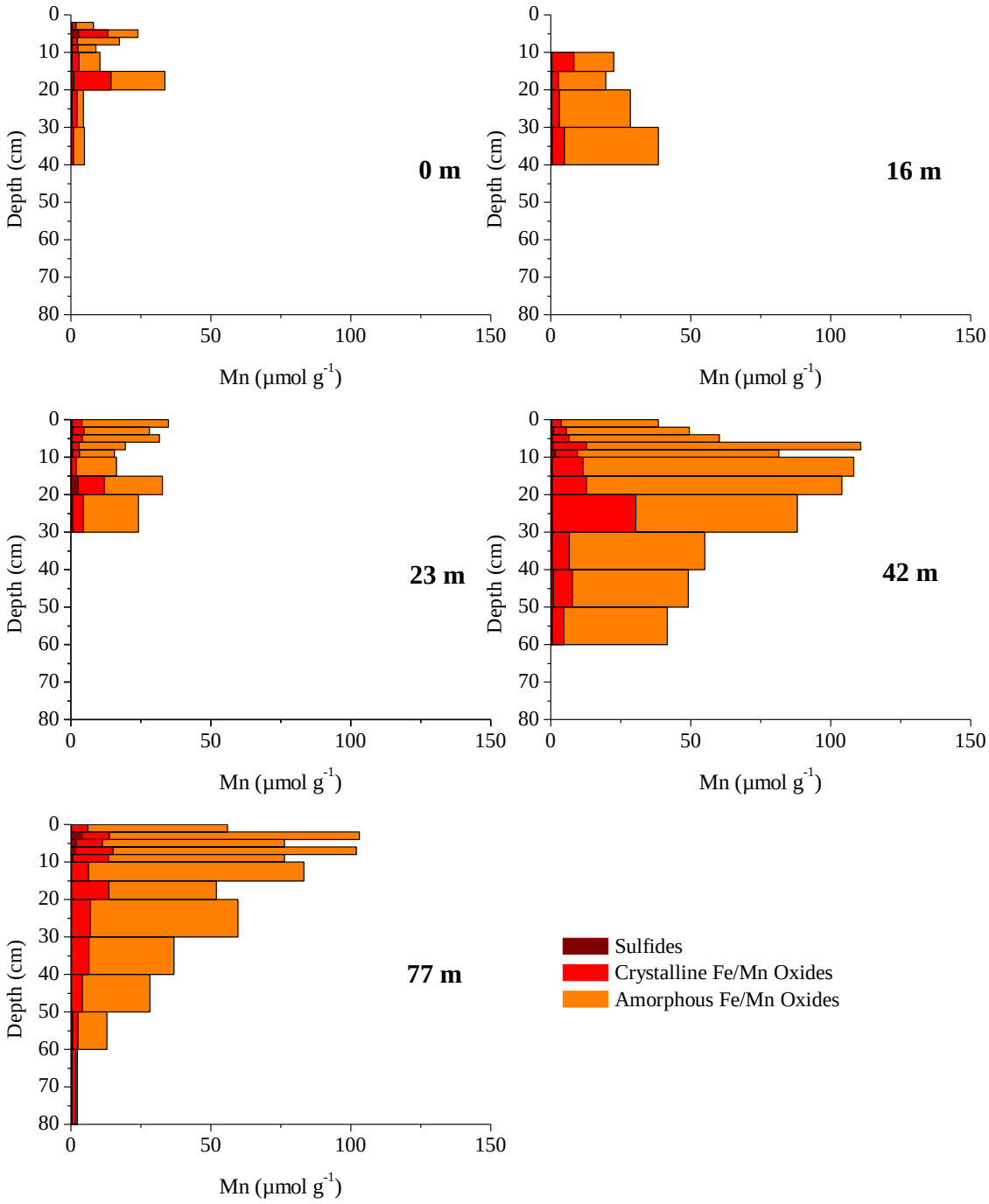

Figure 2.21. Manganese from extraction of metals from sediment collected downstream of the input of acid mine drainage from the Big Five Tunnel into Left Hand Creek. Distances on each graph represent the downstream location of each core collected with 0 m being the point where the drainage enters the creek.

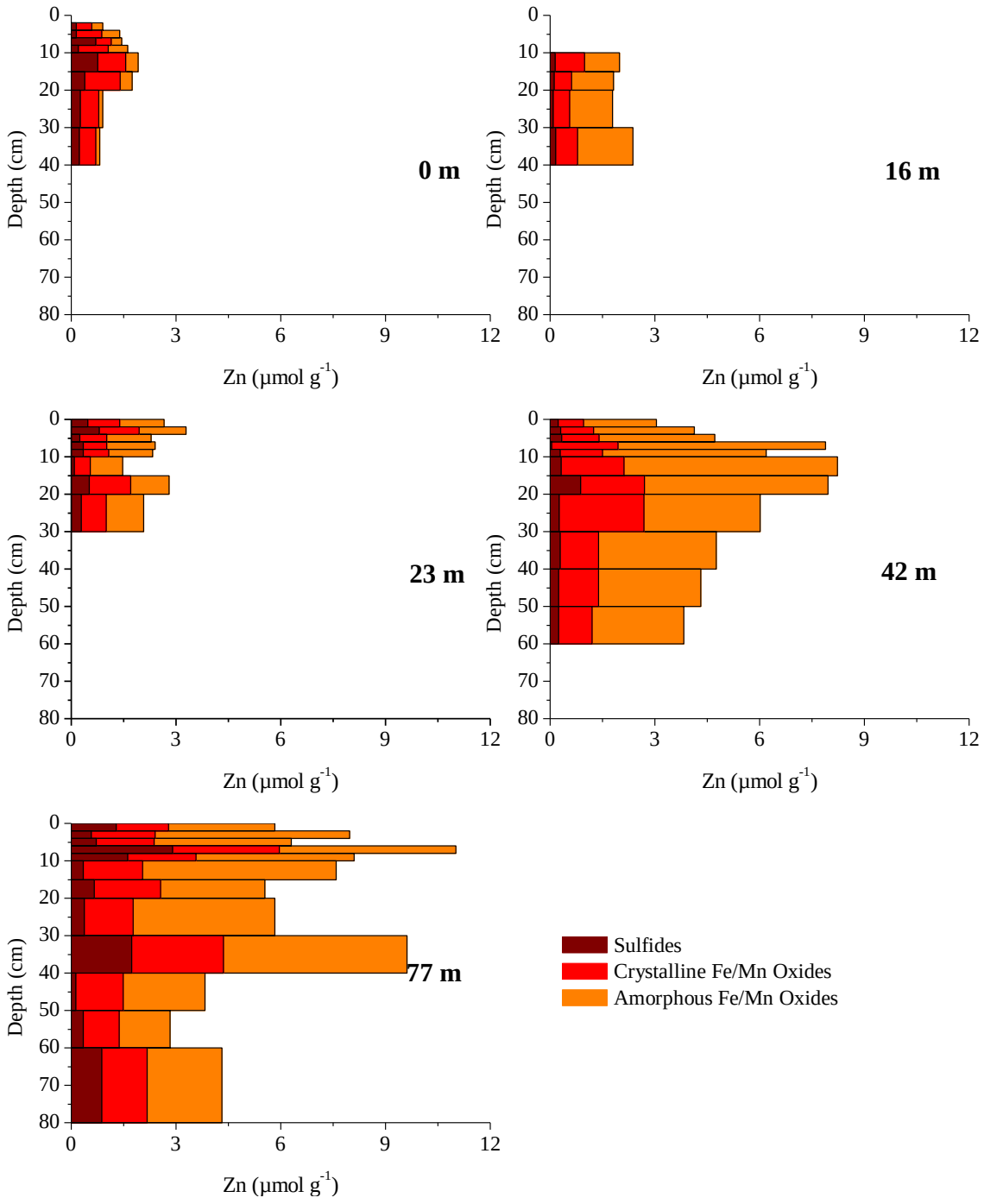

Figure 2.22. Zinc from extraction of metals from sediment collected downstream of the input of acid mine drainage from the Big Five Tunnel into Left Hand Creek. Distances on each graph represent the downstream location of each core collected with 0 m being the point where the drainage enters the creek.

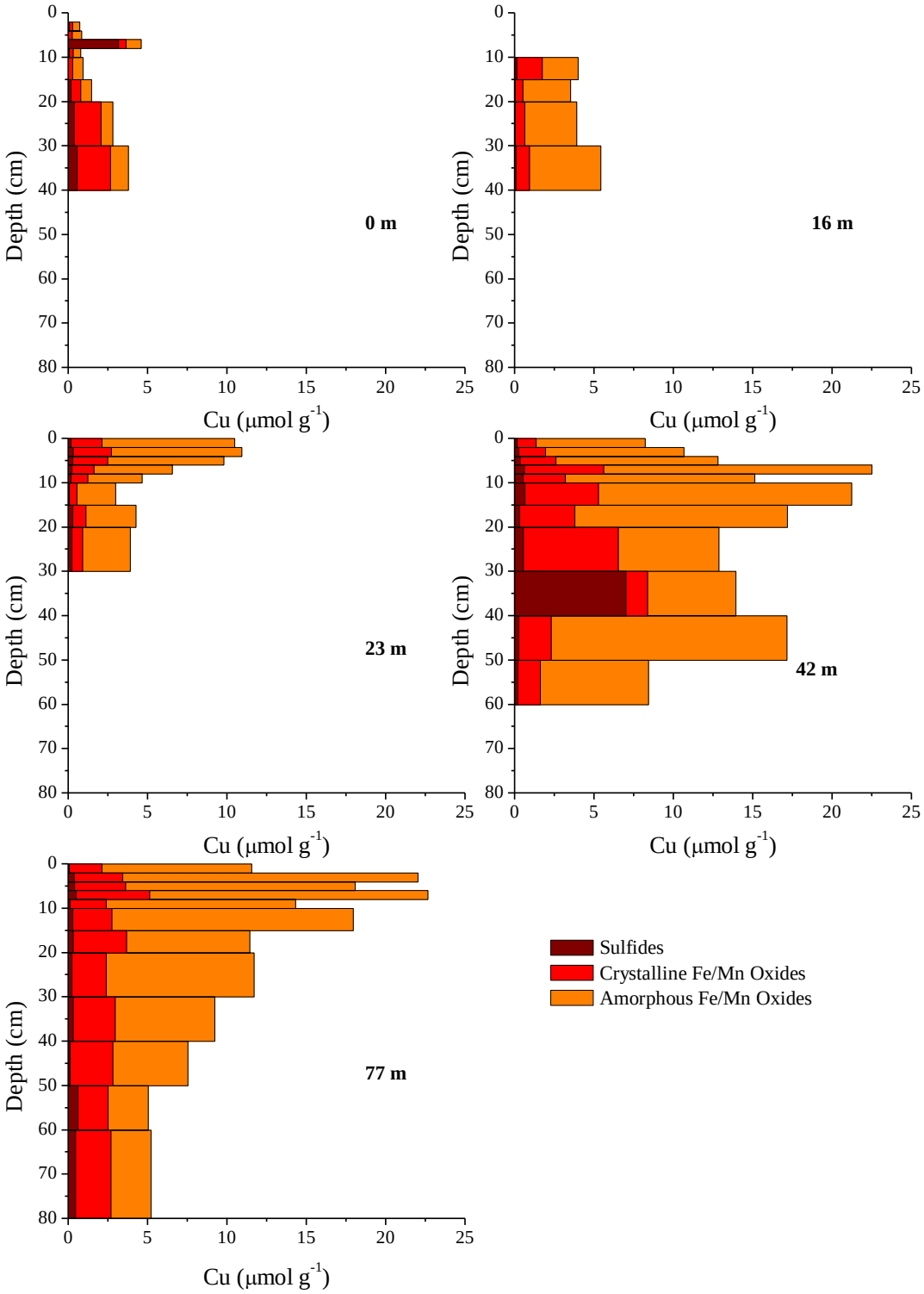

Figure 2.23. Copper from extraction of metals from sediment collected downstream of the input of acid mine drainage from the Big Five Tunnel into Left Hand Creek. Distances on each graph represent the downstream location of each core collected with 0 m being the point where the drainage enters the creek.

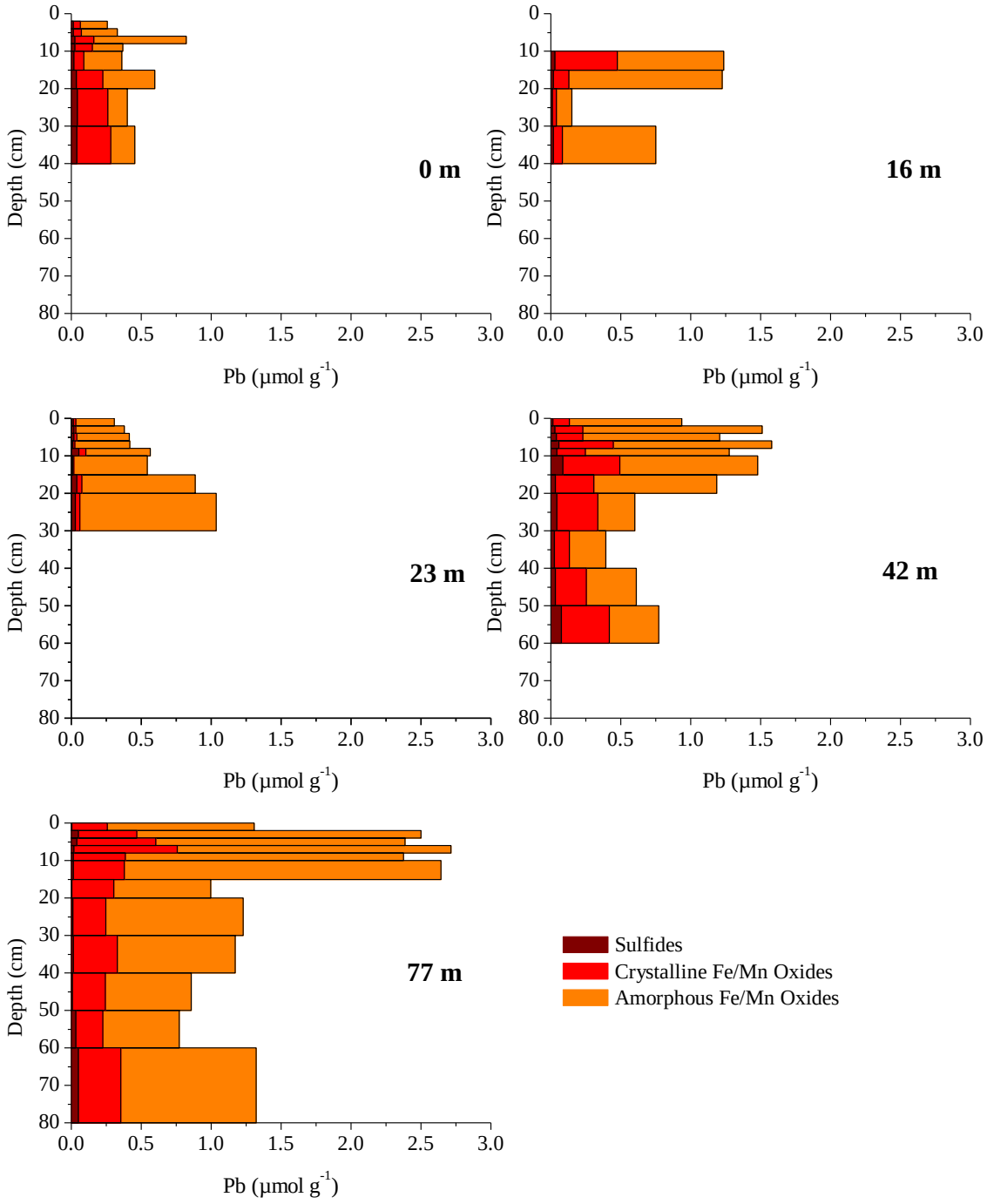

Figure 2.24. Lead from extraction of metals from sediment collected downstream of the input of acid mine drainage from the Big Five Tunnel into Left Hand Creek. Distances on each graph represent the downstream location of each core collected with 0 m being the point where the drainage enters the creek.

Sediment Grain Composition

EDX line scans were performed on polished sediment mounts to determine the composition of sediment coatings and distinguish the coatings from the underlying grains. The linescans show a difference in composition at the edge of the sediment grain at approximately 4 μm, where the amounts of O and Si decline and C, Fe, and Al appears (Figure 2.25B). A typical line scan shown in Figure 2.25 shows a sharp increase in the amount of Fe at the outer edge of the grain, while the abundance of the other elements was low.

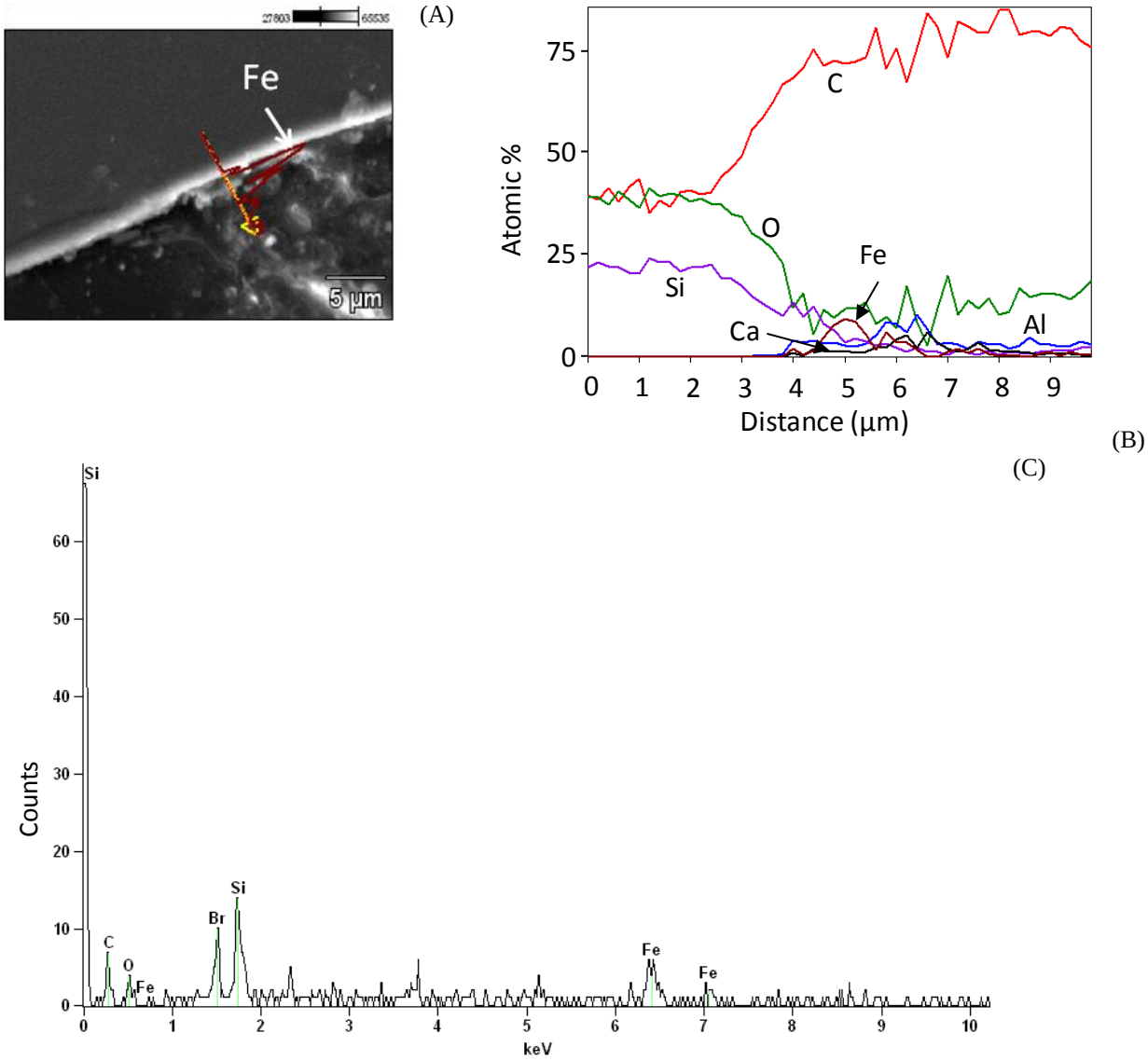

Figure 2.25. SEM micrograph showing the path of the line scan performed (A), graph of the atomic percentages of Al, Si, and Fe along the EDX line scan, with the origin of the line being 0 µm and the head of the arrow being 9 µm (B), and the energy spectrum from one point on the grain coating (C). For ease of comparing (A) and (B), the relative magnitude of the atomic percentage of Fe is plotted on the line scan in (A).

DISCUSSION

Hyporheic exchange is responsible for the transport of stream solutes into the subsurface. This exchange brings metals into contact with the sediments where they may be removed

through adsorption processes. Associations with colloids may change the way that metals are transported in the subsurface pore waters. Metals have varying affinities for colloids, but lead and copper are known to associate extensively with colloids (Kimball et al., 1995; Schemel et al., 2000); therefore colloidal transport may have an important influence on the transport of these metals. In order to determine the importance of hyporheic exchange and colloid association for metal removal in the subsurface, subsurface pore waters were examined for their metal and colloid compositions along with other water chemistry parameters at both high- and low flow conditions. The abundance of chemically mobile metals in the sediment was also measured and tracer dilution tests were used to quantify hyporheic exchange.

Hyporheic Exchange

The subsurface bromide tracer injection measurements indicated that the shallow depths (5 cm) of the hyporheic zone are highly interactive with the stream and that surface water exchange occurred on the timescale of 1 to 5 hours down to depths of 40 cm at pool locations. At some distances down the stream, even deeper exchange (up to 100 cm, the deepest piezometer depths) was indicated by increases in concentrations at the final measurements made at approximately 25 h after the start of the injection (Figure 2.8). The variation in connectivity (Table 2.3) is likely due to subsurface heterogeneity, which causes preferential flow paths through the hyporheic zone.

The metrics based on the OTIS model indicate that hyporheic exchange plays a minor role in solute transport. The hyporheic zone is assumed to be equivalent to the model storage zone due to the lack of observed eddies or pools in the reach. The model of the high flow Br injection described the observations with only advection and dispersion considered. In the low flow case, parameters based on the model indicated that the hyporheic zone area was only 3% of

the stream area (A_s/A = 0.032) and the fraction of median travel time due to transient storage evaluated at 200 m (F_{med}^{200}) was only 0.1%, which indicates that very little of the stream water flowed through with the hyporheic zone. The average storage zone residence time was estimated at 0.4 h and the hydraulic retention factor (average time water remains in storage relative to the hydraulic turnover length, $R_h = A_S/Q$) is 0.3 s m^{-1}. All these values are at the low end of the range observed in other studies of small streams (Runkel, 2002). The thickness of a u-shaped hyporheic zone around the perimeter of the stream was estimated using the model-fit storage zone cross-sectional area (A_s, Table 2.2), measurements of the stream width and depth, and a range of sediment porosities based on the hydraulic conductivities measured in the hyporheic zone (Figure 2.3). Using these parameters, the thickness of the hyporheic zone was estimated to be approximately only 1-2 cm.

Piezometer observations of the bromide tracer suggest that subsurface exchange may be more extensive than the transient storage model indicates. However, the timescale of the most rapid exchange is slow (Table 3) compared to the timescale of transport through the reach (0.5 h for 237 m reach at low flow and 2 min at high flow). The timescale of exchange is too slow to affect the surface concentration significantly. Therefore the model can only indicate minor hyporheic exchange.

The high electrical conductivity of the acid mine drainage entering Left Hand Creek is diluted upon entering the stream such that the electrical conductivity downstream of the acid mine drainage addition is similar to that measured upstream of the acid mine drainage addition. The high electrical conductivities, low pH, and up-gradient flow in the piezometers at 0 m indicate that acid mine drainage was entering the stream not only at the surface, but also through subsurface flow. The elevated electrical conductivities and sodium concentrations at depths

below 30 cm at 16 m and 23 m observed at may also be the result of subsurface flow of acid mine drainage water. Elevated levels of zinc are also observed at these locations.

Hydraulic conductivities and hydraulic head gradients can influence hyporheic exchange. Ryan and Boufadel (2006) showed that more tracer entered the subsurface if the shallow subsurface was of higher conductivity than that of the the underlying sediment. In Left Hand Creek, this was the case in three piezometer locations (-21 m, 0 m, and 16 m). However, head gradients induced by streambed topography can mask this effect. Harvey and Bencala (1993) showed that subsurface flow paths begin at the downstream end of pools prior to an increase in the slope (i.e., the step, or riffle, below the pool), and return to the stream at the upstream end of the next pool. Piezometers at four distances (-21 m, 16 m, 23 m, and 77 m) were located at the downstream end of pools, indicating that the topography and resulting head gradients were driving flow into the subsurface. The remaining piezometer locations (0 m and 42 m) were located in riffles where head gradients were more positive and connectivity was limited to the shallow subsurface.

Hyporheic exchange has been observed to decrease in the spring due to the influence of greater groundwater head (Harvey and Bencala, 1993). The tracer dilution test showed evidence of storage in the low flow case while none was indicated at high flow. However, the subsurface measurements indicated that exchange driven by streambed topography was consistent between the high flow and low flow.

Metal Removal

The pH of the stream and hyporheic zone waters is an important parameter controlling metal transport (Gandy et al., 2007). The pH plays an important role in solubility and adsorption of metals and in the mobility of colloids. As pH increases to the neutral range, protons offer less

competition with metals for binding sites on surface hydroxyls. This results in a larger colloidal fraction of metals at higher pH (Figure 2.26). A trend of increasing colloidal fraction from zinc to copper to lead is also observed as we would expect based on surface complexation constants for the adsorption of these metals on hydrous ferric oxide surfaces: $10^{0.99}$, $10^{2.89}$, and $10^{4.65}$ for zinc, copper, and lead, respectively (Dzombak and Morel, 1990). This trend has also been observed in other AMD-impacted settings (Kimball et al., 1995; Farag et al.,2007).

The shallow subsurface remained near saturation with dissolved oxygen. This maintains the stability of colloids with respect to dissolution. Reducing conditions are unlikely to decrease metal sorption in the hyporheic zone ranging from 5 to 60 cm in depth. Depletion of oxygen occurs below these depths in the subsurface.

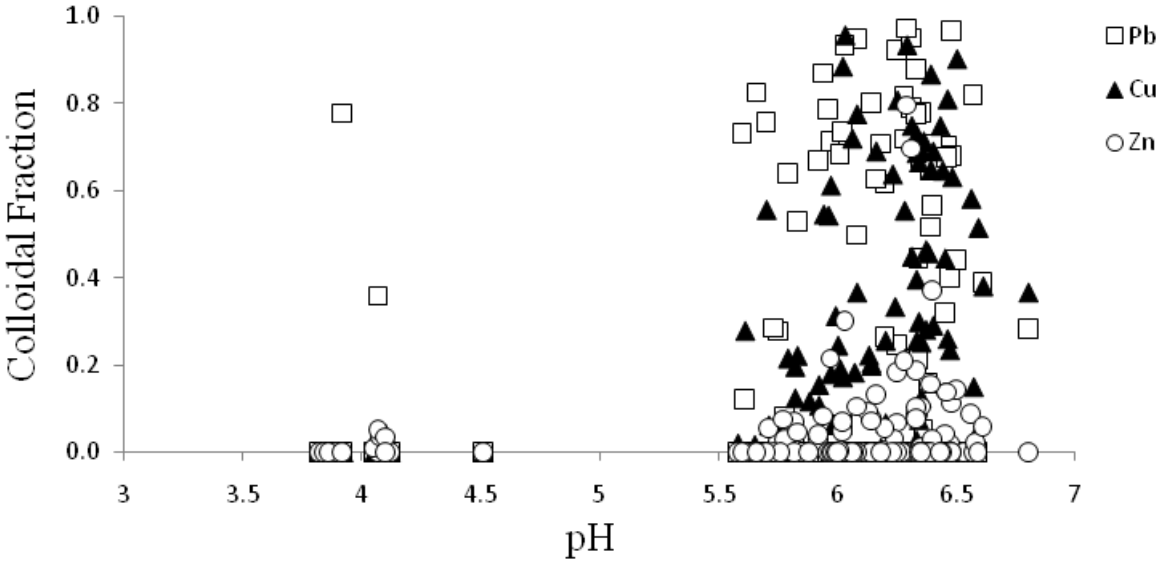

Figure 2.26. The colloidal fractions of lead, copper, and zinc as related to stream acidity in Left Hand Creek.

The high colloidal concentrations of iron and aluminum in the hyporheic zone suggests that these metals occur as colloidal hydrous oxides under the stream flow and chemical conditions present in the study reach. The EDX analysis of the colloids showed that iron and aluminum make up approximately 5-10% of the colloids. XRD on colloids isolated from the

surface water did not show crystalline material with iron and aluminum composition, which is to be expected for colloidal material that precipitates rapidly as a result of the increase in pH. Colloidal manganese was found in the subsurface (Figures 2.10, 2.11, and 2.12); however, EDX did not detect manganese in the colloids. Manganese is likely adsorbed to other colloids rather than precipitated as manganese oxides.

The relationship between the colloidal fractions of lead, copper, and zinc with iron, manganese, and aluminum in the colloidal form was investigated for metals in the hyporheic zone. Colloidal copper in the hyporheic zone is positively correlated with iron, manganese, and aluminum in the colloidal form during both the high- and low flow samplings (Figure 2.27). Many studies have shown the importance of colloids in controlling metal transport in surface waters, but no studies have shown the affect of colloids on metal transport in the hyporheic zone. The colloidal lead fractions were consistently high due to the high affinity of lead for mineral surfaces. Precipitation of lead hydroxides is not expected based on solubility calculations at the observed pH and lead concentrations. Colloidal zinc was not correlated with colloidal Fe, Mn, and Al due to the tendency of zinc to remain largely dissolved.

Deposition of colloids and sorption of dissolved metals forms coatings on the sediment grains. EDX line scans indicated that Fe was an important element of these coatings. These coatings were also quantified by the sequential extraction analysis, where the first step the extraction, identified as the amorphous iron-manganese oxide fraction, represented the coatings. These reducible iron and manganese oxides are considered to be chemically labile because these phases could release trace metals to the environment under certain geochemical conditions; i.e., reducing conditions could remobilize the metals adsorbed to the amorphous iron-manganese oxide fraction. Concentrations of lead, copper, and zinc in the amorphous iron/manganese oxide

fraction of the sediments were all positively correlated with the concentrations of iron, aluminum, and manganese of the same fraction (Figure 2.27). The most positive (steepest slope) correlations for lead, copper, and zinc were with iron. The most linear correlations for lead, copper, and zinc were with manganese. The average lead concentration in the amorphous iron/manganese oxide fraction represented 72% of the total lead concentration. The copper in the amorphous fraction was also high; 72% of the copper was in that fraction. The zinc in the amorphous fraction of the sediment averaged 55% of the total zinc. Previous studies have shown that these metals partition to iron-oxides in acid mine drainage-contaminated sediments following the order of Pb > Cu > Zn (Bencala, 1990; Evans and Davies, 1994; Galan, 2003). The strong tendency of lead to adsorb to sediments or precipitate as an oxide may account for its greater independence from the concentrations of iron, aluminum, or manganese. The high metal levels found in the amorphous fraction may support co-precipitation as an additional mechanism for sequestration in addition to surface precipitation. Co-precipitation of lead, copper, and zinc with amorphous iron hydroxides has been shown to result in high removal rates of these metals from solution and slow release over long periods (Martinez and McBride, 1998).

The metals examined here – lead, copper, and zinc – exhibit a range of affinities for adsorption to mineral surfaces (Dzombak and Morel, 1990; Farag et al., 1998; Schemel et al., 2000; Munk et al., 2002; Galán et al., 2003). Based on these observations, sorption to the streambed sediments was expected to follow the order of Pb > Cu > Zn. In order to assess the relationship between metals in the sediments, we estimated distribution coefficients (K_d) as

$$K_d\ (L\ kg^{-1}) = \frac{C_s(mg\ kg^{-1})}{C_w(mg\ L^{-1})} \tag{2.5}$$

where C_s is the concentration of metal in the solid phase and C_w is the concentration of the metal in the water. Here, the metal concentration in the amorphous Fe/Mn oxide phase was used for C_s

because the majority of the adsorbed metals were present in this phase. The pore water concentrations from both high flow and low flow were used to estimate average K_d values for lead, copper, and zinc: $10^{4.96\pm0.44}$ L kg^{-1} for lead, $10^{4.27\pm0.34}$ L kg^{-1} for copper, and $10^{2.84\pm0.46}$ L kg^{-1} for zinc. This trend corresponds with the trend observed in the colloidal fractions of these metals, where colloidal lead fractions were high, copper showed a medium portion of colloids, and zinc was largely dissolved.

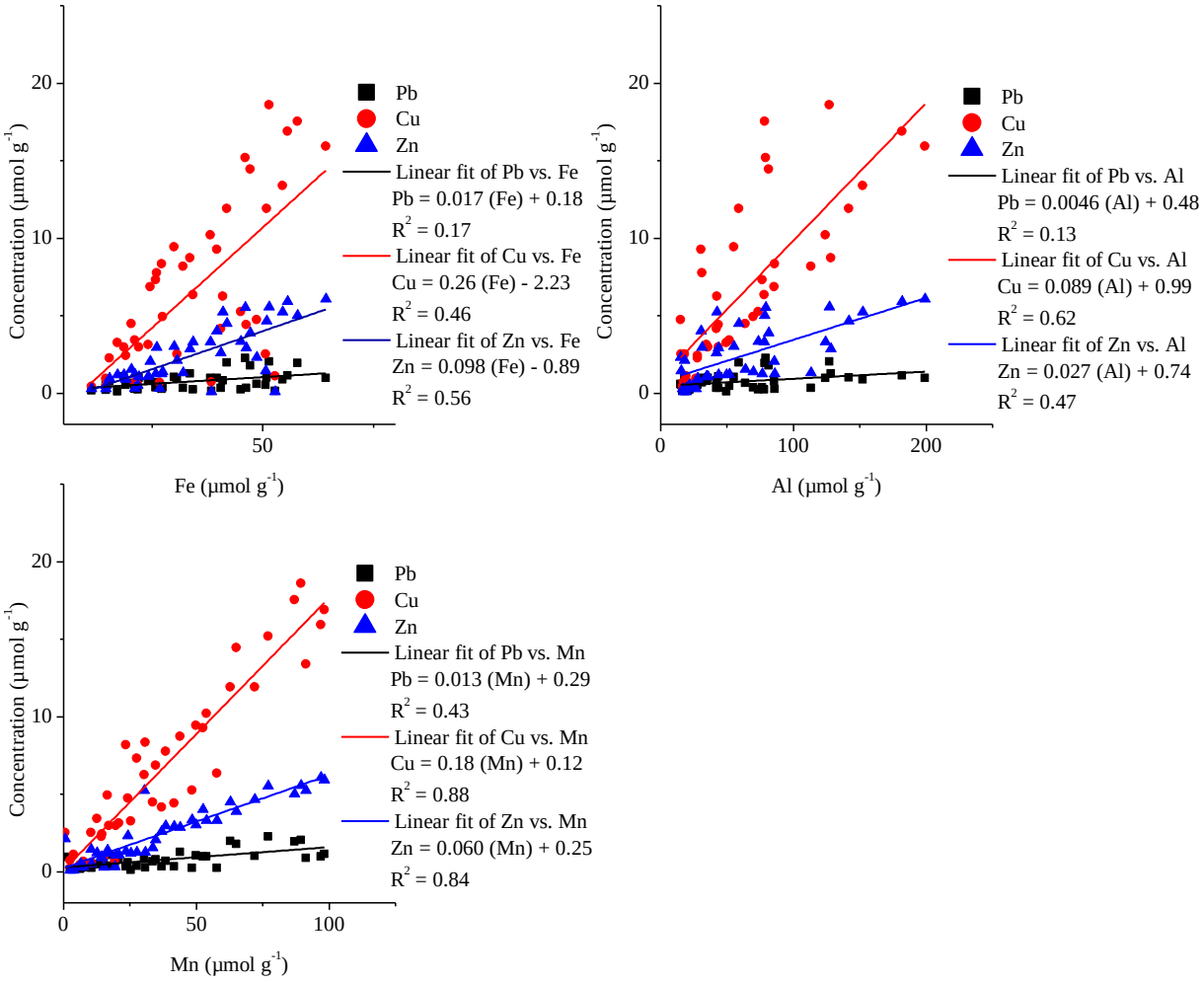

Figure 2.27. Correlations of Pb, Cu, and Zn with Fe, Al, and Mn from the amorphous Fe/Mn fraction of the extraction of sediment taken from the streambed of Left Hand Creek with lead, copper, and zinc from the same fraction.

A key goal in this study was to determine whether colloids enhanced or impeded transport versus the transport of dissolved metals. The removal of dissolved metals was compared with colloidal metals by comparing the normalized concentration of dissolved metal (ratio of dissolved metal concentration in the hyporheic zone to the dissolved metal concentration in the surface) at each location in the subsurface with the normalized concentration of colloidal metal (ratio of colloidal metal in the hyporheic zone to the colloidal metal concentration in the surface). The majority of the time, the normalized colloidal concentration was larger than the normalized dissolved concentration, suggesting that colloid-associated metals are more mobile than dissolved metals. The median values of the dataset of ratios of normalized dissolved concentration to normalized colloidal concentration were 0.82, 0.08, and 0.06 for Pb, Cu, and Zn, respectively. One caveat to this supposition of enhanced transport is that in several instances, the colloidal metal concentration in the subsurface was larger than the concentration in the surface. This indicates that the colloidal metals were generated in the subsurface. These colloids could have been mobilized due to changes in the water chemistry, i.e. ionic strength, pH. It is also possible that immobile colloids were collected during the sampling process, though the careful sampling procedure makes this unlikely. When the instances of apparent colloid generation are removed from the dataset, the colloids still offered enhanced metal transport relative to dissolved metals in the hyporheic zone.

Principle component analysis (PCA) and parallel factor analysis (PFA) were used help determine which processes control metal transport in the hyporheic zone. These analyses work by determining which parameters are most important for explaining the variability in a dataset. Chloride, as a conservative, non-reactive tracer, was used to represent the hydrological processes occurring in the stream system. Ions that covary with the chloride were considered to be largely

behaving conservatively. Variance not related to chloride could be said to show non-conservative behavior and any covariance with other water chemistry parameters might offer a clue to the mechanisms controlling the non-conservative transport. Wilderman et al. (2009) performed a similar analysis on solutes in a river subsurface to distinguish hydrologic processes from Mn-controlled redox processes. Iron, manganese, and aluminum oxides are known to act as adsorbents for other trace metals of interest (Dzombak and Morel, 1990; Gandy et al., 2007). These metal oxides are expected to control trace metal transport through adsorption processes. Physical parameters, such as head gradient and hydraulic conductivity control exchange of stream and hyporheic zone water and flow in the subsurface (Table 2.5). Water chemistry parameters, like pH, conductivity, and dissolved oxygen concentrations, affect metal speciation. The principle component analysis on the data for high flow explains 54% of the variability in the data in the first two principal components (PCs). PCA indicates that dissolved metals are related to chloride while colloidal metals form a distinct cluster (Figure 2.28). The first two principle components from PCA on the low flow data represent 68% of the variance in the data. The PCA on the low flow data shows a distinct cluster of colloidal fractions of all the metals, conductivity, proton activity, head gradient, and hydraulic conductivity. The dissolved metals and the chloride along with dissolved oxygen form another distinct cluster. The first two principle factors in the parallel factor analysis (PFA) explain 43% and 63% of the total variance in the high- and low flow data sets (Figure 2.29). PFA for both high- and low flow indicate that chloride and all of the colloidal metals are consistently important parameters that explain a large portion of the data. This shows the close relationship between all of these variables. Hydrologic processes affect transport of both colloids and dissolved ions.

The divisions between dissolved and colloidal metals indicate that they are controlled by different mechanisms. While the dissolved metals are associated with conservative chloride, the colloidal metals are not entirely controlled by hydrologic processes. Instead, they are subject to other removal processes, such as deposition in the sediments.

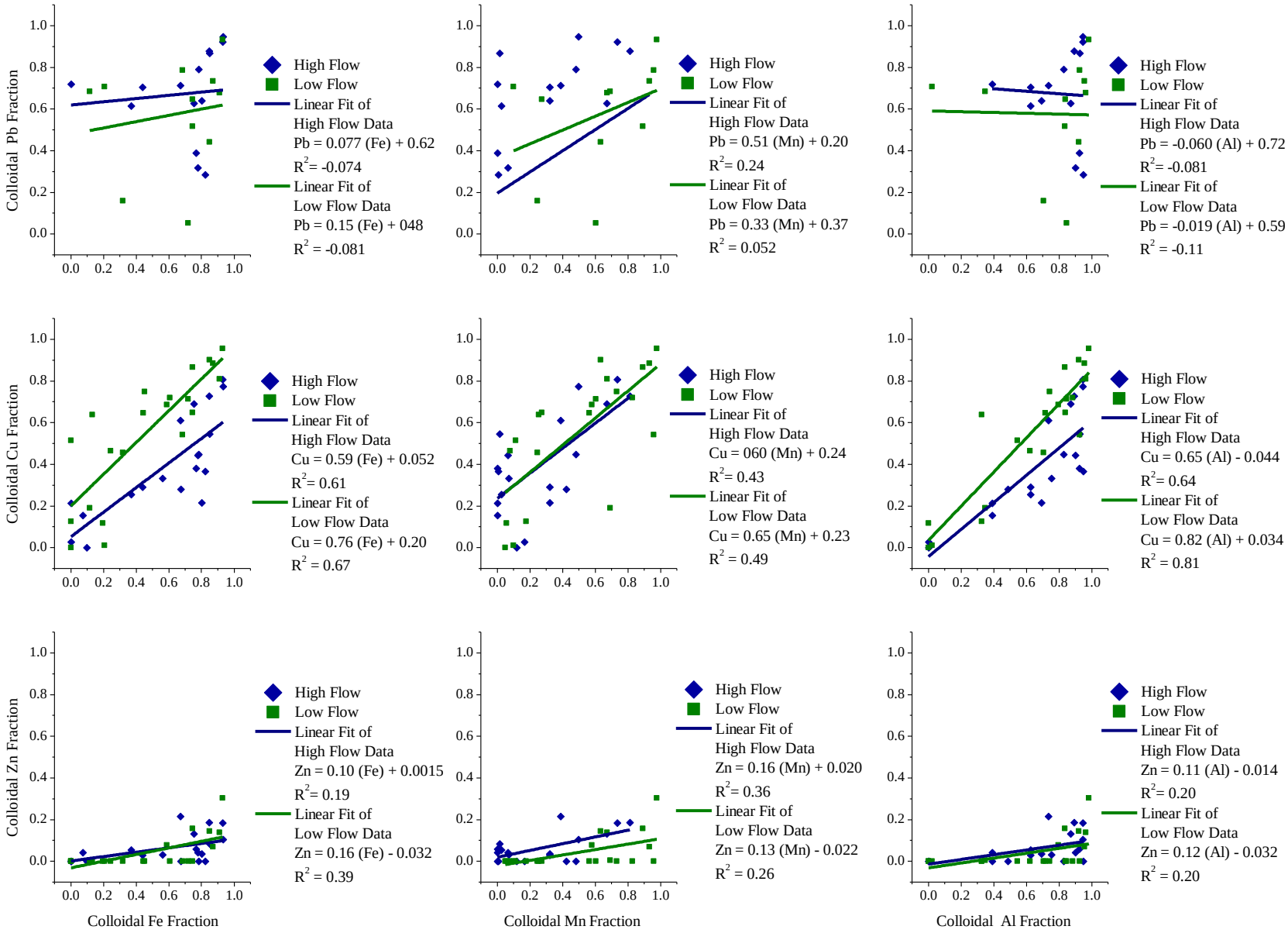

Figure 2.28. Plots of colloidal lead, copper, and zinc vs. colloidal iron, manganese, and aluminum.

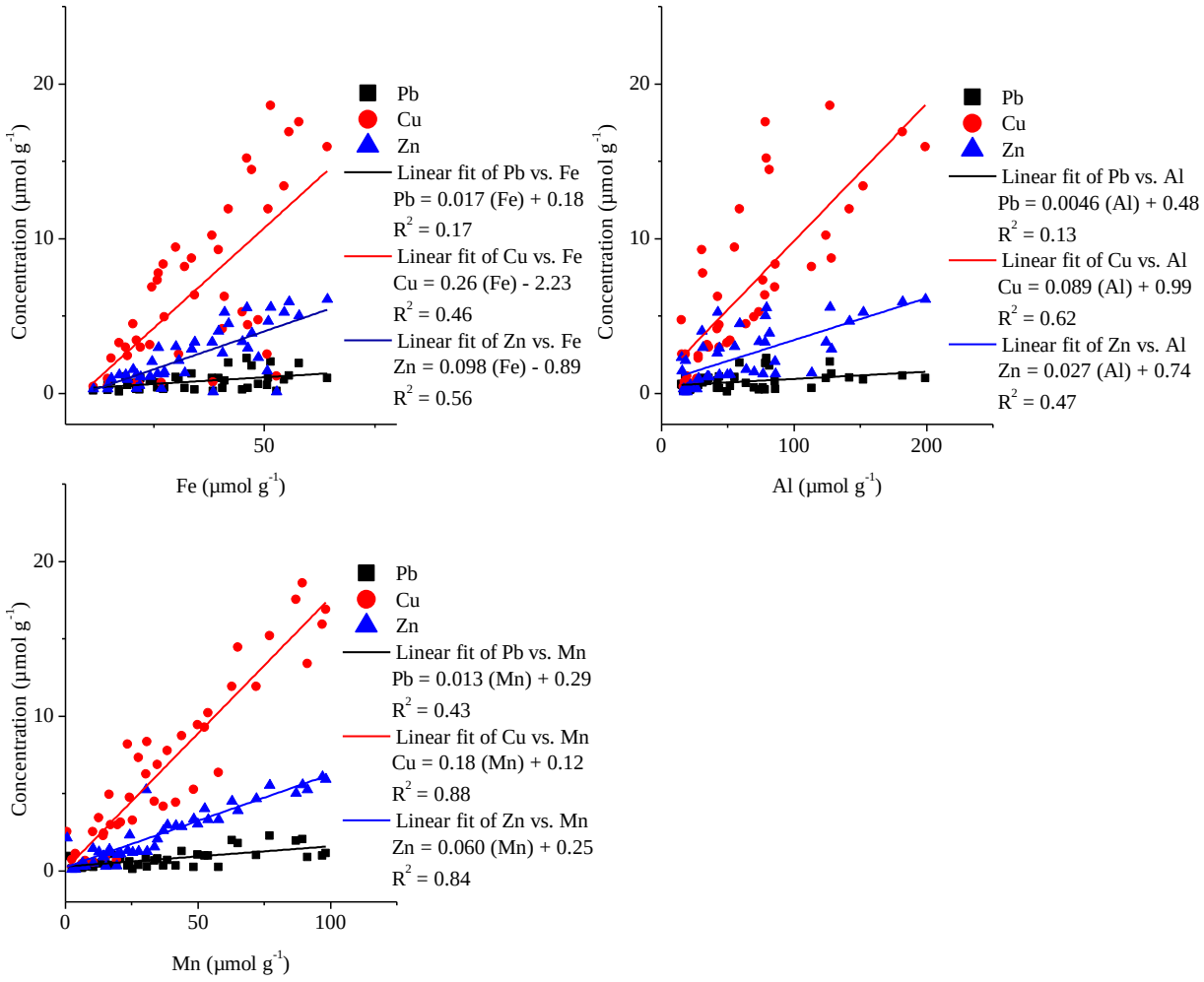

Figure 2.29. Correlations of Pb, Cu, and Zn with Fe, Al, and Mn from the amorphous Fe/Mn fraction of the extraction of sediment taken from the streambed of Left Hand Creek with lead, copper, and zinc from the same fraction.

Table 2.4. Statistics of full data set including the number of observations considered, maximum, minimum, median, mean, standard deviation (SD), and coefficient of variation (CV) of each dataset. Colloidal and dissolved concentrations of a metal are indicated by a subscript (Zn_{coll} = concentration of colloidal zinc and Zn_{diss} = concentration of dissolved zinc).

Statistic	Cl^-	Zn_{diss}	Zn_{coll}	Cu_{diss}	Cu_{coll}	Pb_{diss}	Pb_{coll}	Fe_{diss}	Fe_{coll}	Mn_{diss}	Mn_{coll}	Al_{diss}	Al_{coll}	DO saturation	cond	pH	head gradient	*K*
High-Flow	----------µM----------													(%)	µS cm^{-1}		cm cm^{-1}	cm s^{-1}
Number	54	54	54	54	54	54	54	54	54	54	54	54	54	56	57	57	50	50
Max	71.8	45.4	2.4	56.0	6.7	0.07	0.05	17.1	53.8	54.5	3.5	163.8	77.7	1.00	516.0	4.1	0.87	0.02
Min	10.1	0.5	0.01	0.02	0.001	0.001	0.0001	0.3	0.0040	0.01	0.004	0.2	0.01	0.03	94.3	6.8	-0.40	0.01
Median	49.2	2.9	0.2	0.33	0.07	0.01	0.00	0.7	1.3	0.4	0.2	1.1	2.5	0.73	181.8	6.2	-0.003	0.01
Mean	45.7	8.7	0.3	3.3	0.4	0.01	0.01	1.5	3.4	8.5	0.5	15.5	6.2	0.67	237.5	4.9	-0.02	0.01
SD	14.5	11.2	0.5	8.6	1.0	0.02	0.01	2.8	8.0	17.2	0.8	32.6	11.3	0.25	133.6	4.6	0.19	0.003
CV	31.7	128.9	131.8	256.1	240.8	112.1	166.4	191.2	235.2	202.7	159.2	210.0	183.2	37.0	56.2	241.6	-942.4	22.6
Statistic	Cl^-	Zn_{diss}	Zn_{coll}	Cu_{diss}	Cu_{coll}	Pb_{diss}	Pb_{coll}	Fe_{diss}	Fe_{coll}	Mn_{diss}	Mn_{coll}	Al_{diss}	Al_{coll}	DO saturation	cond	pH	head gradient	*K*
Low flow	----------µM----------													(%)	µS cm^{-1}		cm cm^{-1}	cm s^{-1}
Number	57	57	57	57	57	57	57	57	57	57	57	57	57	50	52	53	50	50
Max	23.1	12.9	0.7	15.2	3.7	0.1	0.3	6.7	52.0	38.8	11.1	99.6	42.2	1.0	564.0	3.8	0.2	0.02
Min	13.2	0.1	0.01	0.01	0.003	0.002	0.0004	0.7	0.04	0.02	0.005	0.4	0.01	0.2	70.2	6.6	-0.8	0.01
Median	18.8	2.2	0.0	0.2	0.05	0.02	0.0004	1.7	0.6	0.2	0.4	1.1	1.8	0.7	139.4	6.0	-0.1	0.01
Mean	18.1	3.7	0.1	2.3	0.3	0.02	0.03	2.4	5.0	5.9	1.5	13.8	5.1	0.7	249.1	4.7	-0.1	0.01
SD	2.8	3.8	0.2	4.8	0.7	0.02	0.1	1.4	10.2	12.2	2.1	30.9	8.4	0.2	173.8	4.3	0.2	0.003
CV	15.5	102.6	204.2	208.5	219.4	91.8	224.7	61.0	203.1	207.9	144.0	223.7	165.4	29.5	69.8	229.6	-151.2	22.6

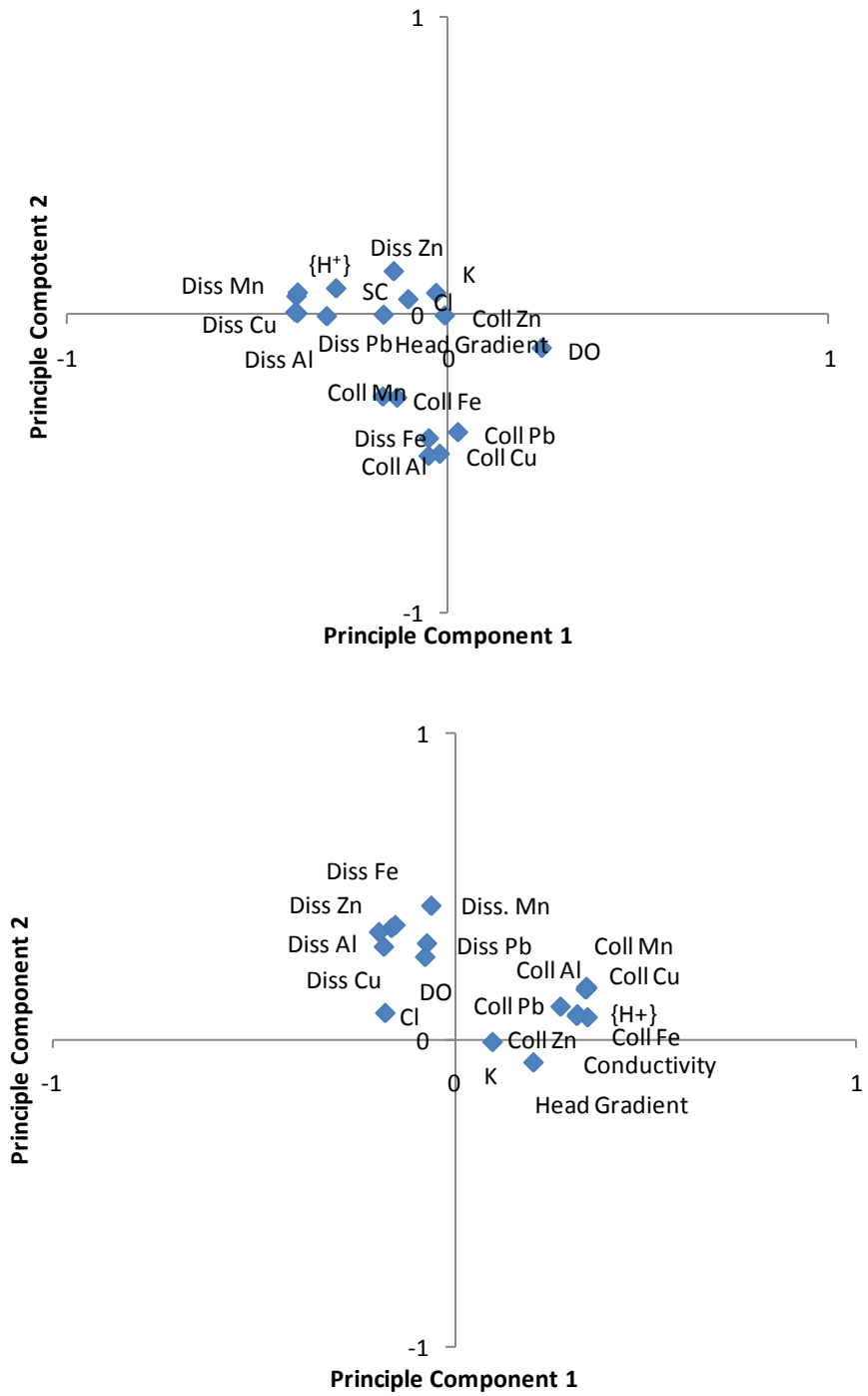

Figure 2.30. High flow (upper) and low flow (lower) loadings (eigenvectors) for the first and second principle components. Principle component analysis was performed on parameters from the high flow and low flow data built from Left Hand Creek surface and subsurface water analyses.

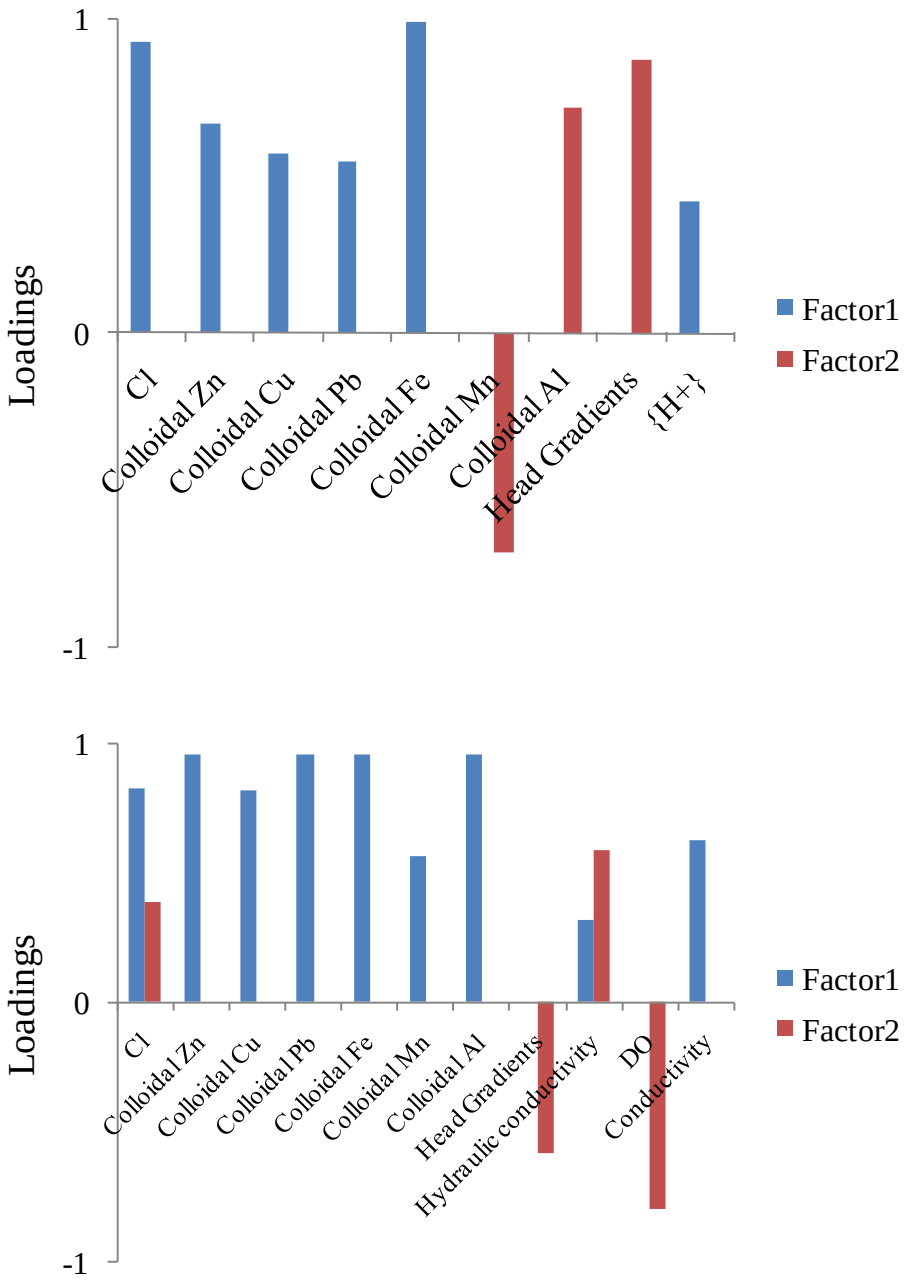

Figure 2.31. Rotated factor correlation coefficients for the Cl, colloidal Zn, Cu, Pb, Fe, Mn, and Al concentrations and physical chemical parameters. Only values greater than 0.3 are shown.

CONCLUSIONS

These experiments illustrate the difficulties in integrating stream and subsurface measurements. Modeling and subsurface measurements indicate differences in the importance of stream-subsurface exchange. Subsurface flows are difficult to track and understand. In this case, there were long, lateral flow paths that supply acid mine drainage water from the flow that spreads out adjacent to the stream. These flows complicated analysis of the stream-subsurface exchange of metals by making the both the groundwater and the surface water a potential source of metals.

Iron, manganese, and aluminum oxides can act as sorbents for other trace metals of interest (Dzombak and Morel 1990; Gandy et al., 2007). The high colloidal concentrations of lead and copper and their close relationship with iron, manganese, and aluminum in the stream and hyporheic zone suggests that they adsorb to mobile colloidal forms of these oxides under the stream flow and chemical conditions present in the study reach. These colloids are likely immobilized by colloidal filtration mechanisms as described by Ren et al. (2000) and constitute the amorphous coatings found on the sediment grains. Colloidal fractions of the lead and copper are highest in the upper 20 cm of the streambed. However, comparison of the colloidal concentrations with dissolved concentrations in the hyporheic zone suggests that colloid-facilitated metal transport does occur.

These results suggest that hyporheic exchange is minor relative to overall stream transport and the impact of exchange on metal removal will be small. However, exchange does occur and these metals accumulate in the sediments over time. In this case, it is likely that contaminant metals in the stream will continue to undergo exchange and accumulate in the sediments for considerable distances downstream of the acid mine drainage input. The extent of

attenuation in other systems will depend on the rate of hyporheic exchange and the rate of transport through the stream. With decreasing flow rate and stream water velocity, Karwan and Saiers (2009) noted an increase in the extent of hyporheic exchange. The resulting large-scale sediment contamination has the potential to complicate cleanup efforts - If remediation projects eliminate the effects of acid mine drainage, the sediment may provide a new source of metal contamination to the stream channel. Metals could be remobilized if changes in chemical conditions cause dissolution from the sediments or if turbulence due to storms and flooding resuspends colloid- and sediment-bound metals (Horowitz, 1990; Kimball et al., 1995; Butler et al., 2008).

REFERENCES

American Public Health Association (2005) Standard methods for the examination of water and wastewater (21st ed): Washington, D.C., published jointly by American Public Health Association, American Water Works Association, and Water Environment Federation, Washington, DC.

Axtmann, E.V., Luoma, S.N. (1991) Large-cale distribution of metal contamination in the finegrained sediments of the Clark Fork River, Montana, USA. *Applied Geochemistry* 6 (1) 75-88.

Bencala, K.E. (1983) Simulation of solute transport in a mountain pool-and-riffle stream with a kinetic mass transfer model for sorption. *Water Resources Research* 19 (3) 732-738.

Bencala, K.E. (1984) Interactions of solutes and streambed sediment 2. A dynamic analysis of coupled hydrologic and chemical processes that determine solute transport. *Water Resources Research* 20 (12) 1804-1814.

Benner, S.G., Smart, E.W., Moore, J.N. (1995) Metal behavior during surface groundwater interaction, Silver-Bow Creek, Montana. *Environmental Science & Technology* 29 (7) 1789-1795.

Butler, B.A., Ranville, J.F., Ross, P.E. (2008) Observed and modeled seasonal trends in dissolved and particulate Cu, Fe, Mn, and Zn in a mining-impacted stream. *Water Research* 42 (12) 3135-3145.

Cahoon, D.R., Lynch, J.C., Knaus, R.M. (1996) Improved cryogenic coring device for sampling wetland soils. *Journal of Sedimentary Research* 66 (5) 1025-1027.

Chapman, B.M., Jones, D.R., Jung, R.F. (1983) Processes controlling metal-ion attenuation in acid-mine drainage streams. *Geochimica et Cosmochimica Acta* 47 (11) 1957-1973.

Cobb, H.S. (1988) *Prospecting Our Past: Gold, Silver and Tungsten Mills of Boulder County*. The Book Lode, Longmont, Colorado.

Davies, S.H.R., Morgan, J.J. (1989) Manganese(II) oxidation-kinetics on metal-oxide surfaces. *Journal of Colloid and Interface Science* 129 (1) 63-77.

Davis, M.W., Streufert, R.K. (1990) Gold occurrences of Colorado. Resource Series 28, Colorado Geological Survey, Denver, Colorado.

Dzombak, D.A., Morel, F.M.M., 1990. *Surface Complexation Modeling: Hydrous Ferric Oxide*. John Wiley & Sons, New York.

Farag, A.M., Woodward, D.F., Goldstein, J.N., Brumbaugh, W., Meyer, J.S. (1998) Concentrations of metals associated with mining waste in sediments, biofilm, benthic macroinvertebrates, and fish from the Coeur d'Alene River Basin, Idaho. *Archives of Environmental Contamination and Toxicology* 34 (2) 119-127.

Farag, A. M., Nimick, D. A., Kimball, B. A., Church, S. E., Harper, D. D., Brumbaugh, W. G. (2007) Concentrations of metals in water, sediment, biofilm, benthic macroinvertebrates, and fish in the Boulder River watershed, Montana, and the role of colloids in metal uptake. *Archives of Environmental Contamination and Toxicology 52*(3) 397-409.

Fuller, C.C., Davis, J.A., (1989) Influence of coupling of sorption and photosynthetic processes on trace element cycles in natural waters. *Nature* 340 (6228) 52-54.

Fuller, C. C., Harvey, J. W. (2000) Reactive uptake of trace metals in the hyporheic zone of a mining-contaminated stream, Pinal Creek, Arizona. *Environmental Science & Technology 34*(7) 1150-1155.

Galán, E., Gomez-Ariza, J.L., Gonzalez, I., Fernandez-Caliani, J.C., Morales, E., Giraldez, I. (2003) Heavy metal partitioning in river sediments severely polluted by acid mine drainage in the Iberian Pyrite Belt. *Applied Geochemistry* 18 (3) 409-421.

Gandy, C.J., Smith, J.W.N., Jarvis, A.P. (2007) Attenuation of mining-derived pollutants in the hyporheic zone: A review. *Science of the Total Environment* 373 (2-3) 435-446.

Ganguli, P.M., Mason, R.P., Abu-Saba, K.E., Anderson, R.S., Flegal, A.R. (2000) Mercury speciation in drainage from the New Idria mercury mine, California. *Environmental Science & Technology* 34 (22) 4773-4779.

Hart, B.T., Noller, B.N., Legras, C., Currey, N. (1992) Manganese speciation in Magela Creek, Northern Australia. *Australian Journal of Marine and Freshwater Research* 43 (2) 421-441.

Harvey, J.W., Bencala, K.E. (1993) The effect of streambed topography on surface-subsurface water exchange in mountain catchments. *Water Resources Research* 29 (1) 89-98.

Harvey, J.W., Wagner, B.J. (2000) Quantifying hydrologic interactions between streams and their subsurface hyporheic zones. In *Streams and Ground Waters*, Jones, J.B., Mulholland, P.J. (Eds.), Academic Press, San Diego, p. 3.

Hill, M.T.R. (1999) A freeze-corer for simultaneous sampling of benthic macroinvertebrates and bed sediment from shallow streams. *Hydrobiologia* 412, 213-215.

Horowitz A. F., Rinella F.A., Lamothe P., Miller T.L., Edwards T.K., Roche R.L., Rickert D.A. (1990) Variations in suspended sediment and associated trace element concentrations in selected riverine cross sections. *Environmental Science & Technology* 24 (9), 1313-1320.

Hvorslev, M.J. 1951. Time lag and soil permeability in groundwater observations. U.S. Army Corps of Engineers, Waterways Experimental Station. Vicksburg, Mississippi, Bulletin 36, 57 p.

Johnson, C.A. (1986) The regulation of trace-element concentrations in river and estuarine waters contaminated with acid-mine drainage – The adsorption of Cu and Zn on amorphous Fe oxyhydroxides. *Geochimica et Cosmochimica Acta* 50 (11) 2433-2438.

Kennedy, V.C., Jackman, A.P., Zand, S.M., Zellweger, G.W., Avanzino, R.J. (1984) Transport and concentration controls for chloride, strontium, potassium and lead in Uvas Creek, a small cobble-bed stream in Santa Clara County, California, U.S.A. 1. Conceptual Model. *Journal of Hydrology* 75 (1-4) 67-110.

Kimball, B.A. Callender, E., Axtmann, E.V., (1995) Effects of colloids on metal transport in a river receiving acid-mine drainage, Upper Arkansas River, Colorado, USA. *Applied Geochemistry* 10 (3) 285-306.

Kimball, B.A., Mcknight, D.M., Wetherbee, G.A., Harnish, R.A. (1992) Mechanisms of iron photoreduction in a metal-rich, acidic stream (St. Kevin Gulch, Colorado, USA). *Chemical Geology* 96 (1-2) 227-239.

Lee, D. R., Cherry, J. A. (1978) A Field Exercise on Groundwater Flow Using Seepage Meters and Mini-piezometers. Journal of Geological Education 27, 6 - 10.

Malcolm, I.A., Soulsby, C., Youngson, A.F., Hannah, D.M., McLaren, I.S., Thorne, A. (2004) Hydrological influences on hyporheic water quality: implications for salmon egg survival. *Hydrological Processes* 18 (9) 1543-1560.

Martinez, C. E. and McBride, M. B. (1998) Solubility of Cd^{2+}, Cu^{2+}, Pb^{2+}, and Zn^{2+} in aged coprecipitates with amorphous iron hydroxides. *Environmental Science & Technology* 32, 743-748.

Munk, L., Faure, G., Pride, D.E., Bigham, J.M. (2002) Sorption of trace metals to an aluminum precipitate in a stream receiving acid rock-drainage; Snake River, Summit County, Colorado. *Applied Geochemistry* 17 (4) 421-430.

Nagorski, S.A., Moore, J.N., Smith, D.B. (2002) Distribution of metals in water and bed sediment in a mineral-rich watershed, Montana, USA. *Mine Water and the Environment* 21 (3) 121-136.

R Development Core Team, 2009. R: A Language and Environment for Statistical Computing. R Foundation for Statistical Computing (Ed.), Vienna, Austria.

Rampe, J.J., Runnells, D.D. (1989) Contamination of water and sediment in a desert stream by metals from an abandoned gold mine and mill, Eureka District, Arizona, USA. *Applied Geochemistry* 4 (5) 445-454.

Ranville, M., Rough, D., Flegal, A.R. (2004) Metal attenuation at the abandoned Spenceville copper mine. *Applied Geochemistry* 19 (5) 803-815.

Reed, S. J. B. (1996) Electron microbe analysis and scanning electron microscopy in geology. Cambridge University Press, New York, 201 pp.

Ren, J.H., Packman, A.I. (2004a) Modeling of simultaneous exchange of colloids and sorbing contaminants between streams and streambeds. *Environmental Science & Technology* 38 (10) 2901-2911.

Ren, J.H., Packman, A.I. (2004b) Stream-subsurface exchange of zinc in the presence of silica and kaolinite colloids. *Environmental Science & Technology* 38 (24) 6571-6581.

Ren, J.H., Packman, A.I. (2005) Coupled stream-subsurface exchange of colloidal hematite and dissolved zinc, copper, and phosphate. *Environmental Science & Technology* 39 (17) 6387-6394.

Ren, J.H., Packman, A.I., Welty, C. (2000) Correlation of colloid collision efficiency with hydraulic conductivity of silica sands. *Water Resources Research* 36 (9) 2493-2500.

Runkel, R.L. (1998) One-dimensional transport with inflow and storage (OTIS): A solute transport model for streams and rivers. Water-Resources Investigations Report 98-4018, U.S. Geological Survey, Denver, Colorado.

Runkel, R.L. (2002) A new metric for determining the importance of transient storage. *Journal of the North American Benthological Society* 21 (4) 529-543.

Runkel, R.L., Kimball, B.A., Bencala, K.E., McKnight D. M. (1999) Reactive solute transport in streams: a surface complexation approach for trace metal sorption. *Water Resources Research* 35 (12) 3829-3840.

Schemel, L.E., Kimball, B.A., Bencala, K.E. (2000) Colloid formation and metal transport through two mixing zones affected by acid mine drainage near Silverton, Colorado. *Applied Geochemistry* 15 (7) 1003-1018.

Schemel, L.E., Kimball, B.A., Runkel, R.L., Cox, M.H. (2007) Formation of mixed Al-Fe colloidal sorbent and dissolved-colloidal partitioning of Cu and Zn in the Cement Creek - Animas River confluence, Silverton, Colorado. *Applied Geochemistry* 22 (7) 1467-1484.

Schwertmann, U., Cornell, R.M. (2000) *Iron Oxides in the Laboratory: Preparation and Characterization*. Wiley-VCH, New York.

Storey, R.G., Howard, K.W.F., Williams, D.D. (2003) Factors controlling riffle-scale hyporheic exchange flows and their seasonal changes in a gaining stream: A three-dimensional groundwater flow model. *Water Resources Research* 39 (2) 1034.

Theobald, P.K., Lakin, H.W., Hawkins, D.B. (1963) The precipitation of aluminum, iron and manganese at the junction of Deer Creek with the Snake River in Summit-County, Colorado. *Geochimica et Cosmochimica Acta* 27 (2) 121-132.

Tonkin, J.W., Balistrieri, L.S., Murray, J.W. (2002) Modeling metal removal onto natural particles formed during mixing of acid rock drainage with ambient surface water. *Environmental Science & Technology* 36 (3) 484-492.

Triska, F.J., Kennedy, V.C., Avanzino, R.J., Zellweger, G.W., Bencala, K.E. (1989) Retention and transport of nutrients in a third-order stream: channel processes. *Ecology* 70 (6) 1877-1892.

USEPA, 2003. Left Hand Creek watershed case study: Use of NPL as a catalyst for abandoned mine cleanup. United States Environmental Protection Agency, 6 p. (accessed on March 17, 2011, at http://www.epa.gov/aml/tech/lefthand.pdf).

USEPA/DOE, 2004. Mine waste technology program: Annual report 2004. United States Environmental Protection Agency and the Department of Energy, 51 p. (accessed March on 17, 2011, at http://www.epa.gov/nrmrl/std/mtb/mwt/annual/annual2004/annual2004.htm).

Wagner, B.J., Harvey, J.W. (1997) Experimental design for estimating parameters of rate-limited mass transfer: Analysis of stream tracer studies. *Water Resources Research* 33 (7) 1731-1741.

Wanty, R.B., Winter, T.C. (2000) A simple device for measuring differences in hydraulic head between surface water and shallow groundwater. Fact Sheet FS-077-00, U.S. Geological Survey, Washington, DC.

Wentz, D.A. (1974) Effect of mine drainage on the quality of streams in Colorado, 1971-72. *Colorado Water Resources Circular* 21, 117 p.

Wondzell, S.M. (2006) Effect of morphology and discharge on hyporheic exchange flows in two small streams in the Cascade Mountains of Oregon, USA. *Hydrological Processes* 20 (2) 267-287.

Wood, A.R. 2004. Characterization and prioritization of mining-related metal sources with metal loading tracer dilution tests, and a review of regulations and mine restoration funding resources, Lefthand Creek watershed, northwestern Boulder County, Colorado. M.S. Thesis, University of Colorado, Boulder, Colorado.

Wroblicky, G.J., Campana, M.E., Valett, H.M., Dahm, C.N. (1998) Seasonal variation in surface-subsurface water exchange and lateral hyporheic area of two stream-aquifer systems. *Water Resources Research* 34 (3) 317-328.

Zaramella, M., Marion, A., Packman, A.I. (2006) Applicability of the transient storage model to the hyporheic exchange of metals. *Journal of Contaminant Hydrology* 84 (1-2) 21-35.

CHAPTER 3 - FERRIC (OXY)HYDROXIDE COLLOID TRANSPORT AND SURFACE-SUBSURFACE EXCHANGE IN AN ACID MINE DRAINAGE-IMPACTED STREAM

ABSTRACT

To assess the role of colloids and hyporheic exchange in controlling metal transport in streams contaminated by acid mine drainage, we studied the exchange of colloids with the hyporheic zone of a contaminated reach. We injected synthesized ferric (oxy)hydroxide colloids into a stream contaminated by acid mine drainage and monitored their transport in the stream and subsurface pore waters. These colloids are similar to those occurring naturally in acid mine drainage-impacted systems. The ferric (oxy)hydroxide colloids were synthesized in the presence of yttrium to differentiate the injected colloids from colloids present in the stream. A one-dimensional transient storage model (OTIS) was used to quantify parameters describing the transport of the ferric (oxy)hydroxide colloids and bromide, which was injected to serve as a conservative tracer. Based on integration of the area under the tracer dilution plots at the upstream and downstream ends of the reach, 12.3% of the colloids were lost from the main channel over the 61 m reach. Comparing the colloids with the conservative tracer in the hyporheic zone reveals that greater than 98% of the colloid attenuation occurred within the upper 40 cm of the streambed at four locations downstream of the injection. Transient storage and first-order removal in the storage zone accounted for the loss of the ferrihydrite colloids from the stream. The rapid decline in the concentrations of colloids in the tail of the breakthrough curves indicates irreversible removal and indicates that modeling using first-order removal is acceptable. Accumulated colloids in the streambed sediments could make the sediments a source of contamination as turbulence due to storms and floods may resuspend colloids trapped in the streambed.

INTRODUCTION

Streams in mining regions of the United States have been contaminated by the flow of acidic, metal-laden discharges from mining sites. Metal contamination impairs aquatic ecosystems. Some metals accumulate in fish and create additional risk for humans who ingest them. As the population increases, the demand for drinking water has made the risk of human exposure through drinking water a larger issue. Understanding metal fate and transport is a key component of planning mine cleanups. Colloids have been shown to dominate the transport and removal of some metals such as lead and copper (Johnson, 1986; Kimball et al., 1995; Ganguli et al., 2000; Tonkin et al., 2002).

In acid mine drainage environments, ferric (oxy)hydroxides are consistently a major colloidal constituent (Benner et al., 1995; Sullivan and Drever, 2001; Zanker et al., 2003; Gandy et al., 2007). Ferric (oxy)hydroxides are formed by the oxidation of ferrous iron, which is released during the weathering of iron sulfide minerals. Generally, ferric (oxy)hydroxide colloids are very small; therefore, they offer high surface areas for adsorption of metals. Because of this adsorption capacity, it is likely that they play a major role in the transport of trace metals (Gandy et al., 2007).

Hyporheic exchange plays an important role in contaminant transport (Triska et al., 1989; Benner et al., 1995; Gandy et al., 2007). Hyporheic flow is driven by head gradients that force stream water into the subsurface, where the stream water mixes with groundwater before it re-enters the surface water downstream. The mixing of stream and groundwater in the hyporheic zone may cause removal and transformations of constituents in the water and on the sediment surfaces.

Colloids may be removed from the stream by settling to the sediment-water interface and through the processes of filtration, straining, and dissolution in the hyporheic zone. Sub-micrometer colloids settle slowly relative to advection in the stream; removal processes in the hyporheic zone have been suggested as the more important mechanism for removal of these small particles (Karwan and Saiers, 2009). Conversely, colloids may aggregate, depending on the stream chemistry, to form larger particles. At a pH near the point of zero charge for the colloid surface, the colloids will be more likely to aggregate. Colloids entering the hyporheic zone will be immobilized through physicochemical filtration (Brownian diffusion, interception, and sedimentation). Packman et al. (2000) described a fundamentally-based physicochemical model for colloid exchange based on the hydraulics of bed form-driven advective pore water flow and subsurface colloid transport processes. The model considered particle settling and physicochemical filtration by the bed sediment. Packman and Brooks (2001) showed that submicron colloids were carried into the subsurface through hydrodynamically-driven stream-subsurface exchange and trapped there. Ren and Packman (2004a) developed a model that predicted stream-subsurface exchange incorporating colloidal contaminant transport. The model was used to explain zinc transport coupled with silica and kaolinite colloids (Ren and Packman, 2004b) and the transport of hematite colloids in the presence of zinc, copper and phosphate(Ren and Packman, 2005) in experiments carried out in a recirculating flume with a sand bed. These studies emphasize that the link between contaminants and colloids makes it necessary to consider their transport simulataneously as colloid-contaminant interactions can alter both colloid and contaminant mobility.

The goal of this work was to quantify ferric (oxy)hydroxide colloid transport in an acid mine drainage-affected stream surface-subsurface system. We hypothesized that colloids would

be removed from the stream through hyporheic exchange and filtration in the bed sediments. A tracer dilution test involving bromide and colloids was conducted with continuous injection concentrations measured downstream in surface and subsurface pore waters. We used the bromide to determine the extent of hyporheic exchange and we compared the colloids with the bromide to determine the extent of colloid removal in the hyporheic zone. This allowed us to determine whether the colloids are removed in the subsurface or if they remain mobile and offer a transport mechanism for associated metals.

The injected colloids were labeled during the synthesis process in order to differentiate them from those already present in the stream. An ideal colloid tracer should be (1) readily distinguished from natural colloids, (2) easily measured at very low concentrations, (3) variable in size, density, and surface properties, (4) available in narrow (monodisperse) size distributions, (5) stable, both colloidally and compositionally, for the duration of the experiments, and (6) environmentally benign (Mahler et al., 1998; Ryan et al., 2000). Labeling of particles has been a useful technique for tracing their movement through groundwater systems (Puls and Powell, 1992; Mahler et al., 1998a, 1998b; Ryan et al., 2000). Puls and Powell (1992) used radiolabeled iron to trace the transport of iron oxides through aquifer material in a laboratory study. Mahler et al. (1998a; 1998b) developed methods of labeling montmorillonite clay to trace the transport of suspended solids in karst aquifers using lanthanides and DNA. Ryan et al. (2000) synthesized silica-coated titania (TiO_2) and zirconia (ZrO_2) colloids to trace mineral colloids for subsurface transport experiments.

The colloid injection performed concurrently with a conservative tracer injection allowed us to evaluate the transport of ferric (oxy)hydroxide colloids. We evaluated the removal of colloids from the stream over the reach of interest using first order removal coefficients in the

transient storage model. Subsurface pore water monitoring allowed for the determination of the extent of colloid transport or removal in the subsurface.

METHODS

Field Site

The colloid injection experiment was carried out on an acid mine drainage-affected reach of Left Hand Creek, a low-order alpine stream (Figure 3.1). The upstream end of the study site is marked by the entrance of acid mine drainage from the Big Five Tunnel, a the main source of metal contamination on the Captain Jack Mill Superfund site, which is located approximately 2.5 km south of Ward, Colorado.

Left Hand Creek originates in glacial and snow-melt waters at an elevation of approximately 4,200 m near the continental divide in northwestern Boulder County. The creek flows through the Ward Mining District, which produced gold and silver from veins that contained pyrite, galena, and chalcopyrite from 1858 to 1993 (Cobb, 1988; Davis and Streufert, 1990; USEPA, 2003). The legacy of this mining is significant metal contamination, with lead, copper, and zinc being the most abundant metals in the mine water.

Flow in Left Hand Creek is regulated by releases from the Left Hand Park Reservoir, which is located 5.5 km upstream of the study site. The reservoir stores snow-melt and spring runoff for agricultural releases throughout the year. The flow rate in Left Hand Creek in the vicinity of the study site ranges from about 0.015 $m^3 s^{-1}$ at base-flow to 0.15 $m^3 s^{-1}$ at high flow conditions during the spring snow-melt (Wood, 2004). A survey of the reach reveals a step-pool configuration characteristic of steep mountain channels with an average slope of 7%.

Field Piezometer Installation

Piezometers bundles were installed in October 2007 to sample pore waters of the hyporheic zone (Figure 3.1). The piezometers were made of polyethylene tubing (0.32 cm inside diameter, 0.64 cm outside diameter) with perforated tips (2.5 cm length, 0.1 cm diameter holes) covered by nylon mesh (0.5 mm) attached with duct tape, a design adapted from Wanty and Winter (2000). Piezometers of nine different lengths were bundled together and installed in the streambed at depths ranging from 5 cm to 100 cm (Figure 3.1). The bundles were installed by driving a steel pipe (5.1 cm diameter) filled with a steel rod into the streambed with a 27 kg electric hammer, removing the rod, inserting the piezometer bundle into the pipe, and withdrawing the pipe with a winch hoist and tripod while the piezometer bundle position was maintained. The target depth was 100 cm, but boulders limited the depth of driving to 60-95 cm in all but one sample location. The piezometer bundles used in this study were installed at four locations downstream of the acid mine drainage (Figure 3.1). The piezometer bundles were placed as near as possible to the thalweg of the stream if not prevented by boulders. Three of the piezometer bundles were located in pools at distances of 16 m, 23 m, and 77 m relative to the acid mine drainage inflow at 0 m. The remaining piezometer bundle at a distance of 42 m was located in a riffle.

Colloid Synthesis and Characterization

Colloids were synthesized using an adaptation of the method of Schwertmann and Cornell (2000) for ferrihydrite ($Fe_5OH_8 \cdot 4H_2O$) synthesis. Yttrium was incorporated into the synthesis method in order to label the colloids and differentiate them from the colloids already present in the stream. Yttrium was chosen because its size made it likely to fit within the structure of the ferrihydrite colloids and sorption of yttrium to ferric hydroxide has been well

characterized (Quinn et al., 2006). Ferric nitrate (0.4 M) was hydrolyzed in the presence of yttrium nitrate (0.2 M) by addition of sodium hydroxide (1 M) at a rate of 1 mL min^{-1} at 21ºC. The addition of 1 M sodium hydroxide resulted in ferric iron (0.4 M $Fe(NO_3)_3 \cdot 9\ H_2O$) hydrolysis at a rate of 333 µmol Fe min^{-1}. The rapid rate of hydrolysis was expected to result in formation of more amorphous, rather than more crystalline, 2-line ferrihydrite. The colloid suspension was centrifuged (2,200 *g* for 15 min), the water was decanted, and replaced with ultrapure (>18 MΩ cm) water, and the ferrihydrite was resuspended by applying a vortex for 10 s. This rinsing process was done five times and the colloids were collected in a 20 L high-density polyethelyne (HDPE) container. The yttrium-labeled ferrihydrite colloids were not dried prior to injection. The colloids were prepared over a period of 14 d before injection.

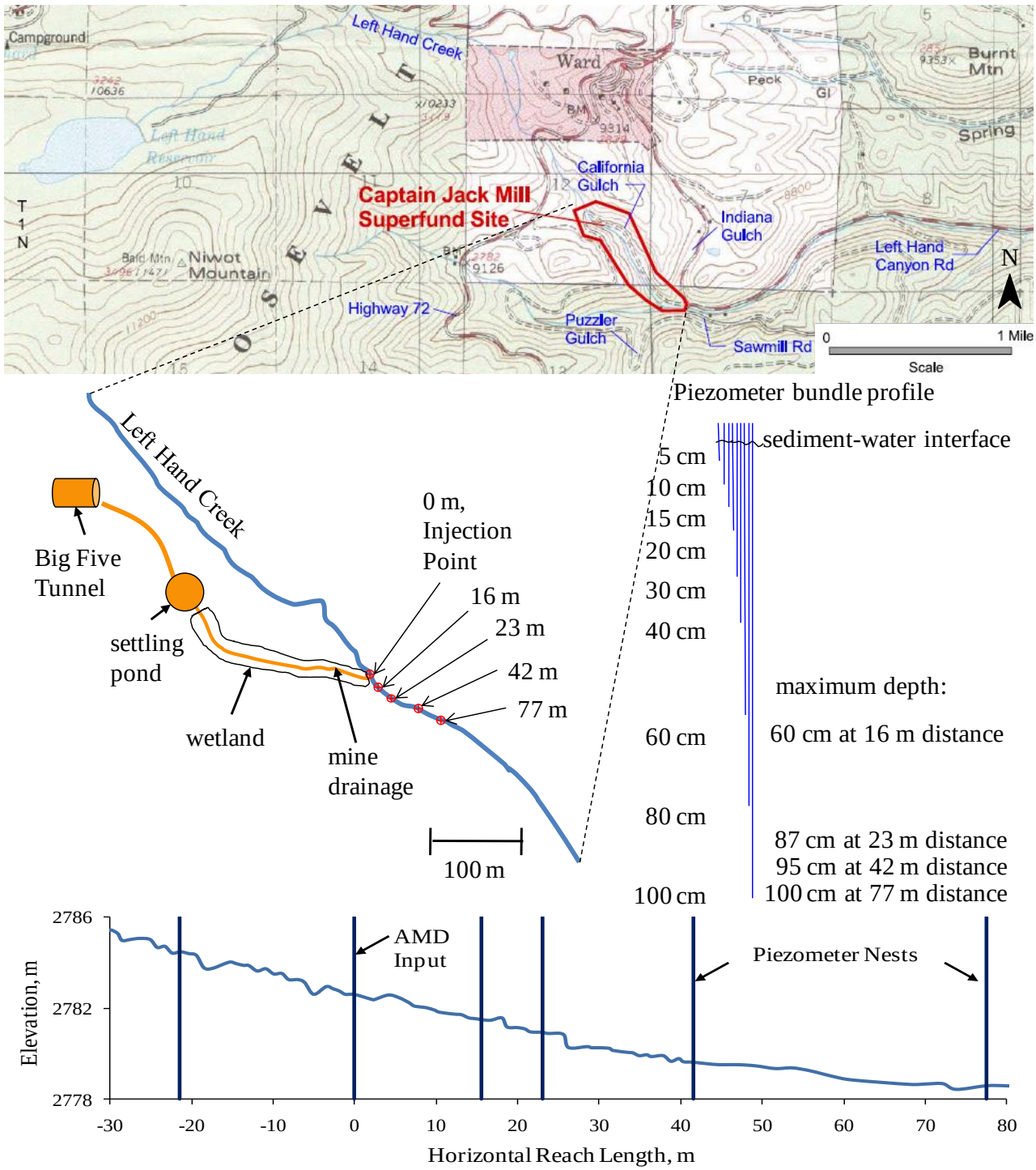

Figure 3.1. Topographic map (USGS 1:24,000; UTM zone 13, NAD 27) of study region along with sketch of field site including major features, sampling locations, piezometer bundle depths, and streambed profile with piezometer locations. The acid mine drainage enters the stream at 0 m. Due to the presence of large boulders in the streambed, some piezometers could not be installed to the intended 100 cm depth – for these, the maximum piezometer depth achieved is noted.

The colloids were analyzed for size, surface charge, elemental composition, and crystalline structure. To assess colloid size, morphology, and surface elemental composition, the colloids were air-dried on silicon wafers or on filters (0.1 μm, Nuclepore) for scanning electron microscopy/energy dispersive x-ray (SEM-EDX) analysis, using a field emission SEM (FESEM; JEOL JSM-7401F). The wafers and filters were taped to aluminum mounts with double-sided carbon tape and, in the case of the nonconductive filters, sputter-coated with a layer of gold and palladium (Cressington Sputter Coater 108auto; 0.08 mbar, 40 milliamps, 40 s) to lessen charging of the sample.

To assess colloid size, samples of the colloidal solution were mixed with stream water (7.2 μM as colloidal Fe) for dynamic light scattering (DLS; Particle Sizing Systems; 380 ZLS) at 21°C. The size was examined using Gaussian analysis of the autocorrelation function obtained from DLS. The number-weighted intensities were considered to be most representative of the colloid suspensions because they were expected to be made up largely of small particles.

The zeta potential of the colloids was measured in a solution of 1 mM KCl with laser Doppler microelectrophoresis (Brookhaven ZetaPALS () at 21°C. The pH of the colloid suspension was adjusted with 50 mM NaOH and allowed to equilibrate. The pH of the suspension was recorded immediately prior to zeta potential measurement.

For assessment of the crystallinity, colloids were dried at 60°C for 24 h and ground before placing on a mount for x-ray diffraction (XRD; D5000 Siemens) analysis. The sample was analyzed between 5 and 65° 2θ at 0.02° steps with a 5 s count per step using Cu K_α radiation. For comparison, ferrihydrite colloids were synthesized without yttrium present and analyzed by XRD. The diffraction patterns were analyzed with Jade 5 (Materials Data Inc.) software.

Tracer Dilution Test

The colloids and a conservative tracer, bromide (added as sodium bromide), were mixed with water pumped from the acid mine drainage into a polyethylene tank of 378 L (100 gal) volume. The concentrations of the injected constituents were 930 µM for Fe, 590 µM for yttrium, and 120 mM for bromide. The colloid suspension was injected into the stream at the point where the acid mine drainage enters the stream. The colloid suspension (378 L) was injected at a rate of 0.70 ± 0.01 L min^{-1} over a period of 9 h; the injection began at 7:00 and was stopped at 16:00. Stream discharge was determined using the tracer dilution method,

$$Q_{stream} = \frac{Q_{injection}[tracer]_{injection}}{[tracer]_{downstream} - [tracer]_{upstream}} \quad (3.1)$$

where Q_{stream} is stream discharge, $Q_{injection}$ is the injection flow rate, $[tracer]_{injection}$ is injection bromide concentration, $[tracer]_{upstream}$ is the upstream bromide concentration, and $[tracer]_{downstream}$ is bromide concentration at any downstream location once a steady concentration was reached. Stream discharge was calculated as 1,300 L min^{-1} (0.022 m^3 s^{-1}). Samples were collected periodically throughout the injection until one hour after the end of the injection. A single sample was collected the day after the injection, approximately 25 h after the start of the injection. To allow for comparison between the transport of the bromide and the colloids in both the stream and subsurface, the concentrations have been normalized by dividing by the maximum concentration of bromide or colloids at 16 m.

The relative breakthrough (*RB*) between the subsurface and main channel were calculated for the each location and depth. The relative breakthrough (%) of an injected constituent is a comparison of the time-integrated mass of the constituent relative to that of the conservative tracer (Harvey et al., 1989):

$$RB\ (\%) = \left[\int_{t_0}^{t_f} \frac{[C]_t}{[C]_0} dt \Big/ \int_{t_0}^{t_f} \frac{[tracer]_t}{[tracer]_0} dt \right] \times 100 \qquad (3.2)$$

where $[C]_0$ is the steady concentration in the surface, $[\text{tracer}]_0$ is the steady bromide concentration in the surface, $[C]_t$ and $[\text{tracer}]_t$ are the concentrations in the subsurface at time t, and t_0 and t_f are the times at the beginning and end of the breakthrough. The attenuation (%) of the injected constituent is 100 – *RB*.

Sample Collection

Samples were collected from the stream at distances of 16 m and 77 m downstream of the injection point. Samples were collected periodically throughout the injection until one hour after the end of the injection. A single sample was collected the day after the injection, approximately 35 h after the start of the injection. Samples were collected from piezometers at 5, 20, 40, and 100 cm (or deepest) depths in the subsurface, with the exception of the 16 m location. Piezometers were not installed to 100 cm depth at 16 m; therefore, the deepest depth at which samples were collected at the 16 m distance was 40 cm. Samples of hyporheic zone water were collected from the piezometers by withdrawing water with a syringe (polypropylene, 30 mL) at a rate of about 15 mL min^{-1} after purging about 1.5 volumes of water standing in the piezometers. The pore volume of each piezometer was calculated based on the length of the tubing below the water line. The depth of the stream was measured to the nearest centimeter prior to drawing water and used to estimate the volume of water standing in the tube. Purging and sample volumes were kept small to avoid cross-sampling between piezometers at nearby depths. A new syringe was used to take a sample from each piezometer with the only cleaning procedure being rinsing the syringe with the purged water. Surface samples were also collected with syringes rinsed with stream water. Because some of the yttrium remained dissolved in the colloidal suspension (Table 3.1), samples were filtered in the field with a 0.1 µm filter (Nuclepore,

polycarbonate). Filtration was assisted by the use of a device similar to a syringe pump which held six filter samples at a time and could be operated manually. The filters and the material on the filters after filtration were collected in bottles (high-density polyethylene, 30 mL) and stored in coolers prior to laboratory analysis. The molar ratio of Y:Fe was determined by measuring the yttrium and iron concentrations in the colloids collected on 0.1 µm filters from samples of the injection suspension and the stream. This ratio was used with further measurements of yttrium in the experimental samples to determine the colloidal iron concentrations.

Laboratory Analysis

Filters collected from the field were digested in the lab by adding 10 mL of 2% nitric acid and soaking in an oscillating (50 rpm) water bath for 16 h at 60°C. Yttrium and iron were measured by inductively coupled plasma-mass spectrometry (ICP-MS; Varian 810MS). Detection limits (DL) for iron and yttrium were 76 nM and 0.25 nM, respectively. Bromide was measured by ion chromatography (IC; Dionex DX-500) with a detection limit of 0.63 µM.

Table 3.1. Results of preliminary analyses showing the colloidal fraction of yttrium in samples of stream water with synthesized colloids added. Colloidal yttrium fraction was determined by the difference between the total and dissolved yttrium divided by the total.

Sample	Total Y ($\mu g\ L^{-1}$)	Dissolved Y ($\mu g\ L^{-1}$)	Colloidal Y Fraction
1	13.11	5.658	0.57
2	116.1	102.4	0.12

Transport Modeling

The surface concentrations from the tracer injections were modeled using OTIS-P (One-Dimensional Transport with Inflow and Storage with Parameter estimation; Runkel, 1998). The model estimates transport parameters using nonlinear regression techniques. The model was fit to the conservative tracer, bromide, to estimate dispersion (D) [$m^2\ s^{-1}$], stream cross-sectional area (A) [m^2], storage zone cross-sectional area (A_S) [m^2], and storage zone exchange

coefficient (α) [s^{-1}]. These parameters where then used in the models of the metal transport to estimate the first order removal rate coefficients for the main channel (λ) [s^{-1}] and the storage zone (λ_S) [s^{-1}]. The transient storage model includes any bodies of stationary water, including eddies and side pools, compared with the fast moving waters of the main channel to be part of the transient storage zone. For the purposes of this study, the storage zone referred to by the model is taken to be essentially equivalent to the stream hyporheic zone due to the lack of observed eddies or pools.

The data from observations made at the 16 m location were used as the upstream boundary conditions to model the reach from 16 m to 77 m. The observations at 77 m were used to fit the model. To allow for comparison between the transport of the bromide and the colloids in both the stream and subsurface, the concentrations have been normalized by dividing by the maximum concentration of bromide or colloids at 16 m.

Several metrics were calculated to evaluate the model and the impact of transient storage: (1) the relative size of the hyporheic zone (A_S/A), (2) the average distance a molecule travels downstream within the main channel prior to entering the storage zone ($L_S = u/\alpha$), (3)the hydraulic retention factor (average time water remains in storage relative to the hydraulic turnover length, $R_h = A_S/Q$), and (4) the fraction of median travel time due to transient storage, F_{med} (Runkel, 2002):

$$F_{med} \cong (1 - e^{-L(\alpha/u)}) \frac{A_S}{A + A_S} \tag{3.3}$$

where u is advective velocity (m s^{-1}) and L is the reach length (m) was also determined. F_{med} was evaluated at the standard distance of 200 m by setting L equal to 200 m (F_{med}^{200}) for comparison with other datasets. Damkohler numbers for transient storage (DaI_α) and colloid removal kinetics (DaI_λ) were calculated as:

$$DaI_{\alpha} = \frac{\alpha\left(1+\frac{A}{A_S}\right)L}{u} \tag{3.4}$$

$$DaI_{\lambda} = \frac{\lambda\left(1+\frac{A}{A_S}\right)L}{u} \tag{3.5}$$

The Damkohler number gives the ratio of the time scale of transient storage or removal to the time scale of advection through the reach.

In order to examine the importance of subsurface removal, colloid transport was also modeled by setting first-order removal rate coefficient for the main channel (λ) equal to zero and estimating the storage zone (λ_S) using OTIS. Underlying this technique is the assumption that all removal is occurring through hyporheic exchange with no removal occurring in the main channel. This procedure was used to determine to what extent subsurface removal could account for the colloid removal.

RESULTS

Colloid Characterization

The yttrium-labeled colloids were analyzed for elemental composition and size using SEM/EDX, ICP-MS, and DLS. The molar ratio of Y:Fe of the colloids was determined by a linear regression of measured values of yttrium and iron; the slope was 0.061 ± 0.001 (Figure 3.2). This ratio was determined by measuring yttrium and iron collected on 0.1 µm filters in samples of the injection suspension (the higher Y and Fe concentrations) and the stream (the lower Y and Fe concentrations). The slopes representing the ratio of Y:Fe were higher for both the stream and tank samples than that corresponding to the overall data (Figure 3.2).

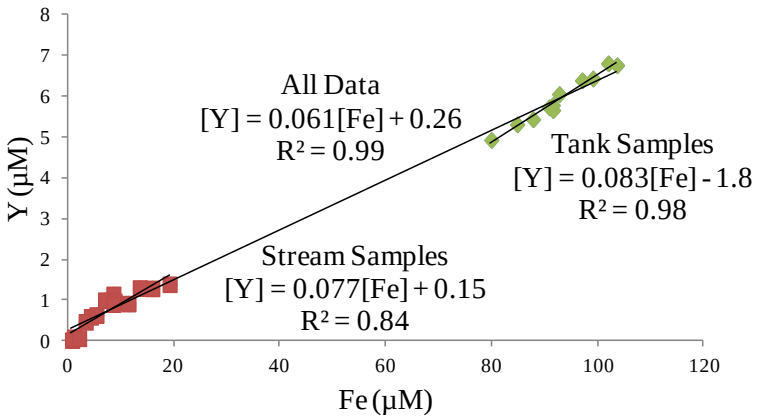

Figure 3.2. Plot of colloidal yttrium concentration as a function of colloid iron concentration in injection tank and stream samples collected during the injection experiment.

The digestion procedure was compared with select samples that were also analyzed by measuring the total yttrium and the dissolved yttrium passing through the 0.1 µm filters. The digestion involved adding 10 mL of 2% nitric acid to bottles containing the used filters and soaking in an oscillating water bath for 16 h at 60°C. The original sample volume (20 mL) filtered was used to calculate the in-stream colloidal yttrium concentration. The difference between the two measurements ranged from 4 to 57% (Table 3.2).

Table 3.2. Analysis of yttrium measurement as a substitute for iron colloid measurement. Colloidal yttrium from filter digestion procedure is compared with colloidal yttrium based on the difference between total and dissolved yttrium.

sample location and collection time	total Y (µM)	dissolved Y (µM)	colloidal Y based on difference between dissolved and total (µM)	colloidal Y based on digestion of colloids trapped on filter (µM)	colloidal Y fraction based on difference between total and dissolved	colloidal Y fraction based on digestion of colloids trapped on filter	difference between 'difference' and 'digestion' methods (%)
16 m, 10:00	1.77	0.48	1.28	0.57	0.73	0.32	55
16 m, 12:00	1.64	0.51	1.14	1.27	0.70	0.77	-12
77 m, 09:00	1.50	0.42	1.08	1.13	0.72	0.75	-4.0
77 m, 12:00	1.42	0.38	1.04	0.45	0.73	0.32	57

The yttrium-labeled colloids imaged by scanning electron microscopy appeared to aggregate during the drying process. Based on SEM images (Figure 3.3), the primary colloids were approximately 50-100 nm in diameter. The images also show evidence of aggregation,

which may have occurred during filtration. Dynamic light scattering was used to determine the colloid size in a dilute aqueous suspension of colloids (7.2 μM as Fe) in stream water at the pH of the stream (6.20). Analysis performed 1 h after mixing of the synthesized colloids indicated a non-Gaussian colloid distribution. The intensity-weighted Gaussian analysis indicated colloid diameter of 510 ± 310 nm while the number-weighted Gaussian diameter was 120 ± 100 nm (Figure 3.4). Zeta potential measurements made as a function of pH indicated that the point of zero charge of the yttrium-labeled colloids was increased compared to colloids composed of ferrihydrite (Figure 3.5).

X-ray diffraction showed low peak intensities indicating low crystallinity for the yttrium-labeled colloids. The peaks correspond with amorphous ferrihydrite as well as lepidocrocite (γ-FeO(OH)) (Figure 3.6). Yttrium precipitates cannot be entirely ruled out with this analysis, though no peaks associated with yttrium (oxy)hydroxides or oxides were identified. The formation of lepidocrocite may have occurred due to differences in the rate of hydrolysis during synthesis. The yttrium-labeled colloids were synthesized in larger quantities than the ferrihydrite; this may have resulted in zones where the pH was elevated due to incomplete mixing.

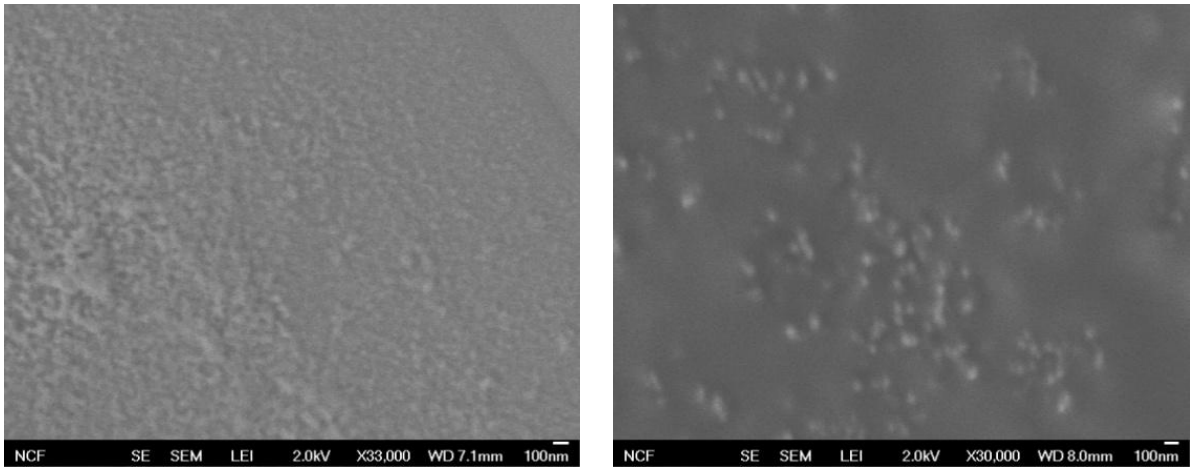

Figure 3.3. SEM images of the yttrium-labeled ferric (oxy)hydroxide colloids: (left) colloids from the injection suspension dried on a silicon wafer at 33,000× magnification; and (right) colloids collected on a filter from a stream sample during the injection experiment at 30,000× magnification. The accelerating voltage was 2 kV and the 100 nm scale bar is located in the lower right corner of each image.

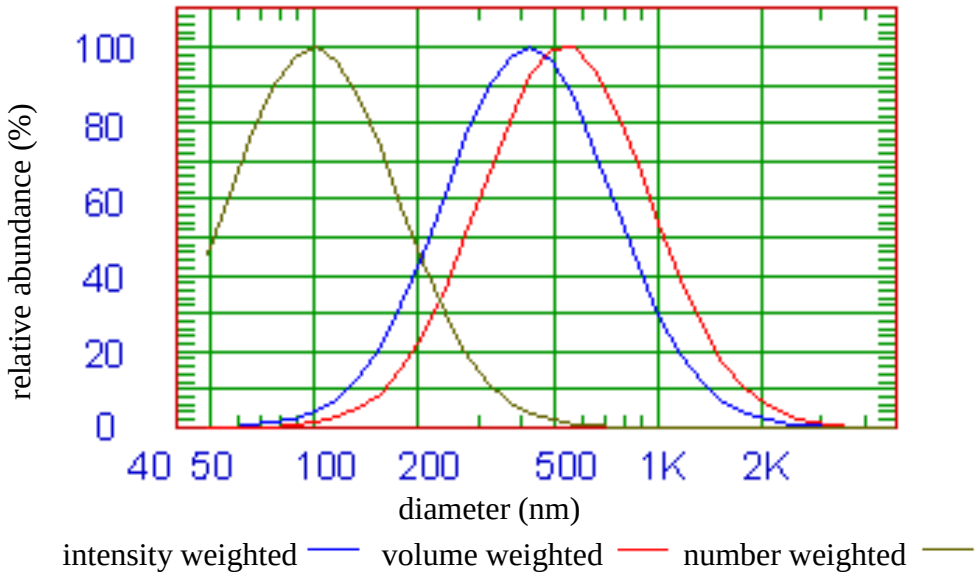

Figure 3.4. Relative abundance as a function of colloid diameter from DLS NICOMP distribution analysis.

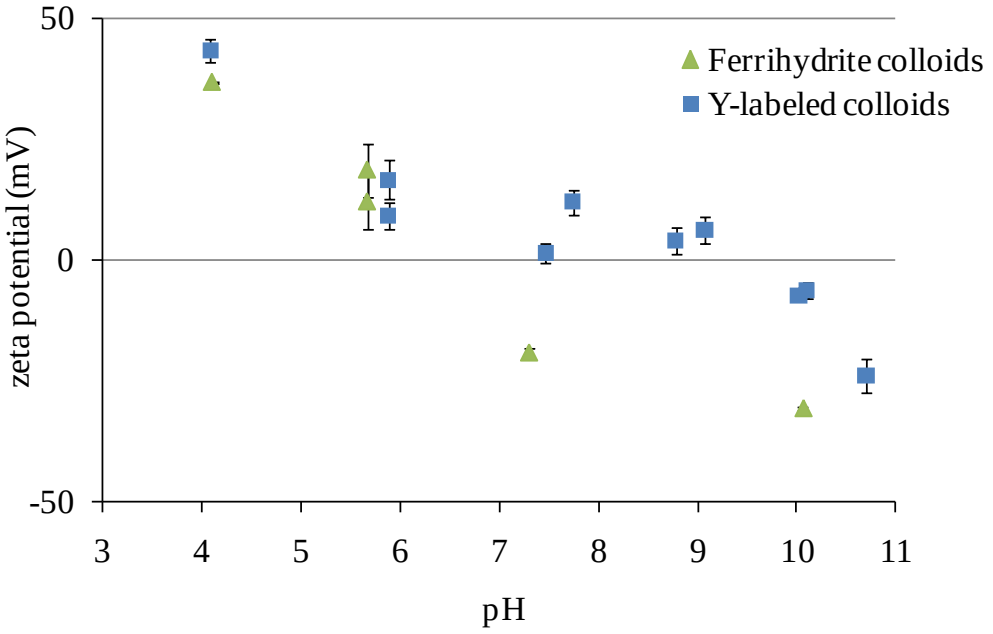

Figure 3.5. Zeta potential as a function of pH for Y-labeled colloids along with ferrihydrite colloids for comparison.

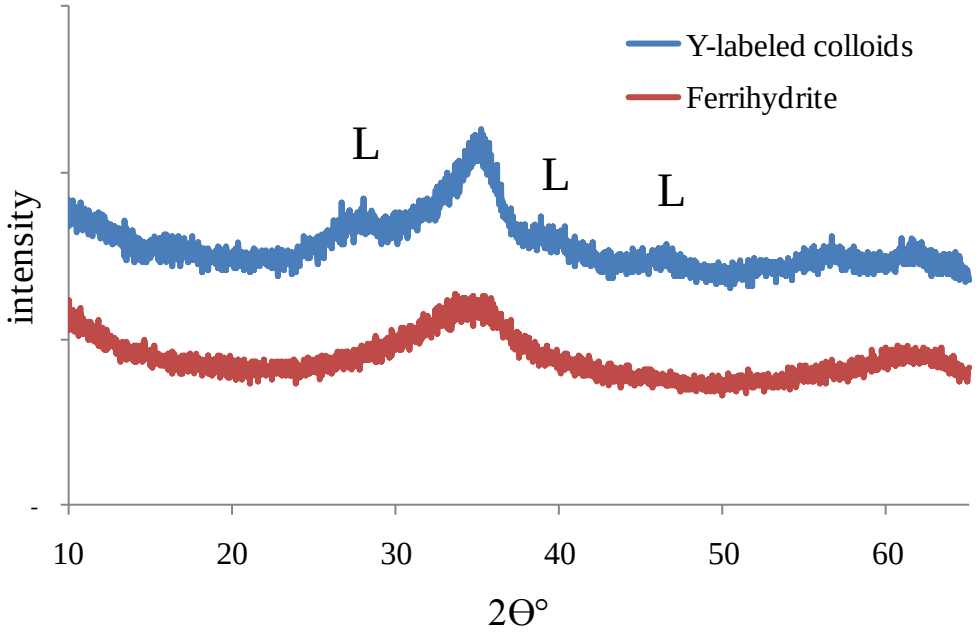

Figure 3.6. X-ray diffraction results showing yttrium-labeled colloids and pure ferrihydrite colloids for comparison. The peaks labeled with L are ascribed to lepidocrocite.

Stream-Subsurface Transport

Bromide measurements in the surface water show that there was little change in flow between the upstream end of the reach at 16 m and downstream end at 77 m (Figure 3.5). This indicates that dilution from tributaries and lateral inflow from groundwater was minor.

The difference in the normalized steady concentration between bromide and colloids indicates that colloids were removed through the reach (Figure 3.5). Comparison of the relative mass of colloids with relative mass of bromide appearing in the piezometers, most of the colloids entering the hyporheic zone are attenuated in the upper 5 cm (Figure 3.6; Table 3.3). The exception is at the 77 m distance, where the relative breakthrough (Equation 3.2) remained as high as 50% at the 5 cm depth.

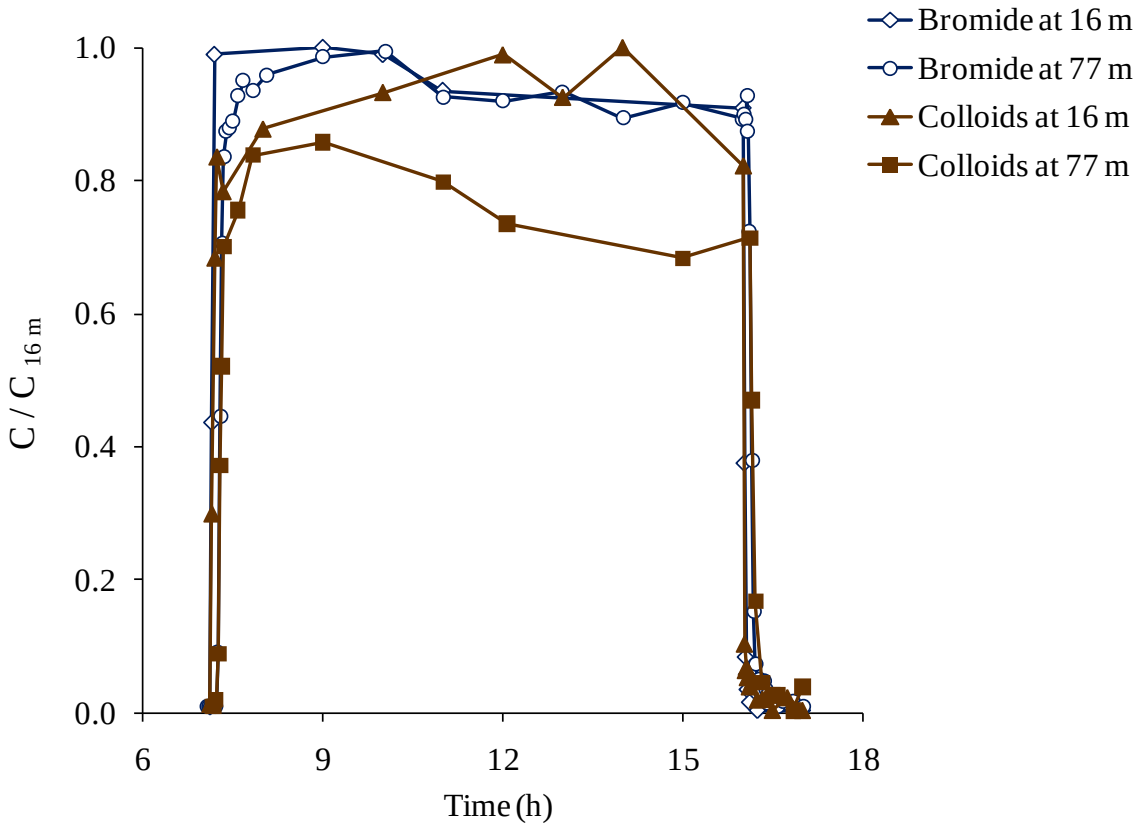

Figure 3.5. Surface water bromide and colloid breakthroughs at the upstream end of the reach (16 m) and the downstream end of the reach (77 m) normalized to the maximum upstream concentration at 16 m ($C_{16\,m}$).

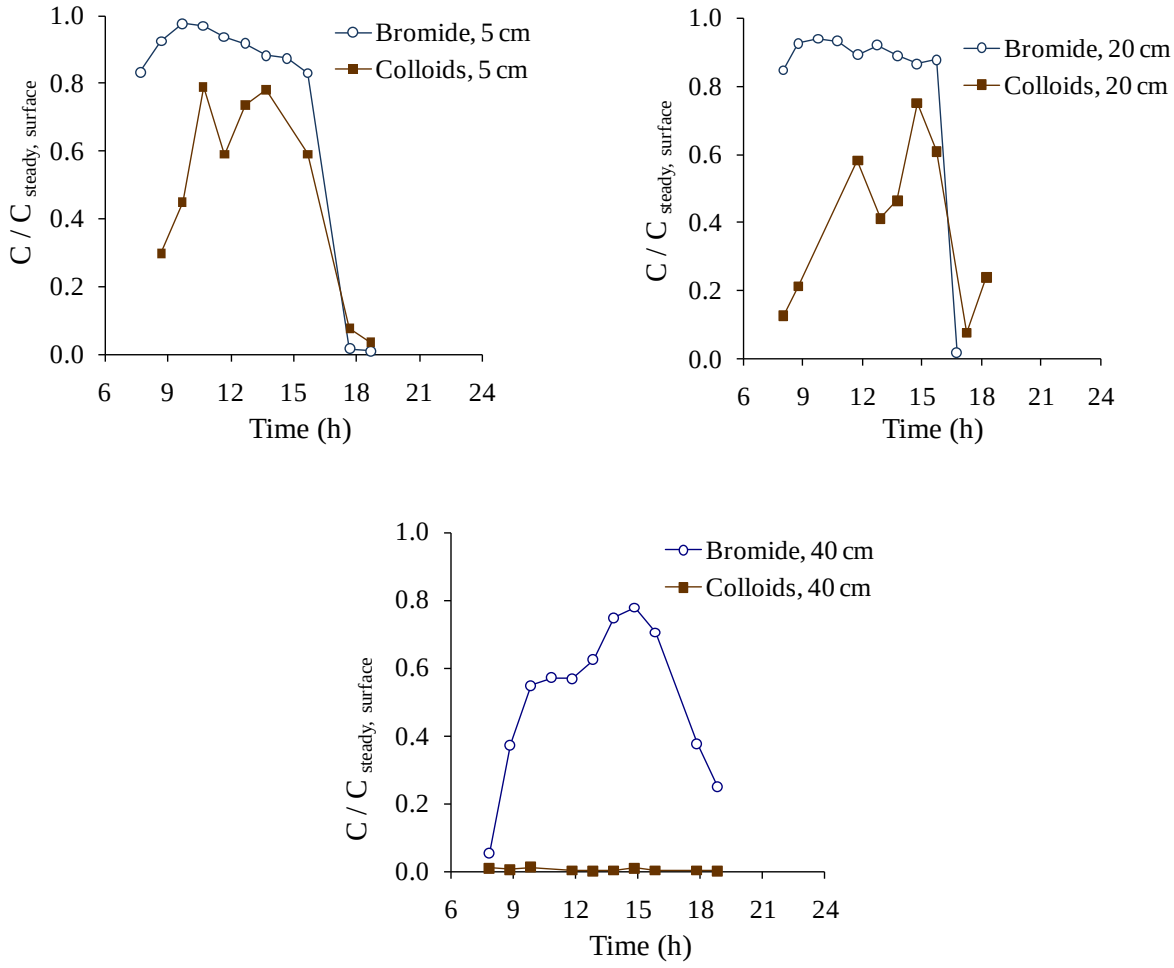

Figure 3.6. Breakthrough curves for colloids and bromide at subsurface depths of 5 cm, 20 cm, and 40 cm at the 77 m distance.

Table 3.3. Maximum normalized concentration for bromide and colloids in the subsurface, colloid relative breakthroughs (RB) calculated using Equation 1, and attenuation calculated as 100-*RB*.

Distance	Depth	bromide $(C/C_0)_{max}$	colloid $(C/C_0)_{max}$	*RB* (%)	Attenuation (%)
16 m	5 cm	0.32	0.011	0.72	99
16 m	20 cm	0.11	nd	nd	nd
16 m	40 cm	0.0087	nd	nd	nd
23 m	5 cm	0.98	0.30	19	81
23 m	20 cm	0.79	0.023	2.4	98
23 m	40 cm	0.059	nd	nd	nd
42 m	5 cm	0.65	0.022	2.4	98
42 m	20 cm	0.083	nd	nd	nd
42 m	40 cm	0.0087	nd	nd	nd
77 m	5 cm	0.98	0.79	63	37
77 m	20 cm	0.94	0.75	50	50
77 m	40 cm	0.78	0.012	1.1	99

nd - not determined with available data due to very low colloid concentrations relative to background concentrations.

Stream Transport Model

The bromide concentration dropped between 10:00 and 11:00, indicating an increase in flow at this time (Figure 3.7). Because the concentration was steady after this time, the flow was calculated based on this part of the injection experiment and the OTIS transport model was fit to the observed stream data collected after 11:30. A summary of model parameters is given in Table 3.4. The OTIS model parameters indicate that the storage zone area was small relative to the stream cross sectional area ($A_S/A = 0.14$). The hydraulic turnover length (L_s), which is the average distance water travels downstream within the main channel prior to entering the storage zone, was 1.0 km. The hydraulic retention factor (R_h), the average time that a water molecule remains in storage relative to the hydraulic turnover length, of 0.97 s m^{-1}. The fraction of median

travel time due to transient storage (F_{med}^{200}) was 0.023, meaning that transient storage accounts for 2.3% of total reach travel time.

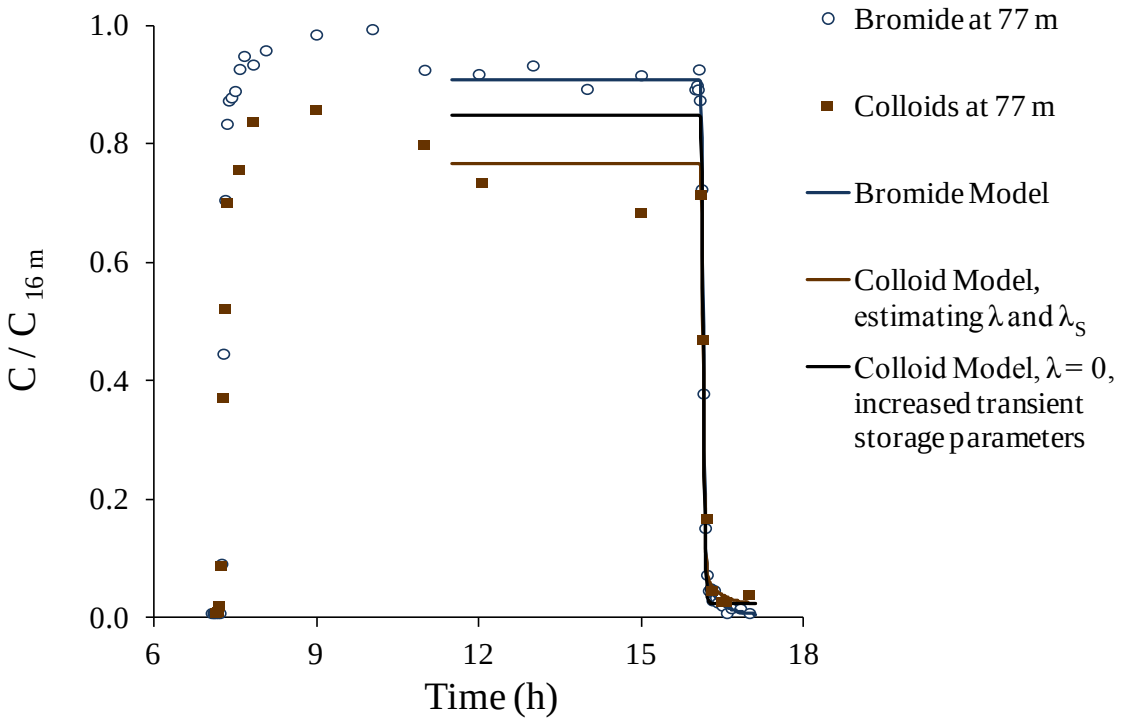

Figure 3.7. Breakthrough and OTIS-P fits of bromide and colloids in the surface water at a downstream distance of 77 m. The two colloid models show the fits of the two models: (1) estimating both main channel (λ) and storage zone (λ_S) removal coefficients and (2) setting $\lambda = 0$ and estimating λ_S. The injection began at 07:00 hours and ended at 16:00 hours; however the model simulation was performed only on data collected when flow was steady after 11:30. The observations at 16 m were used to define the upstream boundary conditions in the models. The concentrations were normalized to the maximum concentrations measured at 16 m.

The storage zone concentrations predicted by the OTIS-P models are compared with piezometer measurements in Figure 3.8. Based on integration of the area under the breakthrough curve, 12.3% of the colloids were lost over the 61 m reach. The colloid removal was modeled based on two scenarios: (1) estimating both main channel (λ) and storage zone (λ_S) removal coefficients and (2) setting $\lambda = 0$ and estimating λ_S. In the first scenario, removal rate coefficients for the main channel (λ) and for the storage zone (λ_S) were 3.0×10^{-4} s^{-1} and

8.6×10^{-17} s^{-1}, respectively. For colloid transport, DaI_{λ}, which is the ratio of the time scale of removal to the time scale of advection in the reach, was 0.14. For comparison, the Damkohler number obtained based on the storage zone removal rate, DaI_{λ_S}, was 4.1×10^{-14}. In the second scenario, the maximum removal rate coefficient for the storage zone (λ_S) obtained by setting $\lambda = 0$ was 5.6×10^{2} s^{-1}. The Damkohler number obtained based on the storage zone removal rate, DaI_{λ_S} was 2.7×10^{5}. The colloid models did not converge to a unique solution for either model scenario. The lack of convergence is likely due to the limited number of observed data points on the falling limb of the concentration plot and indicates that the parameters estimates are very uncertain.

Table 3.4. Summary of parameters based on OTIS-P modeling of tracer dilution tests with bromide and colloids and calculated metrics. The coefficient of variance is given in parentheses beside each modeled parameter.

bromide model	
Q (m^3 s^{-1})	0.021
v (m s^{-1})	0.14
D (m^2 s^{-1})	0.24 (0.10)
A (m^2)	0.15 (0.0093)
A_S (m^2)	0.021 (0.21)
α (s^{-1})	1.5×10^{-4} (0.30)
bromide model *RSS*[a]	0.097
DaI_{α}	0.89
T_{stor} (h)	0.16
R_h (s m^{-1})	1.7
L_s (m)	356
F_{med}^{200}	0.083

colloid model, estimating λ and λ_S	
λ (s^{-1})	3.0×10^{-4} [b]
λ_S (s^{-1})	8.6×10^{-17} [b]
colloid model *RSS*[a]	0.029
DaI_{λ}	0.14
DaI_{λ_S}	4.1×10^{-14}

colloid model, estimating λ_S when $\lambda = 0$	
λ_S (s^{-1}), when $\lambda = 0$	560 [b]
colloid model *RSS*[a]	0.047
DaI_{λ_S}	2.7×10^{5}

[a] *RSS* - residual sum of squares from the model.
[b] CV was not computed because the model did not converge on a unique solution; parameter uncertainty is large.

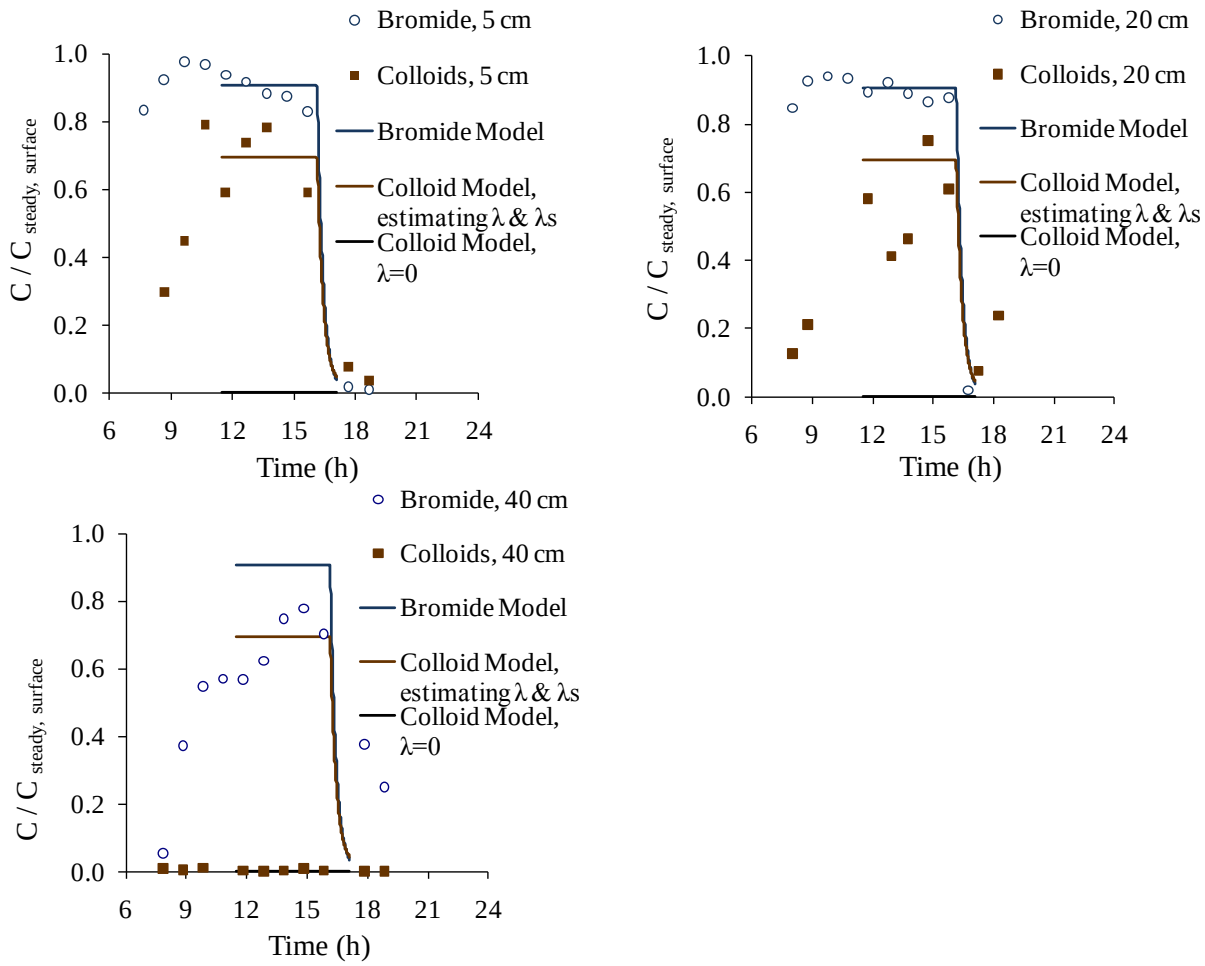

Figure 3.8. Breakthrough curves for colloids and bromide at subsurface depths of 5 cm, 20 cm, and 40 cm at the 77 m distance showing the OTIS-P models of subsurface bromide and colloids under the two scenarios: (1) estimating both main channel (λ) and storage zone (λ_S) removal coefficients and (2) setting $\lambda = 0$ and estimating λ_S.

DISCUSSION

Analysis of Yttrium as a Colloid Tracer

We developed and evaluated the use of yttrium to label ferric (oxy)hydroxide colloids for a stream tracer dilution test in the field. Yttrium labeling provided a cost-effective, relatively easy tracer for distinguishing injected colloids from those already present. The detection limit for yttrium is very low and it can be readily measured by ICP-MS. Yttrium-labeled colloids were similar in size to ferric (oxy)hydroxide colloids synthesized in the lab without yttrium

coprecipitation (Appendix 1). Zeta potential measurements indicate that yttrium labeling increased the point of zero charge (PZC) of the colloids from 6.6 ± 0.41 to 9.0 ± 0.48. The PZC of a crystalline yttrium oxide (Y_2O_3) has been measured to be 9.1 (Sprycha et al., 1992). As less crystalline structures typically have a higher point of zero charge, a fresh yttrium oxide precipitate is expected to have a PZC above 9.1. If the yttrium coprecipitated with the iron, a point of zero charge between that for a yttrium oxide precipitate and that for an iron oxide precipitate is expected. This result suggests that yttrium coprecipitated with the iron while the colloids formed. Comparison of the EDX measurements of the Y:Fe ratio with the digestion results supports this. The EDX measurements, which measure the surface composition, showed a lower Y:Fe ratio (0.03) than the bulk colloid composition, indicating that yttrium is found within the structure of the colloids. The PZC is also consistent with the point of zero charge of lepidocrocite (8.7; Schwertmann and Cornell, 2000), which is consistent with the presence of amorphous ferrihydrite and lepidocrocite as determined by XRD. At the pH of the stream (6.2), the surface charge of the synthesized colloids is expected to be positive and similar to that of pure ferrihydrite.

Yttrium was an environmentally non-toxic element at the levels used in the experiment. The yttrium concentration measured in the stream was approximately 50 µg L^{-1} over a period of 9 h. Also, the bioavailability of the yttrium in the colloidal form is limited. A study of acute toxicity of yttrium has shown an LC_{50}, the concentration resulting in 50% mortality over a 7 day period, for *Hyalella azteca*, commonly called scud, was 183 µg L^{-1} in water with a hardness of 18 mg L^{-1} as $CaCO_3$ and carbonate alkalinity of 14 mg L^{-1} as $CaCO_3$ (Borgmann et al., 2005).

We evaluated the error associated with the measurement of the colloidal yttrium concentration. The colloidal yttrium measured by digestion of the filters varied from the

colloidal yttrium determined by the difference in total and dissolved yttrium; in one sample, the 'digestion' method indicated yttrium was 55% lower than the 'difference' method (Table 3.2). This suggests that some yttrium could have been lost during the extra processing involved with the digestion procedure. If the digestion did not completely remove the colloids from the filter, this would have caused an under-estimation of the colloid concentration. The selected digestion method was chosen after examining a range of acid concentrations and digestion durations. These investigations found that more rigorous digestion did not increase the yttrium recovery. The original concentration in the stream was calculated based on the small sample volume (20 mL) filtered. This sample volume was measured in the field using a 30 mL syringe, which could have been slightly inaccurate and variable depending on the operator. There could also have been filter clogging, which may have limited the ability to pass all of the sample through the filter. This may explain the variation in the colloidal concentration during the steady injection.

The yttrium versus iron slope was reasonably linear over the wide range of concentrations analyzed. The Y:Fe ratio used for the estimate of colloid concentration was that determined by the overall data from Figure 3.2. The selection of this ratio may have led to a slight under-estimation of the colloid concentrations. However, the selection should not affect the model results because all concentrations are internally consistent and concentrations have been normalized to the maximum concentrations measured at 16 m to assist in comparison between the conservative tracer and the colloids.

Hyporheic Exchange

The piezometers indicated that the depth of hyporheic exchange varied throughout the reach with bromide found from 5 cm to 40 cm in the subsurface. The fraction of surface water in

the subsurface based on bromide measurements ranged from 0.32 - 0.98. The subsurface was well connected to 20 cm depth at the 23 m location and to 40 cm at 77 m location.

Several metrics can be used to evaluate the model reliability and the importance of transient storage (Table 3.4). The hydraulic retention factor (R_h) and fraction of median travel time due to transient storage (F_{med}^{200}) reflect rapid exchange with a small storage zone. Model parameters compared with the results of a past experiment on the reach under similar flow conditions show an increase in storage zone area and storage zone exchange rate (Table 3.5). However, these values are still relatively small.

Table 3.5. Comparison of advection and transient storage parameters in this experiment with those of a tracer injection experiment in October 2008. The coefficient of variance is given in parentheses beside each modeled parameter.

parameter	October 2008	this experiment
Q ($m^3 s^{-1}$)	0.020	0.022
v ($m s^{-1}$)	0.11	0.15
D ($m^2 s^{-1}$)	0.27 (0.10)	0.24 (0.10)
A (m^2)	0.18 (0.010)	0.15 (0.0093)
A_S (m^2)	0.0058 (0.48)	0.021 (0.21)
α (s^{-1})	2.3×10^{-5} (1.1)	1.5×10^{-4} (0.30)
RSS[a]	6.3	0.097

[a] RSS - residual sum of squares from the model.

The model parameters offer an overall view of reach-scale subsurface exchange, while pore water measurements offer insight into the complex stream-subsurface interactions. The OTIS-P model provided a good fit with the bromide observations of the well-connected piezometers at shallow depths (Figure 3.8). The depth of the hyporheic zone was estimated assuming the hyporheic zone was a u-shaped area underneath and lateral to the stream. The modeled storage zone cross-sectional area (A_s) along with measurements of the stream width and depth and a range of porosities estimated based on the measured hydraulic conductivities indicated that the depth of the hyporheic zone was approximately 2-8 cm. The model prediction

captures the rapid shallow exchange observed, but does not account for the deeper flow paths observed (Table 3.5). The greater connectivity of the 23 m and 77 m location represent the influence of streambed topography and heterogeneity in the subsurface. Locations 23 m and 77 m were located at the downstream ends of pools and showed good connectivity between the surface and subsurface in other tracer experiments (Chapter 2).

Colloid Exchange

The relative breakthrough of colloids compared to bromide was low in most instances. However, colloids were mobile and reached as deep at 20 cm in the subsurface at the 23 m and 77 m locations, where connectivity with the surface was high based on the bromide measurements. These locations had high concentrations of metals in the amorphous iron/manganese fractions in sequential extractions of the sediments (Chapter 2). This suggests historical exchange of colloid-associated metals at the 23 m and 77 m locations.

Colloid transport was evaluated using two different removal scenarios: (1) modeling main channel and storage zone removal rates simultaneously and (2) modeling the storage zone removal only assuming all removal occurs in the hyporheic zone. The second scenario was evaluated to determine to the extent to which hyporheic exchange could account for the removal in the reach. It was assumed that the majority of removal was due to hyporheic exchange because settling of the colloids should be negligible.

In the first scenario of colloid transport, the Damkohler number, DaI_{λ} was 0.14, which indicates that the time scale of removal was slow compared with advection in the reach. A Damkohler number greater than one indicates that removal is fast relative to travel time and equilibrium can be used to describe the model. For comparison, the Damkohler number obtained

based on the storage zone removal rate coefficient, DaI_{λ_S} , was 4.1×10^{-14}. This small Damkohler number indicates that removal occurs to slowly to be considered by the model.

In the second scenario of colloid transport (no removal in the main channel), the Damkohler number for the storage zone removal rate, DaI_{λ_S} was 2.7×10^{5}. The second scenario Damkohler number reflects the large increase in removal rate needed to account for the observed removal.

The removal rate coefficients (λ, λ_S) can be used to determine the relative colloid removal occurring between the main channel and subsurface following the method described by Runkel (2007). Briefly, OTIS was used to obtain the total mass of colloids exiting the reach due to conservative transport and reactive transport, in which the mass of colloids exiting the reach due to main channel and storage zone removal was determined separately. This comparison indicates that approximately 94% of colloid removal occurs in the main channel and 6% occurs in the subsurface. Settling in the main stream channel is a possible mechanism for removal, however it is unlikely to account for this amount of removal due to the small size of the colloids. The remaining mechanism for colloid removal is filtration. The transient storage parameters based on the bromide do not provide sufficient exchange to account for all of the colloid removal. Therefore, even the relatively large storage zone removal coefficient cannot account for the removal and the model uses the main channel removal rate to account for the remaining removal. In the second modeling scenario, where all the removal is attributed to the storage zone, the mass of colloids removed in the storage zone increased by 54% compared to the storage zone removal in the first scenario. However, the total mass of colloids removed decreased by 46% compared to the first scenario. The inability of the second scenario to account for the observed removal further indicates that transient storage cannot account for all of the colloid removal. The model

must apply the main channel removal coefficient to account for the observed removal (Figure 3.7; Table 3.4). This may indicate that a large portion of colloids are removed at the sediment-water interface. Colloid aggregation may have resulted in appreciable sedimentation to bring colloids in contact with the sediments. Colloid settling is not expected at the stream pH given the stabilizing effects of sorbing organic matter (Gaffney et al., 2008); however, it cannot be ruled out as evidence of aggregation was found on SEM images of filtered colloids and DLS showed a wide range of colloid size (510 ± 310 nm, Gauss intensity weighting), which may indicate that aggregation occurred. The SEM evidence is not conclusive because the aggregation may have occurred during the filtering process. Photoreductive dissolution is another process that could be responsible for the observed removal of ferric (oxy)hydroxides (Kimball et al., 1992; Hrncir and McKnight, 1998; McKnight and Duren, 2004; Gammons et al., 2005).

The OTIS models provided a reasonable match with the colloid observations of the well-connected piezometers at shallow depths (Figure 3.8). As the hyporheic depth based on the bromide model is 2-8 cm, the subsurface model is only expected to apply to the 5 cm piezometer depths. The higher relative breakthroughs at 23 and 77 m are located in pools where downwelling water caused greater flow of both solutes and colloids.

Colloid Filtration

Colloid removal in the stream subsurface can be compared with column transport results by comparison of removal rate coefficients obtained from the transport model with those describing deposition in the column. A laboratory column experiment examining colloid filtration in stream sediments was run in similar conditions to those found in the stream (Appendix 1, baseline conditions of pH ≈ 6, I = 0.2 mM, [fulvic acid] = 2 mg L^{-1} as whole fulvic acid). The colloid deposition rate coefficient (k_d) was determined based on the column

experiment breakthrough according to the following equations from Tufenkji and Elimelech (2004):

$$k_d = \frac{3}{2}\frac{(1-f)}{d_c f} U \alpha \eta_0 \quad (3.6)$$

$$\lambda_f = \frac{3}{2}\frac{(1-f)}{d_c} \alpha \eta_0 \quad (3.7)$$

where f is the porosity, d_c is the diameter of spherical collector [cm], U is the Darcy velocity [cm min^{-1}], α is the attachment efficiency, η_0 is the single collector contact efficiency, and λ_f is the filter coefficient [cm^{-1}]. Equations 5 and 6 can be combined to relate k_d to λ_f:

$$k_d = \frac{\lambda_f U}{f} \quad (3.8)$$

Difficulties with the comparison arise from the difference in colloid concentration and scale between the column experiment and the stream reach injection. The column experiment was conducted with much higher colloid concentrations (416 µM as Fe) than were found in the stream (~7 µM as Fe) during the tracer dilution test. The value of the filter coefficient can vary widely depending on the solution chemistry (Ren and Packman, 2005). This effect was observed in flume studies of colloid transport, but not examined here (Ren and Packman, 2005). The column result represents transport only in a small sample of re-packed, sieved sediment material. While the streambed was composed of a number of large cobbles and boulders, the column material excluded any material larger than 2 mm and the resulting higher surface area of sediment grains per column length should increase the removal of colloids compared with a similar volume of undisturbed sediment. In-stream measurements of hydraulic conductivity (Chapter 2) and estimates of Darcy velocity based on conservative bromide transport were used with the filter coefficient, λ_f, determined in the column experiment to bracket a range of k_d values in the stream (Table 3.6). It should be noted that the piezometer measurements are only local

measurements at discrete distances and depths in the streambed and may not be representative of the entire reach.

The k_d value from the column experiment was 0.0048 s^{-1} based on a filter coefficient of 0.39, Darcy velocity of 0.31 cm min^{-1} and porosity of 0.42 (Appendix 1). The range of k_d values for the stream, based on the filter coefficient, λ_f, obtained from the column experiment and piezometer measurements of hydraulic properties resulted was 0.0012 - 0.012 s^{-1}. The removal rate determined from the column experiment fell within the range of possible removal rates based on the measured subsurface parameters.

The storage zone removal rate coefficient based on the first scenario of the reach-scale OTIS model, considering both main channel and storage zone removal (8.6×10^{-17} s^{-1}), underestimates the rate of exchange expected in the stream (0.0012- 0.012 s^{-1}). In the second scenario, the storage zone removal rate coefficient was 560 s^{-1}, and the model overestimates the rate of exchange in the stream (0.0012- 0.012 s^{-1}). The uncertainty in the model storage zone removal rate coefficients makes it difficult to compare them with the column transport. However, this exercise does illustrate the difficulty in addressing the issues of scale between column experiments and reach scale injection experiments.

Table 3.6. Colloid deposition rate coefficient (k_d) based on a sediment-packed column experiment, and based on the filter coefficient from the column experiment combined with ranges of hydrologic parameters measured in the stream. The OTIS-P storage zone removal rate coefficients are also included for comparison.

parameter	column experiment	stream measurements	stream transport model	
			estimating λ and λ_S	estimating λ_S when $\lambda = 0$
Darcy velocity (cm s^{-1})	0.0052	0.0012-0.0083		
Hydraulic conductivity (cm s^{-1})	not measured	0.0060- 0.019		
porosity	0.42	0.27-0.39		
k_d (s^{-1})	0.0048	0.0012- 0.012		
λ_S (s^{-1})			8.6×10^{-17}	560

ENVIRONMENTAL IMPLICATIONS

Colloid removal through hyporheic exchange processes will vary depending on streamflow. In this experiment, the extent of colloid removal was limited by small hyporheic exchange rates due to the high stream velocity (0.15 m s^{-1}). Karwan and Saiers (2009) found that sub-micron sized titanium dioxide colloids can be removed from the stream despite low settling velocities and suggested that colloid removal from the stream channel was due to porous medium filtration in the streambed after introduction to the subsurface through hyporheic exchange. They observed the greatest removal when discharge was low and stream velocity (0.01 m s^{-1}) gave ample time for hyporheic exchange.

Ferric (oxy)hydroxide colloids do undergo hyporheic exchange and are largely removed in the shallow sediments. If metals sorb to the colloids, the colloids have the potential to carry associated metals into the subsurface. Once there, colloid removal through filtration may provide an additional mechanism for metal removal from acid mine drainage-affected streams. If the colloid exchange is irreversible, as indicated by this study (Figure 3.7), the colloids may provide a long-term sink of metals.

Colloid accumulation in the hyporheic zone has the potential to change the dynamics of hyporheic exchange and impact stream water quality if they are remobilized back to the steam. Colloids may clog the pore spaces of the hyporheic zone and reduce hyporheic exchange over time. Armoring, in which metal oxyhydroxides form precipitates on the stream sediments, has been observed in streams receiving elevated iron inputs (Brunke, 1999). Alternatively, storm events may introduce sufficient turbulence to cause resuspension of colloids and any associated contaminant metals back into the stream (Horowitz, 1990; Kimball, 1995; Butler et al., 2008).

REFERENCES

Axtmann, E.V., Luoma, S.N. (1991) Large-scale distribution of metal contamination in the fine-grained sediments of the Clark Fork River, Montana, USA. *Applied Geochemistry* 6 (1) 75-88.

Benner, S.G., Smart, E.W., Moore, J.N. (1995) Metal behavior during surface groundwater interaction, Silver-Bow Creek, Montana. *Environmental Science & Technology* 29 (7) 1789-1795.

Borgmann, U., Couillard, Y., Doyle, P., Dixon, D.G. (2005) Toxicity of sixty-three metals and metalloids to *Hyalella azteca* at two levels of water hardness. *Environmental Toxicology and Chemistry* 24 (3) 641-652.

Brunke, M. (1999) Colmation and depth filtration within streambeds: Retention of particles in hyporheic interstices. *International Review of Hydrobiology* 84, 99-117.

Butler, B.A., Ranville, J.F., Ross, P.E. (2008) Observed and modeled seasonal trends in dissolved and particulate Cu, Fe, Mn, and Zn in a mining-impacted stream. *Water Research* 42 (12) 3135-3145.

Chapman, B.M., Jones, D.R., Jung, R.F. (1983) Processes controlling metal-ion attenuation in acid-mine drainage streams. *Geochimica et Cosmochimica Acta* 47 (11) 1957-1973.

CDPHE (2003) Captain Jack superfund site aerial photo. Colorado Hazardous Materials and Waste Management Division of the Colorado Department of Public Health and Environment

Cobb, H.S. (1988) *Prospecting Our Past: Gold, Silver and Tungsten Mills of Boulder County*. The Book Lode, Longmont, Colorado.

Davis, M.W., Streufert, R.K. (1990) Gold occurrences of Colorado. Resource Series 28, Colorado Geological Survey, Denver, Colorado.

Galán, E., Gomez-Ariza, J.L., Gonzalez, I., Fernandez-Caliani, J.C., Morales, E., Giraldez, I. (2003) Heavy metal partitioning in river sediments severely polluted by acid mine drainage in the Iberian Pyrite Belt. *Applied Geochemistry* 18 (3) 409-421.

Gammons, C. H., Nimick, D. A., Parker, S. R., Cleasby, T. E. and McCleskey, R. B. (2005) Diel behavior of iron and other heavy metals in a mountain stream with acidic to neutral pH: Fisher Creek, Montana, USA. *Geochimica et Cosmochimica Acta* 69, 2505-2516.

Gandy, C.J., Smith, J.W.N., Jarvis, A.P. (2007) Attenuation of mining-derived pollutants in the hyporheic zone: A review. *Science of the Total Environment* 373 (2-3) 435-446.

Ganguli, P.M., Mason, R.P., Abu-Saba, K.E., Anderson, R.S., Flegal, A.R. (2000) Mercury speciation in drainage from the New Idria mercury mine, California. *Environmental Science & Technology* 34 (22) 4773-4779.

Harvey, R.W., George, L.H., Smith, R.L., LeBlanc, D.R. (1989) Transport of microspheres and indigenous bacteria through a sandy aquifer: Results of natural and forced-gradient tracer experiments. *Environmental Science & Technology* 23 (1) 51-56.

Horowitz A. F., Rinella F.A., Lamothe P., Miller T.L., Edwards T.K., Roche R.L., Rickert D.A. (1990) Variations in suspended sediment and associated trace element concentrations in selected riverine cross sections. *Environmental Science & Technology* 24 (9), 1313-1320.

Hrncir, D. C., Mcknight, D. (1998) Variation in photoreactivity of iron hydroxides taken from an acidic mountain stream. *Environmental Science & Technology* 32(14) 2137-2141.

Johnson, C.A. (1986) The regulation of trace-element concentrations in river and estuarine waters contaminated with acid-mine drainage – the adsorption of Cu and Zn on amorphous Fe oxyhydroxides. *Geochimica et Cosmochimica Acta* 50 (11) 2433-2438.

Karwan, D.L., Saiers J.E. (2009) Influences of seasonal flow regime on the fate and transport of fine particles and a dissolved solute in a new england stream. *Water Resources Research* 45 (11) doi:10.1029/2009WR008077.

Kimball, B.A., Mcknight, D.M., Wetherbee, G.A., Harnish, R.A. (1992) Mechanisms of iron photoreduction in a metal-rich, acidic stream (St.Kevin Gulch, Colorado, USA). *Chemical Geology* 96 (1-2) 227-239.

Kimball, B.A., Callender, E., Axtmann, E.V. (1995) Effects of colloids on metal transport in a river receiving acid-mine drainage, Upper Arkansas River, Colorado, USA. *Applied Geochemistry* 10 (3) 285-306.

Mahler, B.J., Bennett, P.C., Zimmerman, M. (1998a) Lanthanide-labeled clay: a new method for tracing sediment transport in karst. *Ground Water* 36 (5) 835-843.

Mahler, B.J., Winkler, M., Bennett, P., Hillis, D.M. (1998b) DNA-labeled clay: a sensitive new method for tracing particle transport. *Geology* 26 (9) 831-834.

McKnight, D. M., Duren, S. M. (2004) Biogeochemical processes controlling midday ferrous iron maxima in stream waters affected by acid rock drainage. *Applied Geochemistry* 19(7) 1075-1084.

Munk, L., Faure, G., Pride, D.E., Bigham, J.M. (2002) Sorption of trace metals to an aluminum precipitate in a stream receiving acid rock-drainage; Snake River, Summit County, Colorado. *Applied Geochemistry* 17 (4) 421-430.

Nagorski, S.A., Moore, J.N., Smith, D.B. (2002) Distribution of metals in water and bed sediment in a mineral-rich watershed, Montana, USA. *Mine Water and the Environment* 21 (3) 121-136.

Packman, A.I., Brooks, N.H. (2001) Hyporheic exchange of solutes and colloids with moving bed forms. *Water Resources Research* 37 (10) 2591-2605.

Packman, A.I., Brooks, N.H., Morgan, J.J. (2000) A physicochemical model for colloid exchange between a stream and a sand streambed with bed forms. *Water Resources Research* 36 (8) 2351-2361.

Puls, R.W., Powell, R.M. (1992) Transport of inorganic colloids through natural aquifer material: implications for contaminant transport. *Environmental Science & Technology* 26 (3) 614-621.

Quinn, K.A., Byrne, R.H., Schijf, J. (2006) Sorption of yttrium and rare earth elements by amorphous ferric hydroxide: Influence of pH and ionic strength. *Marine Chemistry* 99 (1-4) 128-150.

Rampe, J.J., Runnells, D.D. (1989) Contamination of water and sediment in a desert stream by metals from an abandoned gold mine and mill, Eureka District, Arizona, USA. *Applied Geochemistry* 4 (5) 445-454.

Ranville, M., Rough, D., Flegal, A.R. (2004) Metal attenuation at the abandoned Spenceville copper mine. *Applied Geochemistry* 19 (5) 803-815.

Ren, J.H., Packman, A.I. (2004a) Modeling of simultaneous exchange of colloids and sorbing contaminants between streams and streambeds. *Environmental Science & Technology* 38 (10) 2901-2911.

Ren, J.H., Packman, A.I. (2004b) Stream-subsurface exchange of zinc in the presence of silica and kaolinite colloids. *Environmental Science & Technology* 38 (24) 6571-6581.

Ren, J.H., Packman, A.I. (2005) Coupled stream-subsurface exchange of colloidal hematite and dissolved zinc, copper, and phosphate. *Environmental Science & Technology* 39 (17) 6387-6394.

Runkel, R.L. (1998) One-Dimensional Transport with Inflow and Storage (OTIS): A solute transport model for streams and rivers. Water-Resources Investigations Report 98-4018, U.S. Geological Survey, Denver, Colorado.

Runkel, R.L. (2002) A new metric for determining the importance of transient storage. *Journal of the North American Benthological Society* 21 (4) 529-543.

Runkel, R.L. (2007) Toward a transport-based analysis of nutrient spiraling and uptake in streams. *Limnology and Oceanography-Methods* 5: 50-62.

Ryan, J.N., Elimelech, M., Magelky, R.D., Baseman, J.L. (2000) Silica-coated titania and zirconia colloids for subsurface transport field experiments. *Environmental Science & Technology* 34 (10) 2000-2005.

Schwertmann, U., Cornell, R.M. (2000) *Iron Oxides in the Laboratory: Preparation and Characterization*. Wiley-VCH, New York.

Sprycha, R., Jablonski, J., Matijevic, E. (1992) Zeta-potential and surface-charge of monodispersed colloidal yttrium(iii) oxide and basic carbonate. *Journal of Colloid and Interface Science 149* (2) 561-568.

Sullivan, A.B., Drever, J.I. (2001) Geochemistry of suspended particles in a mine-affected mountain stream. *Applied Geochemistry* 16 (15) 1663-1676.

Theobald, P.K., Lakin, H.W., Hawkins, D.B. (1963) The precipitation of aluminum, iron and manganese at the junction of Deer Creek with the Snake River in Summit County, Colorado. *Geochimica et Cosmochimica Acta* 27 (Feb) 121-&.

Tonkin, J.W., Balistrieri, L.S., Murray, J.W. (2002) Modeling metal removal onto natural particles formed during mixing of acid rock drainage with ambient surface water. *Environmental Science & Technology* 36 (3) 484-492.

Triska, F.J., Kennedy, V.C., Avanzino, R.J., Zellweger, G.W., Bencala, K.E. (1989) Retention and transport of nutrients in a third-order stream in northwestern California: hyporheic processes. *Ecology* 70 (6) 1893-1905.

Tufenkji, N., Elimelech, M. (2004) Correlation equation for predicting single-collector efficiency in physicochemical filtration in saturated porous media. *Environmental Science & Technology* 38 (2) 529-536.

USEPA, 2003. Left Hand Creek watershed case study: Use of NPL as a catalyst for abandoned mine cleanup. United States Environmental Protection Agency, 6 p. (accessed on March 17, 2011, at http://www.epa.gov/aml/tech/lefthand.pdf).

USEPA/DOE, 2004. Mine waste technology program: Annual report 2004. United States Environmental Protection Agency and the Department of Energy, 51 p. (accessed March on 17, 2011, at http://www.epa.gov/nrmrl/std/mtb/mwt/annual/annual2004/annual2004.htm).

Wagner, B.J., Harvey, J.W. (1997) Experimental design for estimating parameters of rate-limited mass transfer: Analysis of stream tracer studies. *Water Resources Research* 33 (7) 1731-1741.

Wanty, R.B., Winter, T.C. (2000) A simple device for measuring differences in hydraulic head between surface water and shallow groundwater. Fact Sheet FS-077-00, U.S. Geological Survey, Washington, DC.

Wood, A.R. 2004. Characterization and prioritization of mining-related metal sources with metal loading tracer dilution tests, and a review of regulations and mine restoration funding resources, Lefthand Creek watershed, northwestern Boulder County, Colorado. M.S. Thesis, University of Colorado, Boulder, Colorado.

Zanker, H., Richter, W., Huttig, G. (2003) Scavenging and immobilization of trace contaminants by colloids in the waters of abandoned ore mines. *Colloids and Surfaces A-Physicochemical and Engineering Aspects* 217 (1-3) 21-31.

Zaramella, M., Marion, A., Packman, A.I. (2006) Applicability of the transient storage model to the hyporheic exchange of metals. *Journal of Contaminant Hydrology* 84 (1-2) 21-35.

CHAPTER 4 - METAL TRANSPORT AND SURFACE-SUBSURFACE EXCHANGE IN AN ACID MINE DRAINAGE-IMPACTED STREAM

ABSTRACT

A key component of human and ecological risk assessments of acid mine drainage is predicting the fate and transport of metals in receiving streams. In order to learn more about the processes that control metal removal in streams, we studied the role of colloids and the stream-subsurface exchange in a stream contaminated by acid mine drainage. The transport of metals strongly associated with colloids, lead and copper, was compared with the transport of zinc, a metal which tends to remain in the dissolved phase in stream systems. A continuous step injection of dissolved lead, copper, zinc, and a conservative tracer (bromide) was performed on a short reach of a low-order subalpine stream contaminated with acid mine drainage metals. We measured metals along a 61 m reach of the creek in the stream channel waters and in the subsurface pore waters using a set of mini-piezometers installed in the streambed. Approximately 17.6% of lead and 4.6% of copper were lost from the main channel of the stream over the reach, while zinc was transported conservatively through the reach (<0.1% removal). Zinc was found to be almost entirely dissolved, while both dissolved and colloidal lead and copper were found in the shallow pore waters of the hyporheic zone, which indicates that metal-associated colloid exchange does occur for metals with high adsorption affinities. Separate models of dissolved and colloidal copper showed higher removal rates of the colloidal phase compared with the dissolved phase in both the stream and subsurface.

INTRODUCTION

The legacy of abandoned mines is the contamination of streams with metals released during the accelerated weathering of waste rock and tailings. Many researchers have observed high concentrations of metals where acid mine drainage is introduced to pristine streams, but in many cases, the metal concentrations decrease rapidly downstream (Theobald et al., 1963; Chapman et al., 1983; Rampe and Runnells, 1989; Kimball et al., 1995; Munk et al., 2002; Ranville et al., 2004). High concentrations of metals are attenuated in streambed sediments affected by acid mine drainage (Axtmann and Luoma, 1991; Nagorski et al., 2002; Galán et al., 2003) and hyporheic exchange is frequently cited as the mechanism by which metal removal occurs (Ranville et al., 2004; Zaramella et al., 2006; Gandy et al., 2007). Some metals, such as lead and copper, are largely associated with colloids (Johnson, 1986; Kimball et al., 1995; Ganguli et al., 2000; Tonkin et al., 2002); therefore, understanding of metal transport and removal in streams will also require understanding of colloid transport and removal.

In acid mine drainage environments, ferric (oxy)hydroxides are consistently a major colloidal constituent (Benner et al., 1995; Sullivan and Drever, 2001; Zanker et al., 2003; Gandy et al., 2007). The dissolution of pyrite in the weathering rock releases ferrous iron that oxidizes to form ferric (oxy)hydroxide colloids as acid mine drainage is diluted in pristine streams. Aluminum oxyhydroxides can also form colloids in acid mine drainage (Zanker et al., 2003). Manganese colloids are less common than ferric iron colloids because of the kinetic limitation on oxidation of Mn^{2+}, but the rate of manganese oxidation can be enhanced by the adsorption of Mn^{2+} onto the surfaces of ferric oxyhydroxides and aluminum oxides (Davies and Morgan, 1989). These ferric iron, aluminum, and manganese oxyhydroxides, whether in the form of colloids or coatings on streambed sediment, can scavenge dissolved metals (Kimball et al., 1992;

Munk et al., 2002; Gandy et al., 2007; Schemel et al., 2007). Generally, ferric (oxy)hydroxide colloids are very small; therefore, they offer high surface areas for adsorption of metals. Because of this adsorption capacity, it is likely that they play a major role in the transport of trace metals (Gandy et al., 2007).

Colloids may be removed from the stream by settling on the streambed and filtration, straining, and dissolution in the bed sediments. Hyporheic exchange is responsible for the introduction of the colloids to the bed sediments. Settling of colloids is expected to be minor because of their small size. The remaining removal that occurs is due to filtration driven by hyporheic exchange.

Metals may be removed from the stream through sorption directly to streambed sediments or, if they associate with colloids, the colloids may provide a mechanism for metal transport or removal in the stream sediments depending on the chemical composition (Figure 4.1; Ren et al., 2000; Ren and Packman, 2004a, 2004b, 2005). Colloid-associated metals will be removed from streams affected by acid mine drainage if the colloids are effectively immobilized by attachment to hyporheic zone sediments and the metals do not desorb from the colloids. The extent of the association between metals and colloids depends on environmental factors such as pH, ionic strength, size and type of colloid, concentrations of both the metal and colloid as well as other competing ions, reaction time and temperature, organic matter, microbes, and photochemistry. Metals span a wide range of ionic radius, charge, electronegativity and hardness, or covalent index. The hardness of the metal most directly impacts its stability with a given ligand. The hard, or A-type, metals have high spherical symmetry and they bind preferentially with hard ligands to form a highly polarized bond similar to purely ionic interactions (Pearson, 1986a, b). The soft, or B-type, metals tend to have increased strength of

covalent bonding. Pb(II), Cu(II), and Zn(II) – three metals that are common in acid mine drainage – span a range of covalent indices with Pb(II) having the highest covalent index ("softest"), followed by Cu(II), and then Zn(II) (Nieboer and Richardson, 1980). The relative extent of adsorption of Pb(II), Cu(II), and Zn(II) often observed in soils, sediments, and colloids in acid mine drainage environments follows the order Pb > Cu > Zn (Johnson, 1986; Evans and Davies, 1994; Rose and Ghazi, 1998; Lee et al., 2002). In addition to adsorption, co-precipitation may result in new surface phases at high adsorbate concentrations (Dzombak and Morel, 1990). Co-precipitation usually results in more tightly bound metals and co-precipitates of heavy metals in iron oxides can provide long-term sinks of these metals (Martinez and McBride, 1998).

Dissolved metals and colloid-associated metals may enter the streambed sediments through hyporheic exchange. Hyporheic exchange is the process by which stream water enters the subsurface and returns to the main channel downstream (Harvey and Wagner, 2000). Hyporheic exchange plays an important role in stream biogeochemistry, nutrient cycling, and contaminant removal (Triska et al., 1989; Benner et al., 1995). Mixing of surface and ground water in the hyporheic zone leads to the formation of physical

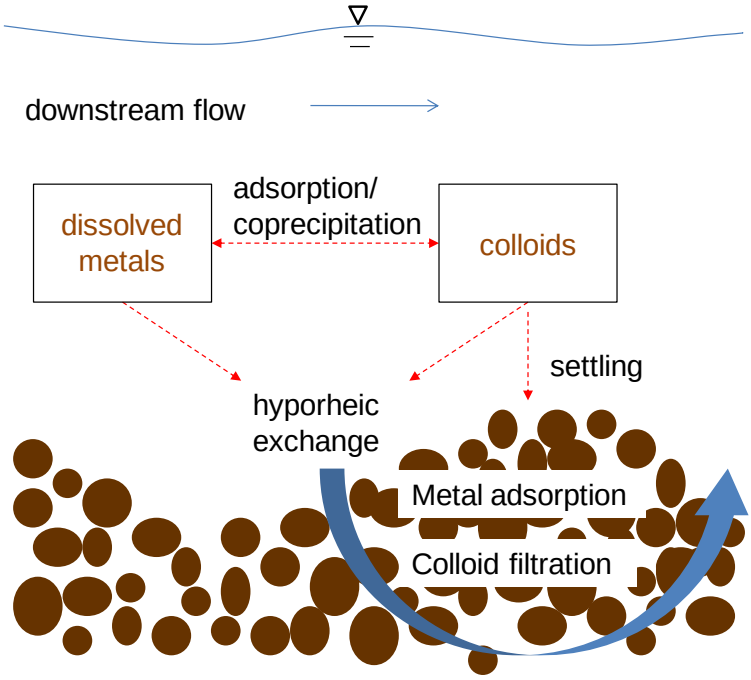

Figure 4.1. Metal and colloid removal processes.

(temperature) and geochemical (pH, organic matter, oxidation-reduction) gradients in the hyporheic zone (Triska et al., 1989).

Coupled metal and colloid transport has been modeled and verified at the laboratory scale. Ren and Packman (2004a) developed a model that predicted stream-subsurface exchange incorporating colloidal contaminant transport. The model was used to explain zinc transport coupled with silica and kaolinite colloids (Ren and Packman, 2004b) and the transport of hematite colloids in the presence of zinc, copper and phosphate (Ren and Packman, 2005). These studies emphasize that the link between contaminants and colloids makes it necessary to consider their transport simulataneously as colloid-contaminant interactions can alter both colloid and contaminant mobility. Zaramella et al. (2006) pointed out the importance of direct injection of the contaminant of interest to determine the appropriate removal parameters in transient storage models. However, metal removal by injection of the metal of interest in a real stream system has not been much examined.

The goal of this work was to examine the influence of hyporheic exchange and colloids on metal transport in a stream impacted by acid mine drainage. We injected dissolved lead, copper, zinc, and a conservative tracer in a step injection in an acid mine drainage-contaminated stream. We measured concentrations of the metals and conservative tracer in the stream channel and in subsurface pore waters to quantify hyporheic exchange and to compare the transport of the three different metals. We expected that strongly-binding metals (e.g., lead) would tend to be largely associated with colloids and their transport controlled by the extent of colloid transport, while weakly-binding metals (e.g., zinc) would be transported as dissolved species.

METHODS

Field Site

The metal injection experiment was carried out on an acid mine drainage-contaminated reach of Left Hand Creek, a low-order alpine stream (Figure 4.2). The upstream end of the study site is marked by the entrance of acid mine drainage from the Big Five Tunnel, a the main source of metal contamination on the Captain Jack Mill Superfund site, which is located approximately 2.5 km south of Ward, Colorado.

Left Hand Creek originates in glacial and snow-melt waters at an elevation of approximately 4,200 m near the continental divide in northwestern Boulder County. The creek flows through the Ward Mining District, which produced gold and silver from veins that contained pyrite, galena, and chalcopyrite from 1858 to 1993 (Cobb, 1988; Davis and Streufert, 1990; USEPA, 2003). The legacy of this mining is significant metal contamination, with lead, copper, and zinc being the most abundant metals in the mine water.

The flow rate in Left Hand Creek in the vicinity of the study site ranges from about 0.015 $m^3 s^{-1}$ at base-flow to 0.15 $m^3 s^{-1}$ at high flow conditions during the spring snow-melt (Wood, 2004). Flow in Left Hand Creek is regulated by releases from the Left Hand Park Reservoir, which is located 5.5 km upstream of the study site. A survey of the reach revealed a step-pool configuration with an average slope of 7% (Figure 4.2).

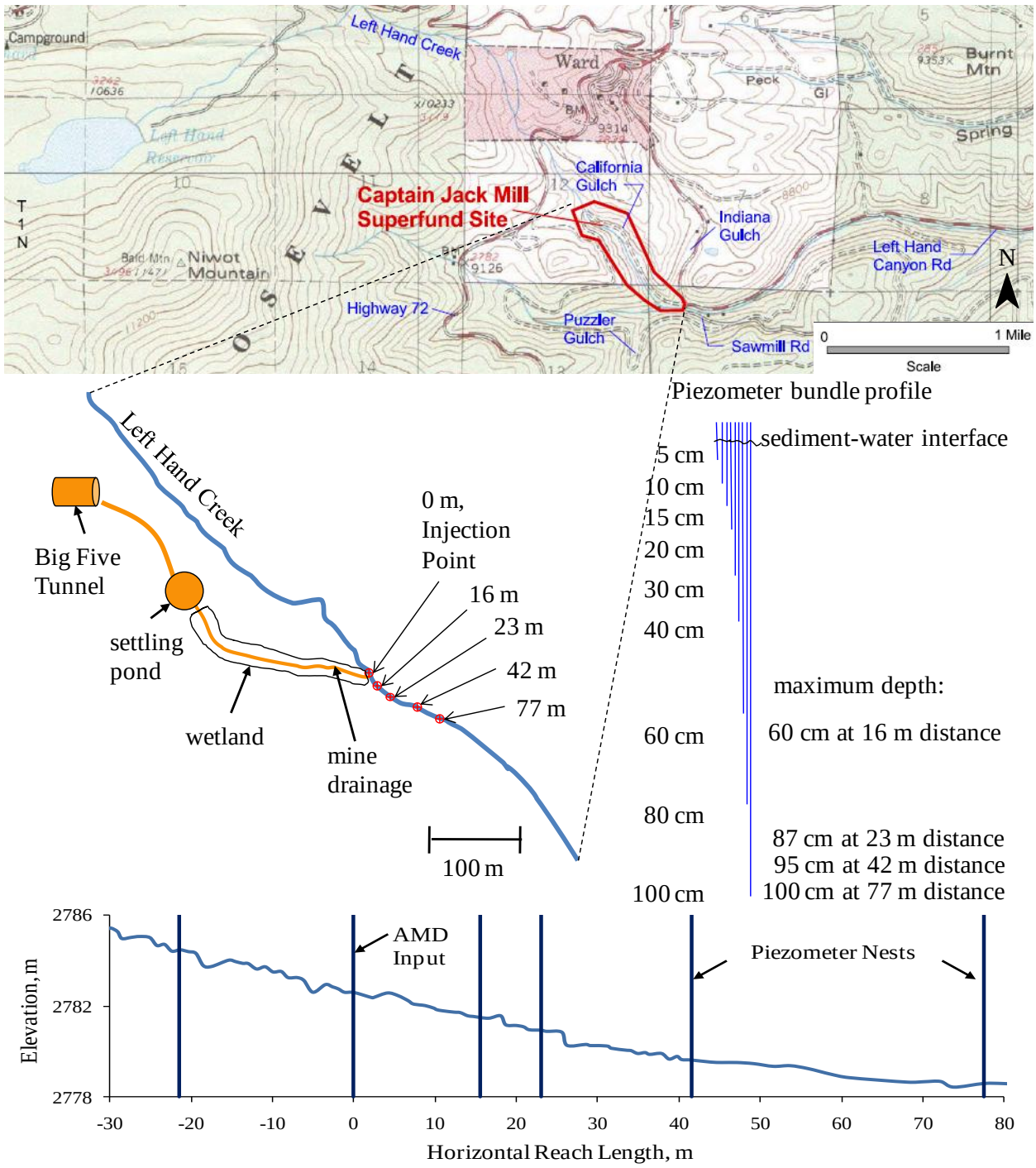

Figure 4.2. Topographic map (USGS 1:24,000; UTM zone 13, NAD 27) of study region along with sketch of field site including major features, sampling locations, piezometer bundle depths, and streambed profile with piezometer locations. The acid mine drainage enters the stream at 0 m. Due to the presence of large boulders in the streambed, some piezometers could not be installed to the intended 100 cm depth – for these, the maximum piezometer depth achieved is noted.

Field Piezometer Installation

Piezometers bundles were installed in October 2007 to sample pore waters of the hyporheic zone (Figure 4.2). The piezometers were made of polyethylene tubing (0.32 cm inside diameter, 0.64 cm outside diameter) with perforated tips (2.5 cm length, 0.1 cm diameter holes) covered by nylon mesh (0.5 mm) attached with duct tape, a design adapted from Wanty and Winter (2000). Piezometers of nine different lengths were bundled together and installed in the streambed at depths ranging from 5 cm to 100 cm (Figure 4.2). The bundles were installed by driving a steel pipe (5.1 cm diameter) filled with a steel rod into the streambed with a 27 kg electric hammer, removing the rod, inserting the piezometer bundle into the pipe, and withdrawing the pipe with a winch hoist and tripod while the piezometer bundle position was maintained. The target depth was 100 cm, but boulders limited the depth of driving to 60-95 cm in all but one sample location. The piezometer bundles used in this study were installed at four locations downstream of the acid mine drainage (Figure 4.2). The piezometer bundles were placed as near as possible to the thalweg of the stream if not prevented by boulders. Three of the piezometer bundles were located in pools at distances of 16 m, 23 m, and 77 m relative to the acid mine drainage inflow at 0 m. The remaining piezometer bundle at a distance of 42 m was located in a riffle.

Metal Tracer Dilution Tests

Lead, copper, and zinc were added to the stream at a constant rate along with a conservative tracer (bromide, added as sodium bromide) to examine their potential for exchange with the subsurface and their speciation – dissolved or colloidal. The injection was carried out at base flow on November 2, 2008. The low flow conditions allowed us to minimize the metal added while obtaining measurable increases in downstream concentration. Lead, copper, and

zinc nitrates (reagent grade, Fisher Scientific) and sodium bromide were mixed with water pumped from the acid mine drainage in a polyethylene tank (378 L) prior to injection. The injected concentrations were chosen so that the maximum in-stream metal concentrations would be 10 times the in-stream background concentrations. Peak concentrations were 22.9 µM zinc, 23.6 µM copper, and 0.121 µM lead. The solution was released into the stream at a constant rate of 0.60 ± 0.01 L min^{-1} for 9 h. Stream discharge was determined using the salt dilution method,

$$Q_{stream} = \frac{Q_{injection}[tracer]_{injection}}{[tracer]_{downstream} - [tracer]_{upstream}} \quad (4.1)$$

where Q_{stream} is stream discharge, $Q_{injection}$ is the injectate flow rate, $[tracer]_{injection}$ is injectate bromide concentration, $[tracer]_{upstream}$ is the upstream bromide concentration, and $[tracer]_{downstream}$ is bromide concentration at any downstream location once a steady concentration was reached. Samples were collected periodically throughout the injection until one hour after the end of the injection. A single sample was collected the day after the injection, approximately 25 h after the start of the injection. To allow for comparison between the transport of the bromide and the colloids in both the stream and subsurface, the concentrations have been normalized by dividing by the maximum concentration of bromide or colloids at 16 m.

The relative breakthrough of each metal was calculated for the each location and depth. The relative breakthrough (*RB*, %) of an injected constituent is a comparison of the time-integrated mass of the constituent relative to that of the conservative tracer (Harvey et al., 1989):

$$RB\ (\%) = \left[\int_{t_0}^{t_f} \frac{[C]_t}{[C]_0} dt \Big/ \int_{t_0}^{t_f} \frac{[tracer]_t}{[tracer]_0} dt \right] \times 100 \quad (4.2)$$

where $[C]_0$ is the steady concentration in the surface, $[\text{tracer}]_0$ is the steady bromide concentration in the surface, $[C]_t$ and $[\text{tracer}]_t$ are the concentrations in the subsurface at time *t*,

and t_0 and t_f are the times at the beginning and end of the breakthrough. The attenuation (%) of the injected constituent is 100 – *RB*.

Sample Collection

Surface samples were collected 16 m and 77 m downstream from the injection point. Piezometers bundles were located at 16, 23, 42, and 77 m. The piezometer bundles were sampled at depths of 5cm, 40 cm, and 100 cm. The samples were withdrawn manually from the piezometer tubes with a syringe (polypropylene, 30 mL) at a constant rate of about 15 mL min^{-1} after purging about 1.5 volumes of water standing in the piezometers. The pore volume of each piezometer was calculated based on the length of the tubing below the water line. The depth of the stream was measured to the nearest centimeter prior to drawing water and used to estimate the volume of water standing in the tube. Purging and sample volumes were kept small to avoid cross-sampling between piezometers at nearby depths. Water samples were collected in bottles (high-density polyethylene, 30 mL) that were washed in acid (10% nitric acid), rinsed three times with ultrapure water (>18 MΩ cm, Millipore Milli-Q), and rinsed three times with stream water at the sampling location. Samples for metals analysis were acidified to a pH of less than 2 with trace metal-grade nitric acid (Fisher Scientific). Samples analyzed as the dissolved fraction were filtered in the field using 0.1 µm membranes (Nuclepore, polycarbonate) and a 12-port vacuum filtration device (Millipore 1225 sampling manifold). This device was thoroughly rinsed with ultrapure water between samples.

Laboratory Analysis

Samples were analyzed for bromide by ion chromatography (IC; Dionex DX-500) and for lead, copper, zinc, aluminum, and manganese by inductively coupled plasma-mass spectrometry (ICP-MS; Varian 810MS). Iron, calcium, potassium, magnesium, sodium, sulfur, and silicate

concentrations were measured by inductively coupled plasma-atomic emission spectrometer (ICP-AES; ARL 3410+). Detection limits for each element are given in Table 4.1.

Table 4.1. Detection limits for elements measured by ICP-MS, ICP-AES or IC.

Element	Detection Limit (μM)	Element	Detection Limit (μM)
Al	0.0080	Ca	0.075
Mn	0.0047	K	0.13
Fe	0.039	Mg	0.041
Cu	0.0063	Na	0.17
Zn	0.012	S	2.8
Pb	0.00039	Si	0.67
Br^-	0.63		

Transport Modeling

The surface concentrations from the tracer injections were modeled using OTIS (One-Dimensional Transport with Inflow and Storage; Runkel, 1998). The model uses a Crank-Nicholson finite-difference solution to solve the advective-dispersion equation along with equations describing transient storage, lateral inflow, and first-order decay. The model can be applied along with nonlinear regression techniques to optimize parameter estimates by minimizing the squared differences between simulated and observed concentrations in a variation of OTIS referred to as OTIS-P. The model was fit to the conservative tracer, bromide, to estimate dispersion (D) [$m^2 s^{-1}$], stream cross-sectional area (A) [m^2], storage zone cross-sectional area (A_S) [m^2], and storage zone exchange coefficient (α) [s^{-1}]. These parameters where then used in the models of the metal transport to estimate the first order removal rate coefficients for the main channel (λ) [s^{-1}] and the storage zone (λ_S) [s^{-1}]. The data from observations made at the 16 m location were used as the upstream boundary conditions to model the reach from 16 m to 77 m. The observations at 77 m were used to fit the model. The residual

sum of squares (*RSS*) was computed for each model to determine the discrepancy between the data (observations at 77 m) and the model estimates. The *RSS* is the sum of the squares of the residuals, or differences between the observations and model estimate. OTIS-P attempts to minimize the *RSS* when determining model parameters. For each modeled parameter, the model computes the standard deviation associated with the parameter. The coefficient of variance, the ratio of the standard deviation to the parameter value, is given allow rapid evaluation of the certainty of the parameter. To allow for comparison between the transport of the bromide and the colloids in both the stream and subsurface, the concentrations have been normalized by dividing by the maximum concentration of bromide or colloids at 16 m.

Several metrics were calculated to evaluate the model and the impact of transient storage: (1) the relative size of the hyporheic zone (A_S/A), (2) the average distance a molecule travels downstream within the main channel prior to entering the storage zone ($L_S = u/\alpha$), (3)the hydraulic retention factor (average time water remains in storage relative to the hydraulic turnover length, $R_h = A_S/Q$), and (4) the fraction of median travel time due to transient storage, F_{med} (Runkel, 2002):

$$F_{med} \cong (1 - e^{-L(\alpha/u)}) \frac{A_S}{A + A_S} \tag{4.3}$$

where u is advective velocity (m s^{-1}) and L is the reach length (m) was also determined. F_{med} was evaluated at the standard distance of 200 m by setting L equal to 200 m (F_{med}^{200}) for comparison with other datasets. Damkohler numbers for transient storage (DaI_α) and colloid removal kinetics (DaI_λ) were calculated as:

$$DaI_\alpha = \frac{\alpha\left(1 + \frac{A}{A_S}\right)L}{u} \tag{4.4}$$

$$DaI_{\lambda} = \frac{\lambda\left(1+\frac{A}{A_S}\right)L}{u} \quad (4.5)$$

The Damkohler number gives the ratio of the time scale of transient storage or removal to the time scale of advection through the reach.

In order to examine the importance of subsurface removal, metal transport was also modeled by setting first-order removal rate coefficient for the main channel (λ) equal to zero and estimating the storage zone (λ_S) using OTIS. Underlying this approach is the assumption that no removal occurred in the main channel. This procedure provided the maximum possible removal that could occur in the hyporheic zone given the amount of transient storage observed.

RESULTS

Stream-Subsurface Transport

Injection of the conservative tracer, bromide, offers a means of quantifying hydrologic characteristics of the stream. Flow rate in the stream at the upstream end of the reach was approximately 1090 L min^{-1} ± 21 L min^{-1} (0.0182 ± 0.0003 m^3 s^{-1}). Bromide measurements in the surface show that there was little change in flow between the upstream end of the reach at 16 m and downstream end at 77 m (Figure 4.3). This indicates that dilution from tributaries and lateral inflow from groundwater was minor. The injected solute concentrations do not reach a stable plateau during the first four hours of the injection due to an increase in stream flow rate.

Subsurface piezometer measurements show that the stream was well-connected with the shallow subsurface, but bromide breakthrough at varied considerably between locations at the 40 cm depth (Table 4.2). For bromide, the maximum concentration reached at 5 cm was equivalent to the surface concentration at all locations except the 23 m distance. At 23 m, the bromide reached 10% of the surface concentration. At the 77 m distance, the bromide reached

100%, while the bromide at 16 m and 42 m reached 5% or less of the surface water concentration at the 40 cm depth. The breakthrough at 100 cm was not assessed at 16 m and 42 m because of the low breakthrough at the 40 cm depth.

The normalized zinc concentrations in the surface are very similar to the conservative bromide concentrations. The difference in the normalized steady concentration between bromide and copper and lead indicates that these metals were removed through the reach. Analysis of the background subtracted mass difference between the upstream and downstream end of the reach by integrating the area under the curve showed that 0.022% of the injected bromide, 0.061% of the injected zinc, 4.6% of the injected copper, and 17.6% of the injected lead were removed in the reach (Table 4.3). Colloidal transport varied between the metals. Zinc was 100% dissolved,

Table 4.2. Maximum normalized concentration for bromide, relative breakthroughs (RB) and attenuation for metals in the subsurface. nm- not measured, nd- not determined with available data due to very low metal concentrations relative to background.

distance	depth	bromide $(C/C_0)_{max}$	zinc RB[a] (%)	copper RB[a] (%)	lead RB[a] (%)	zinc attenuation (%)	copper attenuation (%)	lead attenuation (%)
16 m	5 cm	1.0	30	3	18	70	97	82
16 m	40 cm	0.051	0	0	0	100	100	100
16 m	100 cm	nm	nm	nm	nm	nm	nm	nm
23 m	5 cm	0.29	46	29	0	54	71	100
23 m	40 cm	0.10	0	0	0	100	100	100
23 m	100 cm	0.0033	0	0	0	100	100	100
42 m	5 cm	1.00	100	74	87	0	26	13
42 m	40 cm	0.027	0	0	0	100	100	100
42 m	100 cm	nm	nm	nm	nm	nm	nm	nm
77 m	5 cm	1.00	69	73	nd	31	27	nd
77 m	40 cm	1.00	7	2	0	93	98	100
77 m	100 cm	0.0050	nd	nd	nd	nd	nd	nd

[a] *RB* values calculated using Eqn. 1. Attenuation calculated as 100-*RB* (%).

on average, in the reach surface waters. In the surface, copper was on average 23% colloidal, while lead was approximately 32% colloidal (Figure 4.3, Table 4.3).

Iron, aluminum, and manganese oxides have the potential to sorb metals. Concentrations of iron, aluminum, and manganese were measured in the stream to determine whether there was sufficient colloidal material to offer sorption sites for the injected metals (Figure 4.4).

Table 4.3. Summary of the fraction of mass lost and the average fraction of colloidal metal present in the stream surface samples.

	mass lost over 61 m reach (%)	colloidal metal (%)
total zinc	0.061	0.012
total copper	4.6	23
total lead	17.6	32
dissolved copper	8.6	
colloidal copper	40.3	

Manganese was largely dissolved in the reach, while iron and aluminum colloidal fractions fluctuated throughout the day and became almost entirely dissolved after noon.

Table 4.4. Background metal concentrations and average colloidal fractions in the subsurface. nm-not measured

distance	depth	background zinc (µM)	background copper (µM)	background lead (µM)	colloidal zinc fraction	colloidal copper fraction	colloidal lead fraction
16 m	5 cm	0.865	0.505	0.00646	0.13	0.28	0.21
16 m	40 cm	2.95	0.217	0.0140	0.034	0.13	0.17
16 m	100 cm	nm	nm	nm	nm	nm	nm
23 m	5 cm	1.54	0.631	0.0125	0.087	0.49	0.37
23 m	40 cm	3.16	0.970	0.00484	0.075	0.34	0.37
23 m	100 cm	3.44	0.177	0.00945	0.055	0.34	0.22
42 m	5 cm	1.52	0.970	0.0167	0.10	0.42	0.32
42 m	40 cm	2.66	0.177	0.00834	0.03	0.11	0.08
42 m	100 cm	2.24	0.077	0.00158	0.25	0.25	0.32
77 m	5 cm	1.26	2.36	0.0315	0.12	0.70	0.68
77 m	40 cm	0.754	0.198	0.00670	0.0095	0.34	0.20
77 m	100 cm	7.20	0.213	0.127	0.016	0.16	0.12

The subsurface metals show trends similar to bromide breakthrough with the highest relative breakthoughs at the 5 cm depth (Table 4.2). Little to no zinc or copper reached the 40 cm depth. Lead concentrations were only elevated above background in the 5 cm depths at 16 m and 42 m. Subsurface measurements of lead were suspect because background concentrations were high relative to the concentrations resulting from the injection. The zinc in the subsurface was largely dissolved, though 8.7 to 13% of the zinc was colloidal in the 5 cm depths (Table 4.4). The copper ranged from 11% to 70% colloidal in the subsurface. Lead concentrations in the subsurface were so near the background concentrations that it was only possible to evaluate relative breakthrough at two piezometer locations.

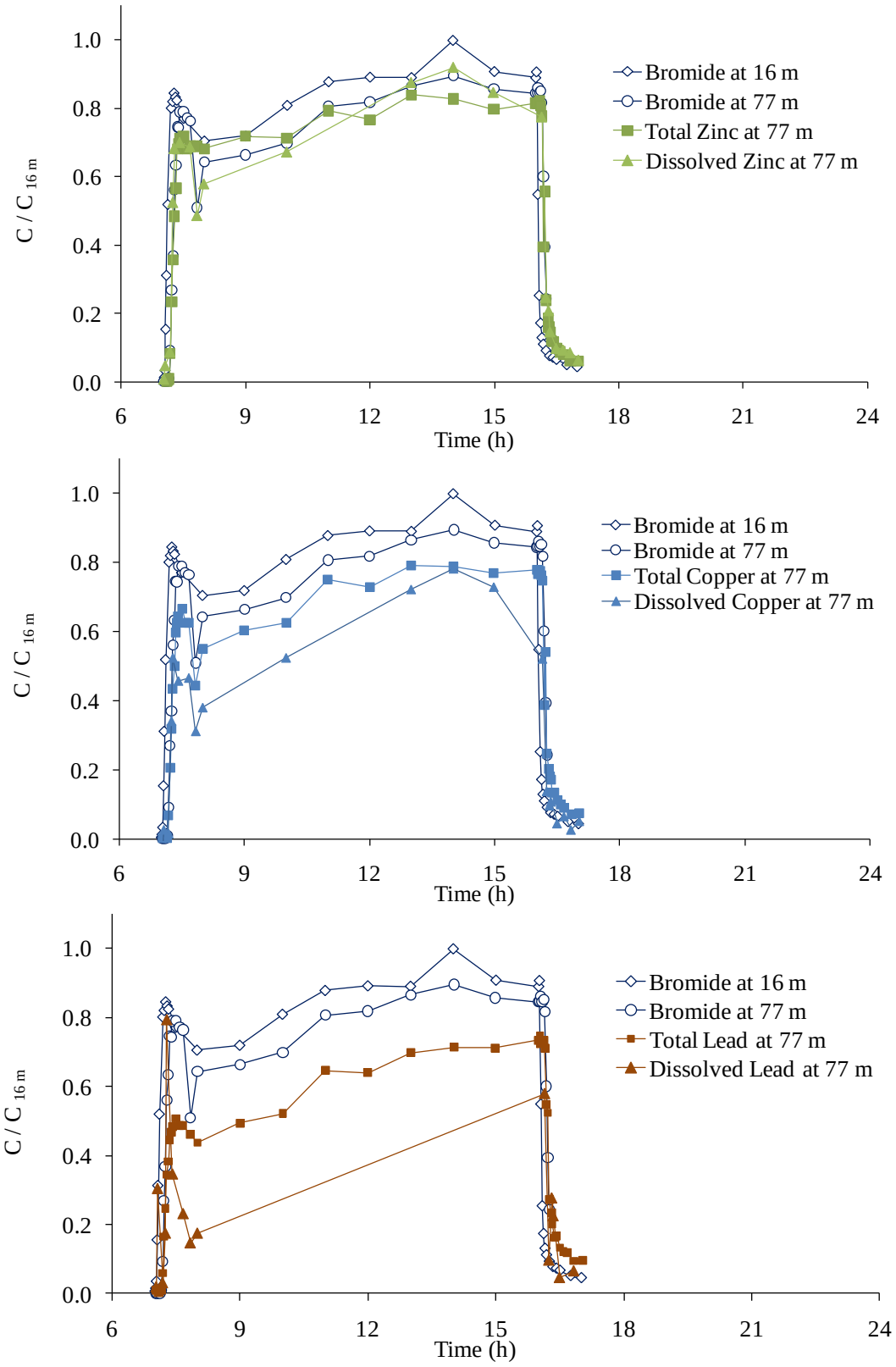

Figure 4.3. Bromide observations at the 16 m and the 77 m location. Total and dissolved metals concentrations are shown for the 77 m location only.

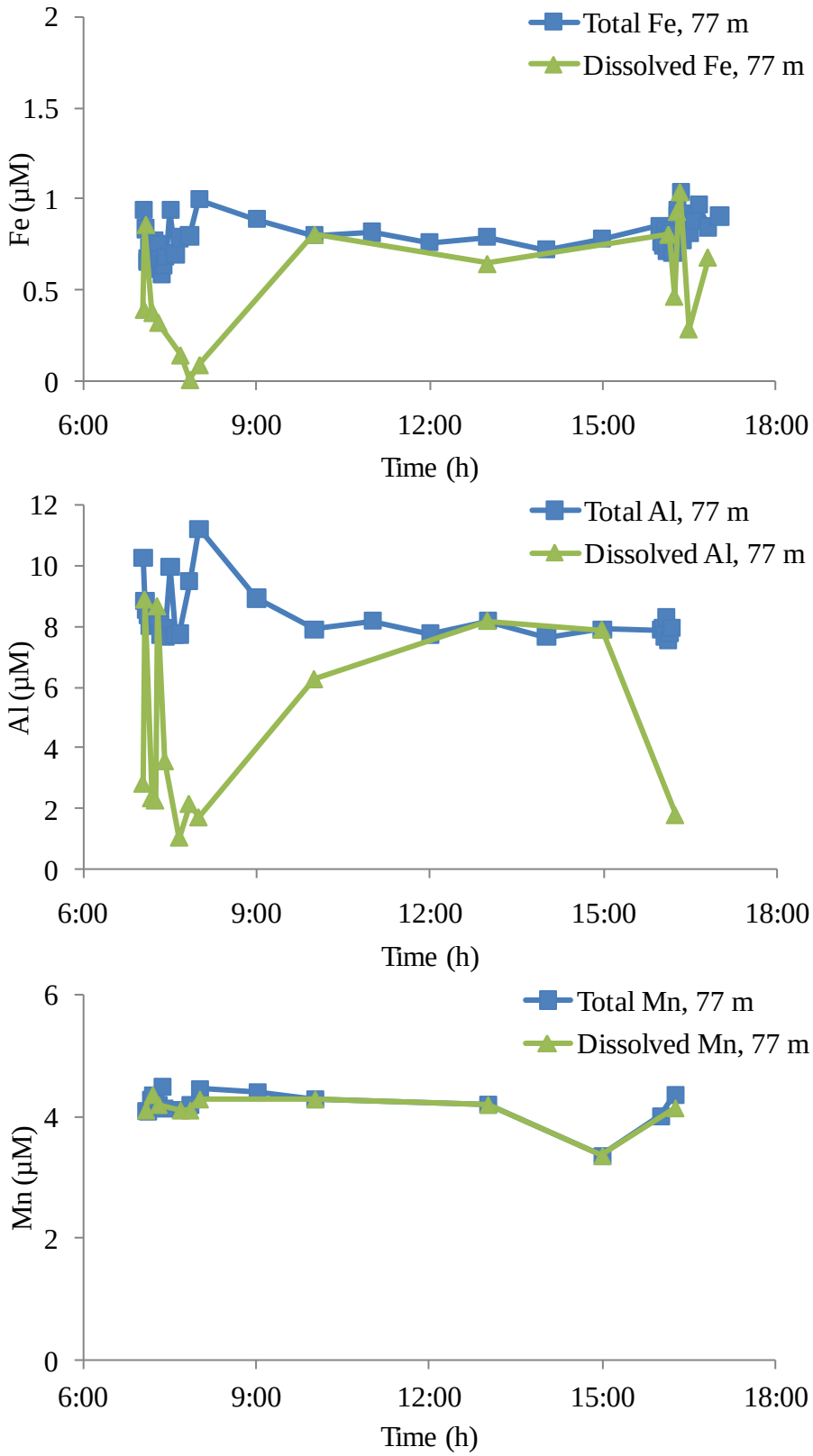

Figure 4.4. Total and dissolved iron, aluminum, and manganese concentrations.

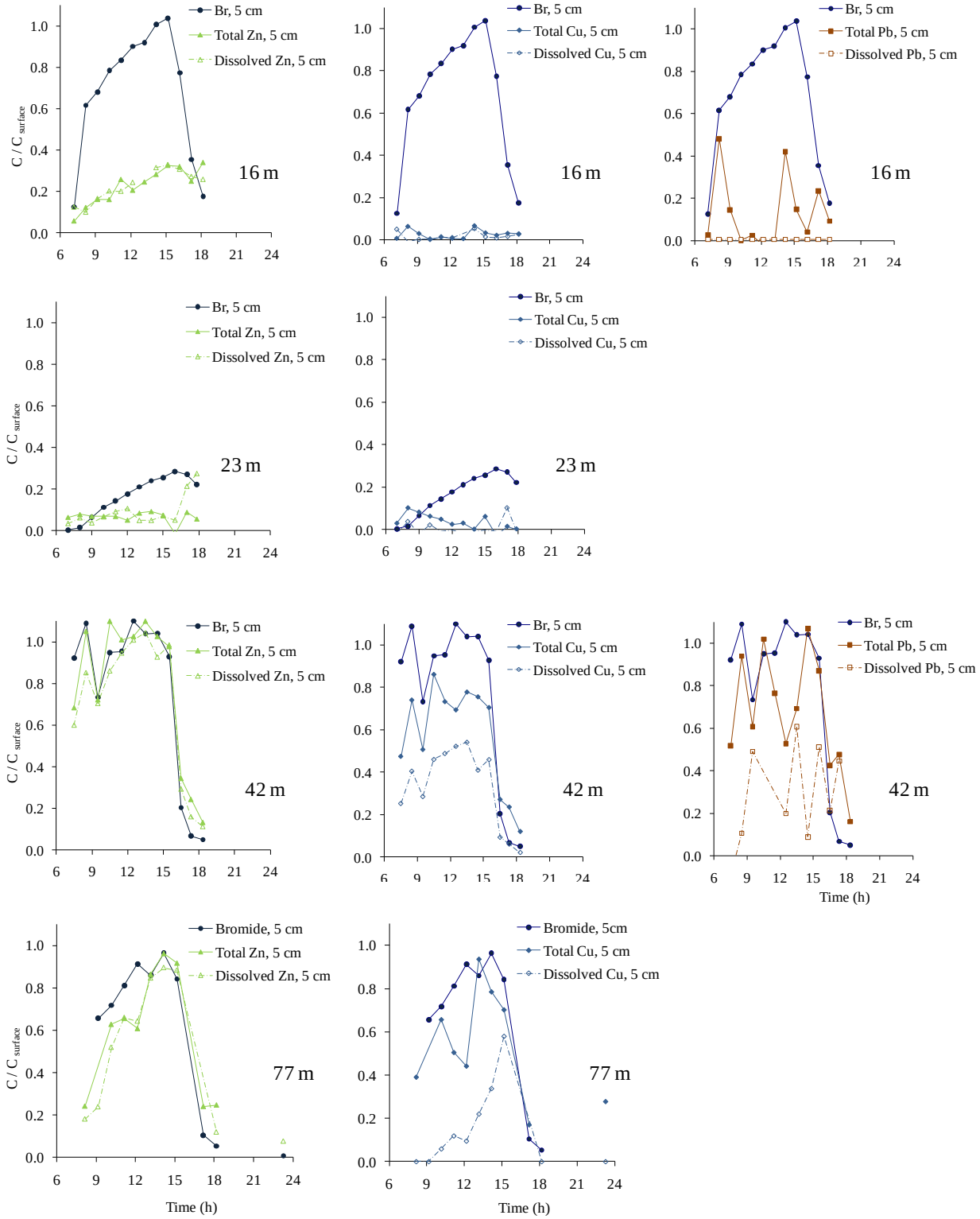

Figure 4.5. Subsurface bromide, total and dissolved zinc, copper, and lead at the 5 cm depth and all locations. The concentrations have been adjusted for background concentrations and normalized to the maximum concentrations at 16 m. Lead measurements at 23 m and 77 m are excluded because concentrations were below background levels.

Metal Tracer Dilution Modeling

The bromide concentration was unsteady in the first 5 h of the injection, indicating changes in flow at this time (Figure 4.6); therefore, the OTIS transport model was fit to the observed stream data collected from 12:00 to 17:00 when the flow was steady (Table 4.5). The cross-sectional area of the hyporheic zone relative to that of the stream (A_s/A) was 0.21 with an average storage zone residence time ($T_{stor} = A_S/\alpha A$) of 0.26 h. The hydraulic turnover length (L_s), which is the average distance water travels downstream within the main channel prior to entering the storage zone, was 490 m. Division of T_{stor} by L_s resulted in a hydraulic retention factor (R_h), the average time a water molecule remains in storage relative to the hydraulic turnover length, of 1.9 s m^{-1}. This suggests that the water is in the hyporheic zone for approximately 21% of the time since the water travels one meter in 9.1 s. However, the hydraulic retention factor is unaffected by the storage zone exchange coefficient. None of the above parameters take into consideration the impacts of all three parameters, u, A_S, and α, which influence transient storage. The fraction of median travel time due to transient storage (F_{med}^{200}) was developed to account the interactions of all three parameters. Here, F_{med}^{200} was 0.058, meaning that transient storage accounts for 5.8% of total reach travel time. The Damkohler number with respect to transient storage, DaI_{α}, was 0.72, which indicates that the time scale of exchange was slow compared with advection in the reach.

Table 4.5. Stream flow characteristics and model parameters describing advection, dispersion, and transient storage based on bromide, the conservative tracer. The coefficient of variance (CV; standard deviation divided by parameter value) is given in parentheses beside each modeled parameter.

	Q ($m^3 s^{-1}$)	v ($m s^{-1}$)	D ($m^2 s^{-1}$)	A (m^2)	A_S (m^2)	α (s^{-1})	RSS[a]
Bromide	0.018	0.11	0.27 (0.25)	0.17 (0.028)	0.035 (0.20)	2.2×10^{-4} (0.44)	0.81

[a] RSS - residual sum of squares from the model.

The total metals data was modeled by setting the parameters describing advection, dispersion, and transient storage (D, A, A_S, α) equal to those determined based on the bromide model and evaluating removal with two scenarios: (1) estimating the removal rate coefficients (λ, λ_S) and (2) setting $\lambda = 0$ and estimating λ_S only (Figure 4.6; Figure 4.7; Table 4.6). For metal transport, the Damkohler number, the ratio of the time scale of removal to the time scale of advection in the reach, was calculated for each metal and each scenario (Table 4.7).

OTIS modeling allows quantification of the differences in transport of total lead, copper, and zinc with main channel and storage zone removal rates (Table 4.6). In the scenario where λ and λ_S were allowed to vary, the metal removal rate coefficient for the surface water, λ, showed a trend of removal of the order Pb > Cu > Zn. The storage zone removal rate coefficients were all very small. For the second scenario, the λ_S values increased compared with those of the first scenario and showed higher values for copper and lead than zinc. The removal rate coefficients for surface and subsurface are very uncertain for most of the metals, as indicated by the high coefficient of variance values and lack of convergence in some cases. By integrating the area under the breakthrough curve for each metal, the mass removed was determined be comparing the upstream with the downstream mass transport. The mass removal follows the trend based on the main channel removal coefficient with removal following the order Pb > Cu > Zn. Only 0.061% of the injected zinc was removed over the 61 m reach, while 4.6% of the copper and 17.6% of the lead were lost from the main stream channel (Table 4.3). Colloidal association followed the same trend as the removal rates. The average colloidal fraction of lead was 32%, followed by copper (23%) and zinc (0.012%).

In order to compare colloidal and dissolved metal transport, colloidal and dissolved copper were modeled separately (Figure 4.8). Zinc and lead phases were not modeled separately

because the zinc remained largely dissolved and there was insufficient dissolved lead data. Both main channel and storage zone removal rate coefficients were estimated (Table 4.6). There was greater certainty in the main channel removal rate coefficients than in the storage zone removal rate coefficients, as indicated by the high coefficients of variance. Both the dissolved copper model removal coefficients decreased compared with the total copper coefficients, while the colloidal model fits showed increases in both removal rate coefficients.

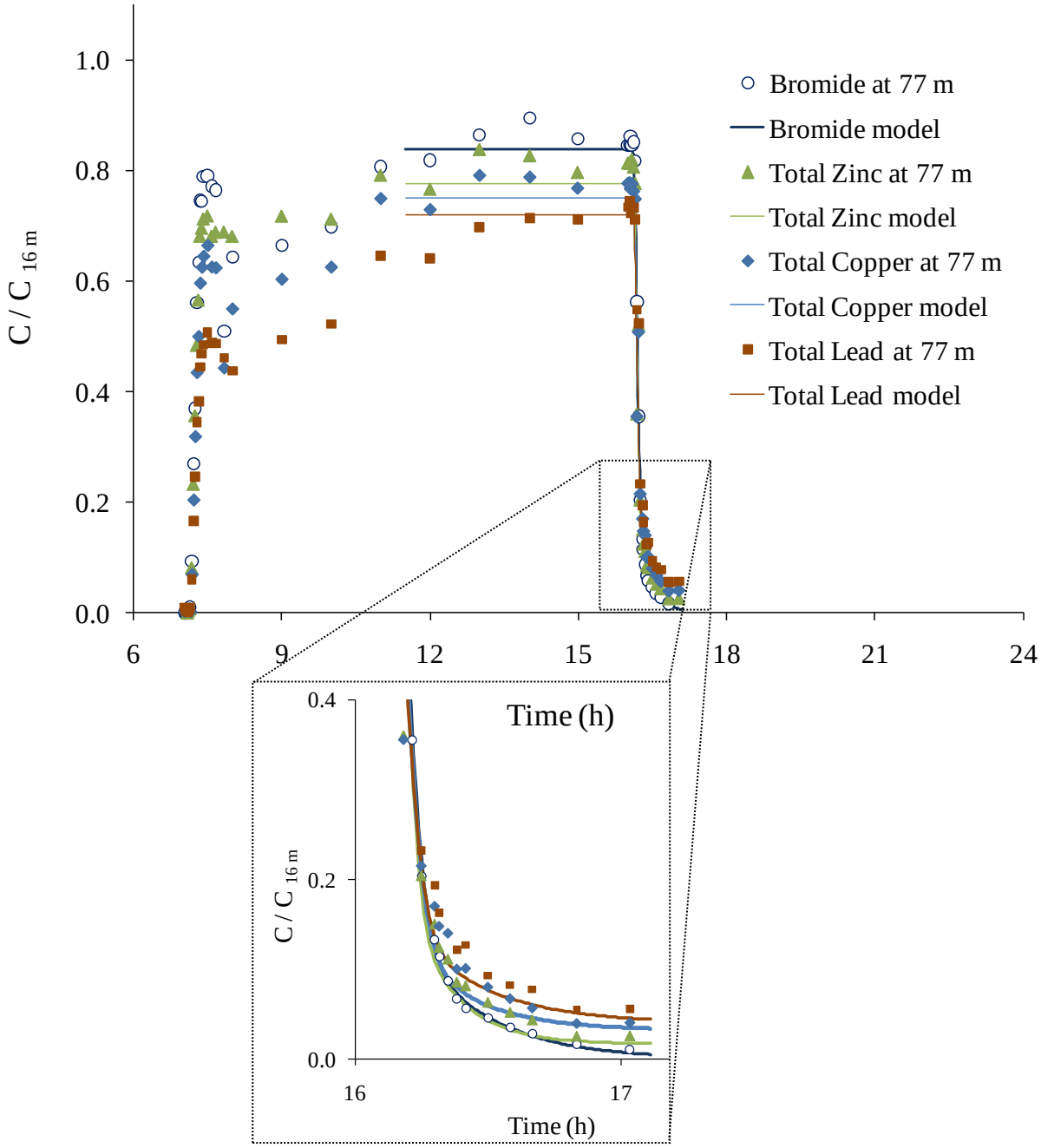

Figure 4.6. Surface bromide and total metal breakthroughs with model fits as a function of time at the 77 m transport distance of the acid mine drainage. The plot shows the model fits obtained by setting $\lambda = 0$ and estimating λ_S.

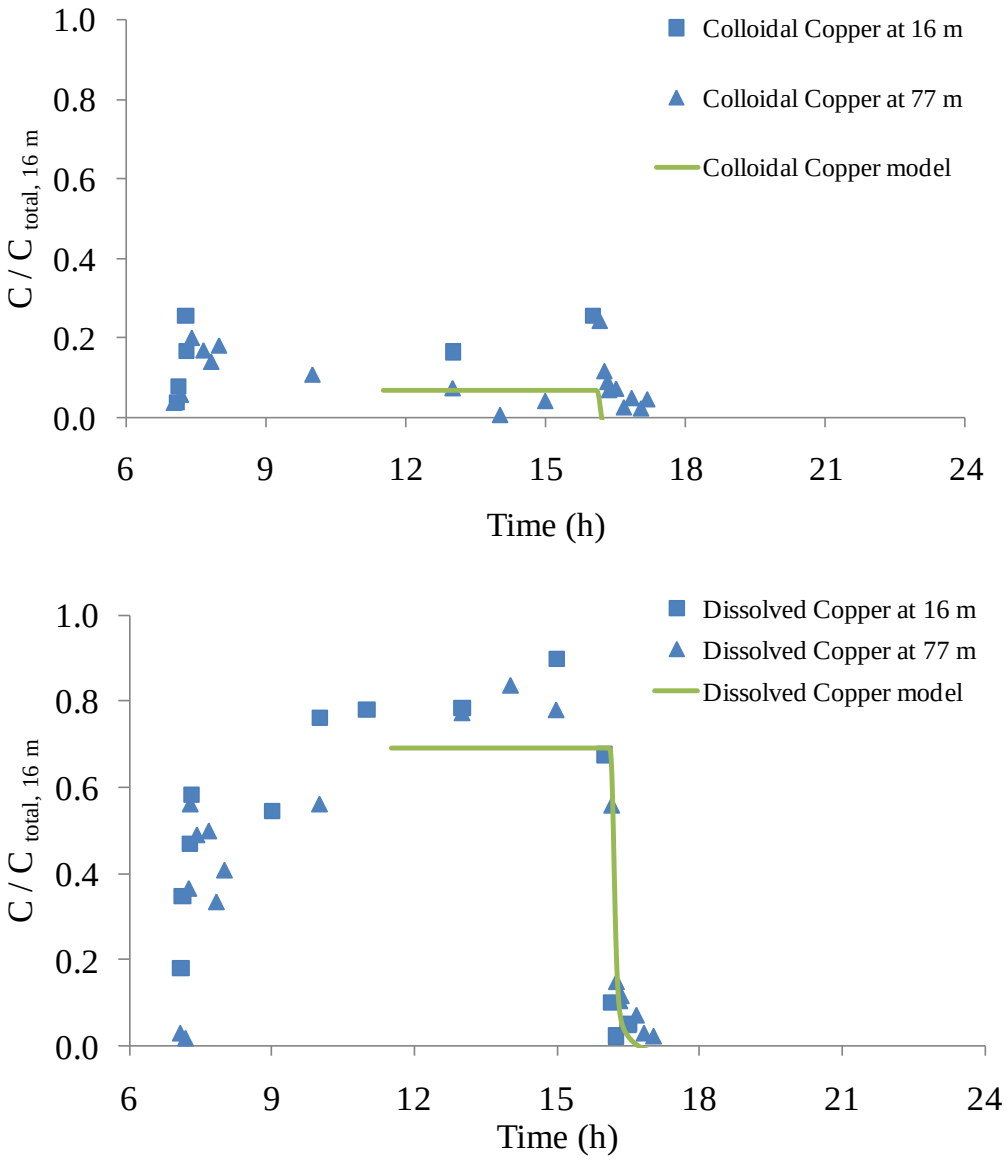

Figure 4.7. Breakthrough for colloidal and dissolved copper along with OTIS model describing the breakthrough at 77 m.

Table 4.6. Summary of removal rates based on the two scenarios used to model metal transport. The coefficient of variance (CV; standard deviation divided by parameter value) is given in parentheses beside each modeled parameter.

	estimating λ and λ_S					estimating λ_S when $\lambda = 0$		
	main channel removal rate, λ (s^{-1})	storage zone removal rate, λ_S (s^{-1})	RSS[b]	DaI_{λ}	DaI_{λ_S}	storage zone removal rate, λ_S (s^{-1})	RSS[a]	DaI_{λ_S}
zinc	6.1×10^{-11} [b]	2.0×10^{-11} [b]	0.16	6.0×10^{-6}	2.0×10^{-6}	7.0×10^{-12} (1.7×10^{16})	0.33	6.8×10^{-7}
copper	9.7×10^{-9} [b]	2.2×10^{-14} [b]	0.28	9.5×10^{-4}	2.0×10^{-9}	1.0×10^{-9} (1.8×10^{-7})	0.28	1.0×10^{-4}
lead	2.2×10^{-4} [b]	3.4×10^{-12} [b]	0.049	22	3.3×10^{-7}	3.2×10^{-9} (1.3×10^{-8})	0.084	3.1 × 10-4
dissolved copper	4.9×10^{-5} (2.5)	3.2×10^{-12} (1.5×10^{8})	0.11	4.8	3.1×10^{-7}			
colloidal copper	6.3×10^{-4} [b]	1.4×10^{-8} [b]	0.029	62	1.4×10^{-3}			

[a] RSS - residual sum of squares from the model.
[b] The model did not converge on a unique solution, indicating that the parameter value is very uncertain.

DISCUSSION

Hyporheic Exchange of Bromide

In situ observations using piezometers in the subsurface are important for gauging hyporheic exchange (Harvey and Wagner, 2000). Piezometer measurements obtained here show that a small, highly interactive hyporheic zone exists in at least the upper 5 cm (Table 4.3). The bromide concentrations in the upper 5 cm depth reached between 29% and 100% of the surface water concentration in all the piezometers.

Several metrics were used to evaluate the model reliability and the importance of transient storage. The storage zone residence time (T_{stor}), hydraulic retention factor (R_h), and fraction of median travel time due to transient storage (F_{med}^{200}) were all at the low end of the range observed in other studies of small mountain streams (Runkel, 2002). The exchange rate

coefficient (α) and the storage zone area (A_S) were larger than those determined in other experiments performed on the same reach of Left Hand Creek (Table 4.7; Chapters 2 and 3). The difference may be due to the slightly lower flow rate and velocity in the creek during this experiment. Other studies have shown increased transient storage with decreasing discharge due to expansion of the hyporheic zone and increased presence of pools which can store water and enhance hyporheic exchange through advective pumping (Harvey et al., 1996; Harvey et al., 2003; Scott et al., 2003; Wondzell, 2006; Mutz et al., 2007; Zarnetske et al., 2007, Karwan and Saiers, 2009).

The depth of the hyporheic zone was estimated assuming the hyporheic zone was a u-shaped area underneath and lateral to the stream. The modeled storage zone cross-sectional area (A_S) along with measurements of the stream width (1.3 to 2.4 m) and a range of porosities estimated based on the measured hydraulic conductivities (0.3 to 0.4) indicated that the depth of the hyporheic zone was approximately 4 - 13 cm. Although the modeled reach scale hyporheic depth is shallower than some of the piezometer measurements show, both the piezometer measurements and the model suggest a relatively small hyporheic zone area undergoing rapid exchange.

Table 4.7. Comparison of advection and transient storage parameters in this experiment, conducted in November 2008, with those of an experiment in October of 2008 and November of 2009.

parameter	October 2008	This experiment, November 2008	November 2009
Q ($m^3 s^{-1}$)	0.020	0.018	0.022
v ($m s^{-1}$)	0.11	0.10	0.15
D ($m^2 s^{-1}$)	0.27 (0.10)	0.27 (0.25)	0.24 (0.10)
A (m^2)	0.18 (0.010)	0.17 (0.028)	0.15 (0.0093)
A_S (m^2)	0.0058 (0.48)	0.035 (0.20)	0.021 (0.21)
α (s^{-1})	2.3×10^{-5} (1.1)	2.2×10^{-4} (0.44)	1.5×10^{-4} (0.30)
RSS	6.33	0.81	0.097

Metal Removal

The amount of each total metal removed followed the order expected based on previous assessments of their tendencies to sorb to mineral surfaces (Johnson, 1986; Evans and Davies, 1994; Rose and Ghazi, 1998; Lee et al., 2002). Essentially all (>99%) of the zinc remained dissolved and was transported conservatively through the reach. Approximately 4.6% of copper and 17.6% of lead was lost over the 61 m reach. Because 23% of the copper and 32% of the lead was colloidal, colloids were expected to play an important role in controlling their transport in the stream and subsurface.

Colloid filtration was high (colloid filtration coefficient coefficient, λ_f, = 0.39 cm^{-1}) in column experiments conducted under similar conditions to the stream (pH ≈ 6, I = 2.0×10^{-4} M, [FA] = 2 mg L^{-1} as fulvic acid; Appendix 1). This result has limited application to stream results due to the sieving of the sediment in the packed column and differences in metal concentrations as described in Chapter 3. The column experiments indicated that colloid facilitated transport occured for lead and copper. Lead was largely colloidal and the lead transport in the column was similar to the colloid transport. Copper was less associated with colloids and was immobilized in the sediments to a greater extent. Zinc was largely dissolved and removal was due to sorption to the sediments.

The dissolved concentrations of iron and aluminum measured throughout the day showed significant variability such that it is difficult to assess their colloidal contribution. The dissolved concentrations increased from 10:00 to 16:00. The ferric (oxy)hydroxide colloids are subject to dissolution in stream systems by photoreduction, which leads to diel variations in the concentrations of ferrous iron and metals (Kimball et al., 1992; Hrncir and McKnight, 1998; McKnight and Duren, 2004; Gammons et al., 2005). Photoreduction may have contributed to the

observed distribution of iron between dissolved and colloidal phases. Aluminum is not subject to photoreduction, but it is possible that aluminum colloids may have dissolved along with the ferric (oxy)hydroxide if the colloids were formed through co-precipitation with the ferric (oxy)hydroxides.

The small number of iron and aluminum oxide colloids in the reach may have limited zinc and copper removal. Concentrations of copper and zinc were higher in the stream than the background concentrations of iron and aluminum. Concentrations in the stream during the injection averaged 19 µM zinc, 17 µM copper, 0.068 µM lead, 0.80 µM iron, and 8.4 µM aluminum (Figure 4.4). These metals may have undergone greater removal if there were more colloids with which to interact. Ren and Packman (2005) observed greater retention of zinc in the sediment bed of a recirculating flume on increase in colloid concentration. Other minerals, such as phyllosilicates, and particulate organic matter may have provided the colloidal constituents in the stream water to explain the observed colloidal concentrations of copper. Colloidal silica concentrations averaged 23 µM. Galan et al. (2003) found that clay minerals were often coated with ferric (oxy) hydroxides and able to act as carriers of metals. Organic matter was not characterized in this experiment, but previous measurements showed dissolved organic matter concentrations ranged from 0.7 - 1.3 mg L^{-1} as C. Organic matter has been shown to bind with metals and enhance their transport by preventing their adsorption to sediments (Breault et al., 1996).

Total metal transport was evaluated using two different removal scenarios: (1) modeling main channel and storage zone removal rates simultaneously and (2) modeling the storage zone removal only assuming all removal occurs in the hyporheic zone. The second scenario was applied to determine how well hyporheic zone removal (as expressed by the storage zone

removal rate coefficient) could explain the observed metal removal. We expected that the majority of metal removal would occur in the hyporheic zone through sorption and filtration of colloid-associated metals. A Damkohler number greater than one was observed for the removal rate of lead in the first scenario, which indicates that removal is fast relative to travel time and equilibrium can be used to describe the model (Table 4.6). The Damkohler numbers for copper and zinc based on the first scenario and all the storage zone removal rates based on the second scenario are less than one, which indicates that the rate of removal is slow relative to the rate of advection and that the kinetics of removal are important. Though uncertainty in the parameters estimates limits interpretations of the differences between the two model scenarios, the second scenario provides an acceptable fit to the metal observations. This suggests that subsurface removal in the hyporheic zone can account for the observed removal.

The removal rate coefficients can be used to determine the relative metal removal occurring between the main channel and subsurface following the method described by Runkel (2007). Briefly, OTIS was used to obtain the total mass of each metal exiting the reach due to conservative transport and reactive transport, and the impacts of main channel removal and storage zone removal were distinguished. This comparison indicates that approximately 97% of lead and greater than 99% of the copper removal was accounted for by the main channel removal coefficients, while all of the minor zinc removal was accounted for by storage zone removal. This main channel removal may represent the processes of metal adsorption and colloid settling on the stream bed sediments. The storage zone removal coefficient is dependent on the transport of metals into the subsurface as modeled by the storage zone exchange coefficient (α) and storage cross-sectional area (A_S). Its relative importance is limited when the storage zone exchange rate coefficient α and the storage zone area A_S are small.

The separate models of dissolved and colloidal copper showed a large difference in main channel and storage zone removal rate coefficients (Table 4.6). Although the parameter values were uncertain, the model describing colloidal transport had removal rate coefficients an order of magnitude larger than those of the model describing dissolved copper transport. This experiment indicated that colloidal metal was transported differently from dissolved metal and suggested that colloids were responsible for the copper removal observed. The large surface removal rate coefficient for the colloidal copper is suggestive of settling, as described above. The storage zone removal rate coefficient for the colloidal copper indicates that the colloids enhance deposition in the hyporheic zone relative to the dissolved copper. This is in contrast to the findings of Chapter 2, where comparison of colloidal and dissolved metals indicated that colloids facilitated transport of lead, copper, and zinc.

Occurrence of metals, both colloidal and dissolved, in the subsurface pore water indicates that the metals did undergo hyporheic exchange. Though exchange was limited, all of the metals were found at the 5 cm depth. Past sequential extractions performed on sediments indicated deposition of metals associated with amorphous iron/manganese oxides at elevated levels at 20-40 cm depths (Chapter 2). This historical record of metal deposition suggests that metals and colloids undergo deeper hyporheic exchange. Analysis of metals at an intermediate depth between 5 and 40 cm may have shown evidence of deeper exchange. Also, a longer sampling time after the end of the injection may have allowed identification of longer flowpaths in the subsurface.

Metals and colloid-associated metals may be removed by adsorption and colloid filtration in the subsurface (Ren and Packman, 2005). Ren and Packman (2005) compared copper and zinc removal in a recirculating flume in the presence of hematite colloids. They measured

settling and filtration independently of the flume experiments by measuring settling velocity directly using a settling column and colloid filtration coefficients from column experiments. They found that model predictions had difficulty matching observations when the colloidal size distribution was complex. Copper was strongly adsorbed to hematite; this caused an increase in colloid size and point of zero charge and resulted in increased hematite filtration and settling in a sand bed, which caused increased removal of copper. Zinc also adsorbed to the hematite colloids, but to a lesser extent than copper. The maximum deposition of zinc was about 25% of the injected concentration compared to about 55% of deposited copper under similar conditions. Although the removal of zinc and copper in Left Hand Creek was much less than that removed in the flume experiment of Ren and Packman (2005), the comparison between copper and zinc follows the same trend. The smaller rate of removal in this experiment may be due to the stabilizing effect of sorbing organic matter, which tends to limit the size of colloids (Gaffney et al., 2008).

IMPLICATIONS

Injections of the contaminant metals of interest allow for a realistic measure of stream transport and removal through interaction with streambed sediments. Models describing metal transport should be calibrated based on direct in-stream observations (Zaramella et al., 2006). This experiment also showed the differences in metal transport behavior between metals and the importance of colloids in influencing transport and removal.

In-stream attenuation of certain metals occurs rapidly downstream of acid mine drainage inputs (Theobald et al., 1963; Chapman et al., 1983; Rampe and Runnells, 1989; Kimball et al., 1995; Munk et al., 2002; Ranville et al., 2004). Metals with high adsorption affinity may adsorb not only to the sediment surfaces, but also to colloids. Metals with a higher sorption affinity; i.e.,

copper and lead, were removed to a greater extent than zinc, which remained dissolved through the main channel reach. Modeling of dissolved and colloidal copper with separate fits indicated that colloidal removal was enhanced compared to removal of the dissolved phase in both the stream and subsurface. Both dissolved and colloidal lead and copper were found in the in the shallow pore waters of the hyporheic zone, which indicates that metal-associated colloid exchange does occur for metals with high adsorption affinities. Though the relative importance of hyporheic exchange is small based on the results of the modeling, the process of hyporheic exchange increases metal contact with sediment surfaces and provides a removal mechanism for colloids and colloid-associated metals through filtration and settling in the sediments.

REFERENCES

Axtmann, E.V., Luoma, S.N. (1991) Large-scale distribution of metal contamination in the fine-grained sediments of the Clark Fork River, Montana, USA. *Applied Geochemistry* 6 (1) 75-88.

Benner, S.G., Smart, E.W., Moore, J.N. (1995) Metal behavior during surface groundwater interaction, Silver-Bow Creek, Montana. *Environmental Science & Technology* 29 (7) 1789-1795.

Breault, R. F., Colman, J. A., Aiken, G. R., McKnight, D. (1996) Copper speciation and binding by organic matter in copper-contaminated streamwater. *Environmental Science & Technology 30*(12) 3477-3486.

Chapman, B.M., Jones, D.R., Jung, R.F. (1983) Processes controlling metal-ion attenuation in acid-mine drainage streams. *Geochimica et Cosmochimica Acta* 47 (11) 1957-1973.

CDPHE (2003) Captain Jack superfund site aerial photo. Colorado Hazardous Materials and Waste Management Division of the Colorado Department of Public Health and Environment.

Cobb, H.S. (1988) *Prospecting Our Past: Gold, Silver and Tungsten Mills of Boulder County*. The Book Lode, Longmont, Colorado.

Davies, S.H.R., Morgan, J.J. (1989) Manganese(II) oxidation-kinetics on metal-oxide surfaces. *Journal of Colloid and Interface Science* 129 (1) 63-77.

Davis, M.W., Streufert, R.K. (1990) Gold occurrences of Colorado. Resource Series 28, Colorado Geological Survey, Denver, Colorado.

Dzombak, D.A., Morel, F.M.M. (1990) *Surface Complexation Modeling: Hydrous Ferric Oxide*. John Wiley & Sons, New York.

Evans, D., Davies, B.E. (1994) The influence of channel morphology on the chemical partitioning of Pb and Zn in contaminated river sediments. *Applied Geochemistry* 9 (1) 45-52.

Gaffney, J. W., White, K. N., Boult, S. (2008) Oxidation state and size of Fe controlled by organic matter in natural waters. *Environmental Science & Technology 42*(10) 3575-3581.

Galán, E., Gomez-Ariza, J.L., Gonzalez, I., Fernandez-Caliani, J.C., Morales, E., Giraldez, I. (2003) Heavy metal partitioning in river sediments severely polluted by acid mine drainage in the Iberian Pyrite Belt. *Applied Geochemistry* 18 (3) 409-421.

Gammons, C. H., Nimick, D. A., Parker, S. R., Cleasby, T. E. and McCleskey, R. B. (2005) Diel behavior of iron and other heavy metals in a mountain stream with acidic to neutral pH: Fisher Creek, Montana, USA. *Geochimica et Cosmochimica Act* 69, 2505-2516.

Gandy, C.J., Smith, J.W.N., Jarvis, A.P. (2007) Attenuation of mining-derived pollutants in the hyporheic zone: A review. *Science of the Total Environment* 373 (2-3) 435-446.

Ganguli, P.M., Mason, R.P., Abu-Saba, K.E., Anderson, R.S., Flegal, A.R. (2000) Mercury speciation in drainage from the New Idria mercury mine, California. *Environmental Science & Technology* 34 (22) 4773-4779.

Harvey, R.W., George, L.H., Smith, R.L., LeBlanc, D.R. (1989) Transport of microspheres and indigenous bacteria through a sandy aquifer: Results of natural and forced-gradient tracer experiments. *Environmental Science & Technology* 23 (1) 51-56.

Harvey, J. W., Wagner, B. J., Bencala, K. E. (1996) Evaluating the reliability of the stream tracer approach to characterize stream-subsurface water exchange. *Water Resources Research 32*(8) 2441-2451.

Harvey, J.W., Wagner, B.J. (2000) Quantifying hydrologic interactions between streams and their subsurface hyporheic zones. In *Streams and Ground Waters*, Jones, J.B., Mulholland, P.J. (Eds.), Academic Press, San Diego, p. 3.

Harvey, J. W., Conklin, M. H., Koelsch, R. S. (2003) Predicting changes in hydrologic retention in an evolving semi-arid alluvial stream. *Advances in Water Resources 26*(9) 939-950.

Hrncir, D. C., Mcknight, D. (1998) Variation in photoreactivity of iron hydroxides taken from an acidic mountain stream. *Environmental Science & Technology* 32(14) 2137-2141.

Johnson, C.A. (1986) The regulation of trace-element concentrations in river and estuarine waters contaminated with acid-mine drainage - the adsorption of Cu and Zn on amorphous Fe oxyhydroxides. *Geochimica et Cosmochimica Acta* 50 (11) 2433-2438.

Karwan, D.L., Saiers J.E. (2009) Influences of seasonal flow regime on the fate and transport of fine particles and a dissolved solute in a new england stream. *Water Resources Research* 45 (11) doi:10.1029/2009WR008077.

Kimball, B.A., Mcknight, D.M., Wetherbee, G.A., Harnish, R.A. (1992) Mechanisms of iron photoreduction in a metal-rich, acidic stream (St.Kevin Gulch, Colorado, USA). *Chemical Geology* 96 (1-2) 227-239.

Kimball, B.A., Callender, E., Axtmann, E.V. (1995) Effects of colloids on metal transport in a river receiving acid-mine drainage, Upper Arkansas River, Colorado, USA. *Applied Geochemistry* 10 (3) 285-306.

Lee, G., Bigham, J. M. and Faure, G. (2002) Removal of trace metals by coprecipitation with Fe, Al and Mn from natural waters contaminated with acid mine drainage in the Ducktown Mining District, Tennessee. *Applied Geochemistry* 17, 569-581.

Martinez, C. E. and M. B. McBride (1998) Solubility of Cd^{2+}, Cu^{2+}, Pb^{2+}, and Zn^{2+} in aged coprecipitates with amorphous iron hydroxides. *Environmental Science & Technology* 32(6) 743-748.

McKnight, D. M., Duren, S. M. (2004) Biogeochemical processes controlling midday ferrous iron maxima in stream waters affected by acid rock drainage. *Applied Geochemistry* 19(7) 1075-1084.

Munk, L., Faure, G., Pride, D.E., Bigham, J.M. (2002) Sorption of trace metals to an aluminum precipitate in a stream receiving acid rock-drainage; Snake River, Summit County, Colorado. *Applied Geochemistry* 17 (4) 421-430.

Mutz, M., E. Kalbus, Meinecke, S. (2007) Effect of instream wood on vertical water flux in low-energy sand bed flume experiments, *Water Resources Research* 43(10) W10424, doi:10.1029/2006WR005676.

Nagorski, S.A., Moore, J.N., Smith, D.B. (2002) Distribution of metals in water and bed sediment in a mineral-rich watershed, Montana, USA. *Mine Water and the Environment* 21 (3) 121-136.

Nieboer, E., Richardson, D.H.S. (1980) The replacement of the nondescript term `heavy metals' by a biologically and chemically significant classification of metal ions. *Environmental Pollution Series B, Chemical and Physical* 1 (1) 3-26.

Pearson, R.G. (1986a) Hard and soft acids and bases, HSAB part 1: fundamental principles. *Journal of Chemical Education* (45) 581-587.

Pearson, R.G. (1986b) Hard and soft acids and bases, HSAB part 2: underlying yheories. *Journal of Chemical Education* (45) 643-648.

Rampe, J.J., Runnells, D.D. (1989) Contamination of water and sediment in a desert stream by metals from an abandoned gold mine and mill, Eureka District, Arizona, USA. *Applied Geochemistry* 4 (5) 445-454.

Ranville, M., Rough, D., Flegal, A.R. (2004) Metal attenuation at the abandoned Spenceville copper mine. *Applied Geochemistry* 19 (5) 803-815.

Ren, J.H., Packman, A.I. (2004a) Modeling of simultaneous exchange of colloids and sorbing contaminants between streams and streambeds. *Environmental Science & Technology* 38 (10) 2901-2911.

Ren, J.H., Packman, A.I. (2004b) Stream-subsurface exchange of zinc in the presence of silica and kaolinite colloids. *Environmental Science & Technology* 38 (24) 6571-6581.

Ren, J.H., Packman, A.I. (2005) Coupled stream-subsurface exchange of colloidal hematite and dissolved zinc, copper, and phosphate. *Environmental Science & Technology* 39 (17) 6387-6394.

Ren, J.H., Packman, A.I., Welty, C. (2000) Correlation of colloid collision efficiency with hydraulic conductivity of silica sands. *Water Resources Research* 36 (9) 2493-2500.

Rose, S., Ghazi, A.M. (1998) Experimental study of the stability of metals associated with iron oxyhydroxides precipitated in acid mine drainage. *Environmental Geology* 36 (3-4) 364-369.

Runkel, R.L. (1998) One-Dimensional Transport with Inflow and Storage (OTIS): A solute transport model for streams and rivers. Water-Resources Investigations Report 98-4018, U.S. Geological Survey, Denver, Colorado.

Runkel, R.L. (2002) A new metric for determining the importance of transient storage. *Journal of the North American Benthological Society* 21 (4) 529-543.

Runkel, R.L. (2007) Toward a transport-based analysis of nutrient spiraling and uptake in streams. *Limnology and Oceanography-Methods* 5: 50-62.

Schemel, L.E., Kimball, B.A., Runkel, R.L., Cox, M.H. (2007) Formation of mixed Al-Fe colloidal sorbent and dissolved-colloidal partitioning of Cu and Zn in the Cement Creek - Animas River Confluence, Silverton, Colorado. *Applied Geochemistry* 22 (7) 1467-1484.

Scott, D. T., Gooseff, M. N., Bencala, K. E., Runkel, R. L. (2003) Automated calibration of a stream solute transport model: implications for interpretation of biogeochemical parameters. *Journal of the North American Benthological Society 22*(4) 492-510.

Sullivan, A.B., Drever, J.I. (2001) Geochemistry of suspended particles in a mine-affected mountain stream. *Applied Geochemistry* 16 (15), 1663-1676.

Theobald, P.K., Lakin, H.W., Hawkins, D.B. (1963) The precipitation of aluminum, iron and manganese at the junction of Deer Creek with the Snake River in Summit County, Colorado. *Geochimica et Cosmochimica Acta* 27 (Feb) 121-&.

Tonkin, J.W., Balistrieri, L.S., Murray, J.W. (2002) Modeling metal removal onto natural particles formed during mixing of acid rock drainage with ambient surface water. *Environmental Science & Technology* 36 (3) 484-492.

Triska, F.J., Kennedy, V.C., Avanzino, R.J., Zellweger, G.W., Bencala, K.E. (1989) Retention and transport of nutrients in a third-order stream in northwestern California: hyporheic processes. *Ecology* 70 (6) 1893-1905.

USEPA, 2003. Left Hand Creek watershed case study: Use of NPL as a catalyst for abandoned mine cleanup. United States Environmental Protection Agency, 6 p. (accessed on March 17, 2011, at http://www.epa.gov/aml/tech/lefthand.pdf).

Wagner, B.J., Harvey, J.W. (1997) Experimental design for estimating parameters of rate-limited mass transfer: Analysis of stream tracer studies. *Water Resources Research* 33 (7) 1731-1741.

Wanty, R.B., Winter, T.C. (2000) A simple device for measuring differences in hydraulic head between surface water and shallow groundwater. Fact Sheet FS-077-00, U.S. Geological Survey, Washington, DC.

Wondzell, S. M. (2006) Effect of morphology and discharge on hyporheic exchange flows in two small streams in the Cascade Mountains of Oregon, USA. *Hydrological Processes 20*(2) 267-287.

Wood, A.R. 2004. Characterization and prioritization of mining-related metal sources with metal loading tracer dilution tests, and a review of regulations and mine restoration funding resources, Lefthand Creek watershed, northwestern Boulder County, Colorado. M.S. Thesis, University of Colorado, Boulder, Colorado.

Zanker, H., Richter, W., Huttig, G. (2003) Scavenging and immobilization of trace contaminants by colloids in the waters of abandoned ore mines. *Colloids and Surfaces A-Physicochemical and Engineering Aspects* 217 (1-3) 21-31.

Zaramella, M., Marion, A., Packman, A.I. (2006) Applicability of the transient storage model to the hyporheic exchange of metals. *Journal of Contaminant Hydrology* 84 (1-2) 21-35.

Zarnetske, J. P., Gooseff, M. N., Brosten, T. R., Bradford, J. H., McNamara, J. P., Bowden, W. B. (2007) Transient storage as a function of geomorphology, discharge, and permafrost active layer conditions in Arctic tundra streams. *Water Resources Research* 43(7) doi:10.1029/2005WR004816.

CHAPTER 5 - CONCLUSIONS AND RECOMMENDATIONS

SUMMARY AND CONCLUSIONS

In this study, we examined the role of hyporheic exchange and colloidal transport for controlling metal transport in a contaminated stream system. Hyporheic exchange offers a mechanism for removal of metals by providing contact with sediment surfaces. The hyporheic zone is an important zone where transformations may occur and metals may be stored. Colloidal transport is an important mechanism to consider for some metals, such as lead and copper.

The link between surface and subsurface flow has been examined. Although a transient storage model describing solute transport indicated that transient storage plays a minor role in solute transport in our study reach, subsurface measurements offer insight into the role of the hyporheic zone. Piezometer results indicated that only the shallow depths (5 cm) are highly interactive with the stream, but the piezometer measurements also revealed well-connected flowpaths to depths of 40 cm and much longer flowpaths were indicated by increases in concentrations at the final measurements made at approximately 25 h at the 100 cm depths. The variation in connectivity is likely due to subsurface heterogeneity which causes preferential flowpaths through the hyporheic zone. The hydraulic head gradients and hydraulic conductivity measurements showed variability in the ability of water to flow through the subsurface and suggested layers of more and less permeable sediments. Despite the small hyporheic zone, the sediments offer a site for the accumulation of metals and colloids through adsorption and filtration.

The chemistry of the hyporheic zone was expected to control the stability of colloids and the likely distribution of metals between dissolved and sorbed phases. Electrical conductivity, pH, and dissolved oxygen measurements with depth in the hyporheic zone showed values similar

to the surface waters in the shallow depths, suggesting that hyporheic exchange provides substantial surface water to enter the subsurface pore waters. Sequential extractions of the sediments showed that trace metals were incorporated in iron and manganese oxide coatings found on the streambed sediments. The high colloidal concentrations of lead and copper and their close relationship with iron, manganese, and aluminum in the stream and hyporheic zone suggests that they adsorb to mobile colloidal forms of these oxides under the stream flow and chemical conditions present in the study reach. These colloids are likely immobilized by colloidal filtration mechanisms and constitute the amorphous coatings found on the sediment grains.

A tracer dilution test involving ferric (oxy)hydroxide colloids showed that colloids are rapidly removed in the sediments. The irreversible colloid removal was modeled as a first order removal process in the storage zone. Piezometer measurements showed that the majority of colloids entering the subsurface are removed in the upper 5 cm. Variability between piezometers was attributed to variation in streambed topography controlling hyporheic exchange and subsurface heterogeneity in the hydraulic conductivities of the subsurface locations. Once the colloids enter the streambed sediments, they undergo physicochemical filtration in the hyporheic zone.

Comparison of lead, copper, and zinc removal in the stream showed a difference in transport between the metals attributed to their sorption affinities. Zinc was largely dissolved, while colloidal fractions of copper and lead affected their transport. Approximately 17.6% of lead and 4.6% of copper were lost from the main channel of the stream over the reach, while zinc was transported conservatively through the reach (0.061% removal). Zinc was found to be almost entirely dissolved, while both dissolved and colloidal lead and copper were found in the

in the shallow pore waters of the hyporheic zone, indicating that metal-associated colloid exchange does occur for metals with high adsorption affinities. Modeling of dissolved and colloidal copper with separate fits indicated that colloidal removal was greatly enhanced compared to removal of the dissolved phase. Though the relative importance of hyporheic exchange is small based on the results of the modeling, the process of hyporheic exchange increases metal contact with sediment surfaces and provides a removal mechanism for colloids through filtration in the hyporheic zone.

Challenges and Future Directions

It is difficult to integrate surface and subsurface transport into our understanding of lotic systems. The time scales of hyporheic exchange are often much slower than that of transport through a stream reach. Modeling using transient storage and the traditional stream tracer approach generally indicates minimal influence of stream-subsurface exchange due to the short advective transport time compared with the time scale of exchange. However, this process can still be important for accumulating nutrients and contaminants in the hyporheic zone where important processes controlling the health of the aquatic ecosystem occur.

Field investigations of contaminant transport should recognize that the traditional stream tracer approach will not capture stream-subsurface exchange that occurs at longer time scales. These longer time scale interactions may still play an important role in controlling the aquatic health of the system. When the impacts to the hyporheic zone are important to an investigation, separate sampling of subsurface pore waters and sediments will be needed.

Modeling of hyporheic transport has been largely focused on waveforms induced in a sand bed, but interactions caused by a solid obstruction such as boulders may also affect exchange. Hutchinson and Webster (1998) conducted flume experiments with a half-buried

spherical object and found that objects such as stones in a streambed caused pressure perturbations which drove surface-subsurface exchange. The effect of this phenomenon on solute transport has not been studied in the field.

Contamination of the sediments by a buildup of metals associated with (oxy)hydroxides may be a source of contamination back to the stream. The chemically labile hydroxides are subject to release back to the stream when chemical conditions cause desorption to occur or when physical events, such as turbulence during flooding, scour loosely held materials. This possibility should be considered in cleanup efforts and goal evaluation and leads to greater complexity in the plans for mine site remediation.

REFERENCES

Hutchinson, P.A., Webster, I.T. (1998) Solute uptake in aquatic sediments due to current-obstacle interactions. *Journal of Environmental Engineering* 124 (5) 419-426.

REFERENCES

Aiken, G. R., McKnight, D.M., Thorn, K.A., Thurman, E.M. (1992) Isolation of hydrophilic organic acids from water using nonionic macroporous resins. *Organic Geochemistry* 18 (4) 567-73.

American Public Health Association (2005) Standard methods for the examination of water and wastewater (21st ed): Washington, D.C., published jointly by American Public Health Association, American Water Works Association, and Water Environment Federation, Washington, DC.

Axtmann, E.V., Luoma, S.N. (1991) Large-cale distribution of metal contamination in the finegrained sediments of the Clark Fork River, Montana, USA. *Applied Geochemistry* 6 (1) 75-88.

Bencala, K. E., Walters, R. A. (1983) Simulation of solute transport in a mountain pool-and-riffle stream - a transient storage model. *Water Resources Research* 19 (3) 718-724.

Bencala, K.E. (1984) Interactions of solutes and streambed sediment 2. A dynamic analysis of coupled hydrologic and chemical processes that determine solute transport. *Water Resources Research* 20 (12) 1804-1814.

Benjamin, M. M., Leckie, J. O. (1981) Multiple-site adsorption of Cd, Cu, Zn, and Pb on amorphous iron oxyhydroxide. *Journal of Colloid and Interface Science 79* (1) 209-221.

Benner, S.G., Smart, E.W., Moore, J.N. (1995) Metal behavior during surface groundwater interaction, Silver-Bow Creek, Montana. *Environmental Science & Technology* 29 (7) 1789-1795.

Borgmann, U., Couillard, Y., Doyle, P., Dixon, D.G. (2005) Toxicity of sixty-three metals and metalloids to *Hyalella azteca* at two levels of water hardness. *Environmental Toxicology and Chemistry* 24 (3) 641-652.

Bradford, S. A., Simunek, J., Bettahar, M., Van Genuchten, M. T. and Yates, S. R. (2003) Modeling colloid attachment, straining, and exclusion in saturated porous media. *Environmental Science & Technology,* 37, 2242-2250.

Breault, R. F., Colman, J. A., Aiken, G. R., McKnight, D. (1996) Copper speciation and binding by organic matter in copper-contaminated streamwater. *Environmental Science & Technology 30*(12) 3477-3486.

Brunke, M. (1999) Colmation and depth filtration within streambeds: Retention of particles in hyporheic interstices. *International Review of Hydrobiology,* 84, 99-117.

Butler, B.A., Ranville, J.F., Ross, P.E. (2008) Observed and modeled seasonal trends in dissolved and particulate Cu, Fe, Mn, and Zn in a mining-impacted stream. *Water Research* 42 (12) 3135-3145.

Cahoon, D.R., Lynch, J.C., Knaus, R.M. (1996) Improved cryogenic coring device for sampling wetland soils. *Journal of Sedimentary Research* 66 (5) 1025-1027.

CDPHE (2003) Captain Jack superfund site aerial photo. Colorado Hazardous Materials and Waste Management Division of the Colorado Department of Public Health and Environment

Chapman, B.M., Jones, D.R., Jung, R.F. (1983) Processes controlling metal-ion attenuation in acid-mine drainage streams. *Geochimica et Cosmochimica Acta* 47 (11) 1957-1973.

CDPHE (2003) Captain Jack superfund site aerial photo. Colorado Hazardous Materials and Waste Management Division of the Colorado Department of Public Health and Environment

Cobb, H.S. (1988) *Prospecting Our Past: Gold, Silver and Tungsten Mills of Boulder County*. The Book Lode, Longmont, Colorado.

Davies, S.H.R., Morgan, J.J. (1989) Manganese(II) oxidation-kinetics on metal-oxide surfaces. *Journal of Colloid and Interface Science* 129 (1) 63-77.

Davis, M.W., Streufert, R.K. (1990) Gold occurrences of Colorado. Resource Series 28, Colorado Geological Survey, Denver, Colorado.

Derjaguin, B. V. and Landau, L. (1941) Theory of the stability of strongly charged lyophobic sols and the adhesion of strongly charged particles in solutions of electrolytes. *Acta Physicochimica URSS,* 14, 633-662.

Dzombak, D.A., Morel, F.M.M., 1990. *Surface Complexation Modeling: Hydrous Ferric Oxide*. John Wiley & Sons, New York.

Eberl, D.D. (2003) User guide to RockJock: a program for determining quantitative mineralogy from x-ray diffraction data. United States Geological Survey, Open File Report 03-78, 40 p.

Evans, D., Davies, B.E. (1994) The influence of channel morphology on the chemical partitioning of Pb and Zn in contaminated river sediments. *Applied Geochemistry* 9 (1) 45-52.

Farag, A.M., Woodward, D.F., Goldstein, J.N., Brumbaugh, W., Meyer, J.S. (1998) Concentrations of metals associated with mining waste in sediments, biofilm, benthic macroinvertebrates, and fish from the Coeur d'Alene River Basin, Idaho. *Archives of Environmental Contamination and Toxicology* 34 (2) 119-127.

Farag, A. M., Nimick, D. A., Kimball, B. A., Church, S. E., Harper, D. D., Brumbaugh, W. G. (2007) Concentrations of metals in water, sediment, biofilm, benthic macroinvertebrates, and fish in the Boulder River watershed, Montana, and the role of colloids in metal uptake. *Archives of Environmental Contamination and Toxicology 52*(3) 397-409.

Feris, K.P., Ramsey, P.W., Gibbons, S.M., Frazar, C., Rillig, M.C., Moore, J.N., Gannon, J.E., Holben, W.E. (2009) Hyporheic microbial community development is a sensitive indicator of metal contamination. *Environmental Science & Technology* 43 (16) 6158-6163.

Fuller, C.C., Davis, J.A., 1989, Influence of coupling of sorption and photosynthetic processes on trace element cycles in natural waters. *Nature* 340 (6228) 52-54.

Fuller, C. C., Harvey, J. W. (2000) Reactive uptake of trace metals in the hyporheic zone of a mining-contaminated stream, Pinal Creek, Arizona. *Environmental Science & Technology* 34 (7) 1150-1155.

Gaffney, J. W., White, K. N., Boult, S. (2008) Oxidation state and size of Fe controlled by organic matter in natural waters. *Environmental Science & Technology 42*(10) 3575-3581.

Galán, E., Gomez-Ariza, J.L., Gonzalez, I., Fernandez-Caliani, J.C., Morales, E., Giraldez, I. (2003) Heavy metal partitioning in river sediments severely polluted by acid mine drainage in the Iberian Pyrite Belt. *Applied Geochemistry* 18 (3) 409-421.

Gandy, C.J., Smith, J.W.N., Jarvis, A.P. (2007) Attenuation of mining-derived pollutants in the hyporheic zone: A review. *Science of the Total Environment* 373 (2-3) 435-446.

Gammons, C. H., Nimick, D. A., Parker, S. R., Cleasby, T. E. and McCleskey, R. B. (2005) Diel behavior of iron and other heavy metals in a mountain stream with acidic to neutral pH: Fisher Creek, Montana, USA. *Geochimica et Cosmochimica Act* 69, 2505-2516.

Gandy, C.J., Smith, J.W.N., Jarvis, A.P. (2007) Attenuation of mining-derived pollutants in the hyporheic zone: A review. *Science of the Total Environment* 373 (2-3) 435-446.

Ganguli, P.M., Mason, R.P., Abu-Saba, K.E., Anderson, R.S., Flegal, A.R. (2000) Mercury speciation in drainage from the New Idria mercury mine, California. *Environmental Science & Technology* 34 (22) 4773-4779.

Hart, B.T., Noller, B.N., Legras, C., Currey, N. (1992) Manganese speciation in Magela Creek, Northern Australia. *Australian Journal of Marine and Freshwater Research* 43 (2) 421-441.

Harvey, J.W., Bencala, K.E. (1993) The effect of streambed topography on surface-subsurface water exchange in mountain catchments. *Water Resources Research* 29 (1) 89-98.

Harvey, J. W., Conklin, M. H., Koelsch, R. S. (2003) Predicting changes in hydrologic retention in an evolving semi-arid alluvial stream. *Advances in Water Resources 26*(9) 939-950.

Harvey, J.W., Fuller, C.C. (1998) Effect of enhanced manganese oxidation in the hyporheic zone on basin-scale geochemical mass balance. *Water Resources Research* 34 (4) 623-636.

Harvey, R.W., George, L.H., Smith, R.L., LeBlanc, D.R. (1989) Transport of microspheres and indigenous bacteria through a sandy aquifer: Results of natural and forced-gradient tracer experiments. *Environmental Science & Technology* 23 (1) 51-56.

Harvey, J.W., Wagner, B.J. (2000) Quantifying hydrologic interactions between streams and their subsurface hyporheic zones. In *Streams and Ground Waters*, Jones, J.B., Mulholland, P.J. (Eds.), Academic Press, San Diego, p. 3.

Harvey, J. W., Wagner, B. J., Bencala, K. E. (1996) Evaluating the reliability of the stream tracer approach to characterize stream-subsurface water exchange. *Water Resources Research 32* (8) 2441-2451.

Hill, M.T.R. (1999) A freeze-corer for simultaneous sampling of benthic macroinvertebrates and bed sediment from shallow streams. *Hydrobiologia* 412, 213-215.

Hiemenz, P.C., Rajagopalan, R. (1997) *Principles of colloid and surface chemistry*. Marcel Dekker, New York.

Horowitz A. F., Rinella F.A., Lamothe P., Miller T.L., Edwards T.K., Roche R.L., Rickert D.A. (1990) Variations in suspended sediment and associated trace element concentrations in selected riverine cross sections. *Environmental Science & Technology* 24 (9), 1313-1320.

Hrncir, D. C., Mcknight, D. (1998) Variation in photoreactivity of iron hydroxides taken from an acidic mountain stream. *Environmental Science & Technology* 32(14) 2137-2141.

Hutchinson, P.A., Webster, I.T. (1998) Solute uptake in aquatic sediments due to current-obstacle interactions. *Journal of Environmental Engineering* 124 (5) 419-426.

Hvorslev, M.J. 1951. Time lag and soil permeability in groundwater observations. U.S. Army Corps of Engineers, Waterways Experimental Station. Vicksburg, Mississippi, Bulletin 36, 57 p.

Johnson, C.A. (1986) The regulation of trace-element concentrations in river and estuarine waters contaminated with acid-mine drainage – The adsorption of Cu and Zn on amorphous Fe oxyhydroxides. *Geochimica et Cosmochimica Acta* 50 (11) 2433-2438.

Karwan, D. L., Saiers, J. E. (2009). Influences of seasonal flow regime on the fate and transport of fine particles and a dissolved solute in a New England stream. *Water Resources Research 45* (11) doi:10.1029/2009WR008077.

Kennedy, V.C., Jackman, A.P., Zand, S.M., Zellweger, G.W., Avanzino, R.J. (1984) Transport and concentration controls for chloride, strontium, potassium and lead in Uvas Creek, a small cobble-bed stream in Santa Clara County, California, U.S.A. 1. Conceptual Model. *Journal of Hydrology* 75 (1-4) 67-110.

Kimball, B.A. Callender, E., Axtmann, E.V., (1995) Effects of colloids on metal transport in a river receiving acid-mine drainage, Upper Arkansas River, Colorado, USA. *Applied Geochemistry* 10 (3) 285-306.

Kimball, B.A., Mcknight, D.M., Wetherbee, G.A., Harnish, R.A. (1992) Mechanisms of iron photoreduction in a metal-rich, acidic stream (St. Kevin Gulch, Colorado, USA). *Chemical Geology* 96 (1-2) 227-239.

Kretzschmar, R., Sticher, H. (1997) Transport of humic-coated iron oxide colloids in a sandy soil: influence of Ca^{2+} and trace metals. Environmental Science & Technology 31 (12) 3497-3504.

Kuwabara, J. S., Leland, H. V., Bencala, K. E. (1984) Copper transport along a sierra-nevada stream. *Journal of Environmental Engineering-ASCE 110* (3) 646-655.

Lee, D. R., Cherry, J. A. (1978) A Field Exercise on Groundwater Flow Using Seepage Meters and Mini-piezometers. Journal of Geological Education 27, 6 - 10.

Lee, G., Bigham, J. M. and Faure, G. (2002) Removal of trace metals by coprecipitation with Fe, Al and Mn from natural waters contaminated with acid mine drainage in the Ducktown Mining District, Tennessee. *Applied Geochemistry* 17, 569-581.

Mahler, B.J., Bennett, P.C., Zimmerman, M. (1998a) Lanthanide-labeled clay: a new method for tracing sediment transport in karst. *Ground Water* 36 (5) 835-843.

Mahler, B.J., Winkler, M., Bennett, P., Hillis, D.M. (1998b) DNA-labeled clay: a sensitive new method for tracing particle transport. *Geology* 26 (9) 831-834.

Malcolm, I.A., Soulsby, C., Youngson, A.F., Hannah, D.M., McLaren, I.S., Thorne, A. (2004) Hydrological influences on hyporheic water quality: implications for salmon egg survival. *Hydrological Processes* 18 (9) 1543-1560.

Martinez, C. E. and McBride, M. B. (1998) Solubility of Cd^{2+}, Cu^{2+}, Pb^{2+}, and Zn^{2+} in aged coprecipitates with amorphous iron hydroxides. *Environmental Science & Technology* 32, 743-748.

McCarthy, J. F. and Zachara, J. M. (1989) Subsurface transport of contaminants. *Environmental Science & Technology,* 23, 496-502.

McDowell-Boyer, L. M., Hunt, J. R. Sitar, N. (1986) Particle transport through porous media *Water Resources Research* 22 (13) 1901-1921.

McKnight, D. M., Duren, S. M. (2004) Biogeochemical processes controlling midday ferrous iron maxima in stream waters affected by acid rock drainage. *Applied Geochemistry* 19(7) 1075-1084.

Munk, L., Faure, G., Pride, D.E., Bigham, J.M. (2002) Sorption of trace metals to an aluminum precipitate in a stream receiving acid rock-drainage; Snake River, Summit County, Colorado. *Applied Geochemistry* 17 (4) 421-430.

Mutz, M., E. Kalbus, Meinecke, S. (2007) Effect of instream wood on vertical water flux in low-energy sand bed flume experiments, *Water Resources Research* 43(10) doi:10.1029/2006WR005676.

Nagorski, S.A., Moore, J.N., Smith, D.B. (2002) Distribution of metals in water and bed sediment in a mineral-rich watershed, Montana, USA. *Mine Water and the Environment* 21 (3) 121-136.

Nieboer, E., Richardson, D. H. S. (1980) The replacement of the nondescript term `heavy metals' by a biologically and chemically significant classification of metal ions. *Environmental Pollution Series B, Chemical and Physica1*1 (1) 3-26.

Packman, A.I., Brooks, N.H. (2001) Hyporheic exchange of solutes and colloids with moving bed forms. *Water Resources Research* 37 (10) 2591-2605.

Packman, A.I., Brooks, N.H., Morgan, J.J. (2000) A physicochemical model for colloid exchange between a stream and a sand streambed with bed forms. *Water Resources Research* 36 (8) 2351-2361.

Pearson, R. G. (1986a) Hard and soft acids and bases, HSAB part 1: fundamental principles. *Journal of Chemical Education* 45, 581-587.

Pearson, R. G. (1986b) Hard and soft acids and bases, HSAB part 2: underlying theories. *Journal of Chemical Education* 45, 643-648.

Puls, R.W., Powell, R.M. (1992) Transport of inorganic colloids through natural aquifer material: implications for contaminant transport. *Environmental Science & Technology* 26 (3) 614-621.

Quinn, K.A., Byrne, R.H., Schijf, J. (2006) Sorption of yttrium and rare earth elements by amorphous ferric hydroxide: Influence of pH and ionic strength. *Marine Chemistry* 99 (1-4) 128-150.

R Development Core Team, 2009. R: A Language and Environment for Statistical Computing. R Foundation for Statistical Computing (Ed.), Vienna, Austria.

Rampe, J.J., Runnells, D.D. (1989) Contamination of water and sediment in a desert stream by metals from an abandoned gold mine and mill, Eureka District, Arizona, USA. *Applied Geochemistry* 4 (5) 445-454.

Ranville, M., Rough, D., Flegal, A.R. (2004) Metal attenuation at the abandoned Spenceville copper mine. *Applied Geochemistry* 19 (5) 803-815.

Reed, S. J. B. (1996) Electron microbe analysis and scanning electron microscopy in geology. Cambridge University Press, New York, 201 pp.

Ren, J.H., Packman, A.I. (2004a) Modeling of simultaneous exchange of colloids and sorbing contaminants between streams and streambeds. *Environmental Science & Technology* 38 (10) 2901-2911.

Ren, J.H., Packman, A.I. (2004b) Stream-subsurface exchange of zinc in the presence of silica and kaolinite colloids. *Environmental Science & Technology* 38 (24) 6571-6581.

Ren, J.H., Packman, A.I. (2005) Coupled stream-subsurface exchange of colloidal hematite and dissolved zinc, copper, and phosphate. *Environmental Science & Technology* 39 (17) 6387-6394.

Ren, J.H., Packman, A.I., Welty, C. (2000) Correlation of colloid collision efficiency with hydraulic conductivity of silica sands. *Water Resources Research* 36 (9), 2493-2500.

Rose, S. and Ghazi, A. M. (1998) Experimental study of the stability of metals associated with iron oxyhydroxides precipitated in acid mine drainage. *Environmental Geology* 36, 364-369.

Runkel, R.L. (1998) One-dimensional transport with inflow and storage (OTIS): A solute transport model for streams and rivers. Water-Resources Investigations Report 98-4018, U.S. Geological Survey, Denver, Colorado.

Runkel, R.L. (2002) A new metric for determining the importance of transient storage. *Journal of the North American Benthological Society* 21 (4) 529-543.

Runkel, R.L. (2007) Toward a transport-based analysis of nutrient spiraling and uptake in streams. *Limnology and Oceanography-Methods* 5: 50-62.

Runkel, R. L., Kimball, B. A., McKnight, D. M., Bencala, K. E. (1999) Reactive solute transport in streams: A surface complexation approach for trace metal sorption. *Water Resources Research 35* (12) 3829-3840.

Runkel, R. L., McKnight, D.M., Rajaram H. (2003) Modeling hyporheic zone processes. *Advances in Water Resources* 26 (9) 901-905.

Ryan, J.N., Elimelech, M., Magelky, R.D., Baseman, J.L. (2000) Silica-coated titania and zirconia colloids for subsurface transport field experiments. *Environmental Science & Technology* 34 (10) 2000-2005.

Schemel, L.E., Kimball, B.A., Bencala, K.E. (2000) Colloid formation and metal transport through two mixing zones affected by acid mine drainage near Silverton, Colorado. *Applied Geochemistry* 15 (7) 1003-1018.

Schemel, L.E., Kimball, B.A., Runkel, R.L., Cox, M.H. (2007) Formation of mixed Al-Fe colloidal sorbent and dissolved-colloidal partitioning of Cu and Zn in the Cement Creek - Animas River confluence, Silverton, Colorado. *Applied Geochemistry* 22 (7) 1467-1484.

Schwertmann, U., Cornell, R.M. (2000) *Iron Oxides in the Laboratory: Preparation and Characterization*. Wiley-VCH, New York.

Scott, D. T., Gooseff, M. N., Bencala, K. E., Runkel, R. L. (2003) Automated calibration of a stream solute transport model: implications for interpretation of biogeochemical parameters. *Journal of the North American Benthological Society 22*(4) 492-510.

Sprycha, R., Jablonski, J., Matijevic, E. (1992) Zeta-potential and surface-charge of monodispersed colloidal yttrium(iii) oxide and basic carbonate. *Journal of Colloid and Interface Science 149* (2) 561-568.

Storey, R.G., Howard, K.W.F., Williams, D.D. (2003) Factors controlling riffle-scale hyporheic exchange flows and their seasonal changes in a gaining stream: A three-dimensional groundwater flow model. *Water Resources Research* 39 (2) 1034.

Sullivan, A.B., Drever, J.I. (2001) Geochemistry of suspended particles in a mine-affected mountain stream. *Applied Geochemistry* 16 (15) 1663-1676.

Theobald, P.K., Lakin, H.W., Hawkins, D.B. (1963) The precipitation of aluminum, iron and manganese at the junction of Deer Creek with the Snake River in Summit-County, Colorado. *Geochimica et Cosmochimica Acta* 27 (2) 121-132.

Tonkin, J.W., Balistrieri, L.S., Murray, J.W. (2002) Modeling metal removal onto natural particles formed during mixing of acid rock drainage with ambient surface water. *Environmental Science & Technology* 36 (3) 484-492.

Toride, N., Leij, F.J., and van Genuchten, M.T. (1995) The CXTFIT code for estimating transport parameters from laboratory or field tracer experiments, version 2.0. Research Report No. 137, U.S. Salinity Laboratory, U.S. Department of Agriculture, Riverside, CA.

Triska, F.J., Kennedy, V.C., Avanzino, R.J., Zellweger, G.W., Bencala, K.E. (1989) Retention and transport of nutrients in a third-order stream: channel processes. *Ecology* 70 (6) 1877-1892.

Tufenkji, N., Elimelech, M. (2004) Correlation equation for predicting single-collector efficiency in physicochemical filtration in saturated porous media. *Environmental Science & Technology* 38 (2) 529-536.

USEPA, 2003. Left Hand Creek watershed case study: Use of NPL as a catalyst for abandoned mine cleanup. United States Environmental Protection Agency, 6 p. (accessed on March 17, 2011, at http://www.epa.gov/aml/tech/lefthand.pdf).

USEPA/DOE, 2004. Mine waste technology program: Annual report 2004. United States Environmental Protection Agency and the Department of Energy, 51 p. (accessed March on 17, 2011, at http://www.epa.gov/nrmrl/std/mtb/mwt/annual/annual2004/annual2004.htm).

Verwey, E. J. W. and Overbeek, J. T. G. (1948) Theory of the Stability of Lyophobic Colloids. Elsevier: Amsterdam, 218 pp.

Wagner, B.J., Harvey, J.W. (1997) Experimental design for estimating parameters of rate-limited mass transfer: Analysis of stream tracer studies. *Water Resources Research* 33 (7) 1731-1741.

Wanty, R.B., Winter, T.C. (2000) A simple device for measuring differences in hydraulic head between surface water and shallow groundwater. Fact Sheet FS-077-00, U.S. Geological Survey, Washington, DC.

Wentz, D.A. (1974) Effect of mine drainage on the quality of streams in Colorado, 1971-72. *Colorado Water Resources Circular* 21, 117 p.

Wondzell, S.M. (2006) Effect of morphology and discharge on hyporheic exchange flows in two small streams in the Cascade Mountains of Oregon, USA. *Hydrological Processes* 20 (2) 267-287.

Wood, A.R. 2004. Characterization and prioritization of mining-related metal sources with metal loading tracer dilution tests, and a review of regulations and mine restoration funding resources, Lefthand Creek watershed, northwestern Boulder County, Colorado. M.S. Thesis, University of Colorado, Boulder, Colorado.

Wroblicky, G.J., Campana, M.E., Valett, H.M., Dahm, C.N. (1998) Seasonal variation in surface-subsurface water exchange and lateral hyporheic area of two stream-aquifer systems. *Water Resources Research* 34 (3) 317-328.

Yao, K.-M., Habibian, M. T. and O'Melia, C. R. (1971) Water and waste water filtration. Concepts and applications. *Environmental Science & Technology* 5, 1105-1112.

Zanker, H., Richter, W., Huttig, G. (2003) Scavenging and immobilization of trace contaminants by colloids in the waters of abandoned ore mines. *Colloids and Surfaces A-Physicochemical and Engineering Aspects* 217 (1-3) 21-31.

Zaramella, M., Marion, A., Packman, A.I. (2006) Applicability of the transient storage model to the hyporheic exchange of metals. *Journal of Contaminant Hydrology* 84 (1-2) 21-35.

Zarnetske, J. P., Gooseff, M. N., Brosten, T. R., Bradford, J. H., McNamara, J. P., Bowden, W. B. (2007) Transient storage as a function of geomorphology, discharge, and permafrost active layer conditions in Arctic tundra streams. *Water Resources Research* 43(7) doi:10.1029/2005WR004816.

APPENDIX A - COLLOID AND COLLOID-ASSOCIATED METAL REMOVAL IN STREAM SEDIMENTS AFFECTED BY ACID MINE DRAINAGE

ABSTRACT

Metals found in acid mine drainage contaminate streams throughout the mining regions worldwide. An important component of assessing the impact of these metals is understanding their transport in the receiving streams. Some contaminant metals are associated with colloids; therefore, understanding the transport of colloids is also required. The hyporheic exchange process transports water from the stream channel into the subsurface. Once in the subsurface colloids and colloid-associated metals may be removed in streambed sediments through physicochemical filtration in the hyporheic zone. The degree of removal was expected to depend on several water chemistry parameters, including pH, ionic strength, and organic matter concentrations. The transport of ferric hydroxide colloids and metals (lead, copper, and zinc) through stream sediments was examined in a series of flow-through column experiments. Baseline conditions were chosen to approximate the chemistry of the impacted stream from which sediments were collected. Additional column experiments showed the influence of variations in pH, ionic strength, and organic matter concentrations on metal and colloid transport. The results of the column experiments conducted under conditions similar to those in the stream showed that 86% of colloids were removed through sorption to the streambed sediments along with 87% of lead, 93% of copper, and 98% of zinc. Most of the lead was associated with the colloids; therefore, lead was more mobile in the presence of colloids than copper or zinc. Changes in pH from 4 – 6 and ionic strength from 0.2 – 10 mM did not significantly influence colloid and metal breakthrough. An increase in the organic matter concentration from 2 mg L^{-1} to 10 mg L^{-1} fulvic acid greatly enhanced colloid and metal breakthrough.

INTRODUCTION

Abandoned mines are responsible for heavy metal contamination in many otherwise pristine streams throughout mining regions of America. The U.S. Environmental Protection Agency (2004) lists over 600,000 abandoned mine sites with an estimated remediation cost range of $32 to $72 billion. Metal contamination impairs aquatic ecosystems. Some metals accumulate in fish and create additional risk for the people who ingest them. Tourism economies may also be adversely affected by the loss of fish habitats. As the population increases, the demand for drinking water has made the risk of human exposure through drinking water a larger issue. Local communities, mining industry leaders, and environmental regulators are under pressure to restore abandoned mine sites and affected streams.

High concentrations of metals are attenuated in streambed sediments affected by acid mine drainage (Axtmann and Luoma, 1991; Nagorski et al., 2002; Galán et al., 2003) and hyporheic exchange is frequently cited as the mechanism by which metal removal occurs (Ranville et al., 2004; Zaramella et al., 2006; Gandy et al., 2007). Hyporheic exchange in the process in which surface water enters the subsurface beneath and lateral to a stream and returns to the stream surface farther downstream (Harvey and Wagner, 2000). Streambed topography, such as pools and riffles, causes the exchange of water between the stream and streambed (Bencala, 1984; Harvey and Bencala, 1993). Hyporheic exchange plays an important role in stream biogeochemistry, nutrient cycling, and contaminant removal (Triska et al., 1989; Benner et al., 1995). Mixing of surface and ground water in the hyporheic zone leads to the formation of physical (temperature) and geochemical (pH, organic matter, oxidation-reduction) gradients in the hyporheic zone (Triska et al., 1989).

Colloids are commonly formed by the oxidation of Fe^{2+} and the precipitation of Fe-(oxy)hydroxides in streams impacted by acid mine drainage (Kimball et al., 1992). They are typically small, amorphous colloids with a high surface area. These Fe-(oxy)hydroxides scavenge other metals whether they are in the form of colloids or coatings on streambed sediment (Kimball et al., 1992; Munk et al., 2002; Gandy et al., 2007; Schemel et al., 2007). Some metals, such as lead and copper, are largely associated with colloids (Johnson, 1986; Kimball et al., 1995; Ganguli et al., 2000; Tonkin et al., 2002); therefore, understanding of metal transport and removal in streams will also require understanding of colloid transport and removal.

In order to understand the transport of colloids undergoing hyporheic exchange in a stream system, it is useful to understand the affects of water chemistry on colloids in a controlled saturated porous media system. Ferric (oxy)hydroxide colloid transport will be limited by physicochemical filtration in the hyporheic zone. The degree of removal will depend on several parameters, including pH, ionic strength, and organic matter concentrations (Gandy, 2007). Near the point of zero charge, colloids will become unstable, resulting in aggregation and settling. Ionic strength also plays an important role in colloid mobility. Increasing ionic strength causes compression of the diffuse double layers around charged surfaces, decreasing the electrical potential at the shear plane (Hiemenz and Rajagopalan 1997). This would result in greater aggregation of colloids which otherwise have repulsive surface charges. Kretzschmar and Sticher (1997) found that addition of organic matter to hematite particles decreased the surface charge of the particles and enhanced transport through a sandy soil matrix.

As water from the stream and groundwater mix, gradients will form with respect to these geochemical parameters. This may result in zones of varied pH, ionic strength and organic

matter concentration. Changing conditions in the hyporheic zone may cause changes in the sorption rates of colloids. The objective of this study was to examine the transport of ferric (oxy)hydroxide colloids through heterogeneous hyporheic zone sediments under varying water chemistry conditions in a series of controlled laboratory column experiments. Colloid and colloid-associated metal transport was assessed over a range of pH, ionic strength, and organic matter concentrations. Metals, such as lead and copper, which have higher affinities for sorption to colloids may be largely controlled by the transport of colloids in the hyporheic zone sediment.

MATERIALS AND METHODS

Porous Medium

The sediments used in the column were collected Left Hand Creek, a stream impacted by acid mine drainage. The sediments were removed from the upper 10 cm of the streambed using a shovel and collected in 1-L HDPE bottles. The sediments were dried in an oven at 60°C and sieved to isolate the 1.0-1.4 mm size grains.

Chemical Constituents

All chemicals used were ACS grade or trace metal grade. Organic matter (OM) was provided by adding hydrophobic organic acid, composed primarily of aquatic fulvic acid, isolated from Lefthand Creek according to the procedure described by Aiken et al. (1992).

Colloid Synthesis and Characterization

Ferrihydrite colloids were synthesized using an adaptation of the method of Schwertmann and Cornell (2000). The addition of 0.5 M sodium hydroxide resulted in ferric iron (0.079 M $Fe(NO_3)_3 \cdot 9\ H_2O$) hydrolysis at a rate of 167 μmol Fe min^{-1}. This rapid rate of hydrolysis encouraged formation of amorphous 2-line ferrihydrite. The colloid suspension was

centrifuged (at 2,200 × g for 15 minutes), the water was decanted, and replaced with ultrapure (<18 MOhm) water, and the ferrihydrite was resuspended by applying a vortex for 10 seconds; this rinsing process was done five times. In the final centrifugation step, colloids smaller than 200 nm in diameter were separated according to Stokes' Law. Only these colloids were used to make the experimental suspension. The colloids were kept in aqueous suspension with ultrapure water at a pH of approximately 4 and used in experiments within 48 h.

The bulk precipitate collected prior to final centrifugation step separated by size was analyzed by x-ray diffraction (XRD; D5000 Siemens) to confirm the mineral identity. One gram of the precipitate was mixed with 0.25 g corundum, milled, and analyzed between 5 and 65° 2θ at 0.02° steps with a 2 s count per step using Cu K_α radiation. A ferrihydrite standard (isolated from Humbug Creek, CA by the USGS) was also analyzed by the same method. The XRD data were analyzed quantitatively for minerals present using the RockJock computer program (Eberl, 2003). The colloid suspension was examined by scanning electron microscopy/energy-dispersive x-ray (SEM-EDX) spectrometry using a field emission SEM (FESEM; JEOL JSM-7401F) for size and elemental composition. The colloidal suspension was collected on a filter, air-dried, taped to aluminum mounts with carbon tape, and sputter-coated with a layer of gold and palladium (Denton Vacuum, Inc., Desk II Cold Sputter/Etch Unit; 50 millitorr, 40 mA, 30 s). Colloids were also analyzed for size and zeta potential using dynamic light scattering (DLS) and laser Doppler microelectrophoresis (Particle Sizing Systems; 380 ZLS). Zeta potential values are based on measurements of electrophoretic mobilities which were converted to zeta potentials using the Smoluchowski equation.

Colloid stability was assessed over a range of pH values. Colloid suspensions were pH-adjusted with 50 mM sodium hydroxide and examined for size within 1 h of pH adjustment. The

size was examined using Gaussian analysis and NICOMP distribution analysis of the autocorrelation function. When the distribution of particles is not uniform, the distribution analysis applies nonlinear least-squares analysis to determine a distribution of particle diameters. The number-weighted intensities were considered to be most representative of the colloid suspensions because they were expected to be made up largely of small particles. Zeta potentials were measured by laser Doppler microelectrophoresis within 24 h of pH adjustment. DLS and zeta potential measurements were carried out at 21°C.

Column Experiments

Column experiments were conducted to assess the role of solution chemistry in the removal of the ferrihydrite colloids in the stream sediments. To determine the hydraulic properties of the column, a conservative tracer, bromide, was injected as sodium bromide into the column prior to injection of the colloid suspension. The colloid suspension was mixed with the metals, organic matter, and pH and ionic strength adjustments were made. The concentrated colloidal suspension was diluted such that the injected suspension consisted of approximately 40 mg L^{-1} ferrihydrite. Metal nitrates were incorporated with the injected suspension for final concentrations of 1800 µg L^{-1} copper, 1800 µg/L zinc, and 100 µg/L lead. Solution ionic strength was controlled using NaCl and pH was adjusted by titrating with 0.05 M sodium hydroxide or 0.05 M hydrochloric acid. This solution was allowed to equilibrate for 1 h prior to injection into the column.

Columns were packed by adding a thin layer (approximately 0.5 cm thick) of dry sediment to the stainless steel column (5 cm length) and flushing it with water from a squirt bottle to settle the grains. This process was repeated until the column was full. Solutes and colloidal suspensions were injected through C-FLEX tubing (Masterflex 6424-14, 1.6 mm ID)

through the column using a peristaltic pump (Cole Parmer L/S 7553-70). The effluent samples (6 mL) were collected on a fraction collector (ISCO Retriever II, Spectra/Chrome CS-1).

The sediments in the column were rinsed prior to the column experiments by passing pH and ionic strength adjusted water through the column for 20 pore volumes to remove any readily-mobilized metals present in the sediments. Metals exiting the column during this pre-experiment flush were measured and the final metals concentrations prior to the experimental injection were used as the background metal concentrations for breakthrough analysis.

Bromide, in the form of sodium bromide, was first pumped into the column, followed by the colloid-metal injection suspension. Both solutions were pumped through the column at a rate of 1.5 mL min^{-1} for 5 pore volumes. This resulted in a Darcy velocity of 0.31 cm min^{-1} through the column. Colloid size and zeta potential of the colloid-metal suspension injected into the column was measured within 24 h of the column experiment. Background metal concentrations measured prior to the start of each experiment were subtracted from the metal breakthrough curves for the purposes of determining metal transport properties. Colloid concentration was determined by weighing a known volume of solution after drying.

Bromide transport was modeled using CXTFIT code (version 2, Toride et al., 1995) to determine the effective porosity of the sediment column. The colloid filtration coefficient, λ, is determined from classical filtration theory with the equation

$$\frac{C}{C_0} = \exp[-\lambda L] \qquad \text{(A.1)}$$

where C_0 is the influent colloid concentration, C is the effluent colloid concentration, and L is the length of the column. The parameter effluent concentrations of colloids and metals were averaged from all the values measured during the steady injection to obtain C/C_0. These values are typically constant with a constant steady injection and flow rate. However, the effluent

concentrations of colloids and metals declined from the maximum over the course of the injection for many experiments. This is noted in Table A.1.

The baseline conditions set for the experiments (pH ≈ 6, I = 2.0×10^{-4} M, [FA] = 2 mg L^{-1} as fulvic acid) were similar to those found in Left Hand Creek. After conducting the baseline column experiment, one of the three chemical parameters, ionic strength, pH, and organic matter concentration, was varied for each subsequent column experiment to determine its influence on colloid removal. For each experiment exploring the affects of chemical composition, one variable was modified at a time. The chemical conditions of each experiment are given in Table A.1.

Laboratory Analysis

Samples for metals analysis were acidified to 2% by volume with trace metal-grade nitric acid. Iron, lead, copper, and zinc were measured with inductively coupled plasma-mass spectrometry (ICP-MS; Varian 810MS). Samples of the column effluent were filtered with 0.1 μm filter (Nuclepore, polycarbonate) prior to acidification to obtain dissolved fractions. Colloidal metal fractions were calculated as the difference between total and dissolved metals. Bromide was analyzed using an electrode and meter (Accumet bromide combination ion selective electrode and Orion 720A meter). Detection limits for bromide, lead, copper, zinc, and iron were 1.0 μM, 0.47 nM, 0.31 nM, 0.67 nM, and 95 nM, respectively.

RESULTS

Colloid characterization

The synthesized colloids were analyzed for structure, elemental composition, and colloidal size. The colloids were a 98.2% match for amorphous, 2-line ferrihydrite (Figure A.1) with impurities of lepidocrocite, hematite, and goethite.

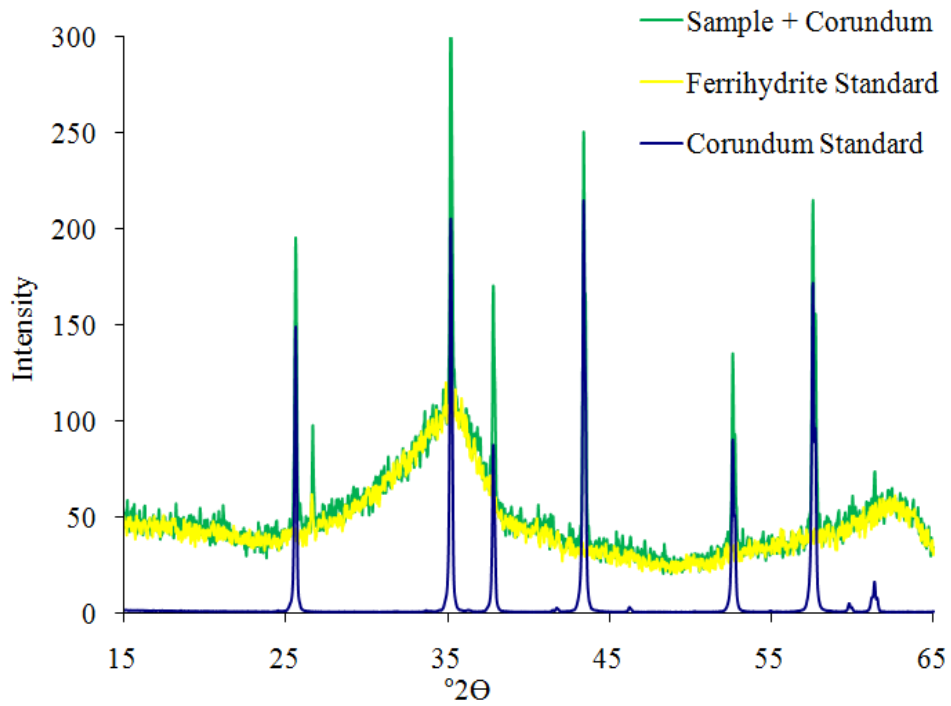

Figure A.1. XRD analysis of synthesized colloids mixed with corundum for quantitative analysis. The sample was a 98.2% match for ferrihydrite with less impurities of lepidocrocite, hematite, and goethite.

SEM examination revealed that the colloids dried on filters (0.1 µm) appeared to be 1-2 µm aggregates of smaller particles about 100 nm in diameter (Figure A.2). The point of zero charge of the colloids was 6.6 as determined by microelectrophoresis (Figure A.3). Near the point of zero charge, the colloids were unstable – dynamic light scattering analysis showed that the average size of the colloid suspension increased from about 100 nm at low pH to as high as 6 µm at pH 6 and 7 (Figure A.4).

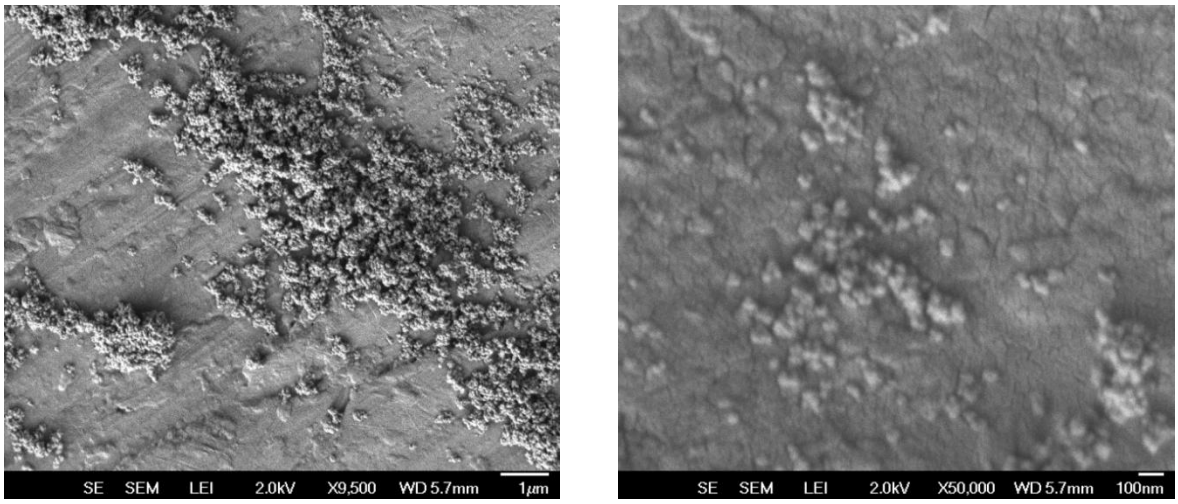

Figure A.2. FESEM images of synthesized ferrihydrite colloids at 9,500× (left) and 50,00× (right) magnification. Scale bars are given on the lower right of each image.

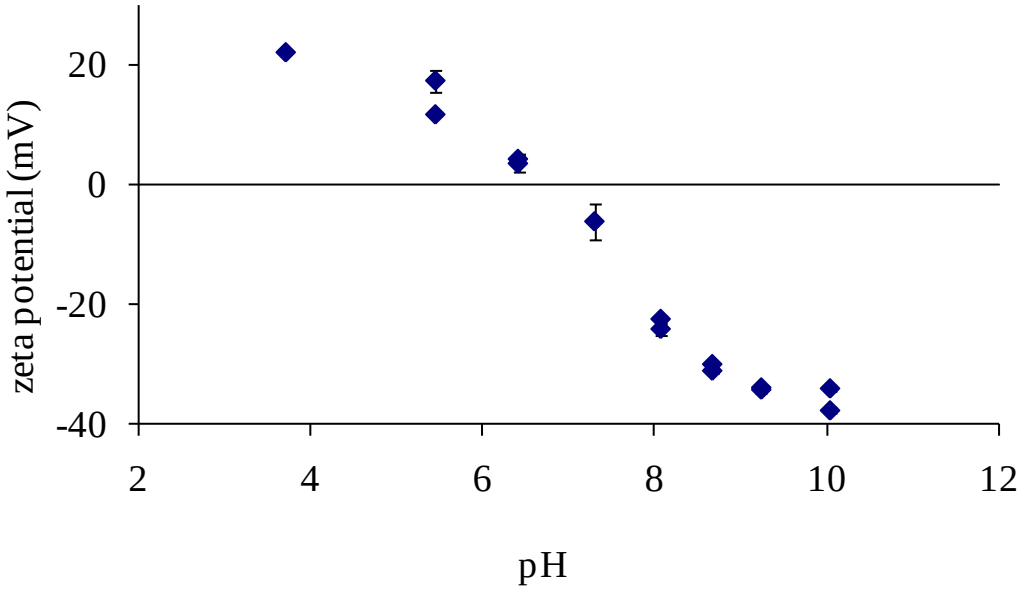

Figure A.3. Zeta potential of the synthesized ferrihydrite colloids as a function of pH as determined by laser Doppler microelectrophoresis in a 1×10^{-4} M NaCl solution. Colloid suspensions were pH- adjusted with 50 mM sodium hydroxide. Error bars represent ± 1 standard deviation.

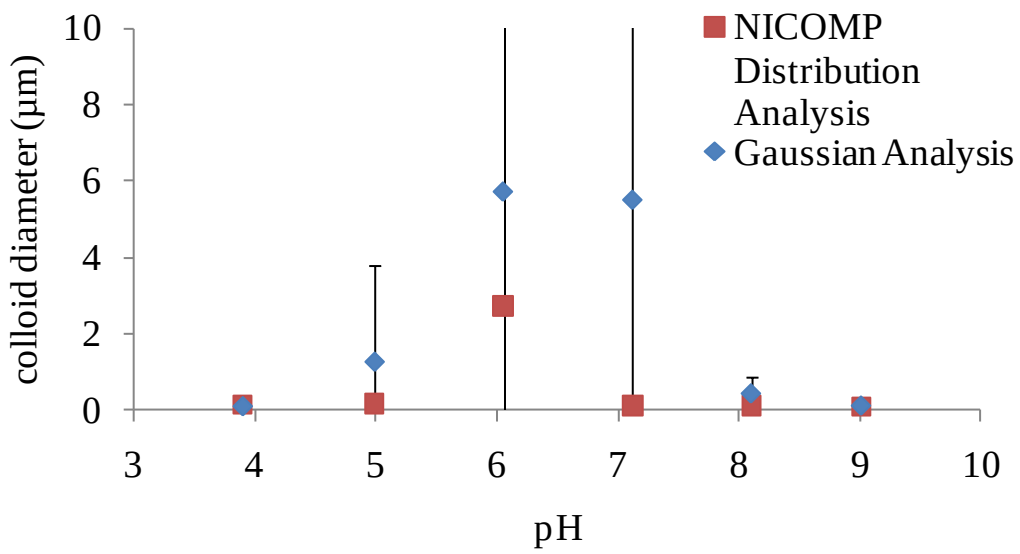

Figure A.4. Number-weighted colloid size as a function of pH in a 2×10^{-4} M NaCl solution after equilibration for 24 h as measured by dynamic light scattering. Values are given for both Gaussian and NICOMP distribution analysis. Error bars give the standard deviation associated with the Gaussian analysis only. Standard deviations cannot be obtained from NICOMP analysis.

Colloid and Metal Filtration Experiments

A series of flow-through column experiments were used to determine the effects of water chemistry on ferrihydrite colloid and metal transport. The baseline conditions set for the experiments (pH ≈ 6, I = 2.0×10^{-4} M, [FA] = 2 mg L^{-1} as fulvic acid) were similar to those found in Left Hand Creek. Under the baseline conditions, the breakthrough of the colloids and lead are similar, copper breakthrough is less than that of lead, and zinc breakthrough is less than that of copper (Figure A.5). For each experiment exploring the affects of chemical composition, one variable was varied at a time. The average C/C_0 values for the iron and other metals normalized to their injection concentrations are given in Table A.1. Measurements of iron indicated that essentially all of the iron entering and exiting the column was colloidal, so the iron values were taken to represent colloidal transport. The colloid sizes and zeta potentials varied widely over the range of conditions analyzed (Table A.1). Increasing the dissolved organic

matter concentration to 10 mg L^{-1} led to the greatest breakthrough for all the metals and colloids (Figure A.6).

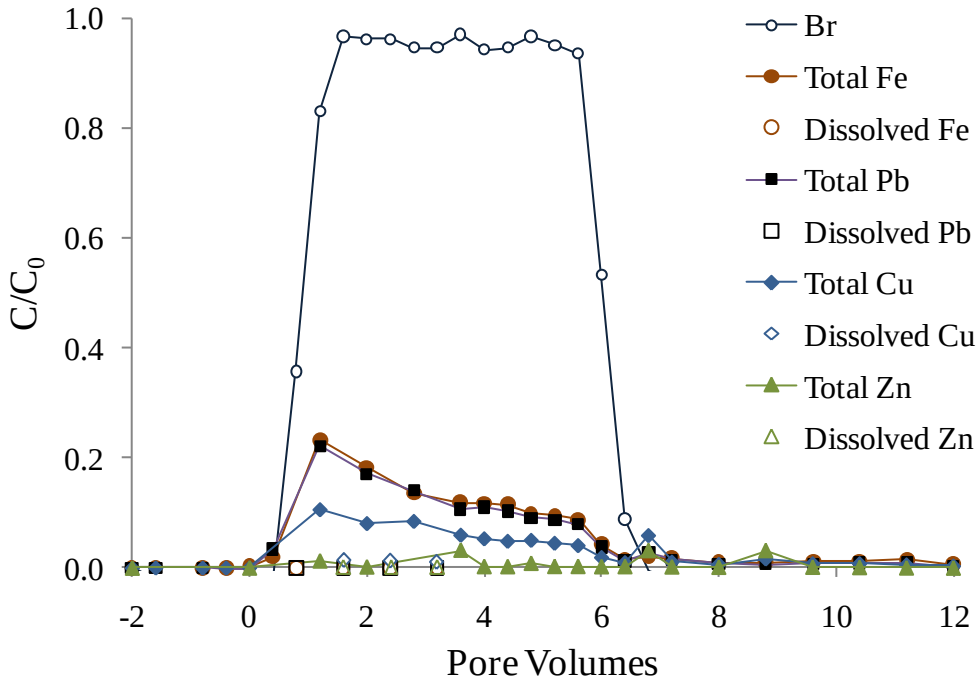

Figure A.5. Normalized breakthrough of bromide and metals that were equilibrated and co-injected under the baseline experimental conditions: pH = 6.0, I = 2×10^{-4} M, [FA] = 2 mg L^{-1}. The bromide was injected prior to the colloids and metals injection and is included here to represent conservative transport.

Table A.1. Average C/C_0 values for metals from column experiments under various values for pH, ionic strength, and organic matter, as fulvic acid (FA). Particle diameter and zeta potentials of influent suspension as well as the resulting colloid filtration coefficient based on Equation 1 are given.

experiment	pH	ionic strength (M)	fulvic acid (mg L^{-1})	NICOMP particle diameter[a] (μm)	Gaussian particle diameter[a] (μm)	zeta potential (mV)	Fe (C/C_0)	Pb (C/C_0)	Cu (C/C_0)	Zn (C/C_0)	colloid filtration coefficient (λ)
baseline	6.0	2.0×10^{-4}	2.0	1.8	0.31 (2.0)	-17.1 (0.93)	0.14[b]	0.13[b]	0.07[b]	0.02[b]	0.39[b]
pH modification	5.1	2.0×10^{-4}	2.0	8.5	10 (14)	3.84 (1.07)	0.01[b]	0.01[b]	0.004[b]	0.002[b]	1.04[b]
pH modification	4.0	2.0×10^{-4}	2.0	8.5	18 (16)	13.34 (0.458)	0.01[b]	0.01[b]	0.02[b]	0.01[b]	0.87[b]
I modification	6.0	1.0×10^{-3}	2.0	NA	NA	-17.1 (0.824)	0.02[b]	0.02[b]	0.01[b]	0.003[b]	0.83[b]
I modification	6.0	1.0×10^{-2}	2.0	3.7	0.87 (11.4)	-20.5 (3.88)	0.05[b]	0.05[b]	0.04[b]	0.004[b]	0.61[b]
FA modification	6.0	2.0×10^{-4}	5.0	1.4	0.45 (6.0)	-10.6 (3.1)	0.03[b]	0.05[b]	0.02[b]	0.06[b]	0.69[b]
FA modification	6.0	2.0×10^{-4}	10.0	0.80	0.15 (0.55)	-15.6 (0.54)	0.83	0.91	0.46	0.14	0.038

[a]The particle diameter given is based on number weighted DLS analysis of influent particles. Standard deviation is given in parenthesis with the Gaussian particle diameter.
NA – not available.
[b]C/C_0 values declined from a maximum during the steady injection

In the column effluent, lead was largely colloidal under all conditions; the fraction of lead in the colloidal form ranged from 69 % to 99 % (Table A.2). The copper speciation varied greatly between experiments; 24 % to 86 % of the copper was colloidal, depending on the chemical composition of the injected solution. Zinc was largely dissolved in all experiments except under baseline conditions, when there was no appreciable breakthrough of zinc. The colloidal fractions of copper and zinc were greatest in the high organic matter experiments.

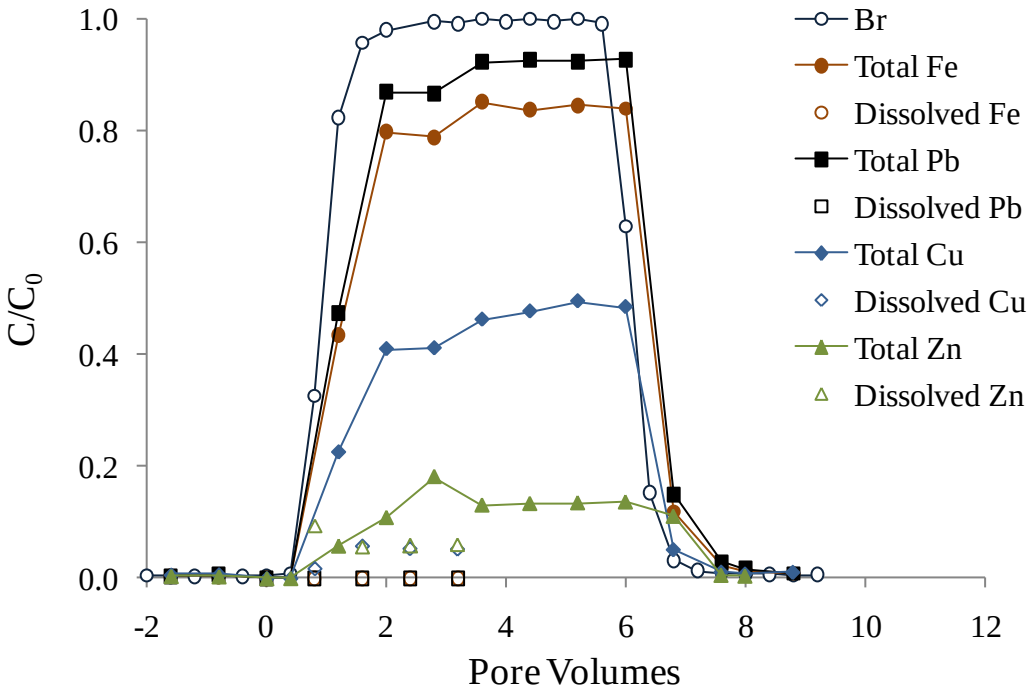

Figure A.6. Fulvic acid modification experimental results showing normalized breakthrough of bromide and metals from a sediment-packed column under experimental conditions: pH = 6, I = 2 x 10-4 M, [FA] = 10 mg L-1 The bromide was injected prior to the colloids and metals injection and is included here to represent conservative transport.

Table A.2. Average fraction of metals entering and exiting the column in the dissolved state (as defined by 0.01 µm filtration). Influent dissolved concentrations were not measured in the pH variation experiments.

		ionic	fulvic	Fe dissolved fraction		Pb dissolved fraction		Cu dissolved fraction		Zn dissolved fraction	
experiment	pH	strength (M)	acid (mg L^{-1})	influent	effluent	influent	effluent	influent	effluent	influent	effluent
Baseline	6.0	2×10^{-4}	2	0.002	0.01	0.0014	0.0087	0.20	0.33	0.89	0.20
Varying pH	5.0	2×10^{-4}	2	--	0.01	--	0.31	--	0.76	--	0.88
Varying pH	4.0	2×10^{-4}	2	--	0.03	--	0.036	--	0.44	--	0.98
Varying I	6.0	1×10^{-3}	2	0.02	0.04	0.023	0.12	0.08	0.63	0.60	0.90
Varying I	6.0	1×10^{-2}	2	0.004	0.03	0.016	0.054	0.46	0.69	0.93	0.73
Varying OM	6.0	2×10^{-4}	5	0.0003	0.03	0.0024	0.18	0.01	0.73	0.38	0.91
Varying OM	6.0	2×10^{-4}	10	0.001	0.00	0.0032	0.0064	0.02	0.14	0.41	0.76

DISCUSSION

Effects of Chemical Composition on Colloids

Changes in the pH, ionic strength, and organic matter concentration all may affect the size and stability of ferric hydroxide particles. Size and zeta potentials of the colloids in a low salt solution showed clear trends with a point of zero charge (PZC) for the colloids of 6.6 and an increase in size from about 100 nm at high and low pH to as high as 6 µm aggregates near the PZC (Figures A.3 & A.4). Trends become more difficult to detect when comparing the colloid characteristics of the column experiment solutions containing organic matter and metals (Table A.1). Replicates of the experiments are necessary to determine whether these results are reproducible.

Decreasing pH was expected to cause a decrease in particle size. However, the colloids at pH 4 and 5 were significantly larger than those at pH 6 with the same ionic strength, fulvic acid, and metal concentrations. The decrease in pH did cause an increase in the zeta potential of the colloids, as expected. The large size of the colloids at pH 4 and 5 led to increased deposition in the column and explains the large colloid filtration coefficients obtained.

Increasing ionic strength caused an increase in colloid size. Though size data for 10^{-3} M NaCl was lost, the increase in size can be seen by comparing the results from 10^{-4} M and 10^{-2} M NaCl experiments. The difference in zeta potential between the 10^{-4} M and 10^{-2} M NaCl experiments is small. The higher ionic strength increased colloid deposition compared with the baseline conditions at 10^{-4} M NaCl, though the trend in the colloid filtration coefficient is not consistent between the 10^{-3} M and 10^{-2} M experiments.

Increasing the fulvic acid concentrations decreased the colloid size, and contributed to the greatest colloid mobility observed in this study. Though the zeta potentials do not indicate a

clear trend of decreasing surface charge with increasing fulvic acid concentration, the coating of the colloids with negatively charged functional groups likely provided the stability of the colloids at smaller sizes. The increase to 5 mg L^{-1} from 2 mg L^{-1} did not decrease filtration, but at a fulvic acid concentration of 10 mg L^{-1} the colloid filtration coefficient decreased substantially.

The equilibration of the metals with the colloids also affected the colloids. Though the effect of metal addition was not examined explicitly in this study, Ren and Packman (2005) observed an increase in diameter of hematite from 1.4 to 3.3 μm in the presence of 3 mg L^{-1} copper or zinc at pH 6.74. It was also observed that copper and zinc increased the point of zero charge of the hematite particles (Ren and Packman, 2005).

Implications for Metal Transport

Though there are some inconsistencies in the trends, differences between the transport of lead, copper, and zinc can be recognized. Because lead associates strongly with the colloids, the lead breakthrough tends to trend with the colloids and shows the greatest transport overall. Copper is less associated with colloids and is immobilized in the sediments to a greater extent. Zinc is largely immobilized through sorption to the sediments.

A decrease in pH was expected to cause a greater faction of metals to be dissolved and result in a greater breakthrough of dissolved metals. However, influent metal speciation was not measured for the pH modification experiments. The overall breakthrough was less than 2% of the influent levels for all the metals at pH 4 and 5 (Table A.1). Most of the dissolved metals were removed through interactions with the sediments, which are presumed to have negatively charged surfaces, though streaming potential measurements of the sediments were not done to confirm this. The effluent zinc followed a trend of increasing dissolved fraction with decreasing

pH, with as much as 98% of the effluent zinc being dissolved at pH 4, while lead and copper speciation did not follow a clear trend with decreasing pH (Table A.2). The metals that were associated with colloids at pH 4 and 5 were largely immobilized due to the high filtration coefficients of the large colloids.

Since the increase in ionic strength caused greater colloid deposition in the sediments, any colloidal metals were also removed to a greater extent with increasing ionic strength. Lead was largely colloidal in the influent and effluent of the ionic strength experiments and breakthrough was similar to the breakthrough for iron. Despite the large removal of colloids, colloidal transport seems to enhance metal transport as breakthrough was greatest for lead, which was mostly colloidal, and lowest for zinc, which was largely dissolved. Sediment capacity for sorbing metals appears to be large, since the dissolved metals are removed at a great extent as are the colloidal metals. All the metals showed greater dissolved fractions in the effluent than in the influent solutions, which may indicate that colloidal metals were preferentially removed (Table A.2).

Increasing the fulvic acid concentration to 10 mg/L increased metal as well as colloid transport in the sediments. Lead breakthrough was 91%, followed by copper (46%) and zinc (14%). Lead was largely colloidal in both the influent and effluent, indicating that it was mobilized through attachment to mobile colloids. Copper was also largely colloidal, but the dissolved fraction in the effluent was higher than in the influent suspension, which indicated that some colloidal material was preferentially removed in the sediments. Zinc also showed a large increase in dissolved fraction in the effluent, indicating that the dissolved zinc was more mobile. Binding of metals to organic matter may also have been a means of enhancing the transport of

metals independently of the ferric hydroxide particles. Copper, for example, may bind with organic matter and thus prevented from adsorbing to sediments (Breault et al., 1996).

SUMMARY

These column experiments show the differences in the behavior of the metals of interest. Because lead associates strongly with the colloids, the lead breakthrough tends to trend with the colloids and shows the greatest transport overall. Copper is less associated with colloids and is immobilized in the sediments to a greater extent. Zinc is largely immobilized through sorption to the sediments. Over the pH and ionic strength ranges analyzed, these parameters do not cause great variations in the colloid or metal transport. More than 86% of the colloids and 85% of the metals are immobilized in the column under a range of conditions that are likely to occur in stream. Only at very high fulvic acid concentrations are the colloids and metals highly mobile.

REFERENCES

Aiken, G. R., McKnight, D.M., Thorn, K.A., Thurman, E.M. (1992) Isolation of hydrophilic organic acids from water using nonionic macroporous resins. *Organic Geochemistry* 18 (4) 567-73.

Axtmann, E.V., Luoma, S.N. (1991) Large-scale distribution of metal contamination in the finegrained sediments of the Clark Fork River, Montana, USA. *Applied Geochemistry* 6 (1) 75-88.

Bencala, K.E. (1984) Interactions of solutes and streambed sediment 2. A dynamic analysis of coupled hydrologic and chemical processes that determine solute transport. *Water Resources Research* 20 (12) 1804-1814.

Benner, S.G., Smart, E.W., Moore, J.N. (1995) Metal behavior during surface groundwater interaction, Silver-Bow Creek, Montana. *Environmental Science & Technology* 29 (7) 1789-1795.

Breault, R. F., Colman, J.A., Aiken, G.R., McKnight, D. (1996) Copper speciation and binding by organic matter in copper-contaminated streamwater. *Environmental Science & Technology* 30 (12) 3477-86.

Eberl, D.D. (2003) User guide to RockJock: a program for determining quantitative mineralogy from x-ray diffraction data. United States Geological Survey, Open File Report 03-78, 40 p.

Galán, E., Gomez-Ariza, J.L., Gonzalez, I., Fernandez-Caliani, J.C., Morales, E., Giraldez, I. (2003) Heavy metal partitioning in river sediments severely polluted by acid mine drainage in the Iberian Pyrite Belt. *Applied Geochemistry* 18 (3) 409-421.

Gandy, C.J., Smith, J.W.N., Jarvis, A.P. (2007) Attenuation of mining-derived pollutants in the hyporheic zone: A review. *Science of the Total Environment* 373 (2-3) 435-446.

Ganguli, P.M., Mason, R.P., Abu-Saba, K.E., Anderson, R.S., Flegal, A.R. (2000) Mercury speciation in drainage from the New Idria mercury mine, California. *Environmental Science & Technology* 34 (22) 4773-4779.

Harvey, J.W., Bencala, K.E. (1993) The effect of streambed topography on surface-subsurface water exchange in mountain catchments. *Water Resources Research* 29 (1) 89-98.

Harvey, J.W., Wagner, B.J. (2000) Quantifying hydrologic interactions between streams and their subsurface hyporheic zones. In *Streams and Ground Waters*, Jones, J.B., Mulholland, P.J. (Eds.), Academic Press, San Diego, p. 3.

Hiemenz, P.C., Rajagopalan, R. (1997) *Principles of colloid and surface chemistry*. Marcel Dekker, New York.

Johnson, C.A. (1986) The regulation of trace-element concentrations in river and estuarine waters contaminated with acid-mine drainage – The adsorption of Cu and Zn on amorphous Fe oxyhydroxides. *Geochimica et Cosmochimica Acta* 50 (11) 2433-2438.

Kimball, B.A. Callender, E., Axtmann, E.V., (1995) Effects of colloids on metal transport in a river receiving acid-mine drainage, Upper Arkansas River, Colorado, USA. *Applied Geochemistry* 10 (3) 285-306.

Kimball, B.A., Mcknight, D.M., Wetherbee, G.A., Harnish, R.A. (1992) Mechanisms of iron photoreduction in a metal-rich, acidic stream (St-Kevin Gulch, Colorado, USA). *Chemical Geology* 96 (1-2) 227-239.

Kretzschmar, R., Sticher, H. (1997) Transport of humic-coated iron oxide colloids in a sandy soil: influence of Ca^{2+} and trace metals. Environmental Science & Technology 31 (12) 3497-3504.

Munk, L., Faure, G., Pride, D.E., Bigham, J.M. (2002) Sorption of trace metals to an aluminum precipitate in a stream receiving acid rock-drainage; Snake River, Summit County, Colorado. *Applied Geochemistry* 17 (4) 421-430.

Nagorski, S.A., Moore, J.N., Smith, D.B. (2002) Distribution of metals in water and bed sediment in a mineral-rich watershed, Montana, USA. *Mine Water and the Environment* 21 (3) 121-136.

Ranville, M., Rough, D., Flegal, A.R. (2004) Metal attenuation at the abandoned Spenceville copper mine. *Applied Geochemistry* 19 (5) 803-815.

Ren, J. H. and Packman, A. I. (2005) Coupled stream-subsurface exchange of colloidal hematite and dissolved zinc, copper, and phosphate. *Environmental Science & Technology* 39 (17) 6387-6394.

Schemel, L.E., Kimball, B.A., Runkel, R.L., Cox, M.H. (2007) Formation of mixed Al-Fe colloidal sorbent and dissolved-colloidal partitioning of Cu and Zn in the Cement Creek - Animas River confluence, Silverton, Colorado. *Applied Geochemistry* 22 (7) 1467-1484.

Schwertmann, U., Cornell, R.M. (2000) *Iron Oxides in the Laboratory: Preparation and Characterization*. Wiley-VCH, New York.

Tonkin, J.W., Balistrieri, L.S., Murray, J.W. (2002) Modeling metal removal onto natural particles formed during mixing of acid rock drainage with ambient surface water. *Environmental Science & Technology* 36 (3) 484-492.

Toride, N., Leij, F.J., and van Genuchten, M.T. (1995) The CXTFIT code for estimating transport parameters from laboratory or field tracer experiments, version 2.0. Research Report No. 137, U.S. Salinity Laboratory, U.S. Department of Agriculture, Riverside, CA.

Triska, F.J., Kennedy, V.C., Avanzino, R.J., Zellweger, G.W., Bencala, K.E. (1989) Retention and transport of nutrients in a third-order stream: channel processes. *Ecology* 70 (6) 1877-1892.

USEPA/DOE, 2004. Mine waste technology program: Annual report 2004. United States Environmental Protection Agency and the Department of Energy, 51 p. (accessed March on 17, 2011, at http://www.epa.gov/nrmrl/std/mtb/mwt/annual/annual2004/annual2004.htm).

Zaramella, M., Marion, A., Packman, A.I. (2006) Applicability of the transient storage model to the hyporheic exchange of metals. *Journal of Contaminant Hydrology* 84 (1-2) 21-35.